NUSCALE™
Power for all humankind

NuScale Standard Plant
Design Certification Application

Chapter Four
Reactor

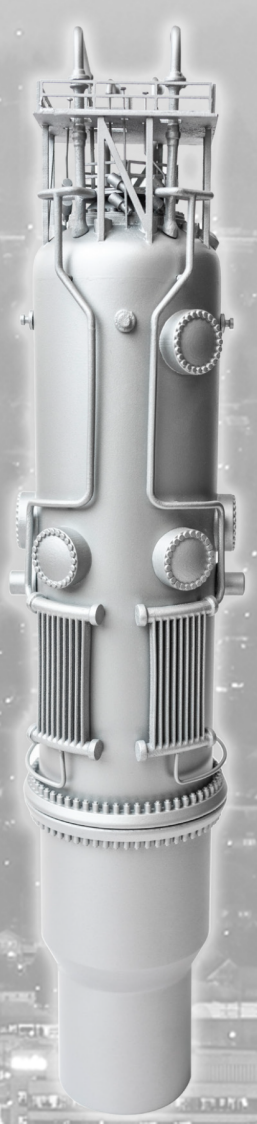

PART 2 - TIER 2

Revision 4.1
June 2020

TABLE OF CONTENTS

TABLE OF CONTENTS

LIST OF TABLES

LIST OF FIGURES

LIST OF FIGURES

LIST OF FIGURES

CHAPTER 4 REACTOR

4.1 Summary Description

The NuScale Power Module (NPM) is a self-contained nuclear steam supply system comprised of a reactor core, a pressurizer, and two steam generators integrated within the reactor pressure vessel (RPV) and housed in a compact steel containment vessel.

This section provides a brief summary of the reactor and the reactor core designs, the fuel rod and fuel assembly design, the core control and monitoring components, and the nuclear and thermal-hydraulic design.

Table 4.1-1 presents a summary of the principal NuScale reactor design parameters. Table 4.1-2 presents the core and fuel assembly design parameters.

4.1.1 Reactor Overview

The reactor vessel internals (RVI) support the reactor core, the control rod assemblies (CRAs), and the control rod drive shafts. The RVI channel the flow from the reactor core to the steam generators within the RPV.

The core configuration consists of 37 fuel assemblies and 16 CRAs. The fuel used in the NuScale design is NuFuel HTP2™. The NuScale fuel assembly design is a 17x17 design that is approximately one-half the length of typical pressurized water reactor fuel. The assembly is supported by five spacer grids, 24 guide tubes, and a top and bottom nozzle that together provide the structural skeleton for the 264 fuel rods. Each fuel assembly has a central instrument tube. The fuel is uranium dioxide (UO_2) with gadolinium oxide (Gd_2O_3) as a burnable absorber homogeneously mixed within the pellet in select locations.

A seamless M5® fuel rod cladding encapsulates ceramic UO_2 pellets which are cylindrically shaped with a spherical dish and chamfer at each end. Each fuel rod has an internal spring system which axially restricts the position of the fuel stack within the rod. The upper end cap has a grippable top-hat shape that allows for the removal of the fuel rods from the fuel assembly if necessary. The fuel rods are pressurized with helium.

The core is surrounded by a stainless steel heavy neutron reflector which improves fuel utilization by preventing the escape of neutrons radially from the core. The reflector also provides the core envelope and directs the flow through the core.

Four HTP™ spacer grids occupy the top four grid positions of a fuel assembly and are formed from interlocking strips that are welded at all intersections and welded to the side plates. Each grid strap is made from a pair of strips welded back-to-back to produce flow channels. The design creates a flow path that is slanted at its outlet creating a vortex flow pattern under normal operating conditions. The spacer grid design provides line contact with the rods, and an enhanced grid-to-rod interface with superior mechanical performance. The bottom spacer grid is an HMP™ design made of Alloy 718 and is similar to the top four grids with respect to spring design, rod-to-grid surface contact, and

manufacturing processes. The bottom spacer grid, however, has enhanced strength and resistance to relaxation and straight (non-mixing) flow channels.

The MONOBLOC™ guide tubes have a constant outer diameter and a reduced inner diameter near the bottom of the tube that forms the guide tube dashpot. The reduced inside diameter of the dashpot creates a hydraulic resistance to decelerate the CRA during rod insertion resulting from a reactor trip. The added thickness in the dashpot of the guide tube also increases the lateral stiffness of the fuel assembly.

The 304 stainless steel bottom nozzle consists of a cast frame of ribs connecting the guide tube locations. The bottom nozzle includes a mesh filter plate that prevents debris from entering the fuel assembly. The top nozzle consists of a machined stainless steel frame that is attached to the guide tubes with quick disconnect features at each of the 24 guide tube locations. The quick disconnect feature allows removal of the top nozzle to gain access to the individual fuel rods if needed.

The fuel cycles are designed for a nominal 2-year length. Gadolinium oxide is used to establish a favorable radial power distribution. The uranium enrichment of individual fuel assemblies varies depending on the position of the fuel assembly in the core. Typically, the assemblies with higher enrichment are placed on the periphery of the reactor core to lower peaking factors. This “out-in” loading pattern is described in Section 4.3.

There are two independent means of reactivity control -- control rods and soluble boron. The CRAs are organized in two banks: a regulating bank and a shutdown bank. The shutdown bank, consisting of eight CRAs symmetrically located in the core, is used during shutdown and reactor trip events. The shutdown bank is organized into two groups of four CRAs each. The regulating bank with eight CRAs (also two groups of four CRAs each) is used during normal plant operation to control reactivity. Each CRA contains 24 individual control rods containing B_4C and Ag-In-Cd (AIC) in the rod tip. The CRA parameters are provided in Table 4.1-3. Movement of the control rod assemblies is provided by the control rod drive system described in Section 3.9.4 and Section 4.6. The boron concentration is adjusted by the chemical and volume control system. Control rods are used for rapid reactivity adjustments and boron concentration is varied throughout the cycle to compensate for fuel burnup.

The core is monitored by the neutron monitoring system (NMS) and the in-core instrumentation system. The NMS is a safety-related instrumentation and controls system that monitors neutron flux from reactor shutdown to full-rated power by the use of three subsystems: 1) source range, 2) intermediate range, and 3) power range.

Neutron flux levels detected by the NMS are used by the module protection system (MPS) to generate reactor protection trips, operating permissives, indication, and alarms for various phases of reactor operation including shutdown conditions.

The in-core instrumentation system continuously monitors neutron flux (including axial offset) within the core and inlet and outlet coolant temperature and provides the parameter values to the module control system and post-accident monitoring system for display and evaluation in the control room.

Core exit temperature provides indication to the MPS as described in Section 7.0.4. The number and location of core exit thermocouples ensure an accurate indication of core exit temperature within each core quadrant.

The thermal-hydraulic design analyses establish that adequate heat transfer is provided between the fuel clad and the reactor coolant. The thermal design takes into account local variations in dimensions, power generation, flow distribution, and mixing. The thermal-hydraulic design is described in Section 4.4.

The NuScale reactor is inherently stable with respect to xenon stability as described in Section 4.3.2 and with respect to thermal-hydraulic stability as described in Section 4.4.7.

A description of the performance and safety functions of the reactor vessel internals is presented in Section 3.9.5.

The analytical techniques used in Chapter 4 are summarized in Table 4.1-4 and are discussed in more detail in Section 4.3 and Section 4.4.

4.1.2 Load Conditions

The fuel assembly component evaluations demonstrate that the primary stresses are lower than the material allowable stresses for both normal operation and faulted conditions for all evaluated components. The fuel load conditions considered in the fuel assembly and CRA design are discussed in Section 4.2.1.5 and Section 4.2.1.6. The dynamic analyses for the control rod drive system and reactor vessel internals are provided in Section 3.9.4 and Section 3.9.5.

Table 4.1-1: NuScale Reactor Design Parameters

Key Reactor Parameter	Value
Core thermal output (MWt)	160
System pressure (psia)	1850
Inlet temperature (°F)	497
Core average temperature (°F)	543
Average temperature rise in core (°F)	100
Best estimate flow (lb/hr)	4.66E+6
Core bypass flow (%)(best estimate)	7.3
Average linear power density (kw/ft)	2.5
Peak linear power for normal operating conditions (kw/ft)	5.0
Normal operation peak heat flux (Btu/hr-ft^2)	170,088
Total heat flux hot channel factor, F_Q	2.0
Heat transfer area on fuel surface (ft^2)	6275.6
Normal operation core average heat flux (Btu/hr-ft^2)	85,044
Core flow area (ft^2)	9.79
Core average coolant velocity (ft/sec)	2.7

Table 4.1-2: NuScale Core Design Parameters

Parameter	Value
Core	
Diameter of active core (ft)	4.94
Number of fuel assemblies	37
Height-to-diameter ratio of active core	1.33
Total cross section area of active core (ft^2)	18.42
Core barrel ID/OD (in)	74/78
Reflector	
Height (in)	91.75
Width (in)	2.5 to 12.2
Fuel Assembly	
Fuel design	NuFuel HTP2™
Length (in)	95.89
Nominal UO_2 per assembly (lb)	549.48
Rods per fuel assembly	264
Fuel assembly pitch (in)	8.466
Fuel rod pitch (in)	0.496
Number of grids per assembly	5
Span of grids (in)	20.1
Number of guide tubes per assembly	24
Number of instrument tubes per assembly	1
Guide tube dashpot region ID (in)	0.397
Guide tube dashpot region OD (in)	0.482
Guide tube above dashpot ID (in)	0.450
Fuel Rod	
Peak rod exposure core design criteria for UO_2 rods (GWd/MTU)	62
Gd_2O_3 concentration	Up to 8%
Cladding outside diameter (in)	0.374
Cladding inside diameter (in)	0.326
Cladding thickness (in)	0.024
Pellet-cladding diametral gap (in)	0.0065
Cladding material	M5®
Fuel column length (in)	78.74
Overall fuel rod length (in)	85
Fuel pellet material	Uranium Dioxide (UO_2)
Fuel pellet diameter (in)	0.3195
Fuel pellet density (%theoretical density)	96.0
Fuel pellet length (in)	0.4
Fissile enrichment	< 4.95%

Table 4.1-3: NuScale Reactor Control Rod Assembly Parameters

Parameter	Value
Silver-indium-cadmium length (in)	12
B_4C length (in)	62
CRA total length (in)	94.37
Neutron absorber material	B_4C and AIC
CRA clad material	304 SS
Maximum CRA bank withdrawal speed (in/min)	15
Number of absorber rods per CRA	24
B_4C outside diameter (in)	0.333
Control rod outside diameter (in)	0.381
Control rod inside diameter (in)	0.344
Silver-indium-cadmium outside diameter (in)	0.336

Table 4.1-4: NuScale Core Design Analytical Tools

Code Name	Type	Application	Additional Discussion
CASMO5	2D lattice transport	Perform fuel design calculations and generate nuclear data required by SIMULATE5.	Multi-group, two-dimensional, lattice physics transport theory code for assembly burnup calculations
COPERNIC	Fuel performance	Perform the thermal and mechanical analyses necessary to accurately simulate the behavior of a fuel rod during its irradiation.	The European TRANSURANUS code is used as a basis for COPERNIC.
SIMULATE5	3-D, steady-state, two-group nodal reactor analysis code core simulator	Steady state reactor analysis including calculation of reactivity coefficients, control rod worth, axial and radial power distributions and core physics inputs for transient analyses.	
SIMULATE-3K	3-D two-group nodal reactor analysis code core simulator	Transient reactor physics analysis	Same calculational foundation as SIMULATE5 extended for transient applications.
MCNP6.1	Monte Carlo collision probability	Evaluate neutron flux distributions for the reactor vessel and containment vessel.	
VIPRE-01	Core thermal hydraulics	Steady-state and transient subchannel analyses and minimum critical heat flux ratio.	Solves the mass, momentum and energy conservation equations.
ANSYS	Finite element structural analysis	Fuel assembly structural analysis	General purpose finite element code used for fuel assembly component structural evaluations, and for guide tube and fuel rod buckling.
CROV	Creep analysis of fuel rod cladding.	Evaluates the resistance of fuel cladding to creep collapse.	Inputs to the analysis include differential pressure, temperature gradients, and fast flux.

4.2 Fuel System Design

The NuScale Power, LLC fuel system is designed to satisfy the following criteria:

- The fuel system will not be damaged as a result of normal operation and anticipated operational occurrences (AOOs) [General Design Criterion (GDC) 10].
- Fuel damage during postulated accidents will not be severe enough to prevent control rod insertion when it is required [Principal Design Criteria (PDC) 27].
- Core coolability is always maintained, even after postulated accidents (PDC 35 and 10 CFR 50.34).
- The number of fuel rod failures is not underestimated for postulated accidents (10 CFR 100).

The NuScale fuel assembly design features are similar to those of existing pressurized water reactor (PWR) 17x17 fuel assemblies. The only significant difference between the NuScale fuel design and other PWRs is the shorter fuel assembly length. The effect of the length on fuel design analyses is tested in full-scale fuel assembly tests and analyzed using NRC-approved methods. The results summarized in this section show that the NuScale fuel design, with its shorter length, demonstrates acceptable fuel performance consistent with the other proven features that make up the NuScale fuel design. Because this is a new application of a proven fuel design, post-irradiation inspection will be performed during the initial three cycles of operation of the first licensed module, as described in Section 4.2.4.6.

Section 4.2.1 presents the design bases for the cladding, fuel material, fuel rod performance, spacer grids, fuel assembly structural design, control rod assembly (CRA), and the surveillance programs that will confirm the adequacy of the design. Section 4.2.2 provides a detailed description of the fuel, the components that comprise the fuel assembly, and the CRA. Section 4.2.3 provides the detailed design evaluation that demonstrates how the design bases are met. Section 4.2.4 discusses fuel and CRA testing and inspection.

The fuel system design evaluations include a fuel rod cladding fatigue analysis that considers power maneuvering in Table 4-3 of Reference 4.2-1. Additional analysis will be performed as part of the detailed design of the cycle-specific core using the methodologies described in Technical Specification 5.6.3. This analysis will include the effects of power maneuvers on CRA absorber depletion, fission gas release, fuel melt limits, transient strain limits, fuel rod components (other than cladding), and guide tube and CRA wear.

COL Item 4.2-1: A COL applicant that references the NuScale Power Plant design certification and wishes to utilize non-baseload operations will provide justification for the fuel performance codes and methods corresponding to the desired operation.

4.2.1 Design Bases

The fuel rod and fuel assembly design bases establish the performance requirements and damage criteria to satisfy the criteria in Section 4.2 of the NUREG-0800 Standard Review Plan.

The fuel assembly structural integrity is assured by setting limits on stresses and deformations due to various loads and by preventing the assembly structure from interfering with the functioning of other components. Three types of loads are considered:

- non-operational loads, such as those due to shipping and handling
- normal loads during normal operation and AOOs
- abnormal loads during infrequent events and postulated accidents

The following are discussed:

- Cladding
- Fuel Material
- Fuel Performance
- Spacer Grids
- Fuel Assembly Structure
- Control Rod Assembly
- Surveillance Programs

4.2.1.1 Cladding

The fuel rod cladding is an advanced zirconium alloy called M5® that was approved for use in the "Evaluation of Advanced Cladding and Structural Material (M5®) in PWR Reactor Fuel" report (Reference 4.2-2). The applicability of this topical report to the NuScale fuel design is described in the "Applicability of AREVA Fuel Methodology for NuScale Design" topical report (Reference 4.2-3).

4.2.1.1.1 Mechanical Properties

The fuel rod cladding properties are defined in Reference 4.2-2.

4.2.1.1.2 Stress-Strain Limits

The methodology and design criteria for analyzing cladding stress are provided in Reference 4.2-2.

The cladding stress analysis follows the guidelines of Section III of the American Society of Mechanical Engineers (ASME) Boiler and Pressure Vessel Code (BPVC), which provides guidance for establishing stress intensity limits. The stress states modeled for the M5® cladding are maximum compression and maximum tension. To determine the stress limits for M5® cladding applications, the design criteria for fuel rod cladding stresses are based on unirradiated yield strength, as approved in Reference 4.2-2. The use of unirradiated values is conservative because irradiation increases the yield and ultimate tensile strengths for M5® and other zirconium alloys.

A cladding buckling analysis determines that the cladding does not buckle when the rod internal pressure is at a minimum, and the system pressure is at a

maximum. The method and equations used for the buckling analysis are presented in Reference 4.2-2.

For cladding strain, the maximum uniform hoop strain (elastic plus plastic) in the cladding does not exceed one percent. This cladding strain criterion has been approved in Reference 4.2-2.

4.2.1.1.3 Fatigue and Vibration

The effect of cyclical loadings on the clad is determined by calculating the clad cumulative fatigue usage factor and ensuring it does not exceed 0.9. The analysis method is consistent with the procedure for fatigue analysis provided in Section III of the ASME BPVC.

The design criterion for fretting is that wear at the fuel rod and grid contact points is limited and precludes fuel failure. Fretting of the clad surface can occur due to flow-induced vibration (FIV) between the fuel rods and fuel assembly grid springs. Forces between the fuel rods and fuel grid springs vary during the fuel life due to clad diameter creep-down combined with grid spring relaxation. Life and Wear testing as described in Section 4.2.3.5.7 demonstrates acceptable grid-to-rod fretting wear performance.

4.2.1.1.4 Chemical Properties

Chemical properties of the cladding are discussed in Reference 4.2-2.

Maintaining the oxide thickness on the cladding within a prescribed limit precludes external hydriding as a cladding failure mechanism. The external cladding oxide thickness limit is established in Reference 4.2-2.

4.2.1.2 Fuel Material

4.2.1.2.1 Thermal-Physical Properties

The thermal-physical properties of the fuel presented in the COPERNIC Code topical report (Reference 4.2-4) are applicable to the NuScale design as demonstrated in Reference 4.2-3.

4.2.1.2.2 Fuel Densification and Fission Product Swelling

Fuel densification and swelling are modeled using the methodology in Reference 4.2-4. The COPERNIC code evaluates cladding strain, fuel temperature, and rod internal pressure using the fuel densification model and the swelling model. The applicability of the COPERNIC code and its thermal models to the NuScale fuel design is demonstrated in Reference 4.2-3.

4.2.1.2.3 Fuel Pellet Chemical Properties

Fuel pellet chemical properties are controlled through a rigorous testing and inspection program to demonstrate that each lot of pellets conforms to design requirements and criteria as described in Section 4.2.4.3.

4.2.1.3 Fuel Rod Performance

The basic fuel rod models and the ability to predict fuel rod operating characteristics are described in Reference 4.2-4. The COPERNIC computer code is used to perform the thermal-mechanical analyses to simulate the behavior of the fuel rod during irradiation, and is also used to verify that the fuel rod design meets design and safety criteria. The critical design bases addressed with COPERNIC include fuel rod internal pressure, cladding temperatures, cladding strain, corrosion, and centerline fuel melt under conditions of normal operation, AOOs, and postulated accidents. Reference 4.2-1 provides additional details concerning the design basis for normal operations and AOOs.

Section 4.4 addresses critical heat flux design criteria. Section 15.4 addresses reactivity-initiated accidents, reactivity insertion accidents, and fuel centerline temperatures. Creep collapse is analyzed with the methods and codes described in Reference 4.2-8. The applicability of Reference 4.2-8 to the NuScale fuel design is justified in Reference 4.2-3.

4.2.1.4 Spacer Grids

The spacer grids are designed to maintain the fuel rods in a coolable configuration (PDC 35 and 10 CFR 50.34), and ensure CRA insertion for AOOs and postulated accidents (PDC 27).

Structural evaluations of the grids determine that the grid strength is sufficient to maintain a coolable geometry and ensure control rod insertion for all resulting impact loads. The evaluation methodology (Reference 4.2-5) uses the load limits that are derived from testing, which are provided in Reference 4.2-1 for the fuel assembly mechanical design.

4.2.1.4.1 Mechanical, Chemical, Thermal, and Irradiation Properties of Grids

The strength criteria of the fuel assembly grid components are based on mechanical strength testing of prototypes, including static and dynamic crush testing.

The design limits are detailed in Reference 4.2-1. The grids are tested to establish a 95 percent confidence level of the mean allowable crushing stress limit for both the unirradiated and a simulated irradiated condition. These limits are sufficient to demonstrate that, under worst-case combined seismic and loss-of-coolant accident (LOCA) events, the fuel assemblies will remain in a coolable geometry (PDC 35 and 10 CFR 50.34) and CRA insertability (PDC 27) is maintained. These criteria are met by showing that the spacer grids experience no significant plastic

deformation exceeding the limit in Reference 4.2-5 as a result of the combined events.

The allowable grid clamping loads during fuel shipment are based on static crush strength testing for static stiffness and elastic load limits. The spacer grids maintain their structural integrity under the maximum lateral shipping loads and the maximum clamping loads. The spacer grid springs are designed to maintain acceptable fuel rod grip forces from the limiting 6 g lateral (transverse) and 4 g axial (longitudinal) shipping loads.

Spacer grid slip load input to the analytical models of the fuel assembly used in the horizontal and vertical faulted analyses are established by mechanical testing.

4.2.1.4.2 Vibration and Fatigue of Grids

The interface between the fuel rods and the spacer grids is maintained throughout the life of the fuel assembly and prevents fuel rod fretting failure. Full-scale fuel assembly testing and a grid-to-rod fretting evaluation detailed in Reference 4.2-1 show that fuel rod cladding wear is expected to be acceptable (see Section 4.2.1.1.3). The grid-to-rod fretting evaluation is performed in accordance with NRC approved methods.

4.2.1.4.3 Chemical Compatibility of Grids with other Core Components

The Zircaloy-4 and Alloy 718 materials of the spacer grids are compatible with the reactor coolant based on extensive operating experience in US PWRs.

4.2.1.5 Fuel Assembly Structural Design

The design bases for evaluating the structural integrity of the fuel assemblies is established by setting design limits on stresses and deformations due to various non-operational, operational, and abnormal loads.

The thermal-hydraulic design basis is presented in Section 4.4.

4.2.1.5.1 Non-Operational Loads

The non-operational load limit is 4 g axial (longitudinal) and 6 g lateral (transverse) with dimensional stability.

4.2.1.5.2 Normal Operating Conditions and Anticipated Operational Occurrences

For AOOs, the fuel assembly component structural design criteria are established for the two primary material categories, austenitic steels and zirconium alloys. The stress categories and strength theory presented in Section III of the ASME BPVC are used as a general guide. The maximum shear theory (Tresca criterion) for combined stresses is used to determine the stress intensities for the austenitic steel components. The stress intensity is defined as the largest numerical difference between the various principal stresses in a three-dimensional field. The design

stress intensity value, S_m, for austenitic steels and zirconium alloys is given by the lowest of the following:

- one-third of the specified minimum tensile strength or two-thirds of the specified minimum yield strength at room temperature
- one-third of the tensile strength or 90 percent of the yield strength at operating temperature, but not to exceed two-thirds of the specified minimum yield strength at room temperature

The stress limits for the austenitic steel components are given below using nomenclature that follows the ASME BPVC, Section III.

- general primary membrane stress intensity limit is S_m
- primary membrane plus bending stress intensity limit is 1.5 S_m
- total primary plus secondary stress intensity limit is 3.0 S_m

The zirconium components, which consist of the Zircaloy-4 guide tube and M5® fuel rod cladding, are divided into two categories because of material differences and functional requirements:

- The fuel rod cladding design criteria are addressed in Section 4.2.1.1.
- The maximum shear theory is used to evaluate the guide tube design. For conservatism, the unirradiated properties are used to define the stress limits.

4.2.1.5.3 Infrequent Events and Postulated Accidents

Seismic loadings typically produce the worst-case faulted loads. For the NuScale Power Plant design, primary system pipe breaks do not result in significant hydraulic loads on the fuel assembly. The design criteria for this category of loadings are as follows:

- Deflections or failures of components cannot interfere with the capability to insert the CRA or emergency cooling of the fuel rods.
- The fuel assembly structural component stresses under abnormal conditions are evaluated primarily using the methods outlined in Reference 4.2-5.

For austenitic steel fuel assembly components, the stress intensity is defined per the rules described above for normal operating conditions. The faulted condition stress limits for fuel assembly structural components are:

- General primary membrane stress intensity limit is the smaller of 2.4 S_m or 0.70 S_u, ultimate strength.
- Primary membrane plus bending stress intensity limit is the smaller of 3.6 S_m or 1.05 S_u.

Due to the requirement to maintain a path for CRA insertion, the guide tube stresses in the faulted condition are evaluated using the Level C criteria in

Subsection NG of the ASME BPVC. For guide tubes, the faulted condition stress intensity limits are:

- The stress intensity limit for the general primary membrane is S_y, yield strength.
- The stress intensity limit for the primary membrane plus bending is 1.5 S_y.
- The axial loads of the guide tubes are limited by buckling limits.

For fuel rod cladding, the faulted condition stress allowables are set based on the provisions in Reference 4.2-2.

4.2.1.5.4 Growth Allowance

A fuel assembly nozzle-to-fuel rod shoulder gap allowance is provided to maintain positive clearance between the fuel rods and the nozzles during the entire fuel assembly lifetime.

A fuel assembly-to-reactor internals gap allowance is provided to maintain a positive core plate gap during the entire fuel assembly lifetime.

4.2.1.5.5 Fuel Assembly Liftoff

The fuel assembly does not unseat or lift off during worst case hydraulic loads during normal operation and AOOs.

4.2.1.5.6 Guide Tube Buckling

Guide tube evaluations demonstrate that buckling does not occur. In addition, the primary and primary-plus-secondary stresses are confirmed to be lower than the material allowable stresses in the ASME BPVC.

4.2.1.5.7 Interface with Adjacent Assemblies

Axial alignment of the spacer grids on adjacent fuel assemblies is maintained for the life of the fuel assembly.

4.2.1.5.8 Fuel Rod Fretting and Wear

As discussed in Section 4.2.1.1.3, the fuel assembly is designed to provide the support needed to limit fuel rod vibration and fretting wear. In addition, core analysis shows that crossflow between assemblies is minimal due to the low axial flow, and testing has shown resistance of the fuel assembly to fretting wear.

4.2.1.5.9 Fuel Rod Bow

Fuel rod bowing is evaluated with respect to the mechanical and thermal-hydraulic performance of the fuel assembly (Reference 4.2-6). The fuel assembly design precludes excessive rod bow during its operational lifetime.

4.2.1.5.10 Control Rod Drop Times

The fuel assembly does not experience any permanent deformations during AOOs that would cause the CRA drop time to increase beyond the drop time used in Chapter 15. This criterion is met by demonstrating the fuel assembly guide tube stresses remain below the limits defined in Section 4.2.1.5.2.

4.2.1.5.11 Loss-of-Coolant Accident and Seismic Loading

The fuel assembly is designed to remain operable during and after an operating basis earthquake (OBE) and to maintain structural integrity, a coolable geometry, and CRA insertion capability during and after a safe shutdown earthquake (SSE) and LOCA.

4.2.1.5.12 Shipping and Handling Loads

The fuel assembly is designed for the maximum loads occurring during shipping and handling, as presented in Reference 4.2-1. The fuel rods do not slip through the spacer grids under the maximum axial shipping loads.

4.2.1.5.13 Material Compatibility

Table 4.2-2 provides a list of fuel assembly components and their materials. The selection of fuel assembly materials is based on extensive operating experience and their compatibility with the service environment and with each other. Each material has been optimized for resistance to adverse changes in material properties from irradiation, and has been evaluated for strength and mechanical properties for the operating temperatures and for the full service life anticipated for each component.

Each material is based on an industry standard and is modified according to specific engineering requirements, such as lowering the cobalt content in stainless steel and nickel-based alloy components, without changing their material performance, in order to reduce activation levels.

4.2.1.5.14 Corrosion

The fuel assembly structural design evaluation considers the effects of thinning from corrosion and the effects of oxide layer formation. Guide tube material corrosion allowances are established from operating experience, design verification testing, and similarities with existing designs. The corrosion allowances for fuel assembly components are presented in Reference 4.2-1.

4.2.1.6 Control Rod Assembly and Burnable Poison Rods

To ensure efficient performance and safe shutdown of the reactor, CRAs are designed such that:

- No significant wear in the control rod cladding occurs during the CRA 20 effective full power year lifetime.

- Insertion of the CRA is not interrupted by misalignment of the CRA guide tubes during normal operation.
- The CRA can be inserted into the fuel assembly during the design basis earthquake that imparts the limiting design load on the fuel assembly, CRA and core internals restraining the CRAs.

Maintaining CRA insertability with respect to the fuel assembly is discussed in Section 4.2.3.5 for both normal operating and faulted conditions, as the fuel assembly is shown to maintain a path for CRA insertion under these conditions. The CRAs are shown to be acceptable given the stresses imparted by the maximum misalignment of the fuel assembly and CRA during a design basis earthquake in which the CRAs are at least partially inserted into the fuel assembly guide tubes.

In addition, the CRAs are designed to ensure that:

- Internal pressure is within limits during normal operation.
- Cladding stresses are within limits during normal, transient, and accident conditions.
- The absorber material is stable considering both thermal expansion and irradiation.
- There is no potential for waterlogging rupture.

There are no discrete burnable poison rods in the fuel design. Burnable poison is integral to some portions of the fuel as discussed in Section 4.2.2.7.

The neutron sources are designed to meet mechanical strength requirements at both ambient and elevated temperatures, to be compatible with the materials and reactor coolant, and to be resistant to radiation degradation. Neutron sources are discussed in Section 4.2.2.9.

4.2.1.7 Surveillance Program

The fuel system surveillance program verifies the adequacy of the fuel design. This program subjects fuel rods and fuel assemblies to post-irradiation examinations that generally include measuring cladding oxide thickness, fuel rod diameter, fuel rod length, fuel rod bowing, fuel rod-to-nozzle shoulder gap, fuel assembly bow and twist, and overall fuel assembly length. The overall fuel rod and assembly conditions are also visually examined during post-irradiation examinations for indications of mechanical damage or abnormalities.

The CRA surveillance program monitors control rod integrity. Visual inspections are performed to determine the presence and extent of cladding wear from interactions with reactor vessel internals and fuel assembly guide tubes. Verification of the cladding integrity also includes monitoring for the absence of excessive cladding strain and potential cracking from silver-indium-cadmium (AIC) absorber swelling. The CRA rod drop time testing is performed prior to and during reactor operation.

Section 4.2.4 discusses the testing and fuel surveillance program that is implemented to ensure the adequacy of the fuel performance and satisfy the design bases. Fuel

surveillance and testing results, as they become available, are used to improve fuel design and manufacturing processes and to confirm that the design bases and safety criteria are satisfied.

4.2.2 Description and Design Drawings

A summary of the fuel assembly and CRA design is provided in Table 4.2-1 through Table 4.2-3 and in Figure 4.2-1 through Figure 4.2-13. Additional details of the fuel assembly and CRA design are provided in Reference 4.2-1.

4.2.2.1 Fuel Assembly Description

The fuel assembly is a 17x17 array of fuel rods that has been designed specifically for use with the core configuration of the NuScale reactor. The main fuel assembly parameters are listed in Table 4.2-1 and the fuel assembly and fuel rods are illustrated in Figure 4.2-1.

The fuel assembly uses five spacer grids, 24 guide tubes, and a top and bottom nozzle, to provide the structural support for the 264 fuel rods. The fuel assembly also includes a central instrument tube in each fuel assembly. The bottom grid is constructed of Alloy 718 strip material and uses the AREVA HMP™ design, while the remaining four HTP™ grids are constructed from Zircaloy-4 strip material. The HMP™ and HTP™ grids provide lateral support for the fuel rods.

Each fuel assembly can be placed in any core location. Proper orientation of the fuel assembly in the core is established by a hole in one corner of the top nozzle which ensures proper interface with the refueling machine via a mating pin on the refueling machine grapple. The refueling machine then provides the correct orientation of the fuel assembly in storage, during refueling transport, and in the reactor core operating position.

4.2.2.2 Spacer Grids Description

The fuel assembly uses HTP™ spacer grids at the intermediate and top spacer locations and an HMP™ spacer grid at the bottom location of the assembly. The HTP™ grids are constructed of Zircaloy-4 alloy strips. The HMP™ grid is constructed of Alloy 718 strips for enhanced strength and low cell relaxation during irradiation.

Each HTP™ grid is a structure of interlocking strips that are welded together at each strip intersection to form a 17 x 17 matrix of square cells (Figure 4.2-7). Each cross-strip is formed by resistance spot welding two stamped halves to form a doublet. The assembled doublet contains channels, slanted at the outlets, which induce a swirling pattern in the coolant flow, as illustrated in Figure 4.2-8. The channels are arranged so that there is no net hydraulic torque on the fuel assembly. These channels also provide the contact surfaces that hold the fuel rods in place. Sideplates are welded to the ends of the doublets and have top and bottom lead-in tabs to avoid assembly hang-up during fuel movement.

The HMP™ grid (see Figure 4.2-9) is constructed of low cobalt, precipitation-hardened Alloy 718 strip material. Resilient spring features are stamped into the strips that

provide frictional axial restraint of each interfacing fuel rod by an interference fit of the fuel rods within each grid cell. Spring and friction contact with each fuel rod is maintained throughout the life of the fuel assembly up to the design burnup. Each HMP™ spacer grid maintains eight individual line contacts per cell with each fuel rod (similar to the HTP™ spacer) and relaxation of the spring within each cell due to irradiation is minimized by the low relaxation properties of Alloy 718 material.

The HMP™ spacer grid is similar to HTP™ spacer grids, except for the material of construction and the flow channels created by the doublet are straight in the HMP™ spacer grid, and do not produce swirling flow around the fuel rods.

To maintain axial alignment of spacer grids with adjacent fuel assemblies, all of the HTP™ grids are spot-welded to the guide tubes. Short Zircaloy-4 sleeves are spot-welded to the guide tube at locations above and below the HMP™ grid to fix its axial position.

4.2.2.3 Quick Disconnect Mechanism Description

A quick disconnect (QD) mechanism attaches the top nozzle to the guide tubes (see Figure 4.2-4 and Figure 4.2-5). The QD design allows the top nozzle to be removed for fuel assembly reconstitution without loose parts. The design consists of a double-spline sleeve made of Zircaloy-4 attached to the guide tube via multiple spot-welds. Machined keyway-type features within the guide tube attachment holes in the top nozzle provide either clearance for removal or restraint for securing the nozzle, based on the radial orientation of the guide tube assembly QD features.

The reconstitution tooling rotates the guide tube QD ring 90° to lock or unlock the guide tube connection and provides a rigid connection when the ring is rotated to its locking position.

4.2.2.4 Top Nozzle Assembly Description

The top nozzle structure (see Figure 4.2-2) consists of a stainless steel frame that interfaces with the reactor upper internals and the core components while providing for coolant flow. The top nozzle flow-hole pattern provides low pressure drop while satisfying strength requirements. The top nozzle design also incorporates a QD feature to attach to the 24 fuel assembly guide tubes, as presented in Section 4.2.2.3. The top nozzle assembly includes four sets of two-leaf hold-down springs.

The leaf springs are made of Alloy 718. The spring system maintains positive fuel assembly contact with the upper core plate under normal operating conditions and AOOs and also minimizes fuel assembly liftoff during seismic events to reduce fuel assembly dynamic stresses. The leaf spring sets are fastened to the top nozzle with Alloy 718 clamp screws. The upper leaf has an extended tang that engages a cutout in the top plate of the nozzle. This arrangement maintains spring leaf retention in the unlikely event of a single leaf spring or clamp screw failure.

4.2.2.5 Bottom Nozzle Description

The NuScale fuel assembly uses a debris-resistant bottom nozzle that includes a filter plate (see Figure 4.2-3). The nozzle frame is constructed of stainless steel, has a frame of deep ribs connecting the guide tube attachment bushings, and has a lower frame and legs with radii that interface with the reactor internals. The frame distributes the primary loads on the fuel assembly through the bottom nozzle. A high strength A-286 alloy filter plate is pinned to the top of the frame. During assembly, the guide tube lower end plugs and shoulder screws clamp the filter plate to the frame (See Figure 4.2-6).

The guide tube lower end plugs are threaded to rigidly connect the guide tubes to the bottom nozzle with cap screws.

4.2.2.6 Guide Tube Description

MONOBLOC™ guide tubes are fabricated from Zircaloy-4 alloy. Each MONOBLOC™ guide tube (see Figure 4.2-4) has two inside diameters (IDs) and a single outside diameter (OD). The larger ID at the top provides a relatively large annular clearance that permits rapid insertion of the CRA during a reactor trip and also accommodates coolant flow during normal operation with inserted CRAs. The reduced ID section (i.e., the dashpot located at the bottom end of the tube) provides a close fit with the control rods to facilitate deceleration toward the end of the control rod travel. This deceleration limits the magnitude of the CRA impact loads on the fuel assembly top nozzle. The guide tube wall thickness at the bottom is greater in the dashpot region than at the upper end to maintain the same OD with the smaller dashpot ID. The MONOBLOC™ design provides a rigid tube and robust guide tube structure that helps to minimize fuel assembly distortion and bow.

Four small holes in the guide tube located just above the dashpot allow both outflow of water during CRA insertion, and coolant flow to the control components during operation. There is also a small flow hole in the guide tube cap screw that enables some coolant flow through the reduced diameter section and drainage of the guide tube, as well as displaced coolant venting during CRA deceleration.

The QD sleeve (Figure 4.2-5) is attached to the upper end of the guide tube and connects to the top nozzle. A stainless steel cap screw threads into a threaded Zircaloy-4 lower end fitting that is welded to the bottom end of each guide tube. The filter plate and bottom nozzle frame are captured and compressed by the fastener to form the joint (see Figure 4.2-6).

4.2.2.7 Fuel Rod Description

The NuScale fuel rod design consists of uranium dioxide (UO_2) pellets contained in seamless M5® zirconium alloy tubing, with end caps welded at each end (see Figure 4.2-10). The use of M5® material is approved in Reference 4.2-2. Compared to earlier zirconium alloys, M5® cladding significantly increases the resistance to corrosion. The fuel rod length and void volume provide acceptable margin against failure by internal pressure buildup. The fuel rod uses one stainless steel spring in the

upper plenum to prevent the formation of fuel pellet stack gaps during shipping and handling, while also allowing for the expansion of the fuel stack during operation. The fuel stack rests on a lower end cap.

The lower end cap has a bullet-nose shape to provide a smooth flow transition in addition to facilitating insertion of the rods into the spacer grids during assembly. The upper end cap has a grippable feature that allows removal of the fuel rods from the fuel assembly if necessary.

The cylindrical fuel pellets are a sintered, high-density ceramic with a dish at each end. The edges of the pellets have chamfers that ease the loading of the pellets into the rod, and the dish and chamfer help reduce the tendency for the pellets to assume an hourglass shape during operation.

The fuel rod design can also utilize axial blanket and gadolinia fuel configurations. The geometry and design of gadolinia fuel rods is identical to the UO_2 fuel rod design. The only variations are in the composition of the fuel stack.

The fuel rods contain a central axial zone of enriched UO_2 pellets or UO_2 plus Gd_2O_3 pellets and axial blanket zones at each end of the stack. The axial blanket region consists of sintered UO_2 pellets with a lower ^{235}U enrichment. The gadolinia serves as a burnable poison to control power peaking or core reactivity.

Table 4.2-1 provides a summary of the major fuel rod design parameters.

4.2.2.8 Control Rod Assembly Description

Each NuScale CRA consists of a group of 24 individual control rods fastened to a spider assembly (see Figure 4.2-11). The individual rods (see Figure 4.2-13) contain B_4C pellets in the upper portion of the rod, and silver-indium-cadmium (AIC) absorber in the tip of the rod. This hybrid configuration of AIC and B_4C is commonly used in commercial PWRs, and is adapted to the NuScale design to reduce the total weight of the CRA. Unlike the AIC material, the B_4C can produce helium gas under neutron fluence leading to the potential buildup of gas pressure in the rod. Thus, the use of B_4C is restricted to the low flux region at the top of the rod where helium production is minimal, and the AIC material is used in the high flux region. The rod internals are sealed within a 304 stainless steel cladding tube to protect the absorber from the coolant. The tube is plugged and welded at each end.

The top ends of the control rods are fastened to a spider using a threaded and pinned joint. The upper end plug is designed with a flex joint which provides the ability to accommodate misalignment between the control rods and the fuel assembly.

The CRA spider (Figure 4.2-12) is a one-piece, stainless steel cast array of vanes on a hub. A spring is located in the lower part of the hub to absorb the kinetic energy of the CRA and driveline following a reactor trip. The spring is preloaded and maintained within the hub by a retaining ring and tension bolt. The CRA is coupled to the control

rod driveline through the coupling section which is machined within a cavity in the top of the hub.

The lower portion of the control rod contains a stack support that resides within a central hole in the AIC. The stack support is comprised of a support column that passes through the AIC central hole and a support platform, upon which the solid portion of the AIC rests (Figure 4.2-13, Item 8). The purpose of the stack support is to prevent the weight of the B_4C column and the plenum spring preload from compressing the lower AIC, which is susceptible to deformation through creep mechanisms at elevated temperatures. By eliminating the axial load acting on the AIC, the stack support reduces the creep mechanism of the lower absorber and thereby reduces cladding strain.

During a refueling outage or after a reactor trip, the spring retainer rests on the fuel assembly top nozzle.

Table 4.2-3 provides the critical nominal design parameters for the CRA, spider, and individual control rods.

4.2.2.9 Stationary Component Assemblies Description

The NuScale design includes primary and secondary sources. The purpose is to provide a minimum detectable neutron flux level at the source range detectors for the initial core and to allow monitoring the change in core multiplication factor during fuel loading and approach to criticality. The primary sources are used in the initial, and possibly second, operating cycle. The secondary sources are used as the controlled neutron source for subsequent cycles.

Primary source material is Californium (Cf-252) and the secondary source material is comprised of antimony and beryllium. The source material is contained in individual stainless steel rods that are connected to a spider hub similar to the CRA. The rods containing the source material are hermetically sealed. The neutron source assemblies are located in diametrically-opposed core positions near the core periphery as close as possible to the ex-core detectors. The neutron source assemblies are statically installed in fuel assembly locations not occupied by a CRA.

The NuScale design does not include the use of thimble plugs. As discussed previously, discrete burnable poison rods are not part of the NuScale design.

4.2.3 Design Evaluation

The fuel rods, fuel assemblies, and control components conform to the guidance of the NUREG-0800 Standard Review Plan 4.2.

Analyses are performed to consider rod operating history, model uncertainties, and dimensional variations. To verify adherence to the design criteria, the evaluation also considers the effects of power transients. The performance of the fuel during AOOs and postulated accidents is presented in Chapter 15 (GDC 10). NuScale addresses anticipated transients without scram in Chapter 15 also.

4.2.3.1 Cladding Evaluation

4.2.3.1.1 Vibration and Wear

Because of the low fuel assembly axial flow and low cross-flow between assemblies, there is little flow energy available to cause vibration in the fuel rods. The grids provide sufficient fuel rod support to prevent significant wear of the clad during the life of the fuel assembly based on operating experience, design analyses, and testing as shown in Reference 4.2-1.

A bending stress is induced in the cladding when coolant flow causes the rod to vibrate against the spacer grids. This FIV bending stress is taken into account in the cladding stress analysis of Section 4.2.3.1.2.

A life and wear test was performed on the NuScale fuel assembly design. The life and wear results, as well as the PWR operating experience of HMP™ and HTP™ grids with M5® clad fuel rods, show that the NuScale fuel design has significant margin to fretting failure for the expected operating conditions (See Reference 4.2-1). See Section 4.2.3.5.7 for additional discussion on the fretting evaluation.

Based on these evaluations as summarized in Reference 4.2-1, the NuScale fuel is not expected to experience flow induced vibration or wear issues.

4.2.3.1.2 Fuel Rod Internal Pressure and Cladding Stresses

The following types of stresses are considered in the cladding stress analysis:

- pressure stresses - membrane stresses from external and internal pressures acting on the fuel rod cladding
- FIV - longitudinal bending stresses from vibration of the fuel rod caused by coolant flow around the rod
- ovality - bending stresses from external and internal pressure on the fuel rod cladding that is oval. This stress does not include the stress resulting from creep ovalization into an axial gap.
- thermal stresses - secondary stresses that arise from the temperature gradient across the fuel rod during reactor operation
- differential growth stresses - localized stresses resulting from the fuel rod slipping through the spacer grids. The slip loads can be caused by differences in the fuel assembly and fuel rod axial expansion rates due to heat-up or irradiation.
- fuel rod to spacer grid interaction - secondary stresses from contact between the fuel rod cladding and the spacer grid
- plenum spring force stress - primary membrane stress; the axial stress is load dependent.

A burnup-dependent fission gas release model in Reference 4.2-2 is used in determining the internal gas pressure as a function of irradiation time.

The classifications of the stresses are as follows:

- pressure stresses - P_m, general primary membrane
- ovality stresses - P_b, primary bending
- fuel rod to spacer grid interaction - Pl, local primary membrane
- FIV - P_b, primary bending
- thermal stresses - Q, secondary
- differential growth - Q, secondary
- plenum spring force - P_m, general primary membrane

The fuel rod cladding is analyzed for the stresses induced during operation using the approved methodology in Reference 4.2-2. Conservative values are used for cladding thickness, oxide layer buildup, external pressure, internal fuel rod pressure, differential temperature, and unirradiated cladding yield strength in accordance with the approved methodology. The fuel rod stress analysis calculates the worst-case cladding stress state based on the thinnest cladding wall and largest cladding ovality allowed by the design. The likelihood of these two conditions occurring at the same location on the cladding is remote; therefore, the consideration of these two conditions together to calculate the cladding stress state is conservative. The analyses of the fuel rod cladding stresses demonstrate positive margins for all operating conditions. The cladding stress safety margins are presented in Reference 4.2-1.

Analysis shows that fuel rod cladding buckling does not occur. Two critical buckling limits, P_{cr} and q_{yp}, are calculated. Buckling limit q_{yp} is the bifurcation buckling pressure of a perfectly circular shell and is calculated to check the elastic stability of the cladding. P_{cr} is the critical load at which buckling occurs. The maximum differential pressure is less than the buckling pressure and the maximum compressive load on the fuel rod is less than the buckling critical load, thereby proving that the cladding will not buckle.

Analysis in Reference 4.2-1 also shows that the maximum internal pressure of the fuel rod over its designated lifetime will not exceed the reactor coolant system pressure. This criterion assures that there is no cladding liftoff or reorientation of hydrides in the radial direction of the cladding.

4.2.3.1.3 Material and Chemical Evaluation

Using the methodology in Reference 4.2-4, the maximum oxide thickness is predicted to be much less than the limit established in Reference 4.2-4. Bounding power histories are used in predicting the oxide thickness. The maximum predicted oxide thickness is provided in Reference 4.2-1.

The absorption of hydrogen on the inside of the cladding is minimized by tight controls on the moisture and hydrogen impurities in the rod during fabrication. The specific moisture and hydrogen content limits are provided in Reference 4.2-1.

4.2.3.1.4 Fretting and Crevice Corrosion

As described in Section 4.2.3.1.1, fretting due to FIV is not expected due to the low axial flow rates during normal operation natural circulation conditions.

PWR operating experience has shown that crevice corrosion is not a likely corrosion mechanism for zirconium alloy cladding material. In general, zirconium alloys are resistant to crevice corrosion. In addition, NuScale coolant chemistry specifications impose tight controls for dissolved oxygen and chlorides, the contaminants that are often associated with crevice attack. See Section 5.2 for the limits on oxygen and chlorides.

4.2.3.1.5 Stress-Accelerated Corrosion

Stress corrosion cracking is addressed for M5® in Reference 4.2-2. M5® cladding improves resistance to stress-accelerated corrosion relative to Zr-4 cladding.

4.2.3.1.6 Cycling and Fatigue

The fuel rod cladding is analyzed for the total fatigue usage factor using the methodology approved in Reference 4.2-2 and the procedure outlined in the ASME BPVC. Testing has determined the fatigue performance of M5® cladding. These tests have shown similar fatigue endurance performance for recrystallized cladding (including M5®) as compared to Zircaloy-4, with the lower yield strength of the recrystallized claddings limiting the applied stresses. A fuel rod life of ten years and a vessel life of 60 years are assumed. The fuel rod cladding will, therefore, experience approximately 16 percent (10/60) of the number of transient cycles the reactor pressure vessel will experience.

The expected normal operating, upset, and test transients are evaluated to determine the total fatigue usage factor experienced by the fuel rod cladding. In accordance with the ASME BPVC, faulted conditions are not included in the fatigue evaluation. Conservative inputs in terms of cladding thickness, oxide layer buildup, external pressure, fuel rod internal pressure, and differential temperature across the cladding were assumed. The results of the fatigue analysis (Reference 4.2-1) for the NuScale fuel rod show that the cumulative fatigue usage factor is well below the allowable limit of 0.9.

4.2.3.1.7 Material Wastage Attributable to Mass Transfer

An oxide thickness limit is established in Reference 4.2-2, and the predicted corrosion is significantly lower than the limit as discussed in Reference 4.2-1.

4.2.3.1.8 Rod Bowing Attributable to Thermal, Irradiation, and Creep Dimensional Changes

Rod bowing is addressed in Reference 4.2-6. This methodology is demonstrated to be applicable to the NuScale fuel in Reference 4.2-3.

4.2.3.1.9 Consequences of Power-Coolant Mismatch

The consequences of power-coolant mismatch are addressed in Section 4.4.

4.2.3.1.10 Irradiation Stability of the Cladding

Considerable operating experience using M5® cladding has proven its irradiation stability. The effects of irradiation on the mechanical integrity of the cladding has been accounted for using the approved COPERNIC model (Reference 4.2-4) for performing the mechanical and thermal analyses, and the effects are shown to be acceptable for the currently approved burnup limit of 62 GWd/MTU established in Reference 4.2-4.

4.2.3.1.11 Creep Collapse and Creepdown

Reference 4.2-2 includes an analysis of creep to evaluate the resistance of the NuScale fuel rod cladding to creep collapse. Inputs to the analysis include differential pressure, temperature gradients, and fast neutron flux.

The following conservatisms are used in determining creep collapse over the life of the fuel rod:

- minimum fuel rod pre-pressure
- no fission gas release
- worst-case or enveloping power history
- worst-case cladding dimensions (including ovality)

Fuel rod creep collapse is determined when either of the following is predicted to occur:

- The rate of creep ovalization exceeds 0.1 mil/hr.
- The maximum fiber stress exceeds the unirradiated yield strength of the cladding.

Using the methodology described above, the fuel rod creep collapse lifetime is greater than the maximum design burnup defined in Reference 4.2-2.

4.2.3.1.12 Cladding Strain

The cladding strain evaluation is discussed in Reference 4.2-1. The calculated linear heat rate for transients that induce one percent cladding strain does not limit the plant operation and is much greater than the maximum transient the fuel rod is expected to experience.

4.2.3.1.13 Pellet-Cladding Interaction

The criterion for transient-induced cladding strain discussed in Section 4.2.1.1.2 also precludes Pellet-Clad Mechanical Interaction (PCMI). The criterion is much greater than the maximum transient the fuel rod is expected to experience. This

method has been previously approved in the "COPERNIC Fuel Rod Design Computer Code" topical report (Reference 4.2-4). The applicability of this topical to the NuScale design is established in Reference 4.2-3.

As discussed in Section 4.2.3.2.3, fuel melting does not occur during normal operation or AOOs. Fuel melting results in a large volume increase which may cause a pellet with a molten center to exert a stress on the cladding. The no centerline melt criteria precludes this type of PCI failure and is used to show an acceptable fuel rod design.

4.2.3.2 Fuel Material Evaluation

4.2.3.2.1 Dimensional Stability

Fuel pellet dimensional stability is provided by a quality inspection program that is used for fuel pellets. Pellets are tested for resinter behavior according to criteria stipulated in the pellet manufacturing specifications. Pellets are also inspected for abnormalities such as discoloration, inclusions, pits, unground areas, cracks, and chips. One hundred percent of the pellets are measured for diameter. To maintain the integrity of the fuel, the other dimensional attributes are measured based on a statistical sampling over the course of pellet grinding and inspection.

4.2.3.2.2 Potential for Chemical Interaction

Standard manufacturing testing is performed to verify fuel pellet stoichiometry (oxygen-to-uranium ratio), uranium content, and isotopic content (^{234}U, ^{235}U, ^{236}U, and ^{238}U). For fuel rods with gadolinia, the gadolinia content and stoichiometry are also measured. Microstructural examinations for grain size and internal porosity provide verification of pellet properties for limiting fission gas release.

Pellet hydrogen and fluorine content are tightly controlled to minimize the potential for hydride blister formation on the cladding inner surfaces. Introduction of unacceptable levels of hydrogen from contamination sources is further prevented by implementing visual inspections of pellets immediately following grinding and immediately prior to loading into the fuel rods. Testing for nitrogen, carbon and oxygen verify sorbed gas limits within the pellets. Testing for elemental impurities and calculation of the equivalent boron content is also performed to prevent unwanted neutron absorption by tramp elements.

4.2.3.2.3 Thermal Stability

Fuel melting does not occur during normal operation or AOOs (Reference 4.2-2). The COPERNIC fuel performance computer code (Reference 4.2-4) is used for the centerline fuel melt analysis. COPERNIC determines the local linear heat rate throughout the fuel rod lifetime that results in centerline temperature exceeding a specified temperature limit (Reference 4.2-4). Staying below this local linear heat rate limit provides a high degree of assurance that fuel melting will not occur.

The local linear heat rate throughout the rod lifetime determined in the centerline fuel melt analysis is used as input to determine the limiting conditions for operation and reactor set points. During normal operation and AOOs, the fuel will not melt because the linear heat rate does not exceed the limit established in the centerline melt analysis.

4.2.3.2.4 Irradiation Stability

The irradiation stability of the fuel rod is confirmed by performing analyses using the COPERNIC code (Reference 4.2-4) that analyzes the fuel throughout the life of the fuel rod.

4.2.3.3 Fuel Rod Performance Evaluation

4.2.3.3.1 Fuel Rod Performance Predictions

COPERNIC is the fuel rod design computer code used to perform thermal and mechanical analyses to accurately simulate the behavior of a fuel rod during irradiation, and to verify the fuel rod design meets design and safety criteria. COPERNIC calculates fuel melting, fuel rod internal gas pressure, cladding strain, cladding peak oxide thickness, and initialization parameters for the cladding creep collapse. The following phenomenological models are utilized in the COPERNIC code:

- radial power distribution
- fuel and cladding temperature distribution
- axial burnup distribution in the fuel
- thermal conductivity of the fuel, cladding, cladding crud, and oxidation layers
- densification of the fuel
- thermal expansion of the fuel and cladding
- fission gas production and release
- solid and gaseous fission product swelling
- fuel restructuring and relocation
- fuel and cladding dimensional changes
- fuel-to-cladding heat transfer coefficient
- thermal conductivity of the fuel rod internal gas mixture
- thermal conductivity in the Knudsen domain
- fuel-to-cladding contact pressure
- heat capacity of the fuel and cladding
- growth and creep of the cladding
- rod internal gas pressure and composition
- sorption of helium and other fill gases

- cladding oxide
- cladding-to-coolant heat transfer coefficient
- thermal conductivity degradation

4.2.3.3.2 Failure and Burnup Experience

Fuel using M5® cladding material was first inserted in a domestic reactor core in 1995, has been used in 22 reactors and more than 7500 fuel assemblies as described in Reference 4.2-1.

4.2.3.3.3 Fuel and Cladding Temperatures

Fuel and cladding temperature analyses are described in Section 4.4.

4.2.3.3.4 Potential Effect of Temperature Transients

The fuel rod experiences many operational transients during its residence in the core. A number of thermal effects must be considered when analyzing the fuel rod performance.

The clad can be in contact with the fuel pellet at some time in the fuel lifetime. Clad-pellet interaction occurs if the fuel pellet temperature is increased after the clad is in contact with the pellet. Clad-pellet interaction is discussed in Section 4.2.3.1.13.

Potential differential axial thermal expansion between the fuel rods and the guide tubes during a transient is considered in the design. Excessive bowing of the fuel rods is precluded because the grid assemblies allow axial movement of the fuel rods relative to the grids. Specifically, thermal expansion of the fuel rods is considered in the grid design so that axial loads imposed on the fuel rods during a thermal transient will not result in excessively bowed fuel rods.

4.2.3.3.5 Analysis of Temperature Effects

Section 4.4 discusses the impact of temperature effects during anticipated operational transients and the effect from fuel rod bow, as well as other fuel rod thermal design bases.

4.2.3.4 Spacer Grids Evaluation

Structural evaluations are performed to ensure the grids maintain their configuration under postulated accidents. These analyses of the grids determined that the resulting impact loads are lower than those allowed to maintain a coolable configuration and control rod insertion. The methodology used to perform these evaluations uses the load limits that are derived by testing, which are provided in Reference 4.2-5.

The maximum impact load on the spacer grids due to a combined SSE and LOCA is provided in Reference 4.2-1. Impact loads were evaluated for scenarios in which both the fuel assembly and spacer grid were either in a beginning of life (BOL), unirradiated

condition or an irradiated condition. An intermediate grid location on a peripheral fuel assembly produced the maximum impact force. The combined loads for seismic and LOCA are below the AREVA-defined limits for plastic deformation of the grid. The requirements to maintain a core coolable geometry and control rod insertion are shown to be met in this worst-case condition in Reference 4.2-1.

The OBE severity for the NuScale Power Plant design is one-third of the severity of the SSE. In accordance with 10 CFR 50 Appendix S that specifies that an OBE earthquake does not need to be evaluated if its severity is less than or equal to one-third of the SSE severity, a separate OBE evaluation of the fuel assembly is not performed.

4.2.3.4.1 Spacer Grid Dimensional Stability

The spacer grids are suitable for use in terms of both irradiation and corrosion effects. This conclusion is based on PWR operating experience with Zircaloy-4 HTP™ and Alloy 718 HMP™ grids in combination with M5™ fuel rods and Zircaloy-4 guide tubes.

The chemical, thermal and irradiation behavior of the Zircaloy-4 HTP™ spacer grids has been determined by extensive operating experience in US PWRs. The operating experience has shown no operating problems associated with the chemistry of the spacer grids. The spacer grids at elevated temperature and with irradiated properties have demonstrated acceptable mechanical performance.

4.2.3.4.2 Spring Loads for Grids

The forces required to slip the HTP™ and HMP™ grids relative to the fuel rods were measured at BOL conditions. These data, which represent the friction force between the grids and fuel rods, were used as input in the analytical models of the fuel assembly.

4.2.3.5 Fuel Assembly Design Evaluation

The NuScale fuel assembly design is evaluated to demonstrate that the fuel assembly satisfies the requirements outlined in the Standard Review Plan. The fuel assembly design evaluation, including the fuel rods, is detailed in Reference 4.2-1 in relation to the Standard Review Plan criteria for fuel system damage mechanisms, fuel rod failure mechanisms, fuel coolability, and CRA insertion. A summary level description of the evaluation is provided in the following sections. A similar summary of the evaluations for the fuel rod design is also presented in Section 4.2.3.1.

Methodologies for the fuel assembly structural and mechanical analyses adhere to the codes and methods used by AREVA (listed below), as demonstrated to be applicable to the NuScale design by Reference 4.2-3 and Reference 4.2-9:

- design criteria for PWR fuel (Reference 4.2-7)
- LOCA-seismic analysis (Reference 4.2-5)
- fuel rod bow evaluation (Reference 4.2-6)

The results of the analyses in Reference 4.2-1 are applicable to fuel assembly operation in the NuScale Power Module.

4.2.3.5.1 Fuel Assembly Structural Design Evaluation

The design criterion for the structural evaluation of the NuScale fuel assembly design is that stress intensities are less than the stress limits based on Section III of the ASME BPVC. The structural design requirements for the NuScale fuel assembly are common to current AREVA PWR fuel designs and incorporate AREVA's design and incore operating experience with similar PWR fuel designs.

The requirements are consistent with the acceptance criteria in the Standard Review Plan. Evaluation results show that the calculated stress intensities are less than the applicable stress limits. Fatigue usage is evaluated and found to be acceptable. ASME Code Service Level A criteria are used for normal operating conditions and Service Level D criteria are generally used for the LOCA and seismic (i.e., faulted) analyses. An exception to this classification is the use of Service Level C criteria for guide tubes when CRA insertability is required for the faulted analyses.

The fuel assembly component evaluations show that the calculated stresses are lower than the material allowable stresses for both normal operation and faulted conditions for all evaluated components. The evaluation of components for LOCA conditions conservatively considered the square root of the sum of the squares combination of the LOCA and SSE loads.

The fuel assembly components evaluated include:

Guide tubes: The guide tubes do not buckle and remain elastic, thereby ensuring the CRAs can be inserted during normal operation. A positive guide tube buckling safety margin is determined for axial loading for all normal operating conditions. The hot zero power condition was determined as the limiting normal operating case for compressive loading compared with hot full power operation. CRA impact loads due to a scram were considered. The critical buckling load was determined with a classical Timoshenko buckling stress model, with results compared to the material yield strength at operating temperature. Initial lateral deflection (column eccentricity) was imposed on the guide tube model at mid-height in the magnitude of the available assembly and baffle clearance in the most limiting row with added limiting manufacturing variance, to account for potential reduction in the critical load due to fuel assembly bow. A positive buckling stress margin was predicted by implicit solution of the Timoshenko buckling stress formulation. Guide tube corrosion, load maldistribution, and temperature effects on material properties were also considered. Guide tube boiling is not predicted to occur during normal operation. Guide tube stresses were also evaluated for faulted conditions and shown to maintain CRA insertion capability by meeting the applicable criteria.

Spacer grids: The spacer grids do not deform beyond the approved limits in Reference 4.2-5 during normal operation and faulted conditions. The mechanical design bases of the spacer grids are confirmed through a series of tests on prototype 17x17 HTP™ grids as discussed in Section 4.2.4.

Bottom nozzle: The evaluation for normal operating conditions is performed in accordance with Subsection NG-3228.2 of the ASME BPVC using a design limit of two-thirds of the collapse load limit obtained by testing and adjusted for operating temperature.

The limit based on the maximum test load is further reduced for operating temperature conditions. Axial loading only is considered because the normal operating loads on the bottom nozzle are applied axially by the guide tubes. The maximum normal operating load used in the evaluation accounts for impact loads from a CRA scram, hold-down spring loads, and the fuel assembly mass.

The evaluation of the bottom nozzle for faulted operating conditions is performed in accordance with Appendix F, Paragraph F-1440(a) of the ASME BPVC using a design limit based on the maximum cold test load. The limit based on the maximum cold test load is further reduced for normal operating temperature evaluations. The maximum normal operating loads used in the evaluation included moment loads, plus the assembly weight, plus LOCA, plus SSE axial loads. Moment loads were considered by calculating the axial load equivalent of the moment couples created by the position of the guide tubes in relation to the center of the bottom nozzle. Margin to the design limit was demonstrated in Reference 4.2-1.

Top nozzle: The top nozzle structure is evaluated for normal operating and shipping and handling loads in accordance with Subsection NG-3228.2 of the ASME Code using a design limit of two-thirds of the collapse load limit obtained by testing and adjusted for operating temperature. The limiting case is evaluated for an axial scram load applied to the top nozzle structural framework and showed that positive margin to the design limit was maintained.

Hold-down spring: Stress analysis of the fuel assembly hold-down spring examines stresses, strains, and fatigue usage to confirm that it does not fail. The evaluation confirmed that the ASME BPVC criteria are satisfied. The spring stresses are treated as secondary stresses since the hold-down spring stresses are controlled by the total separation between the lower and upper core plates.

The secondary stress limits are satisfied by performing a plastic analysis in accordance with Subsection NG-3228.1 of the ASME BPVC. The hold-down springs remain within the elastic range. The maximum normal operating loading bounds the faulted condition loading because the fuel assembly lifts off the lower core plate during some severe seismic events. Therefore, satisfying the normal operating conditions criterion also satisfies the faulted condition. The known spring displacements were converted to stresses to demonstrate the criterion is met.

Structural Connections: The guide tube-to-spacer grid weld connections are evaluated for the limiting applied normal operating condition loads which are caused by the grid slip loads. The applicable load limit was established in accordance with Subsection NG-3228.4 of the ASME BPVC, and is 44 percent of the ultimate collapse load limit obtained by testing and reduced for operating temperature. The connections between the guide tubes, guide tube upper sleeves, and QD sleeve retainers are evaluated with similar NG-3228.4 criterion but with

applied normal operating condition loads of hold-down springs, assembly weight and scram, and conservatively neglecting flow lift loading. The strength of the welded connections between the guide tubes and the guide tube lower end plugs are qualified by the manufacturing specification which bounds the predicted loads from the guide tube analysis. Stress analysis of the guide tube cap screws, threads of the guide tube lower end plugs, and seating interfaces of the guide tube upper sleeve and guide tube lower end plugs found these designs to be acceptable with positive design margins.

Fuel Rod Cladding: The structural evaluation of the fuel rod cladding for normal operation is discussed in Section 4.2.3.1.

4.2.3.5.2 Analysis of Combined Loss-of-Coolant Accident and Seismic Loading

The structural integrity of the fuel assembly has been verified to withstand seismic and LOCA events under both unirradiated (BOL) and irradiated conditions using the methodology described in Reference 4.2-1. The fuel assembly meets the criteria to maintain structural integrity, CRA insertion and a coolable geometry during and after an SSE and a LOCA. The horizontal and vertical loads on the components were first determined with analytical models, and these loads were then combined in the evaluation of each component.

The horizontal component of the faulted analysis determines the structural integrity of the NuScale fuel assembly in the horizontal direction. Loading conditions are evaluated at unirradiated (BOL) and irradiated conditions for an SSE, LOCA, and a combined seismic and LOCA event.

The fuel assembly response to seismic and LOCA excitations is determined using the methodology described in Reference 4.2-5. The NuScale fuel assembly models used for seismic and LOCA analysis were benchmarked using properties established through full-scale prototype testing. Lateral fuel assembly models were combined to represent row configurations of fuel assemblies in the core. Row models with three, five and seven assemblies were created, matching the NuScale core configuration. NuScale seismic SSE and LOCA displacement time histories at the lower core plate and upper core plate were applied to the reactor core model, and the resulting fuel assembly impact loads and deflections were evaluated.

The fuel assembly was evaluated for the vertical SSE and LOCA conditions with a single assembly model described in Reference 4.2-5. Fuel assembly axial stiffness properties and drop impact characteristics were obtained from testing and were used to benchmark the fuel assembly axial model. The evaluation used vertical core plate displacement time histories determined by the NuScale Power Plant seismic model (Section 3.8).

The maximum grid impact forces that were obtained for SSE and SSE plus LOCA conditions for a full-core configuration of NuScale fuel assemblies were less than the allowable limits established by testing, as discussed in Section 4.2.3.4. Other fuel assembly components were evaluated for combined loads and stresses under vertical and lateral SSE plus LOCA conditions. The loads and stresses resulting from lateral SSE and LOCA excitations are the result of fuel assembly deflections under

those excitations. The component stresses were shown to be less than the allowable limits based on Section III of ASME BPVC criteria. The core coolable geometry and CRA insertability are maintained for all the faulted loads and the component stress intensities are less than the allowable limits.

The fuel assembly response to seismic excitations during refueling while the core is located in the reactor flange tool (RFT) was also studied. This evaluation was performed using the methodology described in Reference 4.2-5 with adjustments to account for the lower temperatures experienced in the RFT (Reference 4.2-9). While in the RFT, the fuel is already in a safe shutdown condition and therefore the RFT evaluation serves to confirm the structural integrity of the fuel rod in order to protect against the release of fission products. The same fuel rod analysis criteria from Section 4.2.1.5.3 were conservatively applied to the fuel in the RFT and the fuel rod stresses were shown to be less than the allowable limits as defined in Section 4.2.1.5.3.

4.2.3.5.3 Load Applied in Fuel Handling

Both the fuel assembly and individual components are evaluated for structural adequacy for shipping and handling loads in the amount of 6 g in the lateral direction and 4 g in the axial direction. The evaluations result in positive design margins to the stress limits.

4.2.3.5.4 Axial Growth

A fuel assembly top nozzle-to-fuel rod shoulder gap allowance is provided that maintains positive clearance during the assembly lifetime. The evaluation determined that a positive fuel rod shoulder gap occurs at end of life (EOL) hot conditions and considers the upper tolerance limit for fuel rod growth, minimum guide tube growth, and worst-case tolerances on the length of the fuel rods and guide tubes. The evaluated minimum fuel rod shoulder gap is presented in Reference 4.2-1 and is acceptable.

A fuel assembly-to-reactor internals gap allowance is provided that maintains a positive core plate gap clearance throughout the life of the fuel assembly. The core plate gap allowance considers combined worst-case internals-fuel assembly differential thermal expansion and irradiation-induced axial length changes to the guide tubes. The evaluation determined that a positive fuel core plate gap occurs at EOL cold conditions and considered the upper tolerance limit guide tube growth and worst-case tolerances on the length of the fuel rod and core plate separation. The evaluated minimum core plate gap is presented in Reference 4.2-1 and is shown to be acceptable.

In order to ensure axial alignment of the spacer grids with adjacent fuel assemblies, the HTP™ grids are spot welded to the guide tubes. Sleeves of Zr-4 are spot welded to the guide tubes above and below the HMP™ grids for axial location and restraint. The height of the grids is greater than the worst-case differences in grid elevation at BOL and end of life (EOL). Therefore, grid overlap between adjacent assemblies is maintained for the life of the fuel assembly. Those differences in grid elevation arise due to irradiation-induced length changes of the guide tubes.

4.2.3.5.5 Assembly Liftoff

The fuel assembly liftoff evaluation is performed by comparing the fuel assembly weight and the fuel assembly spring hold-down load with the hydraulic forces under normal operating conditions and AOOs. Hydraulic forces are calculated using pressure loss coefficients from testing a prototypical, full scale NuScale fuel assembly. Results of the analysis show significant margin to liftoff for all AOOs.

4.2.3.5.6 Fuel Rod Bow

Fuel rod bowing is evaluated with respect to the thermal-hydraulic performance of the fuel assembly. The NuScale fuel rod bow performance is expected to be similar to that of other AREVA designs and the analysis methodology discussed in Reference 4.2-6 is applicable. This topical report is demonstrated to be applicable to NuScale fuel in Reference 4.2-3.

4.2.3.5.7 Fuel Rod Fretting

The primary design criterion with regard to fuel rod fretting is that the design must limit fretting to preclude fuel rod failure. The NuScale fuel rod fretting and wear performance is based on the following tests and evaluations:

- full-scale 1000-hour life and wear testing performed on a prototypical, full-scale NuScale test fuel assembly with HMP™ grids modified to simulate EOL conditions
- favorable domestic operating experience with PWR fuel assemblies incorporating M5® fuel rods, and HTP™ and HMP™ grids used on the NuScale fuel design

The fretting operating experience for AREVA 17x17 fuel assemblies can be extended to the NuScale fuel design due to the design similarities and the lower reactor coolant system flow velocity of the NuScale Power Module (the lower flow velocity results in much lower cross flow velocities compared with typical PWRs). The NuScale HTP™ and HMP™ spacer grid designs are identical to those used in AREVA 17x17 fuel assemblies, along with M5® fuel cladding. Operating experience demonstrates that no fretting failures have occurred in the AREVA 17x17 HTP™ PWR fuel design.

The NuScale fuel design does not introduce additional features or characteristics other than the change to the overall length to the evaluation, which is not considered a significant variable in fuel rod fretting. Span lengths are no greater than those used on the existing PWR fuel designs.

No significant fretting marks were found on the life and wear test assembly. The life and wear testing was performed in a full-scale test channel under flow conditions that bound the NuScale operating conditions.

The life and wear test results, as well as the PWR operating experience of HTP™ grids with M5® clad fuel rods, show that the NuScale fuel design has significant

margins against fretting failure for the expected operating conditions including irradiation to extended burnup.

4.2.3.5.8 Corrosion

The corrosion resistance of the alloys used in the fuel assembly has been demonstrated by extensive operating experience as discussed in Reference 4.2-2. This corrosion resistance is the result of both material selection and manufacturing techniques. Rigorous material standards provide high-quality base material, while controlled manufacturing processes produce components with a minimum of surface contamination.

Manufacturing, handling, and assembly procedures prevent contaminants from coming into contact with the metals during fabrication, welding, or annealing operations.

The low carbon in the 304L stainless steels provides resistance to intergranular corrosion and sensitization of the metal. The activity levels caused by neutron activation of non-fuel components in the reactor is minimized by reducing the level of cobalt in the 304L stainless steel and Alloy 718 components used in the fuel assemblies.

Section 5.2.3 provides information on those aspects of the reactor coolant chemistry that provide corrosion protection for stainless steels and nickel alloys. Monitoring and control of primary water chemistry is based on industry experience and the EPRI PWR Primary Water Chemistry Plan.

The selection of corrosion resistant materials proven through extensive in-reactor operation, stringent manufacturing processes, water chemistry controls, and post-irradiation inspections provide assurance that corrosion is not an issue for NuScale fuel.

4.2.3.6 Reactivity Control Assembly and Burnable Poison Rods Evaluation

As described in Reference 4.2-1, the following items are evaluated for the CRAs and shown to be acceptable for their 20 effective full power year lifetime:

- Internal pressure is within limits during normal operation
- Cladding stresses are within limits during normal, transient, and accident conditions
- Thermal stability of the absorber material
- Irradiation stability of the absorber material, taking into consideration gas release and solid and gaseous product swelling

In addition, the design of the CRA precludes the potential for chemical interaction, including possible waterlogging rupture.

Wear rates on the NuScale CRA rods, which are designed with stainless steel cladding, are expected to be low in comparison to those of typical operating PWR plants with

stainless steel cladding given the lower core flow rates (<3 ft/sec) in the NuScale design. In addition, the absence of vessel outlet flow nozzles is also expected to decrease the cross-flows that contribute to control rod wear in typical PWRs. In a typical PWR the flow exits the core and then turns to flow out the nozzles. In the NuScale design the much lower velocity flow continues directly upward into the riser and then into the steam generators. Prototype testing using a full-scale CRA is performed to assess CRA susceptibility to wear. After initial irradiation and operation of the CRA design, inspections are performed so that actual rod wear rates can be compared with the predetermined wear limits to demonstrate acceptable performance.

The CRA structure is also analyzed for loads due to operational stepping, reactor trip, stuck rod, fatigue, and shipping and handling. All stresses in all of the components of the CRA are within limits. The CRA spring is analyzed to show that it can accept all of the energy from a reactor trip without the spring compressing completely and without the spider hub contacting the top nozzle. These analyses are described in more detail in Reference 4.2-1.

In addition, in-reactor surveillance of CRA insertion times is performed in accordance with the Technical Specification to demonstrate satisfactory performance.

As discussed previously, there are no discrete burnable poison rods in the NuScale Power Plant design. The burnable poison is integral with the fuel pellet in selected rods as described in Section 4.2.2.7.

4.2.4 Testing and Inspection Plan

The NuScale fuel design is similar to existing 17x17 designs that have been used successfully in PWRs in the industry. The only significant design difference is the fuel assembly length. The following sections address operating experience, prototype testing, manufacturing testing and inspection, onsite receipt inspection, on-line fuel monitoring, and post-irradiation monitoring that provide confidence that the fuel will meet design requirements.

4.2.4.1 Operating Experience

AREVA has both domestic and international experience with fuel design features that are pertinent to the NuScale fuel assembly design. All of the components in the NuScale fuel assembly design have relevant experience in operating plants, and both components and methods that have been accepted by the NRC for commercial operation. AREVA has extensive PWR operating experience with all of the components and features of the NuScale fuel assembly, including the MONOBLOC™ guide tubes, HTP™ and HMP™ spacer grids, the QD top nozzle assembly, and a mesh filter bottom nozzle. M5® fuel cladding also has extensive operating experience (currently in use in 16 domestic PWRs), including AREVA's 17x17 PWR fuel designs.

HTP™ Grid Experience

The HTP™ spacer is a proven concept in spacer design for PWR fuel. The HTP™ spacer features strip doublets that are shaped such that they not only serve as spring elements to firmly hold the fuel rods in radial alignment, but also produce curved internal flow

channels to achieve the desired thermal-hydraulic performance. The HTP design was first used in a domestic plant in 1988, and the HTP™ design now has 25 years of operational experience in a number of different fuel assembly design variations that include Westinghouse-type 17x17 fuel.

HMP™ Grid Experience

The initial use of the current version of Alloy 718 spacers with straight flow channels, designated HMP™, occurred in 1988. A large operating experience base with fuel featuring the HMP™ spacer is available. Fuel assemblies with HTP™ grids and a lower HMP™ spacer have not had a grid-to-rod fretting failure.

M5® Cladding Experience

M5® is an advanced zirconium alloy developed and implemented by AREVA to improve corrosion resistance, reduce hydrogen uptake, and reduce irradiation growth. In 1999, the NRC approved M5® for domestic use. Since then, extensive operational experience has been gained using M5® material.

As documented in Reference 4.2-3, the above experience applies to the NuScale fuel assembly design.

4.2.4.2 Prototype Testing

A prototype testing program was undertaken to determine the performance characteristics of the NuScale fuel assemblies, CRAs, and fuel assembly components such as grids, upper nozzle, and lower nozzle.

4.2.4.2.1 Assembly Testing

Testing was conducted on full-sized prototype fuel assemblies and on various assembly components. The full-size fuel assemblies were used for structural and thermal-hydraulic testing. The fuel assembly structural tests included lateral deflection tests and axial deflection tests, baffle impact tests, fuel assembly free-and forced-vibration tests, and vertical drop tests. All of these tests were conducted on two prototypical test assemblies, one with grids having BOL characteristics and one having grids with EOL characteristics and the rods seated on the bottom nozzle assembly.

The fuel assembly thermal-hydraulic test scope included assembly pressure drop tests and life and wear testing for 1000 hours.

These tests, summarized in Reference 4.2-1, were conducted in accordance with approved test plans at AREVA test facilities. The test results were used in benchmarking analytical models for the fuel assembly design evaluation addressed in previous Section 4.2.3.5.

Static Stiffness Testing - Forces versus deflection tests were conducted to determine the axial and lateral stiffness of the prototype fuel assembly. In an axial stiffness test, the fuel assembly was compressed along its longitudinal axis by an

application of forces at the nozzles. The lateral stiffness test consisted of loading the fuel assembly laterally near the center of the assembly at the middle spacer grid. The results of this testing are used in the fuel seismic model.

Free- and Forced-Vibration, and Baffle Impact Testing - The vibration tests determine the fuel assembly lateral, dynamic response. The use of free- and forced-vibration tests together cover higher and lower modes of the assembly natural frequency. The baffle impact test determines the assembly response to impacts with the baffle plate (or reflector). This information is used in the fuel assembly seismic model.

Fuel Assembly Drop Testing - Fuel assembly drop tests were performed to obtain impact loads against which the vertical seismic model was benchmarked. The fuel assembly was dropped against an unyielding surface and the impact loads, bottom nozzle displacement, and assembly velocity were recorded. The effects of multiple drops in succession were accounted for in the model benchmark and a suitable correlation to the test results was obtained.

Fuel Hydraulic Flow Testing - Flow testing on a full-scale prototype fuel assembly was performed to establish flow component loss coefficients and other related flow characterization parameters for the NuScale fuel assembly. The form loss coefficients are used in the fuel assembly liftoff analysis.

Fuel Fretting Testing - The prototype fuel assembly with EOL spacer grids was also used to evaluate the fretting and wear performance at the grid-to-rod interfaces. The test was conducted for over 1000 hours under flow conditions that bound those of the NuScale reactor. At the conclusion of the test, several test rods were inspected and showed minimal wear.

4.2.4.2.2 Fuel Assembly Component Testing

In addition to full-scale prototype testing, various components were also characterized by testing. The spacer grid design was subjected to static buckling and dynamic crush tests. The strength of the top and bottom nozzles were also tested. These test results are incorporated into the analytical models used to verify the NuScale fuel design.

4.2.4.2.2.1 Spacer Grid Testing

The mechanical design bases for the spacer grids were confirmed through a series of structural tests on prototype grids. The testing, summarized below, found that the grids provide the necessary design margins:

Dynamic Impact - Dynamic crush tests were performed on HTP™ spacer grids at unirradiated hot and cold conditions and irradiated hot conditions. The tests determined the through-grid stiffness and damping values for the lateral seismic models and the crushing load limits for the grids.

Static Impact - The static crush characteristics (static stiffness and elastic load limit) are used to establish allowable grid clamping loads applied during shipping.

Slip Load - The forces required to slip the grid relative to the fuel rods were measured at BOL conditions for both the HTP™ and HMP™ grids. The slip load values are used in the fuel assembly evaluation.

4.2.4.2.2.2 Strength Test of Top and Bottom Nozzles

Bottom Nozzle - Strength testing of the bottom nozzle was performed to establish the axial load limit for evaluation. A prototype bottom nozzle was tested at room temperature in static axial compression by applying a load to 24 springs on the guide tube positions. The spring stiffness was set to be equal to the guide tube stiffness in order to simulate the load distribution of the guide tubes.

A room temperature test at maximum load was applied without collapse of the structure. This tested maximum load was used to demonstrate the structural adequacy in the design evaluation by comparison with the normal operating and faulted loads, as discussed in Section 4.2.3.5.1 and Section 4.2.3.5.2.

Top nozzle - Strength testing of the top nozzle was performed to establish the axial load limit for evaluation. A prototype top nozzle was tested at room temperature in static axial compression by applying a load to the upper surface of the top nozzle, which was set on 24 springs at the guide tube positions. The spring stiffness was set to be equal to the guide tube stiffness in order to simulate the real load distribution of the guide tubes.

A room temperature test was performed in which a load was applied that exceeds a 4 g assembly load and resulted in no plastic deformation of the structure. This tested maximum load is used to demonstrate the structural adequacy in the design evaluation by comparison with the shipping and handling, normal operating and faulted loads, as discussed in Section 4.2.3.5.

4.2.4.2.3 Control Rod Testing

The NuScale CRA is similar to existing 17X17 CRAs except for the shorter length. The CRA drive shaft is longer than typically used in the industry. Prototype testing is performed to confirm CRA drop times, assess the propensity for wear, and to assess the impact of the maximum expected misalignment of the fuel assembly guide tubes predicted to occur during a joint LOCA and seismic event.

The CRA drop times are calculated using a fluid dynamic computer model that predicts insertion time and impact velocity. When CRAs are dropped into a fuel assembly, the water in the guide tube is displaced through several flow paths. The NuScale fuel assembly design has twenty four guide tubes, each containing two pairs of side flow holes. In addition, water is forced out through the top annulus of the guide tube and through the hole in the cap screw at the bottom of the guide tube assembly. The computer analysis for the CRA drop time is primarily best

estimate but does include some conservatism. The drop time is provided in Figure 4.3-23. The control rod drop time used in Chapter 15 analysis is a more conservative bounding value. The results from the CRA drop testing, described in Section 1.5.1.7, validate the use of the calculated SCRAM curve shown in Figure 4.3-23 as a conservative basis for the CRA drop time.

For the impact velocity, the rod drop calculation is also primarily best estimate but does include conservatism that predicts a higher impact velocity. Testing provides confirmation that these values are conservative for their respective application. This testing is described in more detail in Section 1.5.

The ability of the CRA to insert under conditions of fuel assembly misalignment is assessed in a test that deflects the fuel assembly at the mid-height location. The CRA insertion time is measured and compared to the CRA insertion time testing performed with no deflection of the fuel assembly. The testing is performed to confirm that the CRA insertion is not significantly affected by the maximum expected misalignment.

4.2.4.3 Manufacturing Testing and Inspection

Fuel assemblies and CRAs are manufactured and inspected in accordance with a 10CFR50, Appendix B quality assurance program as described in Chapter 17. In general, components and assemblies are tested and inspected to verify compliance with all design drawing and specification requirements. Quality control procedures are prepared and used for all inspection operations. Quality control maintains a gauge control system for tooling, gauges, templates, and other equipment used to perform inspections. Inspection plans range from 100 percent inspection plans to statistical process control procedures, which require either upper and lower tolerance limits, upper and lower confidence limits, or other statistically-based (attribute or variable) sampling plans.

The quality assurance program requires audits of suppliers and internal audits of manufacturing and inspection operations. Materials are procured from approved suppliers using approved material specifications, which may include industry-approved standards, such as ASME and American Society for Testing and Materials (ASTM) materials specifications or internal specifications. Certified material test reports are required for all safety-related materials and are reviewed for conformance to the specification requirements.

Depending on the particular design requirement to be verified, non-destructive examinations (dimensional, visual, radiographic, ultrasonic, and eddy current inspection) and destructive examinations (chemical composition and metallographic sectioning) are employed for in-process inspections or in support of qualifications.

Manufacturing operations require adherence to cleanliness controls for all components and assemblies. The cleanliness program includes controls for all expendable and consumable materials that come in contact with core components.

Fuel pellets are extensively tested and inspected, including:

- dimensional inspections
- visual examinations to check for surface contamination and surface defects, including the presence of missing pellet surface
- destructive examinations for microstructure (grain pore size distribution)
- resinter densification
- chemical composition
- impurity checks (including hydrogen determination and isotopic content)

Fuel rod cladding tubes are inspected for external and internal defects by approved non-destructive methods. Ultrasonic methods are used for dimensional measurements. Fuel rods have the end cap welds tested by both destructive and non-destructive means, are leak tested using helium detection equipment, and are then gamma-scanned to verify the integrity and position of the internal components and the absence of unacceptable pellet gaps. Automated computer equipment is used to maintain traceability of all fuel components. Fuel pellets, fuel rod end caps and springs are traced on a lot basis. Traceability of fuel cladding and fuel rod assemblies is accomplished by serial number.

Fuel assemblies undergo inspections for bow, twist, dimensional envelope, and fuel rod spacing. Visual examinations are performed as a final check on cleanliness control.

Verification of CRA and component attributes is very similar to those of the fuel assemblies and will be the same for NuScale as for AREVA's typical domestic PWR control components. The absorber composition is verified by an approved supplier through chemical examination. Control rod cladding tubes are inspected for external and internal defects using approved non-destructive methods. The CRAs have the end cap welds tested by both destructive and non-destructive means and are leak tested using helium detection equipment.

4.2.4.4 Onsite Receipt Inspection

When fresh fuel and CRAs are received on site, written procedures are used for inspection of the new fuel assemblies and control rod assemblies. Specific fuel handling procedures define the sequence in which handling and inspection take place.

Fuel shipping containers are externally inspected when received to ensure there was no damage during shipping. This inspection includes examination of the instrumentation that measures acceleration forces during shipping to ensure the forces were within limits.

Removal of the fuel from the shipping container is performed in accordance with written procedures. Following removal of the fuel assembly from the shipping container, a detailed visual inspection of the fuel assemblies and CRAs is performed. All onsite fuel receipt procedures are based on the fuel fabricator's recommendations. The inspection plans for new fuel are essentially the same as those for previously approved plants.

4.2.4.5 On-line Fuel System Monitoring

The chemical and volume control system (Section 9.3.4) contains radiation detection instrumentation that continuously monitors for radioactivity and is capable of detecting a fuel leak. In addition, the process sampling system (Section 9.3.2) contains grab sample capability that allows for more detailed assessment of the radionuclides in the primary system water. Detection of a fuel leak may result in more frequent grab sample analysis.

4.2.4.6 Post Irradiation Monitoring

A detailed surveillance program is planned following the irradiation of the fuel assembly and CRAs from the first licensed module. This program includes the schedule and criteria for inspection of selected fuel assemblies and CRAs. The program includes complete visual inspections of selected assemblies and detailed measurements to capture key attributes such as those listed below. The detailed measurements are taken to confirm that the fuel is performing according to the design analyses described in Section 4.2. The key attributes that are assessed as part of the post-irradiation monitoring program include:

- fuel rod growth
- fuel rod bowing
- fuel assembly growth
- fuel assembly bowing
- crud deposition
- fuel rod cladding corrosion (oxide)
- fuel rod cladding diameter

In addition, visual inspection of guide tubes and control rod cladding is performed for indications of wear.

The post-irradiation program makes sure that the above characteristics are within expected values. This surveillance program is expected to span the initial three cycles of operation of the initial licensed NuScale Power Module, with provisions for during-cycle inspections if operation indicates the presence of fuel abnormalities. The surveillance program includes guidance on the disposition of failed fuel.

4.2.5 References

4.2-1 NuScale Power, LLC, "NuFuel-HTP2™ Fuel and Control Rod Assembly Designs," TR-0816-51127-P, Rev. 2, July 2019.

4.2-2 AREVA Inc., "Evaluation of Advanced Cladding and Structural Material (M5) in PWR Reactor Fuel," BAW-10227P-A, Rev. 1, June 2003.

4.2-3 NuScale Power, LLC, "Applicability of AREVA Fuel Methodology for the NuScale Design," TR-0116-20825-P-A, Rev. 1, June 2016.

4.2-4 AREVA Inc., "COPERNIC Fuel Rod Design Computer Code," BAW-10231P-A, Rev. 1, January, 2004.

4.2-5 AREVA Inc., "PWR Fuel Assembly Structural Response to Externally Applied Dynamic Excitations," ANP-10337P-A, Revision 0, April 2018.

4.2-6 AREVA Inc., "Computational Procedure for Evaluating Fuel Rod Bowing," XN-75-32-P-A, Supplements 1-4, February 1983.

4.2-7 AREVA Inc., "Generic Mechanical Design Criteria for PWR Fuel Designs," EMF-92-116(P)(A), Rev. 0, February 1999.

4.2-8 AREVA Inc., "Program to Determine In-Reactor Performance of BWFC Fuel Cladding Creep Collapse," BAW-10084P-A, Rev. 3, August 1995.

4.2-9 NuScale Power, LLC, "NuScale Applicability of AREVA Method for the Evaluation of Fuel Assembly Structural Response to Externally Applied Forces," TR-0716-50351-P, Rev. 1, July 2019.

Table 4.2-1: Fuel Design Parameters

Parameter	Nominal Value
Fuel Assembly Parameters	
Fuel rods per fuel assembly	264
Guide tubes per fuel assembly	24
Spacer grids per fuel assembly	5
Number of instrument tubes per assembly	1
Pin pitch (in)	0.496
Guide tube OD (in)	0.482
Guide tube ID (Above Dashpot) (in)	0.450
Guide tube ID (In Dashpot) (in)	0.397
Fuel Assembly Length (including springs)(in)	95.89
Fuel Rod Parameters	
Fuel stack height (in)	78.74
Fuel rod length (in)	85.00
Fuel rod OD (in)	0.374
Fuel rod ID (in)	0.326
Fuel pellet OD (in)	0.3195
Pellet length (in)	0.400

Table 4.2-2: Fuel Assembly Materials

Component	Material
Top nozzle	AISI 304 L stainless steel
Bottom nozzle frame	AISI 304 L stainless steel
Mesh Filter plate	Alloy 286
Guide tube and QD sleeves	Zr-4
Top connection (quick disconnect)	Zr-4 and Alloy 718
Bottom cap screw	AISI 316 L stainless steel
HMP™ grid	Alloy 718
HTP™ grid	Zr-4
Fuel rod cladding	M5®
Fuel assembly leaf springs	Alloy 718
Fuel rod plenum springs	AISI 302 stainless steel
Fuel pellets	UO_2 and UO_2 plus Gd_2O_3

Note: Stainless steels are low cobalt.

Table 4.2-3: Control Rod Design Parameters

Dimension	Nominal Value
CRA total mass (lb)	43
CRA total height (in)	94.37
Control rod OD (in)	0.381
Control rod ID (in)	0.344
Control rod bottom end plug length (in)	1.913
B_4C OD (in)	0.333
B_4C stack length (in)	62.0
AIC composition (weight percent)	80% Silver, 15% Indium, and 5% Cadmium
AIC OD (in)	0.336
AIC stack length (in)	12.0
Cladding material	304 stainless steel
Height of CRA spider assembly (in)	10.387
CRA shaft OD (in)	1.804

Figure 4.2-1: Fuel Assembly General Arrangement

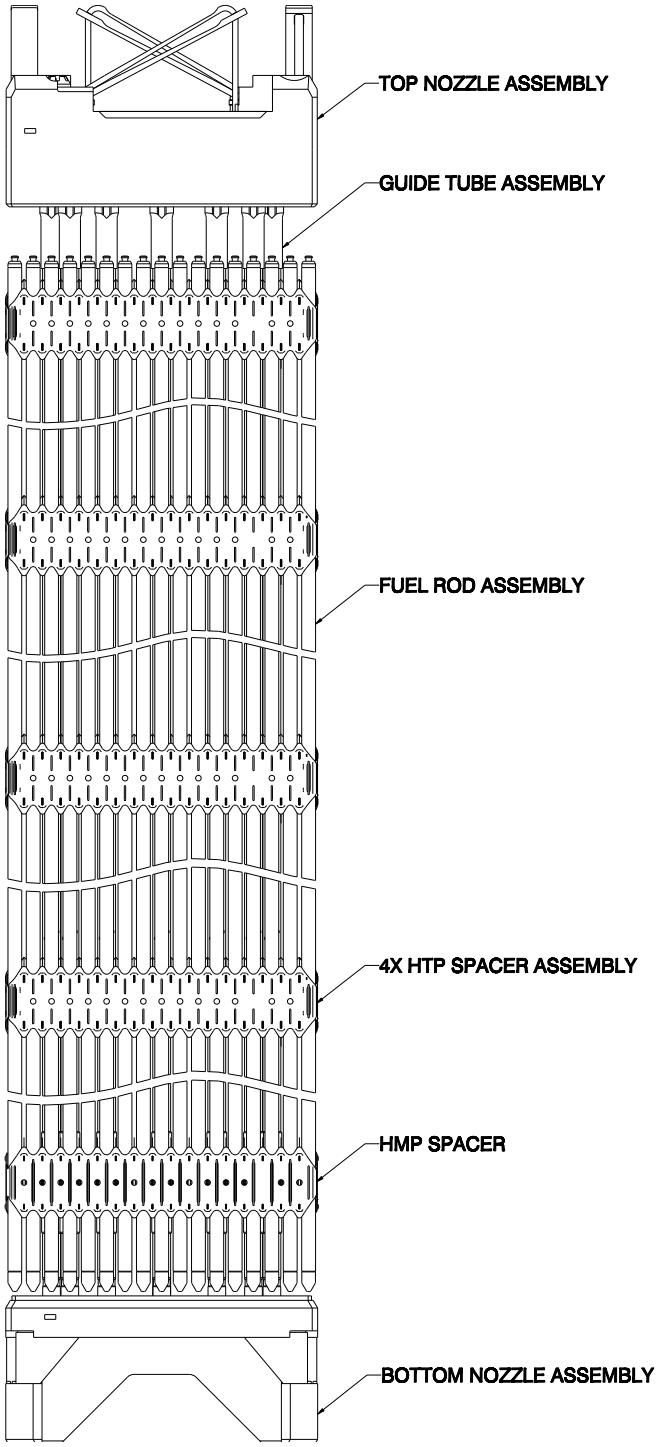

Figure 4.2-2: Top Nozzle

(nominal dimensions)

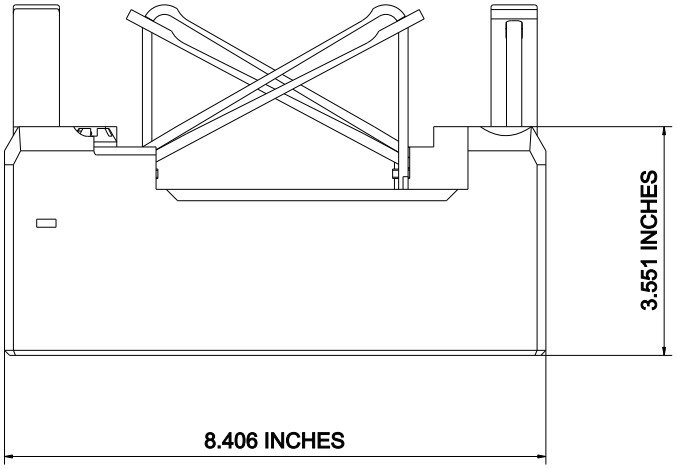

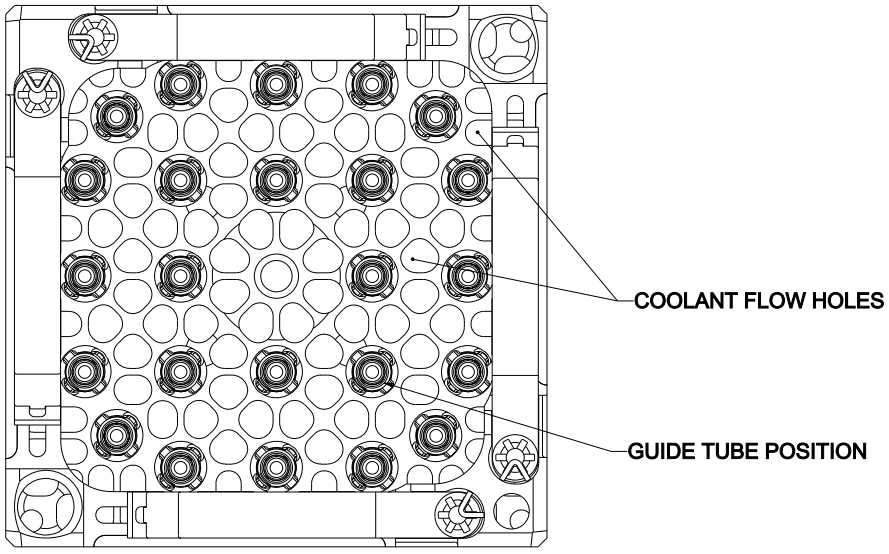

Figure 4.2-3: Bottom Nozzle

(nominal dimensions)

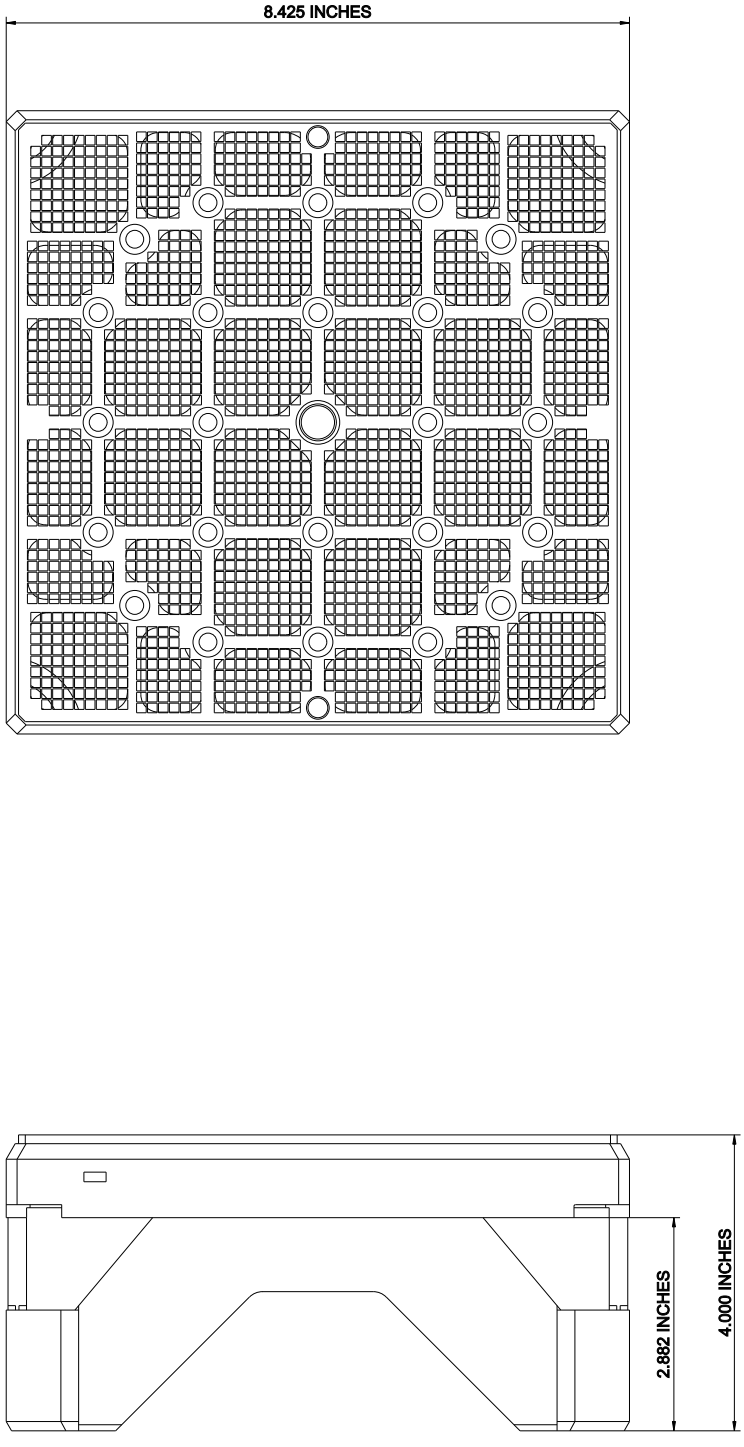

Figure 4.2-4: Guide Tube Assembly

(nominal dimensions)

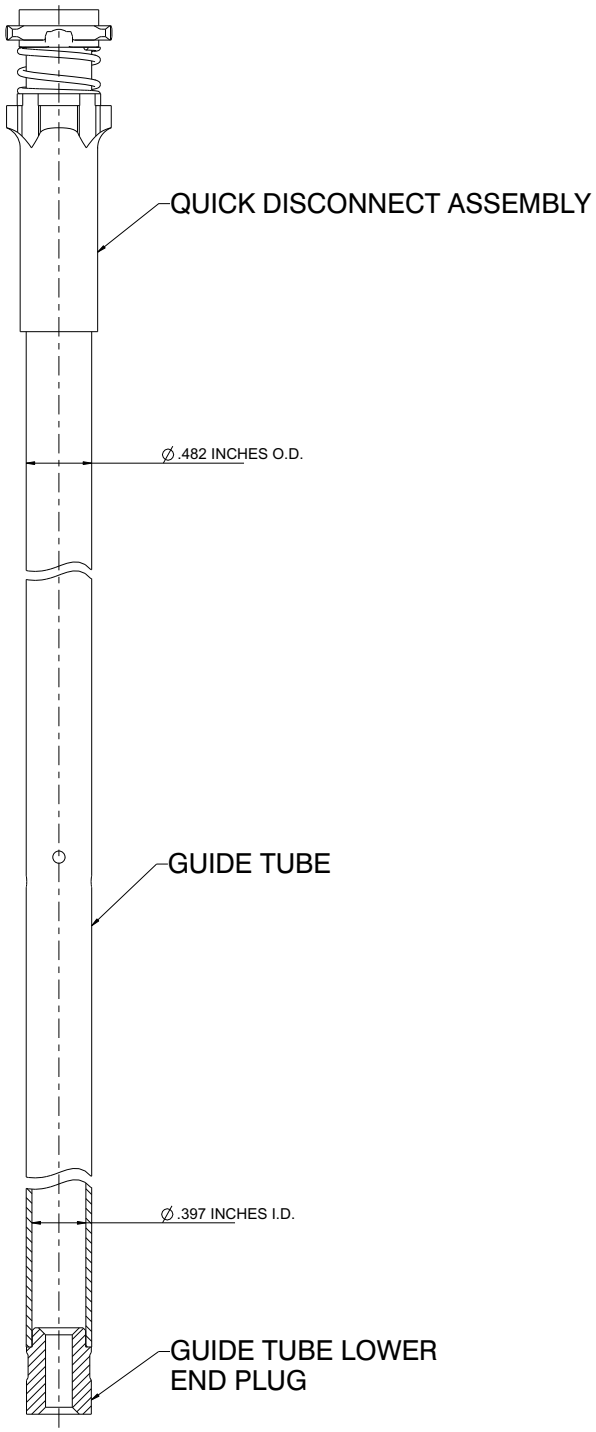

Figure 4.2-5: Guide Tube Quick Disconnect Top Nozzle Connection

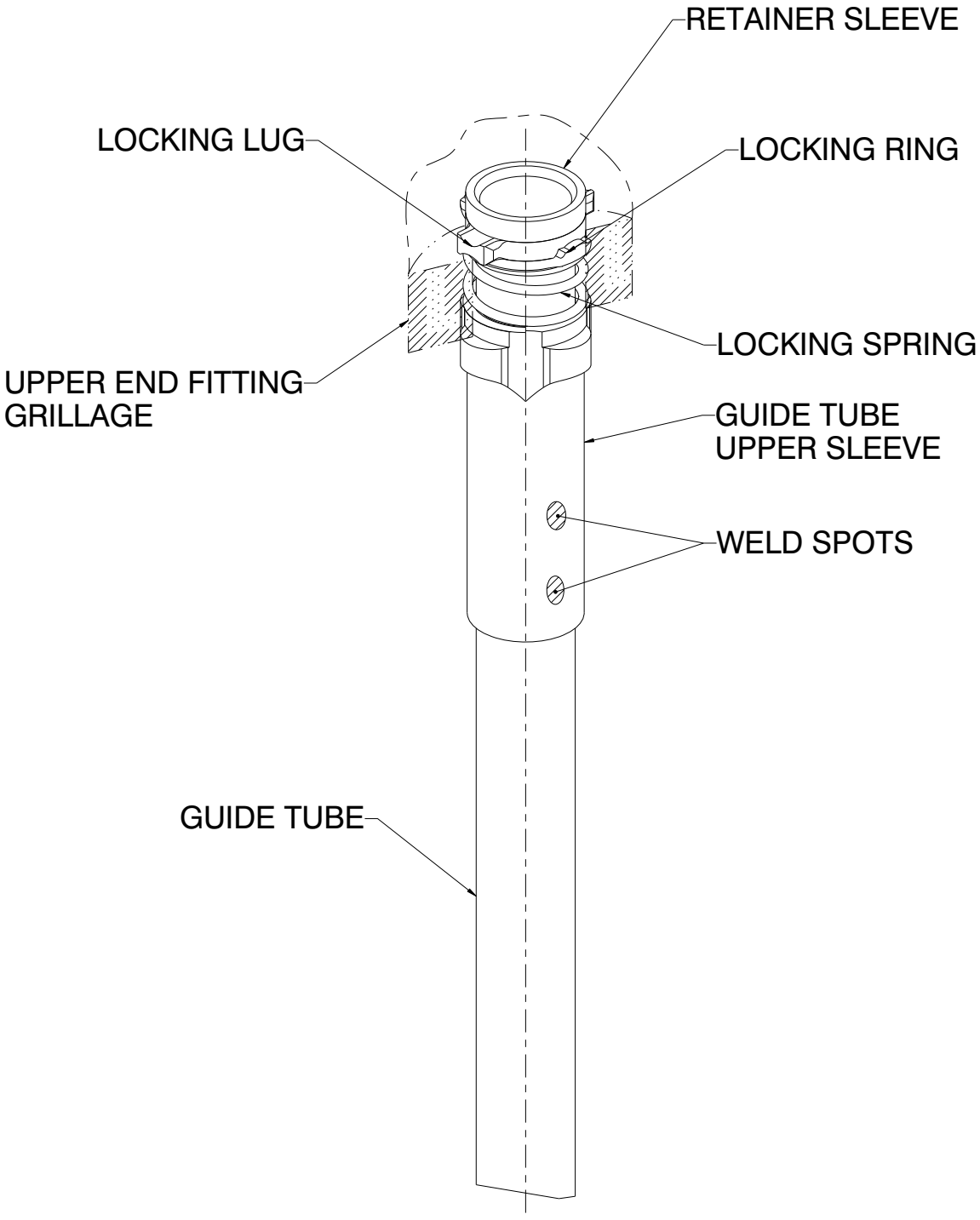

Figure 4.2-6: Cap Screw Bottom Nozzle Connection

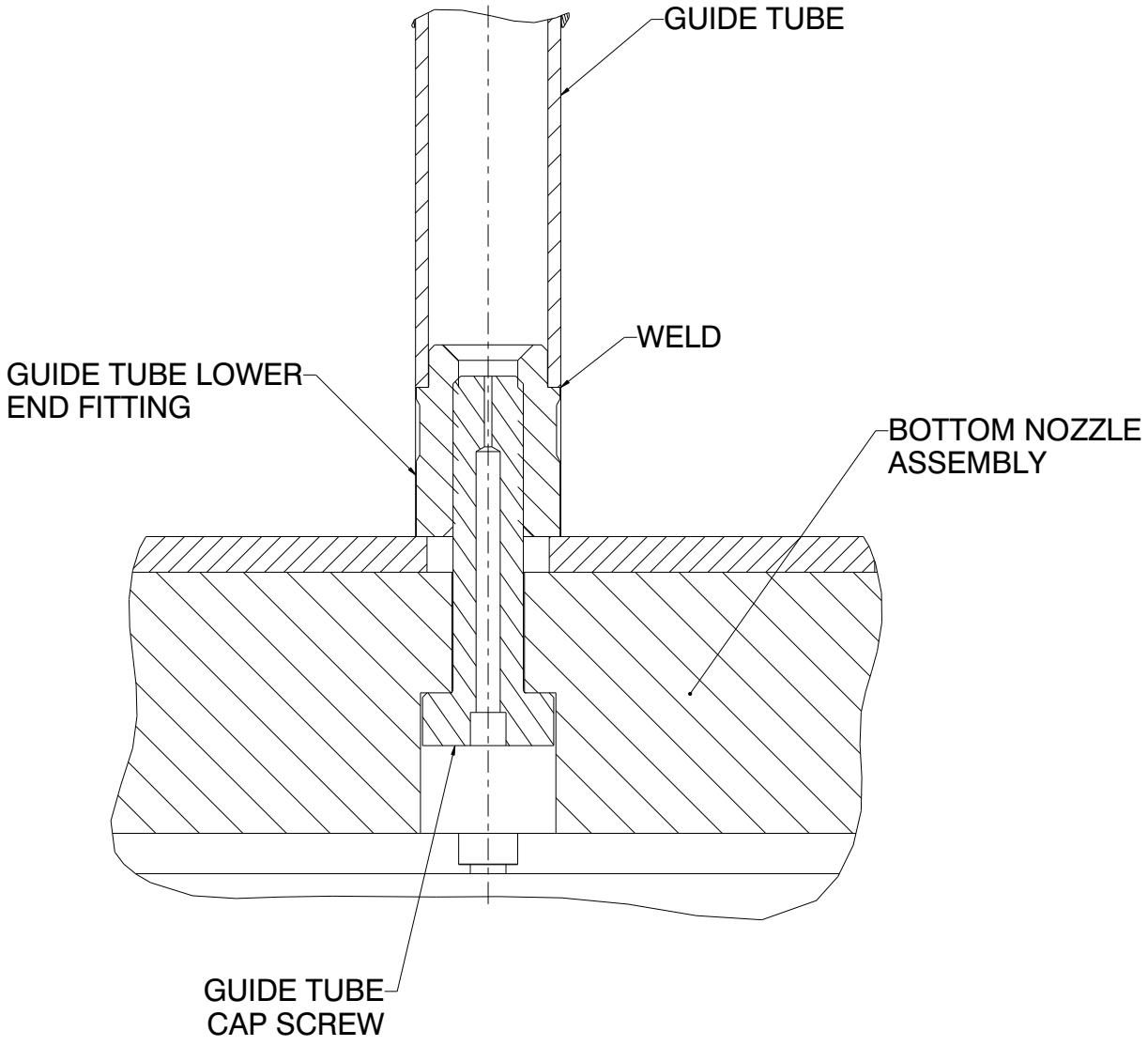

Figure 4.2-7: HTP™ Spacer Grid
(nominal dimensions, one-quarter grid shown)

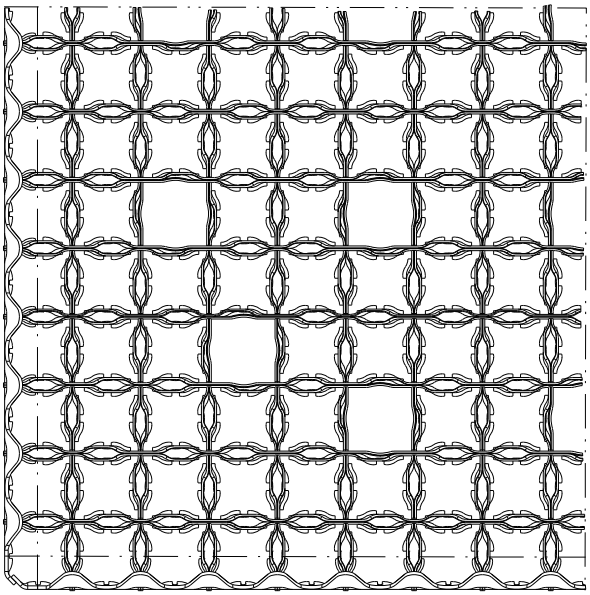

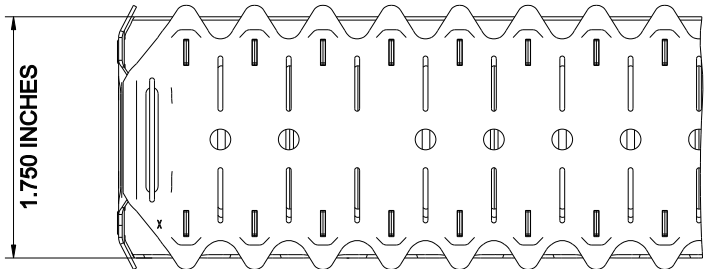

Figure 4.2-8: HTP™ Spacer Grid Characteristics

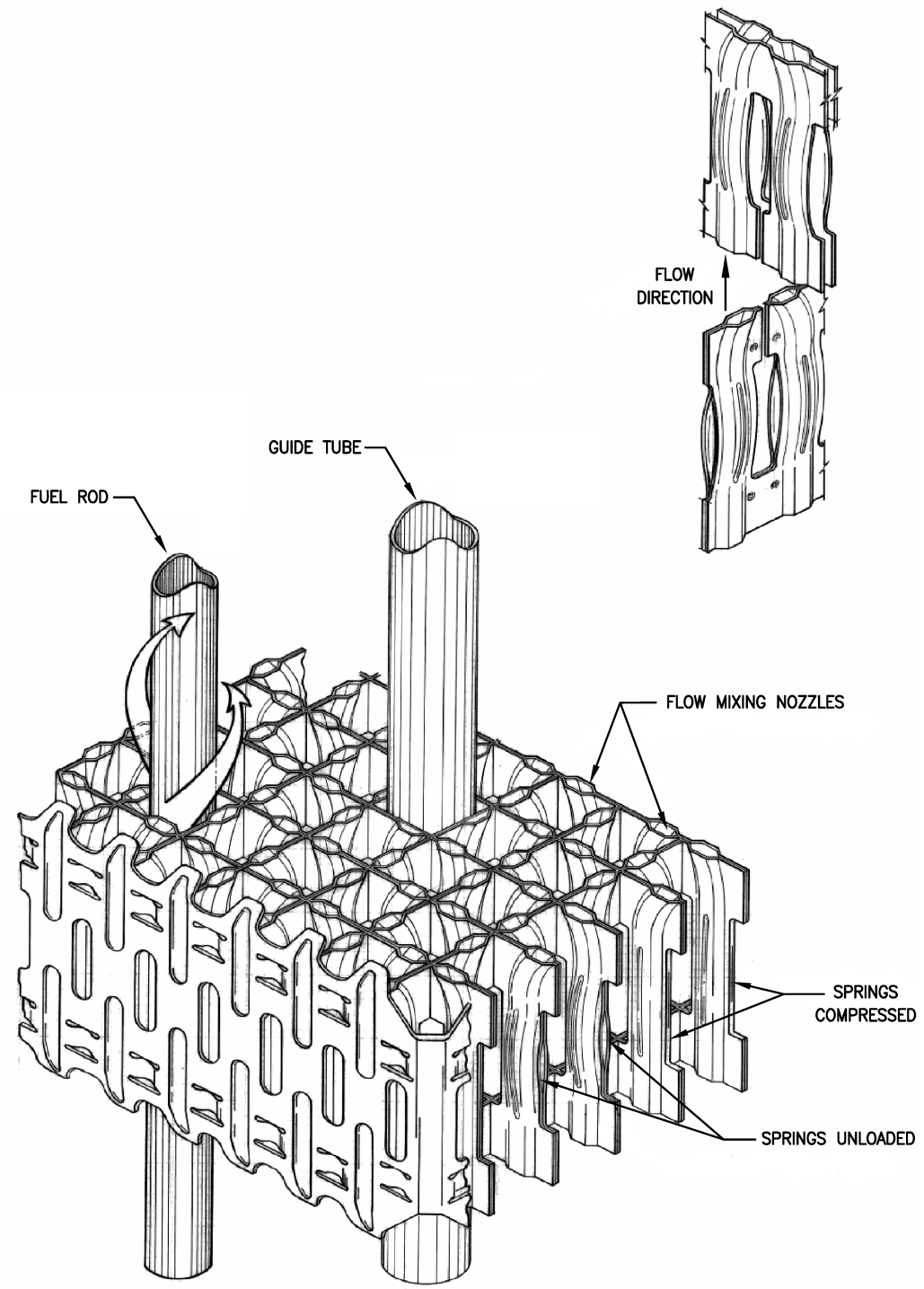

Figure 4.2-9: HMP™ Spacer Grid
(nominal dimensions, one-quarter grid shown)

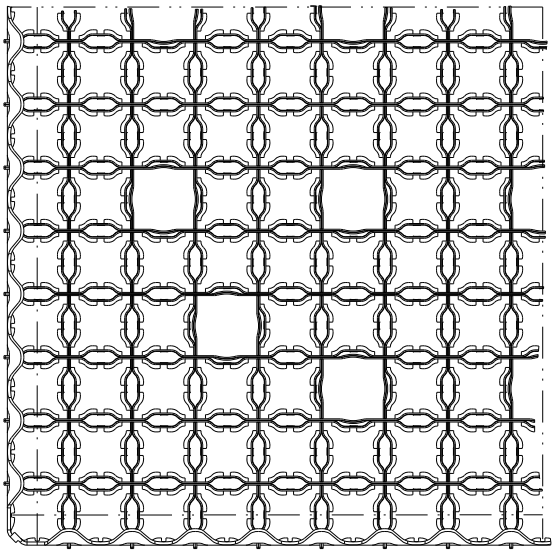

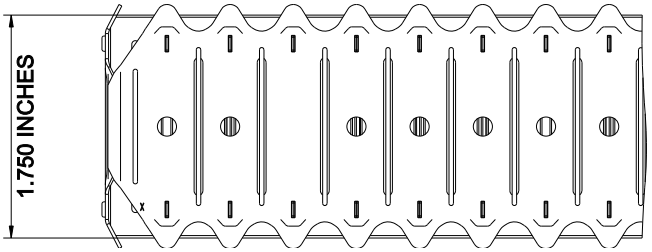

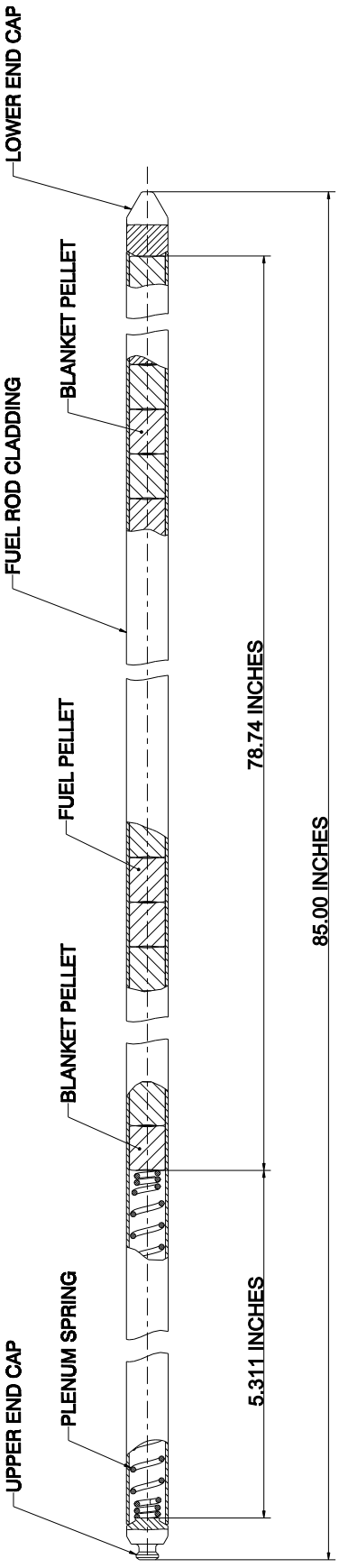

Figure 4.2-10: Fuel Rod Assembly
(nominal dimensions)

Figure 4.2-11: Control Rod Assembly General Arrangement

(nominal dimensions)

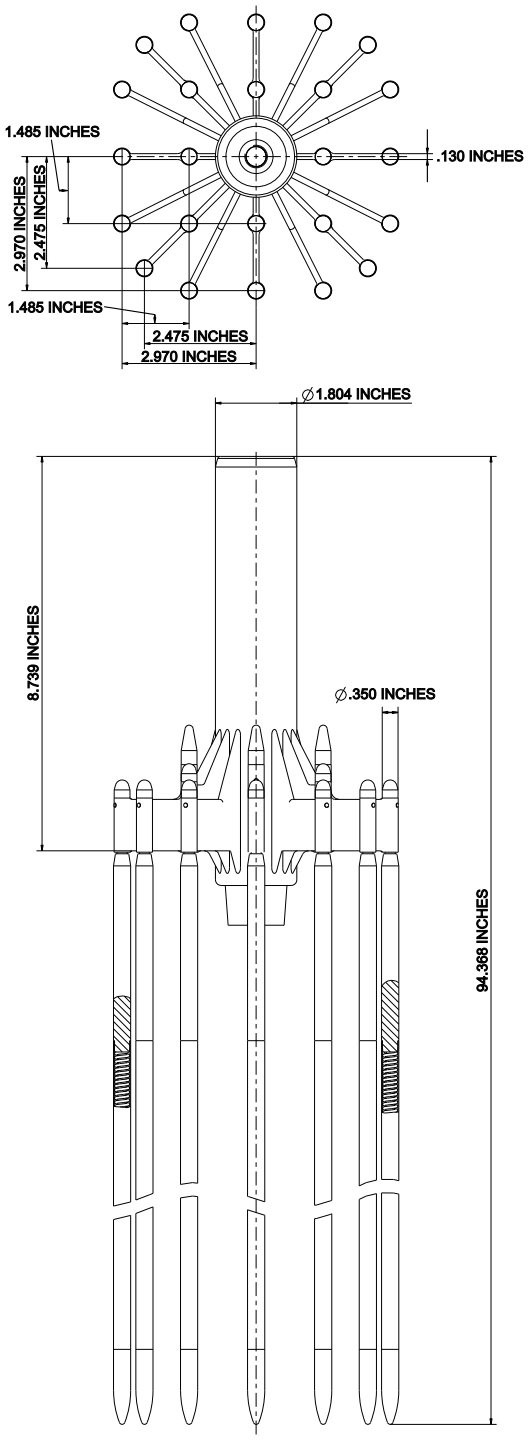

Figure 4.2-12: Control Rod Assembly Cut-Away
(nominal dimensions)

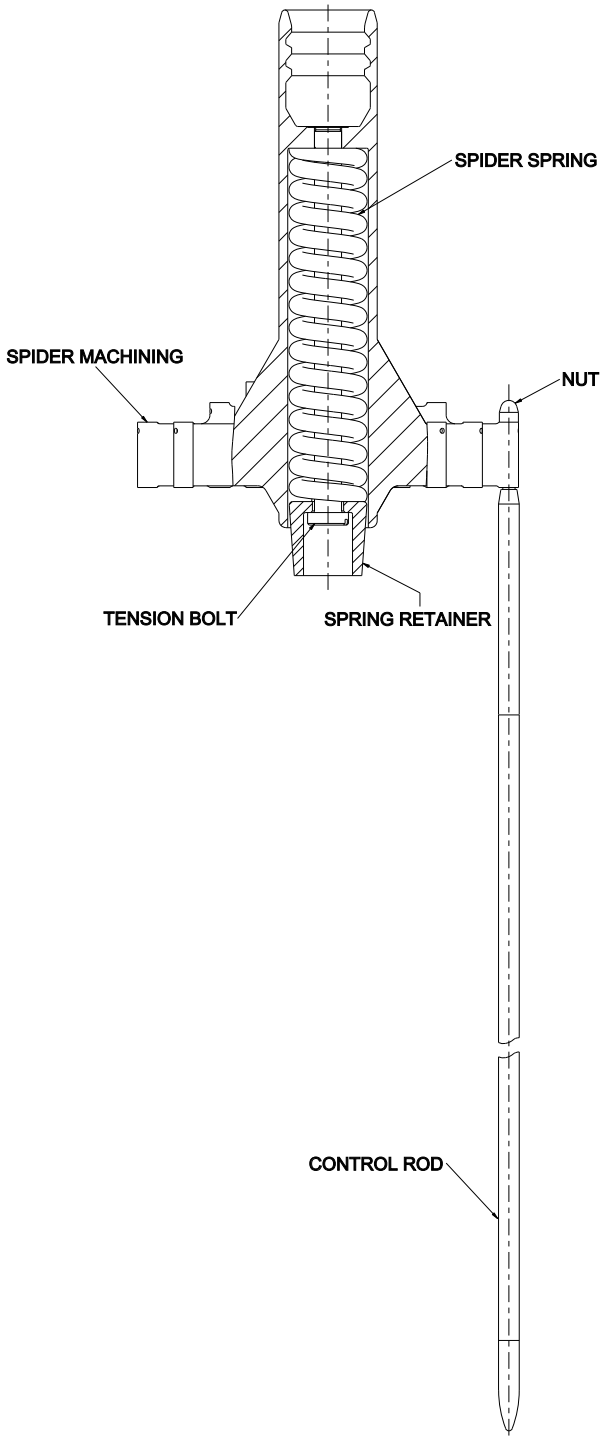

Figure 4.2-13: NuScale Control Rod Assembly Design
(nominal dimensions)

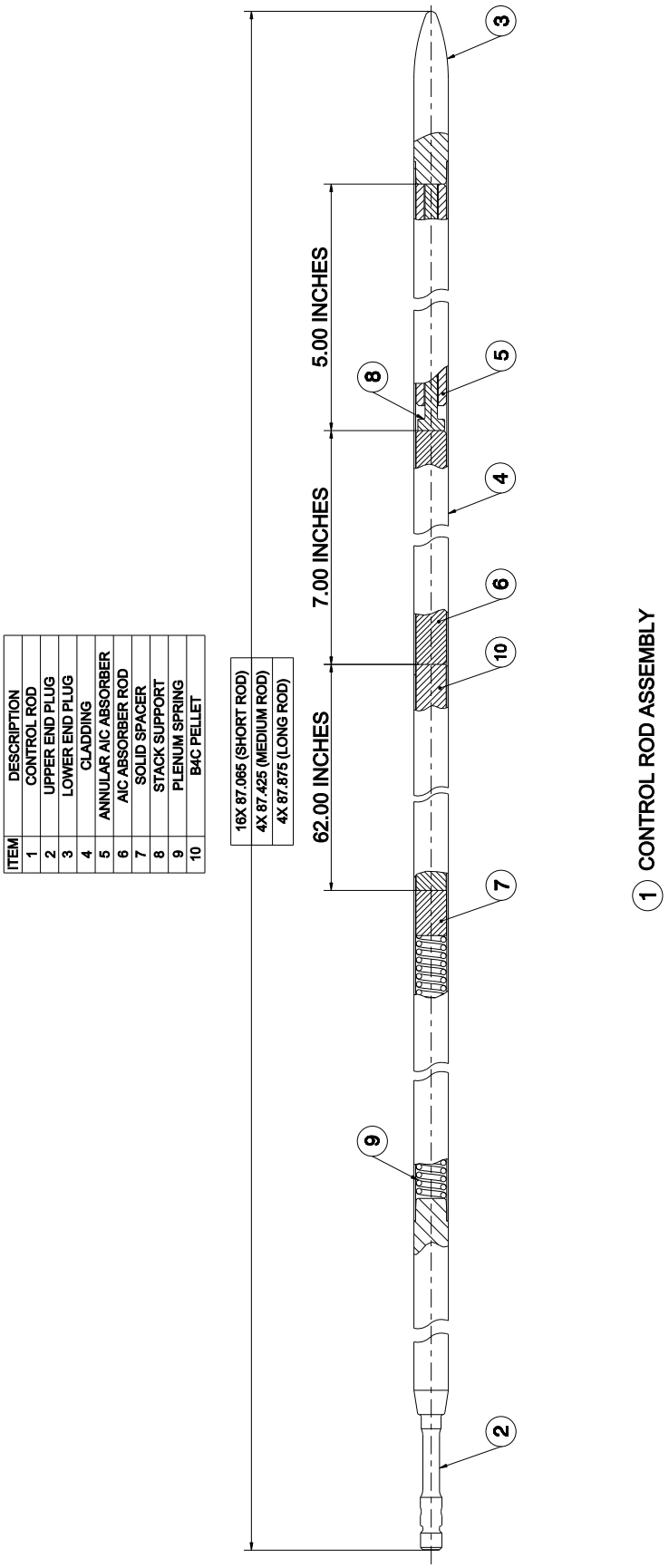

4.3 Nuclear Design

This section describes the nuclear design of the NuScale Power Module (NPM), including the design bases, the nuclear design of the fuel and reactivity control systems, and the analytical methods used to perform the nuclear design. Detailed analytical results for an equilibrium fuel cycle are presented at the end of this section. The equilibrium cycle is representative of a typical fuel cycle design with limits placed on the core design that are applied to the design of other cycles, including the initial and transition cycles.

Section 4.3 is divided into three sections, Design Basis (Section 4.3.1), Nuclear Design Description (Section 4.3.2), and Analytical Methods (Section 4.3.3).

4.3.1 Design Basis

The nuclear design bases for the fuel and reactivity control systems are as follows:

- The reactor core and reactivity control systems are designed with appropriate margin to assure that the specified acceptable fuel design limits (SAFDLs) are not exceeded during normal operation or anticipated operational occurrences consistent with GDC 10.
- The reactor core is designed so that in the power operating range the net effect of prompt inherent nuclear feedback tends to compensate for rapid increase in reactivity consistent with GDC 11.
- The reactor core and reactivity control systems are designed to assure that power oscillations which can result in conditions exceeding SAFDLs are not possible or can be reliably and readily detected and suppressed consistent with GDC 12.
- The reactivity control system withdrawal rate is designed to assure that SAFDLs are not exceeded for accidental withdrawal of control rods consistent with GDC 25.
- There are two independent reactivity control systems based on different design principles, control rods and soluble boron. The control rods and associated rod control system are designed with a positive means for inserting the rods and reliably controlling reactivity changes during normal operation, including anticipated operational occurrences. The control rod design provides assurance that the SAFDLs are not exceeded during an anticipated operational occurrence (AOO) assuming a single stuck control rod. CRAs, with all rods inserted, are capable of holding the reactor subcritical during normal operation, including anticipated operational occurrences, in accordance with GDC 26.
- The control rods and soluble boron system are capable of reliably controlling reactivity changes to assure that under postulated accident conditions and with appropriate margin for stuck rods the capability to cool the core is maintained consistent with Principal Design Criteria (PDC) 27. CRAs, with all rods inserted, are capable of holding the reactor subcritical under postulated accident conditions in accordance with PDC 27.
- The reactivity control systems limit the potential amount and rate of reactivity increase to assure that the effects of postulated reactivity accidents do not result in damage to the reactor coolant pressure boundary greater than limited local yielding nor impair the capability to cool the core consistent with GDC 28.

GDC 13 and GDC 20 also provide requirements that ensure that SAFDLs are met. GDC 13 is discussed in Chapters 6, 7, 8, 9, 11, and 12. GDC 20 is discussed in Chapter 7.

4.3.1.1 Fuel Burnup

Fuel burnup is a measure of the depletion of the fuel based on the energy output and is measured in GWd/MTU (gigawatt days per metric ton of uranium). Core loading patterns are developed with initial excess reactivity to maintain the core critical at full power throughout the cycle as fission products in the fuel build up and fissile material depletes. Burnable poisons and soluble boron are used to compensate for this initial excess reactivity. The end of design cycle life occurs when soluble boron is essentially zero with the control rods positioned to meet operational requirements (fully or close to fully withdrawn). In terms of boron concentration, this end of cycle condition is typically 20 ppm boron or less.

While there is no specific design limit on cycle average burnup, the core average cycle exposure is designed such that the peak fuel rod exposure is less than the approved value in the "Applicability of AREVA Fuel Methodology for the NuScale Design" topical report (Reference 4.3-3).

Section 4.2 discusses the fuel rod design bases.

Meeting the peak rod burnup limit along with the design basis in Section 4.3.1.3 satisfies GDC 10.

4.3.1.2 Negative Reactivity Feedback

The Doppler coefficient and the moderator temperature coefficient (MTC) are the two primary reactivity feedback mechanisms that compensate for a rapid reactivity increase. The Doppler coefficient is characterized by the broadening of absorption peaks with an increase in fuel temperature. The Doppler coefficient is negative for the NuScale fuel design. The MTC is a measure of reactivity feedback associated with a change in the moderator temperature, where changes in density change the neutron energy spectrum. The MTC is negative in the power operating range. The inherent Doppler reactivity characteristics of the fuel provide rapid negative reactivity effects with an increase in fuel temperature. A corresponding increase in moderator temperature which decreases moderator density, provides additional, but slower negative reactivity feedback. The power coefficient, which includes the effects of both the Doppler coefficient and MTC, is discussed in Section 4.3.2.3.3 and is negative for all power levels.

The MTC and the Doppler coefficient together provide inherent reactivity control and satisfy GDC 11.

The moderator and Doppler effects are discussed in more detail in Section 4.3.2.3.

4.3.1.3 Power Distribution

The power distribution and the reactor protection system are designed to ensure that the following SAFDLs are met at a 95 percent probability at a 95 percent confidence level:

- Fuel will not exceed the critical heat flux limits under normal operating and anticipated operational occurrences as described in Section 4.4.
- Peak fuel power under abnormal conditions, including the maximum overpower condition, will not result in fuel melting as discussed in Section 4.4.
- Fuel management is such that the values of fuel rod power and burnup meet the fuel rod mechanical integrity assumptions in Section 4.2.
- Fuel is not operated at a linear power density greater than the design limit for the fuel.

These restrictions along with the burnup restriction in Section 4.3.1.1 satisfy GDC 10. The power distribution limits are discussed in more detail in Section 4.3.2.2.

4.3.1.4 Maximum Controlled Reactivity Insertion

The NuScale design places limits on the worth of the control rod assemblies (CRAs), CRA insertion depth, and maximum CRA withdrawal rate. The maximum controlled reactivity addition rate is limited, such that the SAFDLs are not violated during normal operation, AOOs, or postulated accidents.

For an accidental withdrawal of a bank of CRAs or a single CRA, the maximum withdrawal rate is established such that critical heat flux (CHF) limits are not exceeded as discussed in Section 15.4, consistent with GDC 25. The design maximum rod withdrawal rate is 15 inches/minute as described in Section 3.9.4.1.

The maximum worth of the CRAs and the limits on CRA insertion preclude rupture of the reactor coolant pressure boundary due to a rod withdrawal or rod ejection accident (Section 15.4). The design basis presented in this section satisfies GDC 28. Control rod worth is discussed in more detail in Section 4.3.2.5.

4.3.1.5 Shutdown Margin and Long Term Shutdown Capability

The NuScale design employs two independent means for reactivity control: CRAs and soluble boron. The concentration of soluble boron in the reactor coolant system (RCS) is controlled by the chemical and volume control system (CVCS). These two reactivity control systems satisfy the portion of GDC 26 that requires two independent reactivity control systems of different design principles. Each of the two independent means of reactivity control is capable of controlling the reactivity changes resulting from planned, normal operation.

Shutdown margin (SDM) is defined as the instantaneous amount of reactivity by which the reactor is subcritical, or would be subcritical from its present condition, assuming all CRAs are fully inserted with the highest worth CRA assumed stuck out of the core. Shutdown margin is maintained in accordance with the technical specifications for all

modes of operation, including: operations, hot shutdown, safe shutdown, transition, and refueling. For the operations mode, the technical specification for SDM is based on the limit used for safety analysis. A comparison between the SDM limit used for safety analysis and the available SDM for the equilibrium fuel cycle is presented in Section 4.3.2.5.

During power operations, the CVCS is used to adjust soluble boron concentration to account for reactivity changes due to core burnup and due to power maneuvering, in order to maintain the CRAs within the power dependent insertion limits (PDIL). The PDILs ensure that sufficient SDM is maintained. Using soluble boron preserves the capability of the CRAs to rapidly reduce power and protect fuel design limits upon a reactor trip, and provides a means for controlling the rate of reactivity changes resulting from planned, normal power changes (including xenon burnout) to assure SAFDLs are not exceeded.

For AOOs, rapid CRA insertion after a reactor trip provides protection of fuel design limits. Consistent with GDC 26, the calculation of SDM includes a provision for the highest worth CRA remaining fully withdrawn from the core.

For postulated accidents comprised of infrequent events and accidents as described in Section 15.0, rapid CRA insertion after a reactor trip provides protection of the core. As with AOOs, the CVCS is used to adjust soluble boron concentration and maintain SDM prior to the event. Thus, for postulated accidents, the combined capability of the CVCS and CRAs control reactivity and ensures that the capability to cool the core is maintained as described in Section 15.0. CRAs reliably control reactivity changes after a postulated accident without the need for poison addition.

For design basis events (DBE), the insertion of all CRAs provides the safety related means to shut down the reactor and maintain it in a shutdown condition. Long term shutdown capability is defined as the amount of reactivity by which the reactor is subcritical or would be subcritical from its present condition assuming all CRAs are fully inserted and the RCS is cooled to equilibrium conditions. Long term shutdown capability is evaluated assuming that the core is xenon-free, no decay heat or voiding is present, and equilibrium samarium is accounted for. Insertion of all CRAs satisfies the portion of GDC 26 and PDC 27 requiring that one of the systems shall be capable of holding the reactor core subcritical under cold conditions.

Conservative analysis indicates that a return to power could occur following a reactor trip under the condition that the highest worth CRA does not insert, coincident with the CVCS system being unavailable. The probability of such a return to power is insignificant because the probability of failure of a CRA to insert and the CVCS being unavailable is less than 1E-5 per reactor year. Furthermore, even in a return to power scenario, fuel damage does not occur because the resultant power level is limited and the associated heat generated is within the capacity of the passive heat removal system, as discussed in Section 15.0.6.

LOCA events can result in condensation of unborated water in the CNV and RPV downcomer once the steam generator tubes become uncovered. The ECCS actuation signals on high CNV level and low RCS pressure are specifically designed to ensure ECCS actuation occurs prior to the development of conditions that could result in a core dilution event following ECCS actuation. For small RCS leaks where ECCS actuation

setpoints are not reached within 72 hours, boron mixing is maintained through diverse flow paths until RPV level drops below the riser holes. After the riser holes are uncovered, some downcomer dilution may occur, however, core boron concentration remains above the initial RCS boron concentration. This function supports the exemption to GDC 33 discussed in Section 6.3 and Section 9.3.4.1.

In some Non-LOCA scenarios, DHRS can cool the RCS such that the level drops below the top of the riser and the natural circulation loop is interrupted. Without natural circulation flow, condensation of steam could reduce the downcomer boron concentration. Diverse flow paths through four holes located in the riser promote mixing to preclude positive reactivity insertion when natural circulation is restored. The riser holes are located at the SG midpoint, which is below the level resulting from RCS fluid contraction from DHRS cooldown. The method for evaluating the flow through the riser holes is described in Section 15.0.5.

4.3.1.6 Stability

The design of the reactor and associated systems, and the administrative controls on CRA position provide an inherently stable core with respect to axial and radial power stability.

In addition, oscillations in core power can be readily detected by the fixed in-core detector system which continuously monitors the core flux distribution.

The stability analyses are provided in Section 4.3.2.7.

This stability design satisfies GDC 12.

4.3.2 Nuclear Design Description

4.3.2.1 Nuclear Design Description

The NuScale core design is comprised of 37 fuel assemblies, each arranged in a 17x17 lattice and containing 264 fuel rods, 24 CRA guide tubes, and one central instrumentation tube. The fuel rods are supported by five spacer grids; each fuel rod consists of a column of stacked, cylindrical ceramic pellets of enriched uranium dioxide (UO_2) with gadolinium oxide (Gd_2O_3) as a burnable absorber homogeneously mixed within the fuel in selected locations. The fuel pellets are encapsulated in M5® cladding (a zirconium-based alloy) with an active fuel length of 78.74 inches. The fuel is enriched up to 4.95 percent.

Sixteen (16) of the fuel assembly positions contain CRAs. The CRAs are organized into two banks: a regulating bank and a shutdown bank. The regulating bank contains two groups of four (4) CRAs arranged symmetrically in the core. The regulating bank groups are used during normal plant operation to control reactivity and provide axial power shaping. The shutdown bank contains two groups of four (4) CRAs. The shutdown bank is fully withdrawn during power operation. The shutdown bank is used in the event of a reactor trip and to maintain the reactor shutdown. Each CRA contains 24 individual rods fastened at the top end to a common hub or spider. The rods contain two neutron absorbers, silver-indium-cadmium at the bottom of the rod, and boron carbide (B_4C) in the upper portion of the rod. The CRA rods are clad with stainless steel. More information on the fuel and CRAs is provided in Section 4.2 and Section 4.6.

Power dependent insertion limits restrict the amount by which the two regulating bank groups can be inserted at power. When the regulating groups are inserted, both groups in the regulating bank move together until the Group 2 PDIL is reached. Once both groups reach the Group 2 PDIL, Group 1 can insert further, up to the Group 1 PDIL. When the CRAs are withdrawn, Group 2 cannot be withdrawn from the Group 2 PDIL limit until Group 1 has been withdrawn to meet Group 2. From there, both regulating banks move together for the remainder of the withdrawal. The PDILs are shown in Figure 4.3-2.

The fuel cycles are nominally two years and equivalent to a 12 GWd/MTU cycle length. The nuclear design includes axial and radial enrichment zoning within an assembly. Each fuel rod has a reduced enrichment axial blanket at the top and bottom, with a central fully enriched zone. Assemblies may also incorporate radial zoning to ensure that the peak power rod in any assembly is not on the assembly periphery.

The reload fuel management scheme places fresh fuel on the periphery of the core and shuffles burned fuel into the middle of the core in an "out-in" approach. The "out-in" fuel management, in conjunction with NuScale's heavy reflector design, lowers power peaking and maximizes thermal margin. In this scheme, the maximum power does not reside in the central assemblies and a flatter radial power distribution across the core is achieved. This approach provides for analysis and operational simplicity compared to the more traditional low-leakage core loading patterns. Additionally, the "out-in" approach minimizes the burnable poison loading requirement because of the inherently flatter power distribution. As a result, boron concentration and power peaking are usually greatest at the beginning of the cycle.

The NuScale reactor is designed with a heavy reflector (Figure 4.3-25) to improve neutron economy. The reflector is made of stainless steel, which reflects fast neutrons back into the core and flattens the power distribution to improve fuel performance. The reflector is located between the core periphery and the core barrel and provides the core envelope and directs flow through the core.

The soluble boron concentration is adjusted throughout the cycle to compensate for the reactivity changes due to fuel burnup, fission product poisoning, and burnable poison depletion. The higher concentration at beginning of cycle balances the excess reactivity that is designed into the cycle to achieve the nominal two-year cycles. The equilibrium cycle has an initial boron concentration of 1235 ppm.

Burnable poison in the form of gadolinia (Gd_2O_3) is used in strategic locations within the fuel assemblies. The gadolinia is homogeneously mixed with the UO_2 in selected fuel rods to provide a favorable radial power distribution, hold down reactivity, and minimize power peaking within an assembly. Although gadolinia is physically compatible with UO_2, its addition to the fuel degrades some of the material properties of the UO_2. For this reason, fuel containing gadolinia is limited to a lower power generation rate than fuel containing only UO_2 based on consideration of centerline melting.

The equilibrium cycle is the reference for which analysis is presented in this section. The exact loading patterns, the initial and final positions of assemblies, and the number of fresh assemblies and their placement will ultimately depend on the energy

requirements and the specific power history of the individual cycle. The loading pattern for the reference equilibrium cycle is shown in Figure 4.3-1.

Table 4.3-1 and Table 4.3-2 summarize the reactor core design parameters used in the analysis. Table 4.3-5 summarizes the plant operating modes for the NuScale design.

4.3.2.2 Power Distribution

Power distribution calculations are discussed in the "Nuclear Analysis Codes and Methods Qualification" topical report (Reference 4.3-1). This report contains a discussion of power distribution uncertainty, including application and a means for updating the uncertainty values.

4.3.2.2.1 Definitions

Maximum $F_{\Delta H}$

The maximum enthalpy rise hot channel factor, $F_{\Delta H}$, is defined as the ratio of the maximum integrated fuel rod power to the average fuel rod power. The limit on $F_{\Delta H}$ is established to ensure that the fuel design criteria are not exceeded and the accident analysis assumptions remain valid. This limit ensures that the design basis value for the CHF ratio is met for normal operation, anticipated operational occurrences, and infrequent events. The $F_{\Delta H}$ limit is representative of the coolant flow channel with the maximum enthalpy rise. This channel has the highest power input to the coolant and therefore the highest probability for CHF.

The NuScale design limit for $F_{\Delta H}$ is 1.50 and is based on the safety analysis.

Maximum F_Q

The heat flux hot channel factor (or total peaking factor), F_Q, is the ratio of maximum local heat flux on the surface of a fuel rod to the average fuel rod heat flux for the entire core. The maximum F_Q value is used to calculate the peak linear heat generation rate (LHGR). The maximum value of F_Q is used to ensure the specified acceptable fuel design limit for fuel centerline melting is not exceeded.

Axial Peaking Factor F_z

The axial peaking factor, F_z, is the maximum relative power at any axial point in a fuel rod, divided by the average power of the fuel rod.

Engineering Hot Channel Factor, F_E

The engineering heat flux hot channel factor, F_E, accounts for manufacturing tolerances on such parameters as enrichment, pellet density, and pellet diameter.

Measurement Uncertainty Factor, F_M

The measurement uncertainty factor, F_M, accounts for the measurement error associated with power distribution predictions. F_M is accounted for in the nuclear

reliability factor (NRF) determined for F_Q. The NRF is discussed in more detail in Section 4.3.2.2.7 and in Reference 4.3-1.

Additional uncertainties on the limiting $F_{\Delta H}$ value which is used in the CHF ratio calculation are included in the subchannel analysis discussed in Section 4.4.

Peak Linear Heat Generation Rate

The peak LHGR is the maximum heat flow per unit length of the fuel rod. A design limit is placed on the peak LHGR to ensure that the fuel performance limitations are not exceeded.

Axial Offset

Axial offset (AO) is the ratio of the difference in power between the top half of the core and the bottom half of the core to the total core power as shown in the equation below:

$$\text{Axial Offset (fraction)} = \frac{\text{Power in Top of Core} - \text{Power in Bottom of Core}}{\text{Total Power in Core}} \quad \text{Eq. 4.3-1}$$

The axial offset window is defined as a function of reactor power and the AO analytical limit is provided in Figure 4.3-3.

The AO typically becomes more negative during a cycle and also as power increases from hot zero power (HZP) to full power.

4.3.2.2.2 Radial Power

The core radial power distribution is a function of the core loading pattern, control rod pattern, control rod insertion, and location of fresh and burned fuel assemblies.

Figure 4.3-4, Figure 4.3-5, and Figure 4.3-6 show the total and radial peaking factors (F_Q and $F_{\Delta H}$) at the beginning of cycle (BOC), the middle of cycle (MOC), and at the end of cycle (EOC) as a function of power level based on a nominal cycle depletion with all CRAs out, followed by an instantaneous insertion of the regulating bank CRAs to the PDIL. As can be seen from the results, the peaking factors are higher with CRAs inserted to the PDIL. Also, peaking factors generally decrease as the cycle proceeds.

Figure 4.3-11 provides the fuel assembly relative radial power distribution at BOC, MOC, and EOC. A conservatively flat power distribution within the fuel assembly is assumed in the CHF subchannel analysis as described in Section 4.4.

4.3.2.2.3 Assembly Power

A typical radial power distribution within a fuel assembly relative to average core power is shown in Figure 4.3-7. This pin-by-pin power distribution is for a center fuel assembly at BOC and EOC for the equilibrium cycle.

Figure 4.3-8, Figure 4.3-9, and Figure 4.3-10 show a pin-by-pin power distribution relative to average core power for a first batch (fresh), second batch (once burned), and third batch (twice burned) fuel assembly. These are also shown for BOC and EOC. In the case of the central assembly, the power distribution within the assembly is symmetric. For the non-central assemblies, the power distribution within the assembly is non-symmetric.

4.3.2.2.4 Axial Power

The axial power shape is influenced by the position of the regulating bank, the moderator density, fission product distribution, fuel burnup, and the Doppler effect. An axial offset window is developed that encompasses axial offsets achievable during normal operation by considering depletion over various durations. The depletions consider different power levels and CRA insertions. Swings in axial xenon distribution and concentration resulting from these CRA insertions and withdrawals produce a wide range of axial offsets to be enveloped by the AO window. The range of axial power shapes that may be achieved while operating within allowed conditions is also used to evaluate the appropriateness of the AO window. During an operating cycle, the axial offset is maintained within the analytically based AO window (see Figure 4.3-3) by controls specified in the Technical Specifications. The axial power shape can also be determined from the in-core instrumentation system described in Section 4.3.2.2.9.

Figure 4.3-12 provides the core average axial power shape for the equilibrium cycle at BOC, MOC, and EOC. The effect of neutron absorption by the spacer grids can be observed in the power shapes in the figure.

4.3.2.2.5 Local Power

Fuel densification has been observed in nuclear power plants due to irradiation. Densification causes the fuel pellets to shrink and in some cases results in gaps in the fuel column. These gaps, if significant, can cause reduced neutron absorption and can result in power peaking in nearby rods. Modern fuel designs and manufacturing practices have eliminated this phenomenon. No penalty is taken for local power spikes due to fuel densification in the NuScale fuel design.

4.3.2.2.6 Limiting Power Distributions

Limiting power distributions are used for the steady state and transient analyses that are performed in Section 4.4 and Chapter 15.

Radial Power Distribution

The radial power distribution is primarily determined by the cycle design.

For each cycle core design, a limit is imposed on the maximum allowed $F_{\Delta H.}$ This design limit is then conservatively applied in the subchannel analysis as described in Section 4.4. Except for events in Section 15.4 (Reactor and Power Distribution Anomalies) that do not involve CRA motion, radial power distributions are held

constant through the evolution of the transient. Additionally, for Section 15.4 events that do involve CRA motion the radial power shapes account for the possible radial asymmetry of the event and radial power information specific to each event is provided for the subchannel analysis.

Axial Power Distribution

The core average axial flux shape (F_Z) can be affected by operator action. The core average axial power profile can experience significant and rapid changes because of control rod motion and load changes, and slower changes because of changes in the xenon distribution and cycle burnup.

An analysis of the possible axial power shapes is performed to identify the bounding axial power shapes for use in the CHF and transient analyses. These shapes are generated as a function of cycle burnup, control rod position, xenon distribution, and core thermal-hydraulic conditions. Bounding axial power shapes are held constant through the evolution of transients analyzed in Chapter 15, with the exception of some events in Section 15.4 that involve CRA motion. The axial power shapes for these Section 15.4 events account for the change in axial shape caused by the movement of one or more CRAs, as characterized by the event.

The specific assumptions related to power distribution used in the steady state and accident analysis for power distribution are described in more detail in Section 4.4 and Chapter 15. The values of $F_{\Delta H}$ and F_z are conservatively selected for use in the transient analysis such that they are expected to be bounding for all cycles. If the calculated power distributions for a given cycle are not bounded by the values assumed in the accident analysis, the core design is revised to bring the calculated power distribution within the bounding value or the transient analysis is reperformed.

The limiting power distributions are confirmed during operation by technical specifications that require operation within the AO window and within the PDILs. In addition the fixed in-core flux measurements and resulting power distribution that continuously display in the control room provide further assurance that the power distributions both axially and radially are not deviating from those expected and assumed in the analysis.

4.3.2.2.7 Verification of Power Distribution Analysis

The NuScale analytical methods have been benchmarked against other higher-order computer codes, experimental reactors, and against measured data from operating commercial reactors. The results of the benchmarking are discussed in detail in Reference 4.3-1 and are used to derive NRFs. The NRF accounts for calculational error in the nuclear methods and ensures conservatism in the safety-related application of the parameter. The NRFs may be adjusted as measurements are collected and benchmarked against the nuclear methods.

4.3.2.2.8 Testing

A startup testing program is implemented for the initial startup to confirm that the nuclear design analyses are in agreement with predictions. The initial startup program is described in Section 14.2. Since not all limiting situations can be created at the beginning of core life (BOL), the main purpose of the tests is to provide confirmation of the calculation methods used for predicting the test conditions. Tests performed at the beginning of each reload cycle verify the selected safety-related parameters of the reload design.

The purpose of startup physics testing (low-power testing and power-ascension testing) is to measure the neutronic characteristics of the core and compare those measurements with predictions to verify that the core is operating as designed, validate the analytical models, and verify the correctness or conservatism of assumptions used in the safety analyses. Also, as discussed in Section 4.3.2.2.7, the comparison between measured and calculated values during start-up testing is used to assess the continued applicability of the NRF values, or the data is used to update the NRF values depending on the agreement between the measured and calculated values.

There are five characteristics that must be confirmed for each newly loaded core:

- reactivity balance
- reactivity control
- power distribution
- shutdown capability
- shutdown requirement

The reactivity balance is confirmed by the measurement of the HZP all rods out (ARO) boron concentration. Agreement between the measured value and the predicted value means that the total amount of fissile material and absorbing material in the core is consistent with the design. Reactivity control is determined by measurement of the HZP isothermal temperature coefficient (ITC) and comparison to the predicted value. Agreement means that the response of the core to temperature changes is consistent with the design. Power distributions are confirmed by measuring the neutron flux throughout the core at low, intermediate, and higher power levels and comparing the measurements to design predictions. The power distribution at lower power levels must be confirmed before increasing to higher power levels. Control rod worth measurements confirm the capability of the core to be shut down, and the shutdown requirement is confirmed by measuring the power defect (reactivity difference between zero power and full power).

Additional detail on startup physics testing is provided in Reference 4.3-1.

4.3.2.2.9 Monitoring

The in-core instrumentation system (ICIS) continuously monitors core neutron flux distribution and core inlet and outlet temperatures. The core neutron flux information is provided to the module control system to ensure that power distribution is in agreement with predictions. The core inlet and outlet temperature information is provided to the module protection system to ensure that adequate core cooling is being provided for post-accident conditions.

During normal operation, the ICIS is used to synthesize core-wide three-dimensional power distributions. These power distributions are compared to predicted core power distributions to verify the core is operating as designed. Axial power distributions are continuously monitored to validate the AO operating window, and actions required by the technical specifications are initiated based on this information. Also, power distributions from the ICIS are used to calibrate the ex-core neutron flux detectors. When the rod position indication system is not working properly, the ICIS has the capability to determine the relative position of a stuck or misaligned control rod.

The ICIS processes raw input signals from the in-core neutron flux detectors and sends the processed signals to the module control system which uses algorithms to determine the three-dimensional power distribution. The module control system displays this information to the operators. The module control system provides alarms to alert the operators to power distributions that are approaching limits.

During reactor startup, the in-core neutron flux detectors are used to verify proper fuel loading, calibrate the ex-core detectors, measure core peaking factors, and confirm core behavior. During normal power operation, the ICIS is used to measure the power distribution to ensure the peaking factors are within limits.

During post-accident conditions, the core inlet and core outlet thermocouples are used to monitor adequate core cooling and provide the operating staff information to assist them in monitoring critical safety functions.

The ICIS uses self-powered neutron detectors (SPNDs) that require no external power supply. SPND type instrumentation has been widely used in the industry for over 40 years. The self-powered neutron detectors are designed to withstand design temperatures and pressures.

The ICIS instrument strings operate in twelve (12) core locations. The reactor vessel internals provide guide tubing and structural support for the ICIS instrument strings to be properly inserted and retracted when appropriate. The 12 ICIS instrument strings are inserted at the beginning of the cycle and remain in place until the end of the cycle. The ICIS instrument strings are withdrawn for refueling. Figure 4.3-18 shows the 12 in-core locations, designated as ICI1 through ICI12. The in-core instrument strings are inserted in the center instrument tube location of a fuel assembly.

During startup, the core inlet and core exit thermocouples are calibrated against the reactor coolant system narrow- and wide-range temperature measurements.

The neutron flux detector synthesized power distribution is compared against analytical predictions.

The ICIS is comprised of four SPNDs that are fixed in evenly-spaced axial positions; they are placed in twelve well-distributed fuel assembly locations in the core with a spatial density comparable to other plants in the industry that use fixed in-core detectors. The NuScale SPND detector signals occur from neutron activation, generating an electrical current proportional to the incident neutron flux. These signals are then synthesized into three-dimensional assembly and peak rod power distributions through the use of pre-fit coefficient data from detailed SIMULATE5 code calculations. Core power and peak rod power distributions are continuously updated from SPND signals in the control room, and verified to remain within Technical Specification Limiting Condition for Operations (LCOs).

The following uncertainties are considered in the determination of the power distribution:

- Uncertainty in the measured detector signal
- Uncertainty in the relationship between the detector signal and power
- Uncertainty in the predicted relationship between assembly power and peak rod power

4.3.2.2.10 Power Distribution Controls

Design basis events are analyzed from bounding initial conditions and analytical limits. Operation within these bounding conditions and analytical limits is ensured using a variety of mechanisms including TS Limiting Conditions for Operation (LCOs), continuous monitoring, and surveillances. Operation within the limiting power distributions is ensured by the following:

- Position of the shutdown and regulating CRA banks is determined via the rod position indication system; operation of the regulating bank within the PDILs and operation of both banks within the TS modes is ensured via a pre-defined limit and control room alarms as the limit is approached.
- Axial offset is surveilled by continuous monitoring of the flux and power distribution; axial offset is an LCO and alarms are used to indicate if the AO window limit is approached.
- CRA alignment is an LCO.
- In addition to power distributions, the core pressure, flow rate, and temperature are continuously monitored and used to verify LCO limits on $F_{\Delta H}$.

The collective combination of administrative controls, continuous monitoring, and alarms provides assurance that analytical limits are not exceeded and the most limiting power distributions assumed for analysis of design basis events remain bounding.

4.3.2.3 Reactivity Coefficients

The kinetic characteristics of the reactor core determine the core response to a change in plant conditions or to operator adjustments made during normal operation, as well as the core response during AOOs or accidents. These kinetic characteristics are quantified in the reactivity feedback coefficients. The reactivity coefficients reflect the changes in the neutron multiplication due to varying plant conditions, such as thermal power, moderator and fuel temperatures, flow rates, or soluble boron concentration. Since reactivity coefficients change during the cycle, ranges of coefficients are employed in transient analysis to determine the response of the plant throughout life. The results of these analyses and the reactivity coefficients used are presented in Chapter 15.

The reactivity coefficients are calculated with approved nuclear methods. These methods are described in Section 4.3.3. These models and methods have been qualified and benchmarked for core design and analysis as described in Reference 4.3-1.

The effect of radial and axial power distribution is implicit in the reactivity coefficient calculations.

4.3.2.3.1 Doppler Coefficient

The Doppler fuel temperature reactivity coefficient is a measure of the reactivity change associated with a change in fuel temperature. The Doppler coefficient is also referred to as the Fuel Temperature Coefficient. The Doppler coefficient is negative for the NuScale design. The decrease in reactivity with increasing temperature is due the Doppler broadening of ^{238}U and ^{240}Pu resonance absorption peaks. The Doppler coefficient is calculated by uniformly perturbing the fuel temperature. The variation in Doppler coefficient is small over the range of exposure, power level, flow, and temperatures of the NuScale core. The Doppler coefficient becomes more negative as a function of burnup as the ^{240}Pu content increases, thereby increasing the effective ^{240}Pu resonance absorption. The Doppler coefficient is calculated for a range of fuel temperatures by varying the time in cycle, coolant temperature, and power level, with the regulating bank in both the ARO and PDIL positions. Table 4.3-6 demonstrates the range of the Doppler coefficient over this spectrum of parameters.

4.3.2.3.2 Moderator Coefficients

The MTC is a measure of the relative change in reactivity associated with a change in moderator temperature. The MTC is calculated over the range of powers and burnup by increasing the moderator temperature by 5 degrees Fahrenheit above the mean temperature. The calculation of MTC includes the effects of moderator density changes.

The MTC is constrained by design, operational practices, and administrative controls to be negative during power operations so that increases in moderator temperature in the core are accompanied by decreased reactivity.

The primary parameters that affect MTC are soluble boron concentration, burnup, burnable poison, CRA position, and power level. At the higher soluble boron concentrations, the effect of increasing temperature (and decreasing moderator density) results in decreased boron density, which tends to increase reactivity, making the MTC more positive. The maximum MTC typically occurs at the beginning of a cycle at low power levels. Burnup tends to make the MTC more negative because of the decrease in boron concentration and buildup of plutonium and other fission products. The minimum MTC is typically achieved at the end of a cycle.

The MTC is shown in Figure 4.3-13 and Figure 4.3-14 for a range of moderator temperatures at full power and at zero power for the reference equilibrium cycle. While the MTC may be slightly positive at some conditions, as discussed in Section 4.3.2.3.3, the power coefficient is negative at all power levels.

The moderator pressure coefficient is a change in reactivity in relation to a change in reactor coolant pressure. A change in pressure causes a change in reactivity through a change in the coolant density.

The effects of voiding are accounted for in the density portion of the MTC.

The isothermal temperature coefficient (ITC) is the change in reactivity due to the combined change in core average moderator and fuel temperature when the temperature is uniform across the core. This is distinguished from the MTC which is the change in reactivity due to a change only in moderator temperature. The ITC is important because it is the quantity that can be measured in the plant and is used to develop the NRFs for MTC as described in Reference 4.3-1.

4.3.2.3.3 Power Coefficient

The power coefficient is the sum of the moderator temperature, fuel temperature, and void coefficient, and is measured over the percent change in power. The power defect is the sum of the reactivity contributions of each of these feedback mechanisms for a cumulative change in power down to 0 percent power. A three-dimensional calculation is performed in determining total power coefficients and total power defects, and as a result, axial redistribution is implicitly included.

The maximum and minimum power defect for a typical equilibrium cycle is shown in Figure 4.3-15. The maximum and minimum power coefficient is shown in Figure 4.3-16. As can be seen from Figure 4.3-16, the power coefficient is negative at all power levels.

4.3.2.3.4 Boron Worth Coefficient

The boron worth coefficient is a measurement of the change in reactivity associated with a change in the boron concentration. The boron worth coefficient for the equilibrium cycle is provided in Figure 4.3-21.

4.3.2.3.5 Flow Coefficient

The flow coefficient of reactivity is a measure of the relative reactivity change associated with a core flow change. The flow coefficient is determined by calculating the change in reactivity that results from a perturbation of the core average flow. This coefficient is determined at BOC, MOC, and EOC, and for a number of initial power levels, both in ARO and PDIL CRA configurations. Results for minimum and maximum flow coefficient are shown in Figure 4.3-22.

4.3.2.3.6 Comparison of Calculated and Experimental Reactivity Coefficients

A comparison of calculated and experimental reactivity coefficients is provided in Reference 4.3-1.

Uncertainty factors developed from the reactivity coefficient comparison results are used to derive NRF as described in Reference 4.3-1.

Reactivity coefficients are verified during startup testing.

4.3.2.3.7 Reactivity Coefficients in Transient Analysis

The reactivity coefficients, specifically the moderator temperature and Doppler coefficients, are analysis inputs to Chapter 15 transients.

The bounding values are used as design limits in the transient analysis. The exact values of the coefficient used in the analysis depend on whether the transient of interest is examined at the beginning of life or end of life, whether the most negative or the most positive (least negative) coefficients are appropriate to provide conservatism, and whether spatial non-uniformity must be considered in the analysis. Conservative values of coefficients, considering various aspects of analysis, are used in the transient analysis. The details and assumptions for each transient are described in Chapter 15.

The conservative values for reactivity coefficients are selected in such a way that the need for a reevaluation of any accident in a subsequent cycle is minimized. However, if the coefficients fall outside of the conservatively selected values, the core design is changed or reanalysis of the transient is performed.

The list of limiting physics parameters, and the direction that is conservative for each Chapter 15 event is provided in Reference 4.3-1.

4.3.2.4 Control Requirements

Soluble boron is added to the coolant to maintain the required SDM when a cooldown to ambient conditions is required. Table 4.3-2 shows the boron concentrations for various core conditions for the equilibrium cycle.

The CRAs are required to provide negative reactivity to account for the power defect from full power to zero power and to provide the required SDM, assuming the highest worth CRA is stuck out of the core. The reactivity addition resulting from power

reduction includes contributions from Doppler, moderator temperature, flux redistribution, and reduction in voids as discussed in the following sections. The CRAs, with all control rods inserted, provide negative reactivity to maintain long term shutdown capability. Reactivity addition accounted for when evaluating long term shutdown capability includes power defect (from full power to zero power), change in moderator temperature during cooldown and xenon decay as discussed in the following sections. The ability to accomplish shutdown and to maintain long term shutdown capability is demonstrated in Table 4.3-3 and Table 4.3-4 for BOC, MOC, and EOC conditions for the reference equilibrium cycle. The SDM and long term shutdown capability include an uncertainty of 12 percent in the CRA worth. This uncertainty is discussed and shown to be acceptable in Reference 4.3-1.

4.3.2.4.1 Doppler Effect

The Doppler effect is the result of the narrowing of the ^{238}U and ^{240}Pu resonance cross-sections as the fuel temperature decreases. This effect is most noticeable over the range of full power to zero power due to the significant decrease in fuel pellet temperature over the full power range.

4.3.2.4.2 Moderator Temperature

The moderator temperature decreases significantly from 100 percent to 0 percent power. When the MTC is negative, reactivity is added with power reduction. Since the MTC becomes more negative with fuel depletion, this has a significant effect on SDM at the EOC and the long term shutdown capability is also affected.

4.3.2.4.3 Flux Redistribution

During normal operation, the coolant density decreases with higher elevation in the core. This density profile results in less fuel depletion near the top of the core, resulting in an axial power distribution skewed slightly towards the bottom of the core. At HZP, the coolant density is uniform and the power distribution is skewed towards the top of the core. Since a three-dimensional calculation is performed in determining the total power defect, flux redistribution is inherently included in the calculation. The bottom peaked flux shape in the beginning of the cycle results in more burnup in the bottom of the core, causing power to shift towards the top of the core at EOC.

4.3.2.4.4 Void Content

There is a very small void presence in the core due to nucleate boiling at full power and the impact of collapsing of voids on a reduction in power is minimal.

4.3.2.4.5 Rod Insertion Allowance

At power, the regulating bank is moved within a prescribed band to compensate for small changes in boron concentration, changes in moderator temperature, and small changes in xenon. When the CRAs reach the PDIL, changes in soluble boron are required to compensate for additional reactivity changes. The PDIL prevents

large axial offsets and reduces reactivity insertion for a rod ejection accident. Alarms alert the operators when the regulating bank is approaching the PDIL.

4.3.2.4.6 Excess Reactivity for Depletion

Excess reactivity is designed into the cycle to provide sufficient reactivity to compensate for fuel depletion and fission product buildup throughout the cycle. This reactivity is controlled by the addition of soluble boron to the coolant and by burnable poison that is integral with the fuel. The soluble boron concentration for several core configurations and the boron worth are given in Table 4.3-2 for the equilibrium cycle. Since the excess reactivity for burnup is controlled by soluble boron and burnable poison, it is not included in control rod requirements.

4.3.2.4.7 Xenon and Samarium Poisoning

Changes in xenon and samarium concentration take place at a slow rate and the resulting change can be controlled by changing the soluble boron concentration.

4.3.2.4.8 pH Effects

Reactor coolant system chemistry is maintained within a narrow band and changes in reactivity due to changes in coolant pH are small enough and change slowly enough to be controlled by soluble boron.

4.3.2.4.9 Experimental Confirmation

The nuclear design methods are described in Section 4.3.3. The benchmark of these methods against calculated and experimental results is provided in Reference 4.3-1.

4.3.2.4.10 Control

Core reactivity is controlled by soluble boron in the reactor coolant, CRAs, and burnable poison that is integral to the fuel pellets, as described in the following sections.

4.3.2.4.11 Soluble Boron

NuScale uses natural boron for soluble boron control. The soluble boron concentration is changed to control relatively slow reactivity changes due to:

- moderator temperature changes from ambient conditions to HZP.
- transient xenon and samarium poisoning due to planned power changes.
- reactivity effects of fissile inventory depletion and buildup of fission products.
- depletion of burnable poison.

The boron concentration variation for the reference equilibrium cycle is shown in Figure 4.3-17.

4.3.2.4.12 Control Rod Assemblies

There are 16 CRAs in the core design. The CRAs provide control and shutdown capability for:

- shutdown margin for HZP with the highest worth rod stuck out of the core.
- reactivity compensation as a result of an increase in power above HZP (power defect, including Doppler, and moderator reactivity changes).
- fluctuation in boron concentration, coolant temperature, or xenon.
- reactivity changes from load changes.
- design basis events with a stuck rod.
- long term shutdown capability.

CRA insertion is restricted to ensure that there is sufficient negative reactivity available to maintain shutdown capability and to limit the amount of reactivity insertion possible during the rod ejection accident. The PDILs are set sufficiently high to meet these criteria while also being low enough that operators have a reasonable range of CRA movement for power maneuvers. In general, deeper CRA insertion is allowed at lower power levels. Operators are alerted if the PDIL is approached. The PDILs are shown in Figure 4.3-2.

Power distribution, rod ejection, and CRA misoperation analyses are based on the arrangement of CRAs shown in Figure 4.3-18.

During a startup, the shutdown bank is withdrawn before the regulating bank withdrawal is initiated. The approach to criticality is initiated by a combination of boron dilution to the appropriate boron concentration and withdrawal of the regulating bank. Additional detail on startup is provided in Section 14.2.

4.3.2.4.13 Burnable Poisons

Gadolinia (Gd_2O_3) is used as an integral burnable absorber in selected fuel rods to provide partial control of the excess reactivity available during the cycle. In addition, the burnable absorber also reduces the requirement for soluble boron at the beginning of the cycle, eliminating the possibility of a positive MTC during power operations at the beginning of the cycle (at power). In addition, burnable absorbers reduce power peaking within the fuel assembly.

4.3.2.4.14 Peak Xenon

Startup from the peak xenon condition is accomplished using CRAs and boron dilution.

4.3.2.4.15 Burnup

Cycles are designed with excess reactivity to offset the effect of burnup during the cycle. Control of this excess reactivity is accomplished using soluble boron and burnable poison. The boron concentration is limited during operating conditions

to maintain the MTC negative. The end of a fuel cycle is reached when the soluble boron concentration approaches 20 ppm or less as discussed in Section 4.3.1.1.

4.3.2.4.16 Power Maneuvering

Power changes are normally accomplished by means of regulating CRA position or soluble boron concentration. The CRA position is limited by the PDIL and helps maintain the core within the axial offset limits. While power maneuvering operations within the capabilities of the rod control system are anticipated to support power system demands, continuous power maneuvering of the NuScale Power Module where the CRA position is used to achieve power changes was not assumed in the analysis of the representative equilibrium cycle. However, planned power maneuvers will be considered as part of a cycle-specific core design using the methodologies described in Technical Specification 5.6.3. The analysis of the impact of power maneuvering on the nuclear design will include the effects on axial and radial flux shapes that are used in the safety analysis in Chapter 15.

4.3.2.5 Control Rod Patterns and Reactivity Worth

The NuScale reactor module design utilizes 16 of the possible 37 assembly locations for CRAs. There are two CRA banks, a regulating bank and a shutdown bank. The regulating bank contains two groups of four CRAs each. The shutdown bank contains two groups of four CRAs each. Figure 4.3-18 shows the location of the CRA banks. Additional details on the CRAs are provided in Section 4.2 and Section 4.6.

The SDM is the instantaneous amount of reactivity by which the reactor is subcritical or would be subcritical from its present condition assuming all CRAs (shutdown and regulating banks) are fully inserted (while accounting for the power defect, CRAs being at the PDIL, SDM uncertainties, and flux redistribution), except for the single CRA of highest reactivity worth, which is assumed to remain fully withdrawn.

The design limit on minimum SDM is set by the safety analysis for all power levels (including HZP) and operating modes. The limit assures that there is sufficient negative reactivity following a reactor trip, under all credible operating conditions, to shut the reactor down and prevent exceeding the specified acceptable fuel design limits.

Allowable deviations due to misaligned CRAs are controlled by the technical specifications. The allowance for CRA misalignment is based on the assumed uncertainty in the rod position indication (RPI) system. The nominal RPI system performance requirement is that the position is measured within three steps (out of 224 total); the acceptable analytical CRA misalignment is six steps and accounts for abnormal operating conditions such as a failure of half the sensor coils in the system or failure of an AC power source to the RPI system.

The reactivity insertion during a reactor trip is determined from the CRA drop time and differential reactivity worth versus CRA position. The CRA position versus time of travel after rod release is provided in Figure 4.3-23. This curve is based on a calculation described in Section 4.2. The results from the CRA drop testing, described in Section 1.5.1.7, validate the use of the calculated SCRAM curve shown in Figure 4.3-23 as a conservative basis for the CRA drop time. A more conservative bounding CRA drop

time is used in the Chapter 15 analyses. The reactivity worth versus CRA position is calculated by a series of steady-state calculations at various CRA positions, assuming the CRAs are at the PDIL as the initial position in order to minimize the initial reactivity insertion rate. The CRA with the highest worth is assumed stuck out of the core, and the flux distribution is assumed to be skewed to the bottom of the core. The reactivity worth versus CRA position at BOC and EOC is provided in Figure 4.3-24.

The individual CRA worth is calculated for the reference equilibrium cycle starting from hot full power (HFP) and HZP at BOC, MOC, and EOC. In addition, individual CRA worth is also calculated with the regulating groups at the PDILs at HFP and HZP at BOC, MOC, and EOC. These best estimate results are summarized in Table 4.3-7 and Table 4.3-8. The results are calculated for all 224 steps of CRA travel. Figure 4.3-19 shows the differential CRA worth for BOC and EOC at multiple power levels for the equilibrium cycle. Figure 4.3-20 shows the integral regulating bank worth (from the PDIL).

The loss of CRA worth due to the depletion of the absorber material is negligible. A conservative calculation over a 20 EFPY CRA lifetime demonstrates that less than 2 percent of the boron in the upper portion of the CRA is lost due to depletion. The silver-indium-cadmium in the lower portion of the CRA is also evaluated for a loss of worth due to depletion and found to have an insignificant impact on the available worth of the CRAs over their lifetime. Typical reactor operation with the rods withdrawn from the core while at full power limits the potential for CRA absorber depletion. Rod worth is confirmed at the beginning of each cycle during start-up physics testing.

Past PWR operating experience has identified a phenomenon associated with potential boron build-up on the fuel rods that could affect shutdown margin. Build-up of boron in crud at the top of the core can cause the reactivity at the bottom of the core to increase. Such a redistribution of power adversely affects the worth of the CRAs. The NuScale uncertainty analysis of the CRA worth includes comparisons to operating data from existing PWRs. Also, constant monitoring of core axial offset and comparison of that offset to predicted values, identifies any build-up of boron on the cladding surface during operation. Further, post-irradiation examinations as described in Section 4.2 measure oxide build-up and crud deposition on the fuel rods to ensure that boron deposits on the cladding do not adversely affect the rod worth.

4.3.2.6 Criticality of the Reactor During Refueling

Criticality during a refueling is prevented by maintaining an effective neutron multiplication factor (k_{eff}) of 0.95 or less at all times. Refueling is performed with CRAs inserted in the fuel assemblies. Calculation of the required boron concentration for refueling assumes that the two highest worth CRAs are not inserted.

4.3.2.6.1 Criticality Design Method Outside the Reactor

Criticality of fuel assemblies outside the reactor is precluded by adequate design of fuel transfer and storage facilities and by administrative control procedures. The two principal methods of preventing criticality are limiting the fuel assembly array size and limiting assembly interaction by fixing the minimum separation between

assemblies or inserting neutron poisons between assemblies. The details of the methodology used for the fuel storage rack criticality analysis are included in Section 9.1.

4.3.2.6.2 Soluble Boron Credit

See Section 9.1.

4.3.2.7 Stability

The NuScale reactor core is designed to assure that power oscillations that can result in conditions exceeding SAFDLs are not possible and can be readily detected and suppressed. The NuScale reactor is inherently stable with regards to power oscillations due to the overall negative reactivity coefficients at power. Therefore, only xenon-induced power distribution oscillations require evaluation. There are three potential modes of oscillations that are possible in PWRs - azimuthal, radial, and axial. Azimuthal oscillations are not likely due to the inherent symmetry of the NuScale core loading pattern. Radial and axial oscillations are evaluated at BOC, MOC, and EOC for the equilibrium cycle.

The parameter used to characterize the stability of an oscillation is the stability index, which measures the rate of decay of the oscillation over the oscillation period. The rate at which the oscillation decreases is expressed by an exponential function of the form:

$$A(t) = A_0 e^{\alpha t} \qquad \text{Eq. 4.3-2}$$

Where A(t) is the time dependent oscillation amplitude (1/hr), and A_0 is the initial value, and t is time.

The oscillation stability index, α, is obtained using equation:

$$\alpha = \frac{1}{T} \ln\left(\frac{A^{n+1}}{A^n}\right) \qquad \text{Eq. 4.3-3}$$

Where T is the oscillation period (in hours), n is oscillation number.

A positive stability index indicates that the oscillations are diverging and therefore, unstable. A negative stability index indicates that the oscillations are converging, and therefore, stable. A stability index of zero indicates a neutrally stable oscillation.

There are two modes of xenon oscillation that are evaluated, axial and radial oscillations. The stability calculations are performed using the SIMULATE5 code at various times during the equilibrium cycle.

4.3.2.7.1 Axial Oscillations

The oscillations are initiated by instantaneously inserting the regulating bank to the PDIL. The axial xenon oscillations are then observed. Stability calculations are performed at various times in core life and from 25 percent to 100 percent power. The resulting stability indices are summarized in Table 4.3-9.

4.3.2.7.2 Radial Oscillations

Radial oscillations are initiated by instantaneously inserting a single CRA, which results in both radial and axial oscillations. The stability indices are shown in Table 4.3-10 and Table 4.3-11.

For both axial and radial oscillations, all stability indices are negative (i.e. stable) and the oscillation periods are large (on the order of 50 hours). The NuScale reactor is stable with respect to xenon oscillations.

The ICI system continuously monitors power distribution in the core and allows prompt detection of an axial or radial xenon oscillation.

Figure 4.3-26 shows the axial offset peaks from a typical xenon oscillation at 100 percent power at BOC. As can be seen in the figure, the oscillation is quickly damped, and a second peak is hard to distinguish, meaning the core returns to near equilibrium within one oscillation period. Figure 4.3-26 is representative of both the axial and radial behavior seen for all cases, and demonstrates the inherent stability of the NuScale core.

4.3.2.7.3 Stability Methodology Comparison with Experimental Data

As discussed in Section 4.3.2.7, SIMULATE5 calculations are used to demonstrate the NuScale core is stable with respect to axial and radial xenon oscillations. The ability of SIMULATE5 to accurately predict xenon oscillations is dependent on the code's ability to accurately predict reactivity feedback effects, including Doppler and moderator temperature feedback. Validation of the SIMULATE5 code to accurately predict xenon transient behavior is performed by modeling xenon transient behavior from operating PWRs, and comparing predictions against measured data (Reference 4.3-4). The code vendor, Studsvik Scandpower, compared SIMULATE5 predictions of transient xenon behavior from Westinghouse 3-loop PWRs Ringhals-2, Ringhals-3, and Ringhals-4. The code was used to model load follow and coast down maneuvers, and results showed the ability of SIMULATE5 to accurately predict xenon transients. The code is demonstrated to accurately predict moderator and fuel temperature reactivity effects for the NuScale core in Reference 4.3-1.

The ability of the code to predict xenon transient behavior for the NuScale design is demonstrated by the accurate predictions against measured data for operating PWRs, and the accurate predictions of reactivity feedback affects for the NuScale core.

4.3.2.8 Vessel Irradiation

The vessel irradiation and surveillance program is provided in Section 5.3.1.

The heavy neutron reflector, the core barrel, and the water annuli protect the vessel from radiation damage by attenuating neutrons originating in the core and gamma rays originating from both the core and structural components.

The Monte Carlo N-Particle transport code (MCNP6) version 1.0 is used to perform the vessel fluence calculations. The specific cross-section set used is based on ENDF/B-VII. The calculations are performed for 60 years of operation at a 95 percent capacity factor. The values are based on the reference equilibrium cycle. A cross-section view of the MCNP6 model used to calculate vessel flux is provided in Figure 4.3-25.

Neutron flux distribution values (in units of n/cm^2-sec) are summarized in Table 4.3-12. The core average flux value in Table 4.3-12 is calculated using SIMULATE5 instead of MCNP6. SIMULATE5 is used because it provides a more accurate calculation of neutron flux in the core. This SIMULATE5 calculation is based on exposure averaged axial and radial power profiles with soluble boron concentrations that correspond to the nominal middle of cycle concentration. The other Table 4.3-12 values are calculated with MCNP6 using assumptions consistent with Reference 4.3-6. The flux and radiation damage estimates are verified through the analysis of actual surveillance test samples from the irradiation surveillance program as described in Section 5.3.1. The methodology used by NuScale to calculate neutron fluence on the NPM pressure vessel and containment vessel is provided in Reference 4.3-6.

4.3.3 Analytical Methods

The NuScale nuclear analysis is performed with the Studsvik Scandpower Core Management Software simulation tools. These simulation tools include the lattice physics code CASMO5, the linkage code CMSLINK5 for nuclear data library generation, and the core simulator code SIMULATE5 for power distribution and stability calculations. These codes and the modelling methodology are described in detail in Reference 4.3-1. The SIMULATE-3K code is used for transient core physics calculations and is described in detail in Reference 4.3-5. In addition, the MCNP6 code is used to perform fluence calculations.

These codes are used to perform both steady-state and transient neutronic analyses of light water reactors for core design and input to safety analysis.

As described in Reference 4.3-1, the methodology for the design and analysis of a single core is independent of the presence of other NPMs. A conservative neutron flux attenuation analysis, which considers the barriers between modules (several feet of both borated water and concrete wall) confirms that the neutron flux contributed by the next closest NPM operating at full power has an insignificant neutronic impact on the reactor core of a neighboring NPM.

CASMO5

CASMO5 is a multi-group transport theory physics code which uses two-dimensional methods of characteristics transport theory for fuel assembly analysis and isotopic depletion. Cross sections and group constants are generated based on a wide range of potential conditions and cover several hundred energy groups and isotopes. CASMO5 uses the ENDF/B-VII cross section library. CASMO5 calculates eigenvalue results, power and flux distributions, reaction rates, and flux discontinuity factors for individual or multiple assemblies in two dimensions. Multi-group cross section and discontinuity factor data is required for the generation of a cross section library.

CMSLINK5

CMSLINK5 collects input generated by CASMO5 and compiles the data into a single binary library with functional dependencies represented in multi-dimensional matrices of data. The format of the library is readily available for downstream use in both SIMULATE5 and S3K.

SIMULATE5

SIMULATE5 performs steady-state three-dimensional reactor analysis using the multi-group nodal diffusion equation. Thermal-hydraulic capabilities are coupled to the neutronic solution and over depletion state points; neutronic and thermal-hydraulic iterations ensure convergence and agreement of operating conditions, nuclear data, power distributions, and assembly exposure. SIMULATE5 is used to perform core design and optimization, develop a neutronic characterization of the core by determining reactivity feedback coefficients and CRA worth, calculating axial and radial power and flux distributions, and calculation of other values required as input for safety analysis. SIMULATE5 is also used as input to plant monitoring systems.

CASMO5 and SIMULATE5 are used together to perform stability calculations.

S3K

S3K is used for transient reactor core analysis for calculations where time-dependent kinetic behavior is more important on small time scales. S3K has the same computational foundation as SIMULATE5 and requires a model that is initialized in SIMULATE5 as input, but has been extended for transient applications.

MCNP6

MCNP6 is a general-purpose code that can be used for neutron, photon, electron, or coupled neutron photon electron transport. The code treats an arbitrary three dimensional configuration of materials in geometric cells bounded by first and second degree surfaces and some special fourth-degree surfaces. Point-wise (continuous energy) cross section data are available with MCNP6. The MCNP6 code is a higher order code than CASMO5/SIMULATE5 and is used for code-to-code comparisons of the CASMO5, CMSLINK, SIMULATE5 suite of codes in Reference 4.3-1.

4.3.4 References

4.3-1 NuScale Power, LLC, "Nuclear Analysis Codes and Methods Qualification," TR-0616-48793, Rev. 0, August 2016.

4.3-2 Los Alamos National Laboratory, “Initial MCNP6 Release Overview - MCNP6 Version 1.0," LA-UR-13-22924.

4.3-3 NuScale Power LLC, "Applicability of AREVA Fuel Methodology for the NuScale Design," TR-0116-20825-P-A, Rev. 1, June 2016.

4.3-4 Krimer, M., G. Grandi, and M. Carlsson, "PWR Transient XENON Modeling and Analysis Using Studsvik CMS," Proceedings of 2010 LWR Fuel Performance/Top Fuel/WRFPM, Orlando, Florida, September 26-29, 2010.

4.3-5 NuScale Power, LLC, "Rod Ejection Accident Methodology," TR-0716-50350, Rev. 0, December 2016.

4.3-6 NuScale Power, LLC, “Fluence Calculation Methodology and Results,” TR-0116-20781, Rev. 1, July 2019.

Table 4.3-1: NuScale Reactor Core Description

Parameter	Value
Core	
Core diameter (in)	59.25
Active fuel height (in)	78.74
Mass of UO_2 per foot (lb/ft)	0.3172
Fuel Assemblies	
Number	37
Rod array	17x17
Fuel assembly length (in)	94
Fuel assembly pitch (in)	8.466
Fuel rod pitch (in)	0.496
Number of spacer grids	5
Grid height (in)	1.75
Number of Fuel rods	264
Number of Guide tubes	24
Number of Instrumentation tubes	1
Fuel Rods	
Number	264
Diametral gap (in)	0.0065
Cladding material	M5®
Cladding outside diameter (in)	0.374
Cladding inside diameter (in)	0.326
Cladding thickness (in)	0.024
Fill gas	helium
Fuel Pellets	
Density, % TD	96
Material	UO_2 (sintered)
Diameter (in)	0.3195
Length (in)	0.40
Control Rod Assemblies	
Number	16
Upper absorber material	boron carbide
Lower absorber material	silver-indium-cadmium
Cladding	304 stainless steel
Fill gas	helium
Burnable Absorbing Material	
Type	integral with fuel
Material	gadolinia (Gd_2O_3)
Number	Up to 32 per assembly

Table 4.3-2: Nuclear Design Parameters (for Equilibrium Cycle)

Core Average Linear Power (kw/ft)	2.5	
Total Heat Flux Hot Channel Factor	1.860	
Nuclear Enthalpy Hot Channel Factor	1.386	
Reactivity Coefficients		
	Best Estimate	Design
Doppler temperature coefficient (pcm/F)	-1.63 to -2.07	-1.4 to -2.25
Moderator temperature coefficient (HZP-HFP) (pcm/F)	0 to -32.5	+6 to -43
Boron coefficient (pcm/ppm)	-7.6 to -13.7	-10
Effective Delayed Neutron Fraction and Prompt Neutron Lifetime		
$ß_{eff}$ BOC	0.0059	
$ß_{eff}$ EOC	0.0052	
Prompt lifetime BOC (10^{-6}seconds)	18.35	
Prompt lifetime EOC (10^{-6}seconds)	21.91	
Control Rods		
CRA requirement	See Table 4.3-3	
Maximum ejected rod	See Section 15.4	
Bank Worth	BOC	EOC
Regulating bank (from the PDIL) ($)	0.630	1.261
Shutdown bank		
Boron Concentration	BOC	EOC
Design Basis Refueling	2000	2000
Reduction with fuel burnup (ppm)	See Figure 4.3-17	
Safe Shutdown, k_{eff}=0.98, Highest Worth CRA Out, No Xenon	1164	240
Refueling, k_{eff}=0.95, 2 Highest Worth CRAs Out, No Xenon	1746	736

Table 4.3-3: Reactivity Requirements for Control Rods

1.	**Control Rod Assembly Worth (pcm)**	**BOC**	**MOC**	**EOC**
a.	Total Available CRA Worth	14414	14800	15553
b.	Power Dependent Insertion Limits	381	502	663
c.	Worst Rod Stuck Out	4766	4922	5249
d.	Uncertainty	0.12	0.12	0.12
e.	Subtotal (a-b-c)*(1-d)	8154	8250	8484
2.	**Power**			
a.	Defect	1637	2595	3740
b.	Axial Redistribution	391	180	7
c.	Subtotal (a+b)	2028	2775	3747
3.	**Worth Balance**			
a.	Required Shutdown Margin	2041	2041	2041
b.	Gross Margin (1e-2c)	6126	5475	4737
c.	Net Margin to Shutdown Margin (b-a)	4085	3434	2696

Table 4.3-4: Reactivity Requirements for Long Term Shutdown Capability

1.	**CRA Worth**	**BOC**	**MOC**	**EOC**
a.	Total Available CRA, pcm	14414	14800	15553
b.	PDIL, pcm	381	502	663
c.	Uncertainty Factor	0.12	0.12	0.12
d.	Subtotal, pcm (a-b-c)*(1-d)	12349	12582	13103
2.	**Reactivity Insertion**			
a.	Defect, pcm	1637	2595	3740
b.	Axial Redistribution, pcm	391	180	7
c.	Moderator Cooling, pcm	3019	4293	5886
d.	Xenon Worth	2203	2381	2515
e.	Subtotal	7250	9449	12148
3.	**Worth Balance**			
a.	Net Margin to Critical, pcm (1d-2e)	5099	3133	955

Table 4.3-5: Modes of Operation Definition

Mode	Mode Title	k_{eff}	Average Coolant Temperature (°F)
1	Operations	≥ 0.99	> 420
2	Hot shutdown	< 0.99	≥ 420
3	Safe shutdown	< 0.99	< 420
4	Transition	< 0.95	N/A
5	Refueling	N/A	N/A

Table 4.3-6: Range of Doppler Coefficient for NuScale Design

Value	Doppler Coefficient (pcm/°F)	Time in Cycle
Maximum Doppler coefficient	-1.63	BOC
Minimum Doppler coefficient	-2.07	EOC

Table 4.3-7: Individual Control Rod Assembly Worth with Control Rod Assemblies Fully Withdrawn

Time	Condition	CRA Location	Worth (pcm)
BOC	HFP ARO	Group 2	3575.1
		Group 4	4832.3
		Group 3	4825.6
		Group 1	1352.8
MOC	HFP ARO	Group 2	3683.2
		Group 4	4967.4
		Group 3	4967.4
		Group 1	1478.9
EOC	HFP ARO	Group 2	4184.1
		Group 4	5288.6
		Group 3	5290.7
		Group 1	1781.9
BOC	HZP ARO	Group 2	3561.0
		Group 4	4824.2
		Group 3	4817.0
		Group 1	1291.2
MOC	HZP ARO	Group 2	3675.0
		Group 4	4945.4
		Group 3	4944.2
		Group 1	1364.3
EOC	HZP ARO	Group 2	4199.0
		Group 4	5257.3
		Group 3	5257.3
		Group 1	1569.8

Note: See Figure 4.3-18 for CRA Locations

Table 4.3-8: Individual Control Rod Assembly Worth with Regulating Groups Inserted to Power Dependent Insertion Limits

Time	Condition	CRA Location	Worth (pcm)
BOC	HFP PDIL	Group 2	3577.6
		Group 4	4834.3
		Group 3	4827.7
		Group 1	1361.0
MOC	HFP PDIL	Group 2	3682.6
		Group 4	4970.2
		Group 3	4970.2
		Group 1	1494.6
EOC	HFP PDIL	Group 2	4178.8
		Group 4	5289.4
		Group 3	5292.6
		Group 1	1813.6
BOC	HZP PDIL	Group 2	3564.6
		Group 4	4826.0
		Group 3	4818.9
		Group 1	1303.6
MOC	HZP PDIL	Group 2	3678.7
		Group 4	4951.9
		Group 3	4950.7
		Group 1	1389.6
EOC	HZP PDIL	Group 2	4198.8
		Group 4	5266.8
		Group 3	5268.0
		Group 1	1618.6

Note: See Figure 4.3-18 for CRA Locations

Table 4.3-9: Stability Indices for Axial Oscillation Analysis

Time-in-Life	Rated Power (%)	Stability Index (hrs^{-1})
BOC	100.00	-0.071
BOC	75.00	-0.023
BOC	50.00	-0.012
BOC	25.00	-0.005
EOC	100.00	-0.040
EOC	75.00	-0.029
EOC	50.00	-0.013
EOC	25.00	-0.005

Table 4.3-10: Stability Indices for Radial Oscillation due to Radial Perturbation

Time-in-Life	Rated Power (%)	Stability Index (hrs^{-1})
BOC	100.00	-0.074
BOC	75.00	-0.101
BOC	50.00	-0.090
BOC	25.00	-0.095
EOC	100.00	-0.090
EOC	75.00	-0.082
EOC	50.00	-0.071
EOC	25.00	Stable

Table 4.3-11: Stability Indices for Axial Oscillation due to Radial Perturbation

Time-in-Life	Rated Power (%)	Stability Index (hrs^{-1})
BOC	100.00	-0.063
BOC	75.00	-0.011
BOC	50.00	-0.005
BOC	25.00	-0.002
EOC	100.00	-0.013
EOC	75.00	-0.017
EOC	50.00	-0.006
EOC	25.00	-0.002

Table 4.3-12: Typical Fast Neutron Flux Levels (n/cm^2-sec) in the Reactor Core and Reactor Pressure Vessel at Full Power

Location	E $\geq$ 1.0 MeV
Core average	3.41E+13
Reflector block at mid-height	2.81E+13
Upper core plate	1.34E+11
Lower core plate	1.12E+12
Pressure vessel inside diameter azimuthal peak	9.57E+09

Figure 4.3-1: Loading Pattern for Reference Equilibrium Cycle

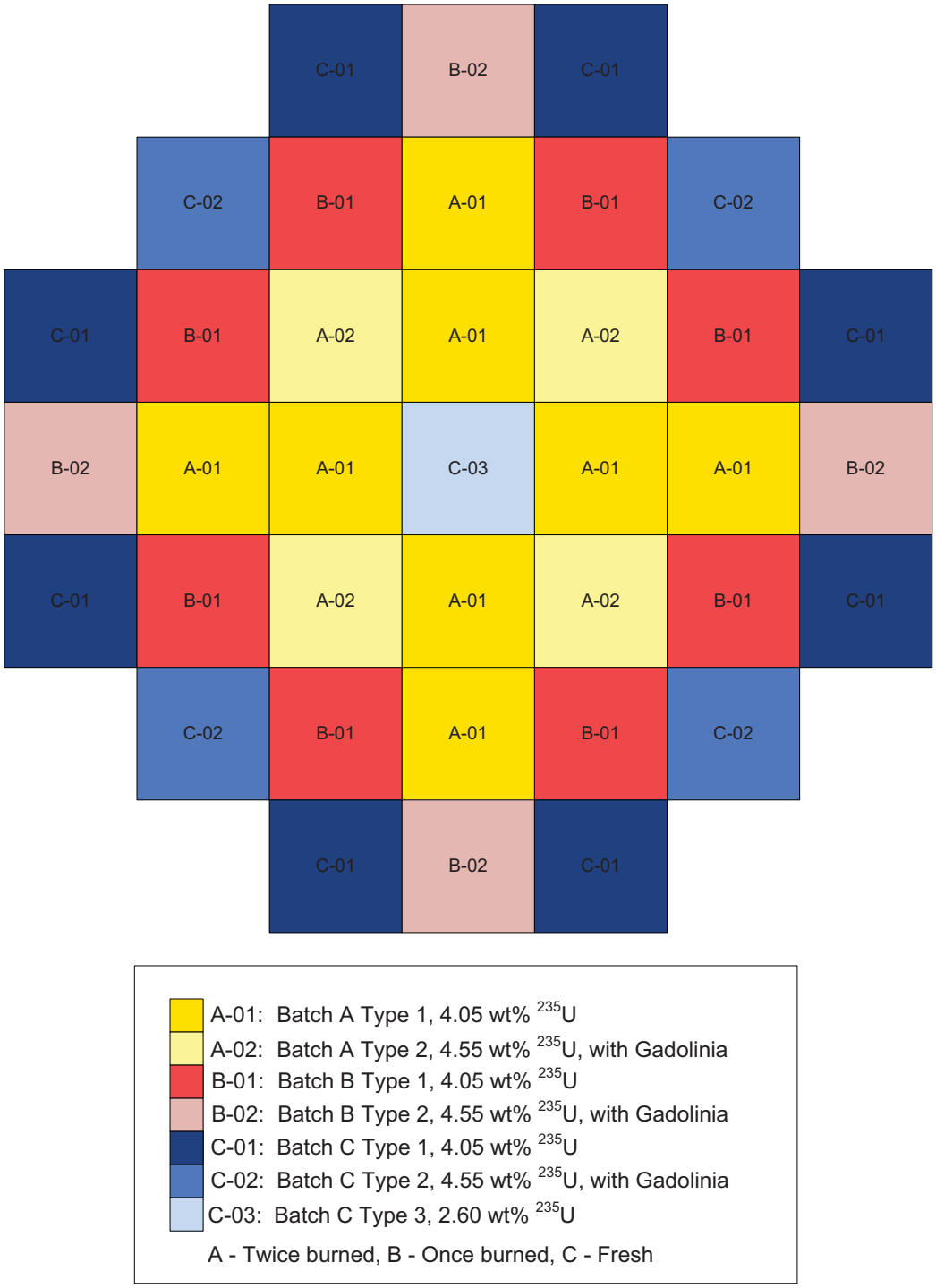

Figure 4.3-2: Power Dependent Insertion Limits

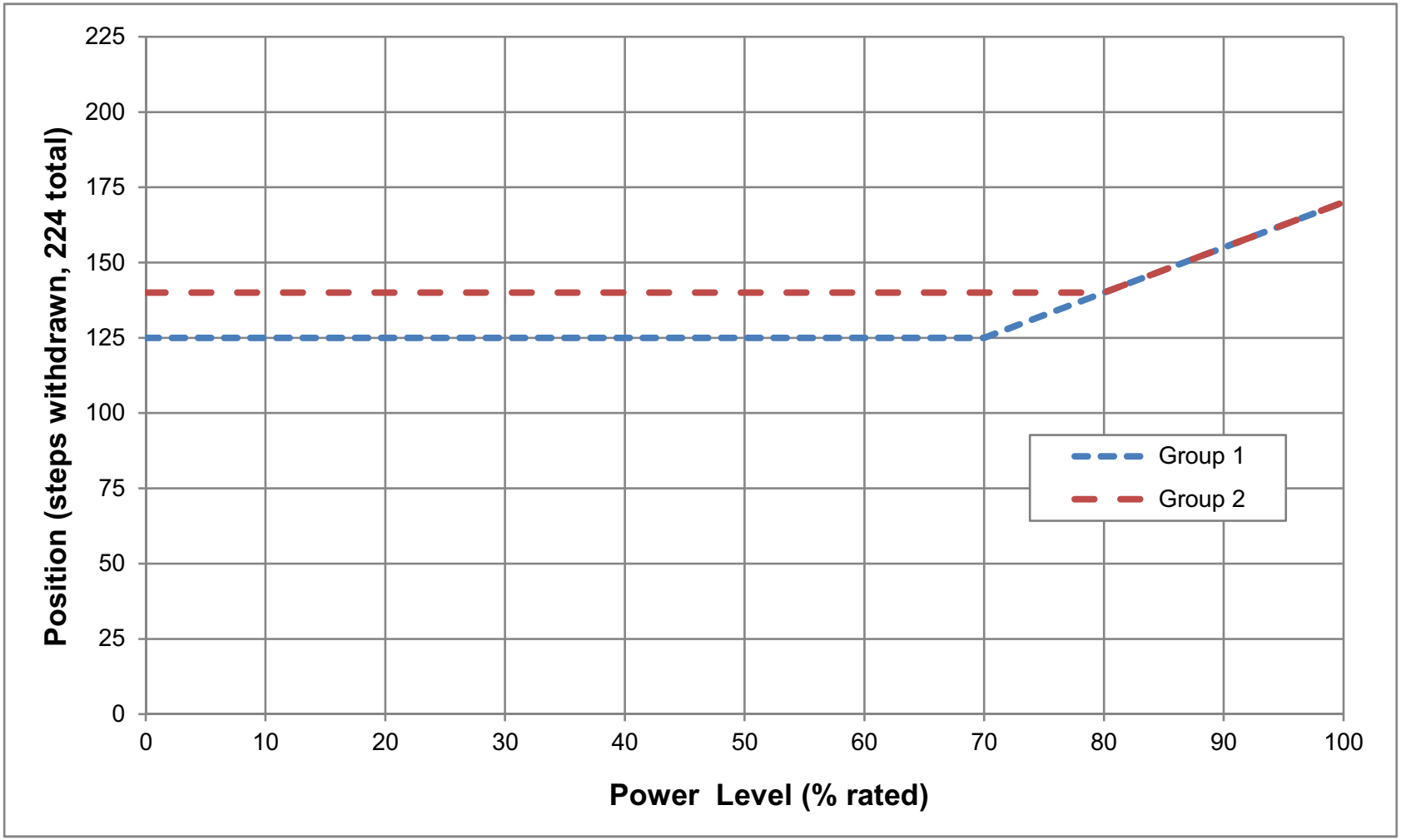

Figure 4.3-3: Axial Offset Window

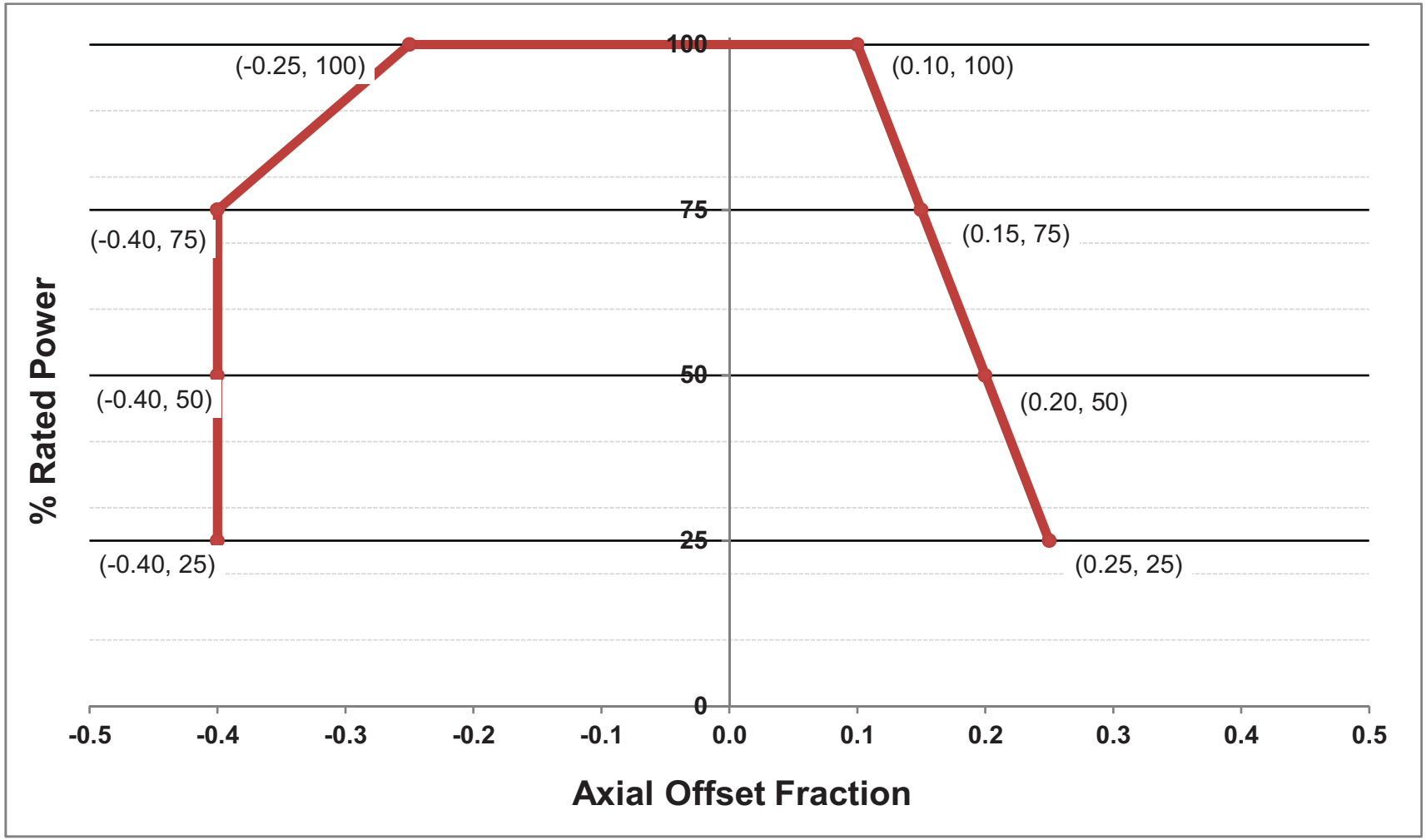

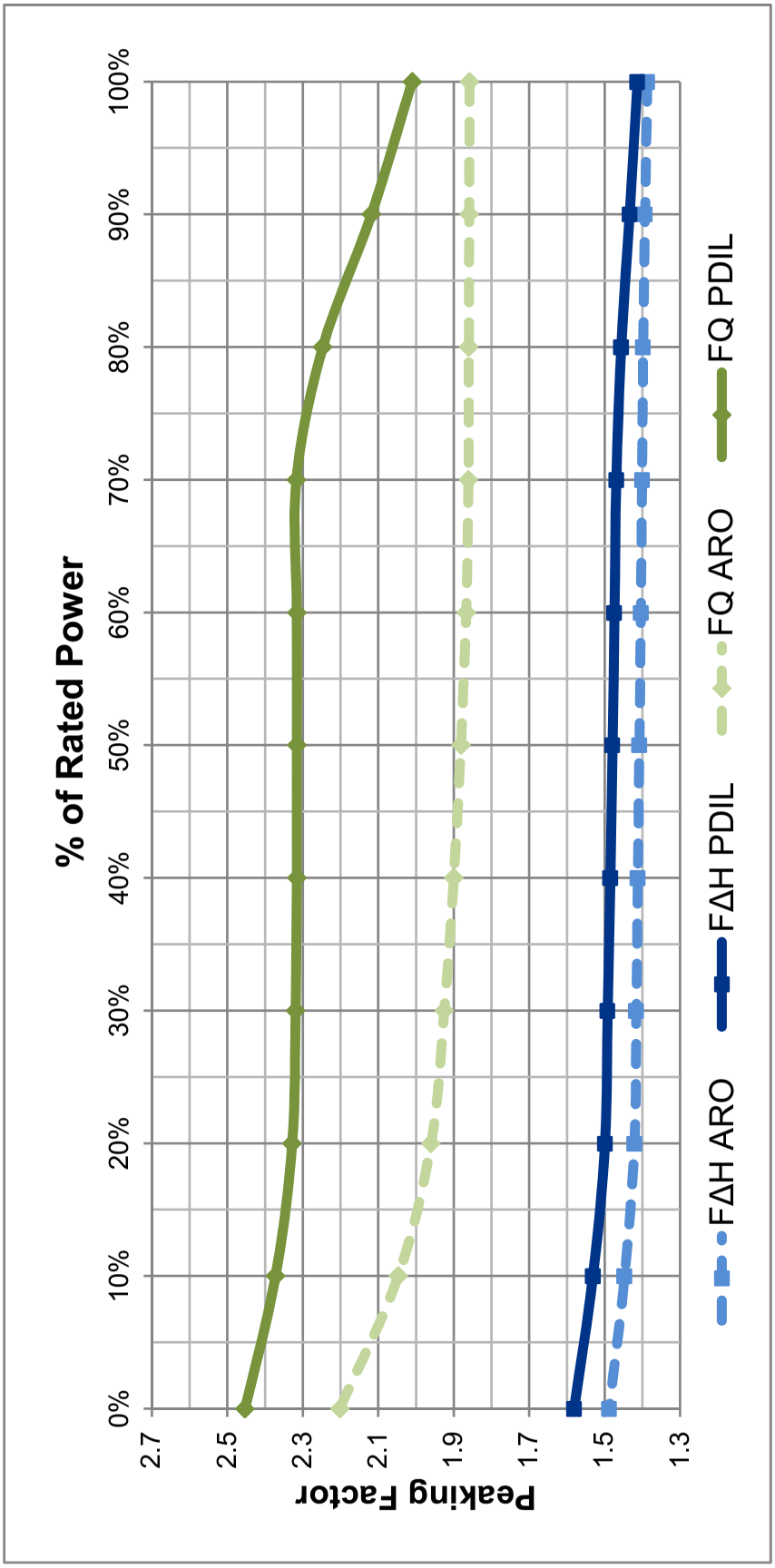

Figure 4.3-4: Power Peaking as a Function of Power Level and Rod Position at Beginning of Cycle

Figure 4.3-5: Power Peaking as a Function of Power Level and Rod Position at Middle of Cycle

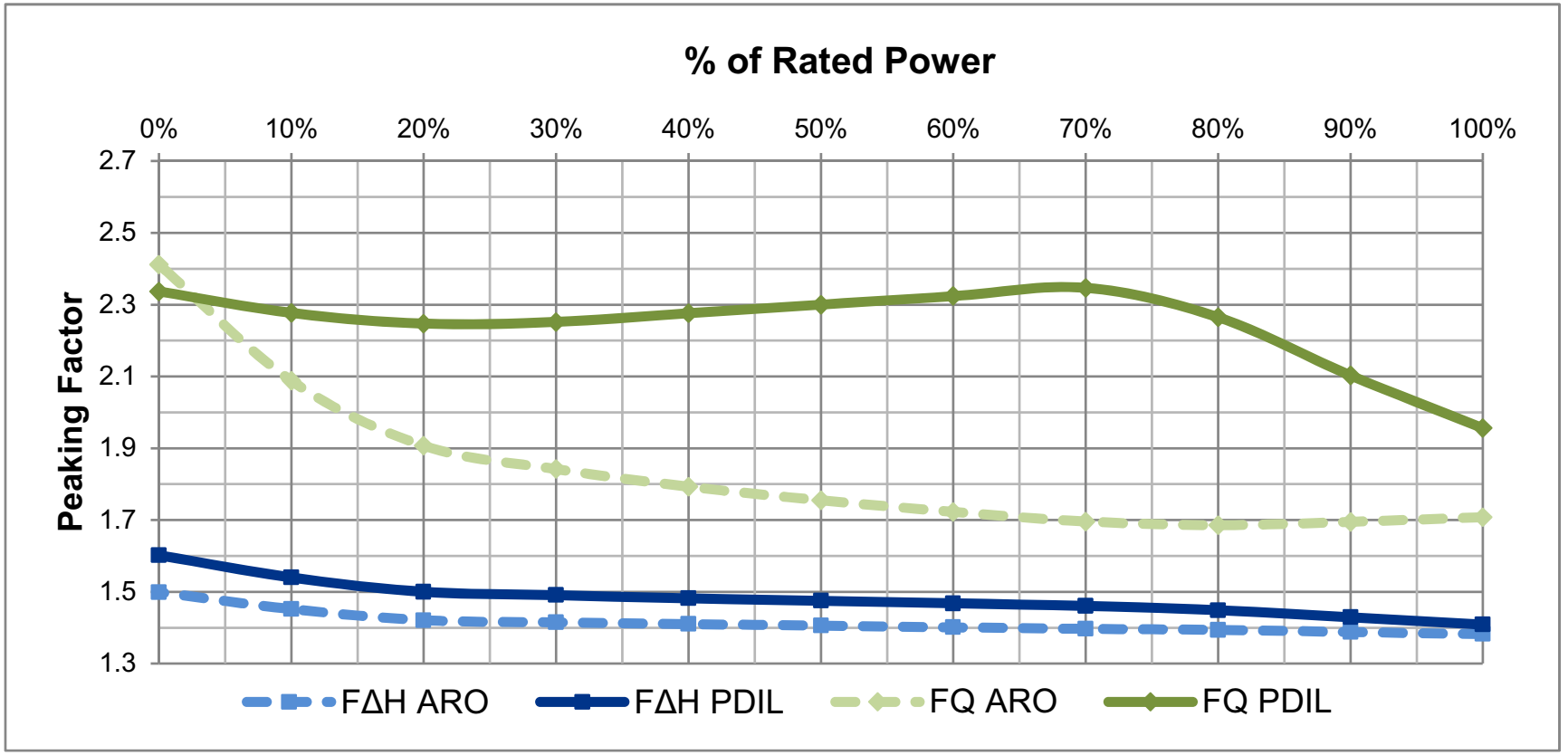

Figure 4.3-6: Power Peaking as a Function of Power Level and Rod Position at End of Cycle

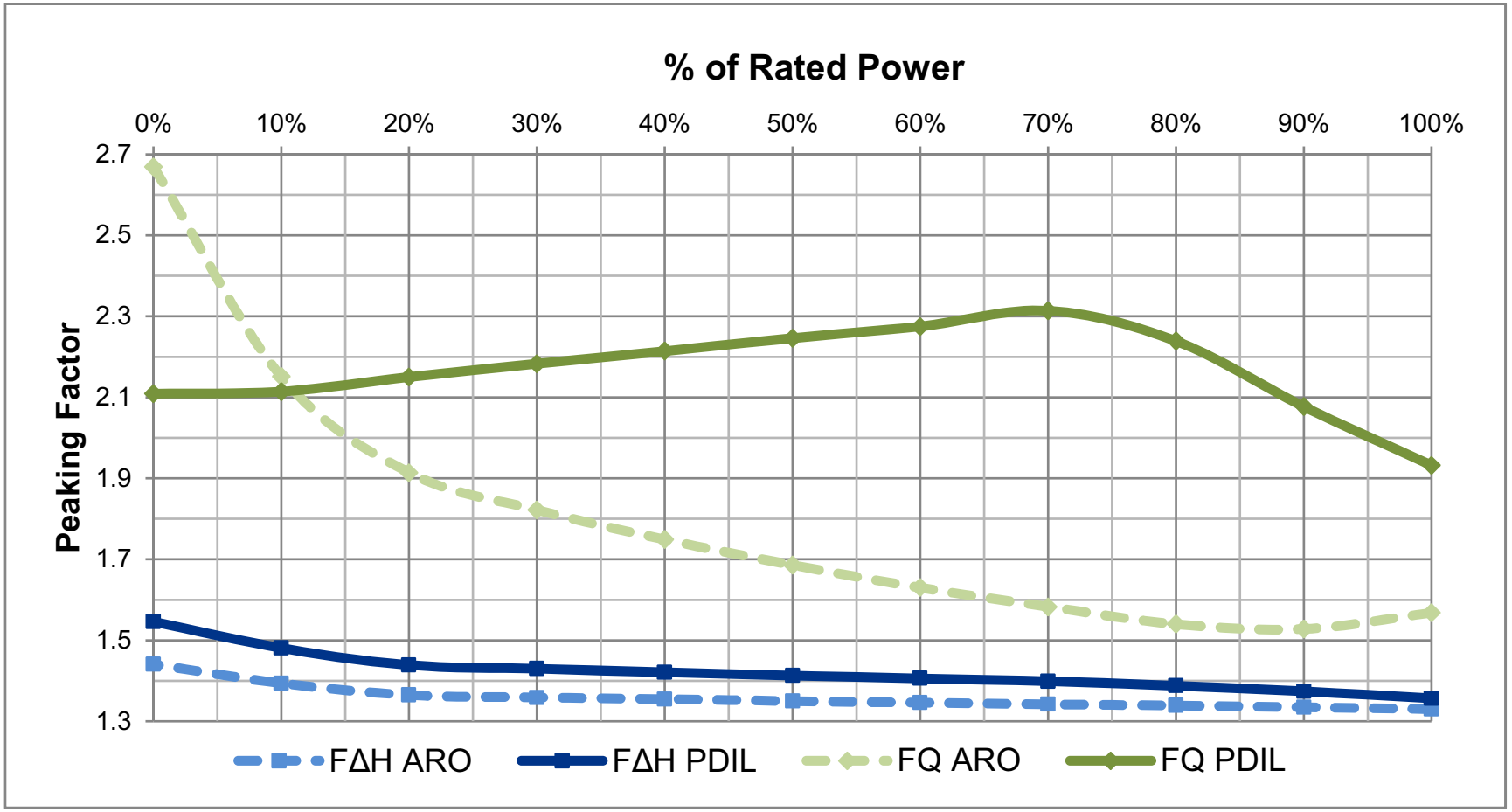

Figure 4.3-7: Radial Relative Power Distribution within a Fuel Assembly

Equilibrium Cycle, BOC, Central Assembly

0.93	0.95	0.97	0.99	1.00	1.01	1.01	1.01	1.02	1.01	1.01	1.01	1.00	0.99	0.97	0.95	0.93
0.95	0.98	1.01	1.04	1.06	1.09	1.07	1.07	1.09	1.07	1.07	1.09	1.06	1.04	1.01	0.98	0.95
0.97	1.01	1.06	1.11	1.13		1.13	1.13		1.13	1.13		1.13	1.11	1.06	1.01	0.97
0.99	1.04	1.11		1.16	1.16	1.13	1.13	1.16	1.13	1.13	1.16	1.16		1.11	1.04	0.99
1.00	1.06	1.13	1.16	1.16	1.17	1.15	1.15	1.17	1.15	1.15	1.17	1.16	1.16	1.13	1.06	1.00
1.01	1.09		1.16	1.17		1.18	1.18		1.18	1.18		1.17	1.16		1.09	1.01
1.01	1.07	1.13	1.13	1.15	1.18	1.16	1.16	1.19	1.16	1.16	1.18	1.15	1.13	1.13	1.07	1.01
1.01	1.07	1.13	1.13	1.15	1.18	1.16	1.16	1.19	1.16	1.16	1.18	1.15	1.13	1.13	1.07	1.01
1.02	1.09		1.16	1.17		1.19	1.19		1.19	1.19		1.17	1.16		1.09	1.02
1.01	1.07	1.13	1.13	1.15	1.18	1.16	1.16	1.19	1.16	1.16	1.18	1.15	1.13	1.13	1.07	1.01
1.01	1.07	1.13	1.13	1.15	1.18	1.16	1.16	1.19	1.16	1.16	1.18	1.15	1.13	1.13	1.07	1.01
1.01	1.09		1.16	1.17		1.18	1.18		1.18	1.18		1.17	1.16		1.09	1.01
1.00	1.06	1.13	1.16	1.16	1.17	1.15	1.15	1.17	1.15	1.15	1.17	1.16	1.16	1.13	1.06	1.00
0.99	1.04	1.11		1.16	1.16	1.13	1.13	1.16	1.13	1.13	1.16	1.16		1.11	1.04	0.99
0.97	1.01	1.06	1.11	1.13		1.13	1.13		1.13	1.13		1.13	1.11	1.06	1.01	0.97
0.95	0.98	1.01	1.04	1.06	1.09	1.07	1.07	1.09	1.07	1.07	1.09	1.06	1.04	1.01	0.98	0.95
0.93	0.95	0.97	0.99	1.00	1.01	1.01	1.01	1.02	1.01	1.01	1.01	1.00	0.99	0.97	0.95	0.93

Equilibrium Cycle, EOC, Central Assembly

1.05	1.05	1.06	1.07	1.08	1.09	1.09	1.09	1.10	1.09	1.09	1.09	1.08	1.07	1.06	1.05	1.05
1.05	1.05	1.06	1.08	1.10	1.13	1.11	1.11	1.13	1.11	1.11	1.13	1.10	1.08	1.06	1.05	1.05
1.06	1.06	1.09	1.13	1.15		1.15	1.14		1.14	1.15		1.15	1.13	1.09	1.06	1.06
1.07	1.08	1.13		1.17	1.16	1.15	1.14	1.16	1.14	1.15	1.16	1.17		1.13	1.08	1.07
1.08	1.10	1.15	1.17	1.16	1.17	1.15	1.15	1.16	1.15	1.15	1.17	1.16	1.17	1.15	1.10	1.08
1.09	1.13		1.16	1.17		1.17	1.17		1.17	1.17		1.17	1.16		1.13	1.09
1.09	1.11	1.15	1.15	1.15	1.17	1.16	1.16	1.18	1.16	1.16	1.17	1.15	1.15	1.15	1.11	1.10
1.09	1.11	1.14	1.14	1.15	1.17	1.16	1.16	1.17	1.16	1.16	1.17	1.15	1.14	1.14	1.11	1.09
1.10	1.13		1.16	1.16		1.18	1.17		1.17	1.18		1.16	1.16		1.13	1.10
1.09	1.11	1.14	1.14	1.15	1.17	1.16	1.16	1.17	1.16	1.16	1.17	1.15	1.14	1.14	1.11	1.09
1.10	1.11	1.15	1.15	1.15	1.17	1.16	1.16	1.18	1.16	1.16	1.17	1.15	1.15	1.15	1.11	1.09
1.09	1.13		1.16	1.17		1.17	1.17		1.17	1.17		1.17	1.16		1.13	1.09
1.08	1.10	1.15	1.17	1.16	1.17	1.15	1.15	1.16	1.15	1.15	1.17	1.16	1.17	1.15	1.10	1.08
1.07	1.08	1.13		1.17	1.16	1.15	1.14	1.16	1.14	1.15	1.16	1.17		1.13	1.08	1.07
1.06	1.06	1.09	1.13	1.15		1.15	1.14		1.14	1.15		1.15	1.13	1.09	1.06	1.06
1.05	1.05	1.06	1.08	1.10	1.13	1.11	1.11	1.13	1.11	1.11	1.13	1.10	1.08	1.06	1.05	1.05
1.05	1.05	1.06	1.07	1.08	1.09	1.09	1.09	1.10	1.09	1.09	1.09	1.08	1.07	1.06	1.05	1.05

Figure 4.3-8: Typical Radial Relative Power Distribution within a Batch 1 Fuel Assembly at Beginning and End of Equilibrium Cycle

BOC Batch 1

1.00	1.00	1.01	1.02	1.02	1.03	1.03	1.02	1.01	0.99	0.98	0.97	0.94	0.91	0.87	0.82	0.74
0.98	1.15	1.16	1.18	1.20	1.23	1.20	1.19	1.20	1.16	1.15	1.15	1.09	1.05	0.99	0.91	0.69
0.97	1.15	1.17	1.22	1.25		1.22	1.21		1.18	1.16		1.12	1.07	0.98	0.88	0.65
0.97	1.15	1.21		1.24	1.22	1.17	1.16	1.18	1.13	1.11	1.13	1.11		1.00	0.87	0.64
0.96	1.15	1.21	1.22	1.20	1.20	1.15	1.14	1.15	1.11	1.09	1.10	1.06	1.04	0.98	0.87	0.63
0.95	1.17		1.19	1.18		1.16	1.15		1.11	1.09		1.04	1.00		0.86	0.61
0.93	1.11	1.15	1.13	1.12	1.14	1.10	1.09	1.10	1.05	1.04	1.04	0.98	0.94	0.91	0.82	0.60
0.91	1.09	1.12	1.09	1.09	1.11	1.07	1.06	1.07	1.02	1.01	1.01	0.95	0.91	0.89	0.79	0.58
0.88	1.07		1.08	1.08		1.06	1.05		1.01	0.99		0.93	0.90		0.77	0.55
0.84	1.00	1.04	1.02	1.01	1.03	0.99	0.98	0.98	0.93	0.92	0.92	0.86	0.83	0.80	0.71	0.52
0.81	0.97	1.01	0.98	0.98	0.99	0.96	0.94	0.95	0.90	0.88	0.88	0.83	0.80	0.77	0.69	0.50
0.78	0.96		0.98	0.97		0.95	0.93		0.89	0.87		0.82	0.79		0.67	0.47
0.74	0.89	0.93	0.94	0.92	0.92	0.88	0.87	0.87	0.82	0.81	0.81	0.78	0.76	0.71	0.63	0.45
0.70	0.83	0.88		0.88	0.86	0.83	0.81	0.82	0.78	0.76	0.76	0.75		0.68	0.59	0.43
0.65	0.76	0.79	0.82	0.82		0.79	0.78		0.74	0.72		0.69	0.67	0.61	0.54	0.40
0.59	0.69	0.69	0.70	0.71	0.72	0.70	0.69	0.69	0.65	0.64	0.63	0.60	0.57	0.53	0.48	0.36
0.50	0.51	0.50	0.50	0.51	0.50	0.50	0.49	0.48	0.46	0.45	0.43	0.42	0.41	0.38	0.36	0.31

EOC Batch 1

1.06	1.04	1.04	1.05	1.05	1.06	1.05	1.04	1.04	1.02	1.02	1.00	0.97	0.95	0.90	0.85	0.78
1.03	1.12	1.13	1.14	1.16	1.18	1.15	1.14	1.15	1.12	1.11	1.11	1.06	1.02	0.96	0.90	0.72
1.01	1.11	1.13	1.17	1.19		1.16	1.15		1.12	1.12		1.07	1.04	0.95	0.87	0.69
1.00	1.11	1.15		1.18	1.16	1.12	1.11	1.12	1.08	1.07	1.08	1.06		0.96	0.85	0.66
1.00	1.12	1.16	1.17	1.14	1.14	1.10	1.09	1.10	1.06	1.06	1.06	1.02	1.01	0.95	0.85	0.66
0.99	1.12		1.13	1.13		1.10	1.09		1.06	1.05		1.00	0.97		0.84	0.63
0.97	1.08	1.10	1.08	1.07	1.09	1.05	1.04	1.05	1.01	1.00	1.00	0.95	0.92	0.88	0.81	0.62
0.95	1.06	1.08	1.06	1.05	1.07	1.03	1.02	1.03	0.99	0.98	0.98	0.92	0.90	0.86	0.78	0.60
0.92	1.05		1.05	1.04		1.02	1.01		0.98	0.97		0.91	0.88		0.77	0.58
0.89	0.99	1.01	0.99	0.99	1.00	0.97	0.95	0.96	0.92	0.91	0.90	0.85	0.83	0.79	0.72	0.55
0.87	0.97	1.00	0.97	0.97	0.97	0.94	0.93	0.94	0.89	0.88	0.88	0.83	0.80	0.77	0.70	0.53
0.84	0.96		0.96	0.95		0.93	0.92		0.88	0.86		0.82	0.79		0.68	0.50
0.79	0.89	0.92	0.93	0.91	0.90	0.87	0.85	0.86	0.82	0.81	0.81	0.78	0.76	0.71	0.64	0.48
0.75	0.84	0.88		0.88	0.86	0.83	0.81	0.82	0.78	0.77	0.77	0.75		0.69	0.60	0.46
0.69	0.77	0.79	0.82	0.81		0.78	0.77		0.74	0.73		0.69	0.68	0.62	0.55	0.42
0.63	0.70	0.70	0.71	0.72	0.73	0.70	0.69	0.69	0.66	0.65	0.65	0.61	0.58	0.54	0.50	0.38
0.55	0.54	0.54	0.54	0.54	0.53	0.53	0.52	0.51	0.49	0.48	0.46	0.45	0.43	0.41	0.38	0.33

Figure 4.3-9: Typical Radial Relative Power Distribution within a Batch 2 Fuel Assembly at Beginning and End of Equilibrium Cycle

BOC Batch 2

0.82	0.85	0.89	0.92	0.94	0.97	0.98	0.99	1.00	1.01	1.02	1.03	1.02	1.02	1.01	1.02	1.06
0.86	0.96	0.98	1.01	1.05	1.08	1.08	1.09	1.11	1.11	1.12	1.14	1.12	1.11	1.09	1.11	1.04
0.90	0.99	1.02	1.06	1.09		1.10	1.11		1.13	1.14		1.15	1.15	1.11	1.11	1.04
0.93	1.02	1.07		1.11	1.11	1.09	1.10	1.12	1.11	1.13	1.16	1.16		1.15	1.12	1.05
0.96	1.07	1.11	1.12	1.12	1.13	1.11	1.11	1.14	1.12	1.14	1.16	1.15	1.19	1.17	1.15	1.06
0.99	1.11		1.13	1.13		1.14	1.14		1.15	1.16		1.16	1.18		1.18	1.07
1.01	1.11	1.13	1.12	1.12	1.14	1.13	1.13	1.16	1.14	1.15	1.17	1.14	1.15	1.17	1.16	1.07
1.03	1.13	1.15	1.13	1.14	1.16	1.14	1.15	1.17	1.15	1.16	1.18	1.15	1.16	1.17	1.17	1.07
1.05	1.17		1.17	1.18		1.18	1.18		1.19	1.20		1.19	1.20		1.20	1.08
1.07	1.17	1.19	1.17	1.17	1.19	1.17	1.17	1.20	1.18	1.19	1.20	1.18	1.18	1.19	1.19	1.08
1.08	1.20	1.22	1.19	1.19	1.21	1.19	1.19	1.22	1.20	1.20	1.22	1.19	1.20	1.21	1.20	1.08
1.10	1.23		1.23	1.23		1.22	1.22		1.22	1.23		1.22	1.23		1.22	1.09
1.09	1.21	1.24	1.25	1.22	1.23	1.20	1.20	1.22	1.20	1.21	1.23	1.22	1.24	1.22	1.19	1.08
1.10	1.21	1.25		1.27	1.25	1.22	1.21	1.24	1.22	1.22	1.25	1.25		1.22	1.18	1.07
1.10	1.19	1.20	1.24	1.25		1.23	1.23		1.23	1.24		1.24	1.23	1.18	1.16	1.06
1.12	1.21	1.20	1.21	1.22	1.25	1.22	1.22	1.24	1.22	1.22	1.24	1.21	1.19	1.16	1.17	1.06
1.16	1.12	1.10	1.10	1.11	1.11	1.11	1.10	1.10	1.10	1.10	1.09	1.08	1.07	1.05	1.05	1.08

EOC Batch 2

0.79	0.82	0.85	0.89	0.90	0.93	0.94	0.95	0.96	0.96	0.97	0.98	0.97	0.98	0.97	0.98	1.02
0.83	0.92	0.94	0.98	1.00	1.03	1.03	1.04	1.06	1.05	1.06	1.08	1.07	1.06	1.05	1.07	1.02
0.86	0.95	0.99	1.03	1.05		1.06	1.07		1.08	1.10		1.11	1.11	1.08	1.08	1.03
0.90	0.99	1.03		1.07	1.08	1.07	1.07	1.09	1.08	1.09	1.12	1.12		1.12	1.10	1.04
0.93	1.02	1.06	1.08	1.09	1.10	1.09	1.09	1.11	1.10	1.11	1.13	1.13	1.15	1.14	1.13	1.06
0.96	1.06		1.09	1.10		1.11	1.12		1.12	1.13		1.13	1.15		1.15	1.07
0.97	1.07	1.09	1.09	1.10	1.12	1.11	1.11	1.13	1.12	1.13	1.14	1.13	1.14	1.15	1.14	1.08
0.99	1.08	1.11	1.11	1.11	1.13	1.12	1.13	1.14	1.13	1.14	1.15	1.13	1.15	1.15	1.15	1.08
1.00	1.11		1.13	1.14		1.15	1.15		1.15	1.16		1.15	1.17		1.17	1.09
1.01	1.11	1.13	1.12	1.13	1.15	1.14	1.14	1.16	1.14	1.15	1.16	1.14	1.15	1.16	1.16	1.09
1.03	1.13	1.15	1.15	1.15	1.17	1.16	1.16	1.18	1.16	1.17	1.18	1.16	1.17	1.18	1.17	1.09
1.04	1.15		1.17	1.18		1.18	1.18		1.18	1.19		1.18	1.20		1.19	1.10
1.04	1.14	1.17	1.19	1.18	1.18	1.17	1.16	1.18	1.16	1.17	1.19	1.18	1.21	1.19	1.17	1.09
1.05	1.14	1.18		1.21	1.20	1.18	1.18	1.20	1.18	1.19	1.21	1.21		1.20	1.17	1.09
1.05	1.13	1.15	1.19	1.20		1.19	1.19		1.19	1.20		1.20	1.20	1.16	1.15	1.08
1.07	1.15	1.16	1.17	1.19	1.21	1.19	1.19	1.21	1.19	1.19	1.21	1.18	1.17	1.15	1.16	1.09
1.11	1.09	1.09	1.10	1.11	1.11	1.11	1.11	1.11	1.11	1.11	1.11	1.10	1.09	1.08	1.09	1.11

Figure 4.3-10: Typical Radial Relative Power Distribution within a Batch 3 Fuel Assembly at Beginning and End of Equilibrium Cycle

BOC Batch 3

0.94	0.91	0.90	0.91	0.90	0.91	0.91	0.90	0.90	0.89	0.89	0.89	0.88	0.89	0.88	0.89	0.93
0.90	0.96	0.95	0.96	0.97	0.98	0.97	0.97	0.98	0.96	0.96	0.97	0.96	0.95	0.94	0.95	0.91
0.89	0.95	0.96	0.98	0.99		0.98	0.98		0.97	0.97		0.98	0.98	0.95	0.95	0.90
0.89	0.95	0.97		0.98	0.98	0.97	0.96	0.97	0.96	0.96	0.97	0.98		0.97	0.95	0.89
0.88	0.95	0.97	0.98	0.97	0.98	0.96	0.96	0.97	0.95	0.96	0.97	0.97	0.99	0.98	0.96	0.89
0.88	0.96		0.97	0.97		0.97	0.97		0.96	0.97		0.97	0.98		0.97	0.89
0.88	0.95	0.96	0.95	0.95	0.96	0.95	0.95	0.96	0.95	0.95	0.96	0.95	0.96	0.96	0.96	0.89
0.88	0.95	0.96	0.95	0.95	0.97	0.95	0.96	0.96	0.95	0.96	0.97	0.95	0.96	0.97	0.96	0.89
0.88	0.96		0.96	0.96		0.97	0.97		0.96	0.97		0.96	0.98		0.97	0.89
0.88	0.95	0.96	0.95	0.95	0.97	0.96	0.96	0.97	0.95	0.96	0.97	0.95	0.97	0.97	0.96	0.89
0.88	0.96	0.97	0.97	0.97	0.98	0.97	0.97	0.98	0.96	0.97	0.98	0.97	0.98	0.98	0.97	0.89
0.89	0.97		0.98	0.98		0.98	0.98		0.98	0.98		0.98	0.99		0.98	0.89
0.88	0.96	0.98	0.99	0.98	0.99	0.97	0.97	0.98	0.97	0.98	0.99	0.98	1.00	0.99	0.97	0.89
0.90	0.96	0.99		1.02	1.01	0.99	0.99	1.00	0.99	1.00	1.01	1.01		1.00	0.97	0.90
0.90	0.96	0.98	1.00	1.01		1.01	1.01		1.00	1.01		1.01	1.01	0.98	0.97	0.90
0.91	0.98	0.99	1.00	1.01	1.03	1.02	1.02	1.03	1.01	1.01	1.02	1.00	1.00	0.99	0.99	0.92
0.95	0.94	0.95	0.95	0.96	0.97	0.96	0.96	0.96	0.95	0.95	0.95	0.94	0.94	0.93	0.94	0.96

EOC Batch 3

0.95	0.94	0.93	0.93	0.93	0.93	0.93	0.93	0.93	0.92	0.92	0.92	0.91	0.91	0.90	0.90	0.91
0.94	0.98	0.97	0.98	0.99	0.99	0.99	0.98	0.99	0.98	0.98	0.98	0.97	0.96	0.95	0.95	0.91
0.93	0.98	0.98	1.00	1.01		1.00	0.99		0.99	0.99		0.99	0.99	0.96	0.95	0.91
0.93	0.98	1.00		1.01	1.00	0.99	0.99	0.99	0.98	0.99	0.99	0.99		0.97	0.96	0.91
0.93	0.99	1.00	1.01	1.00	1.00	0.99	0.99	0.99	0.99	0.99	1.00	0.99	1.00	0.99	0.97	0.91
0.93	0.99		1.00	1.00		0.99	0.99		0.99	0.99		0.98	0.99		0.98	0.91
0.93	0.99	0.99	0.99	0.99	1.00	0.99	0.98	0.99	0.98	0.99	0.99	0.98	0.98	0.98	0.97	0.92
0.93	0.99	0.99	0.99	0.99	1.00	0.99	0.99	0.99	0.99	0.99	0.99	0.98	0.99	0.98	0.97	0.92
0.93	0.99		1.00	1.00		1.00	0.99		0.99	1.00		0.99	0.99		0.98	0.92
0.93	0.99	1.00	0.99	0.99	1.00	0.99	0.99	0.99	0.99	0.99	0.99	0.98	0.99	0.98	0.98	0.92
0.94	0.99	1.00	1.00	1.00	1.01	1.00	1.00	1.00	1.00	1.00	1.00	0.99	1.00	0.99	0.98	0.92
0.94	1.00		1.01	1.01		1.01	1.00		1.00	1.01		1.00	1.01		0.99	0.92
0.93	0.99	1.01	1.02	1.01	1.01	1.00	1.00	1.00	0.99	1.00	1.01	1.00	1.01	1.00	0.98	0.92
0.94	0.99	1.02		1.03	1.03	1.01	1.01	1.02	1.01	1.02	1.02	1.02		1.00	0.98	0.92
0.94	0.99	1.00	1.02	1.03		1.02	1.02		1.01	1.02		1.01	1.01	0.99	0.97	0.92
0.95	1.00	1.00	1.01	1.02	1.03	1.02	1.02	1.03	1.02	1.02	1.02	1.01	1.00	0.98	0.98	0.92
0.97	0.96	0.96	0.97	0.97	0.98	0.98	0.97	0.97	0.97	0.97	0.96	0.95	0.95	0.94	0.94	0.94

Figure 4.3-11: Assembly Radial Power Distribution at Beginning, Middle, and End of Cycle

BOC

		0.895	0.911	0.888		
	1.033	1.137	0.957	1.135	1.033	
0.888	1.135	1.054	0.967	1.054	1.136	0.895
0.911	0.957	0.967	1.091	0.967	0.957	0.911
0.895	1.136	1.054	0.967	1.054	1.135	0.888
	1.033	1.135	0.957	1.137	1.033	
		0.888	0.911	0.895		

MOC

		0.887	0.907	0.883		
	1.053	1.119	0.965	1.118	1.052	
0.883	1.118	1.057	0.983	1.057	1.118	0.887
0.907	0.965	0.983	1.112	0.983	0.965	0.907
0.887	1.118	1.057	0.983	1.057	1.118	0.883
	1.052	1.118	0.965	1.119	1.053	
		0.883	0.907	0.887		

EOC

		0.886	0.915	0.883		
	1.029	1.105	0.980	1.105	1.029	
0.883	1.105	1.064	1.003	1.064	1.105	0.886
0.915	0.980	1.003	1.123	1.003	0.980	0.915
0.886	1.105	1.064	1.003	1.064	1.105	0.883
	1.029	1.105	0.980	1.105	1.029	
		0.883	0.915	0.886		

Figure 4.3-12: Axial Power Distribution at Beginning, Middle, and End of Cycle

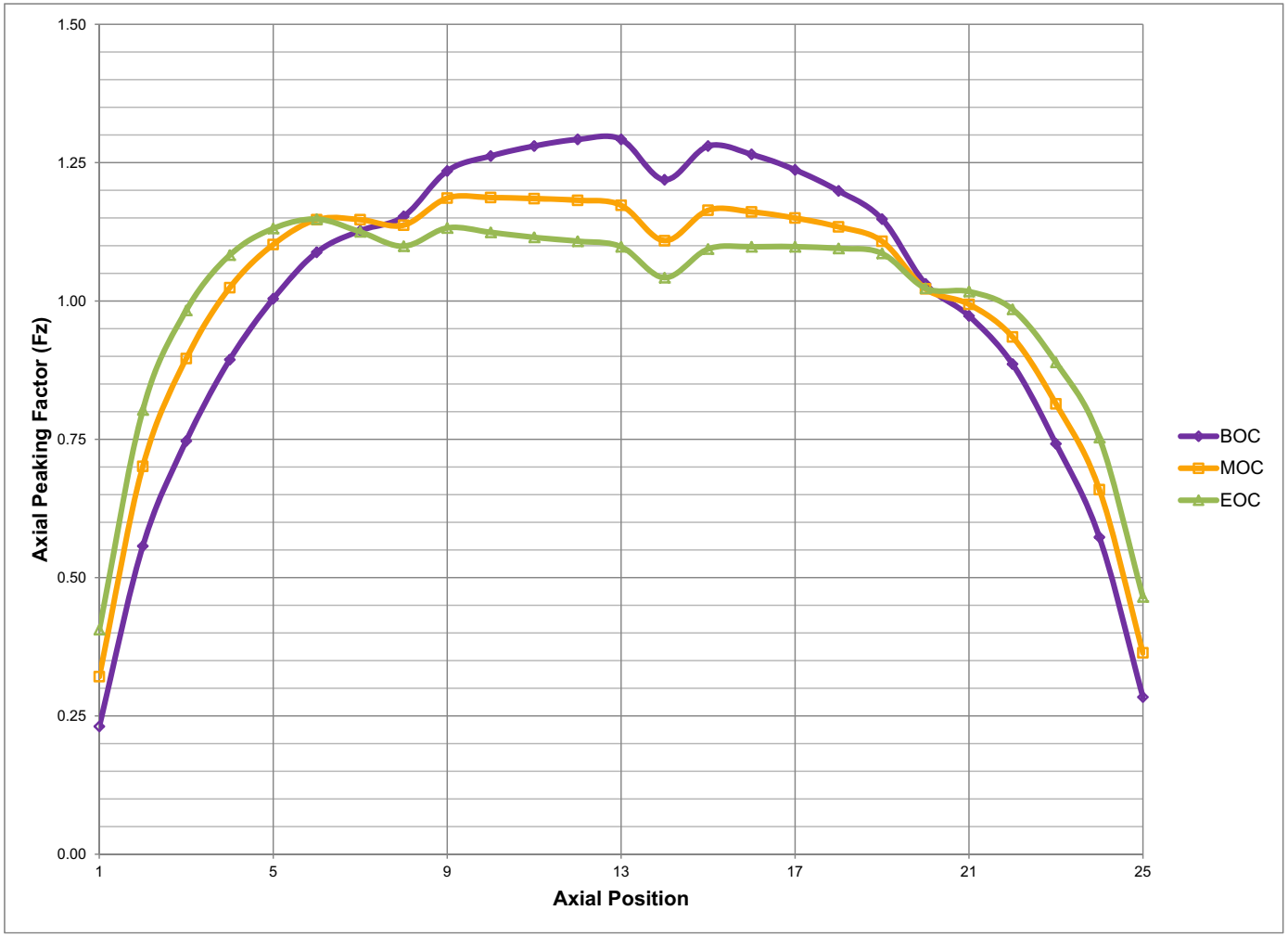

Figure 4.3-13: Moderator Temperature Coefficient of Reactivity at Full Power

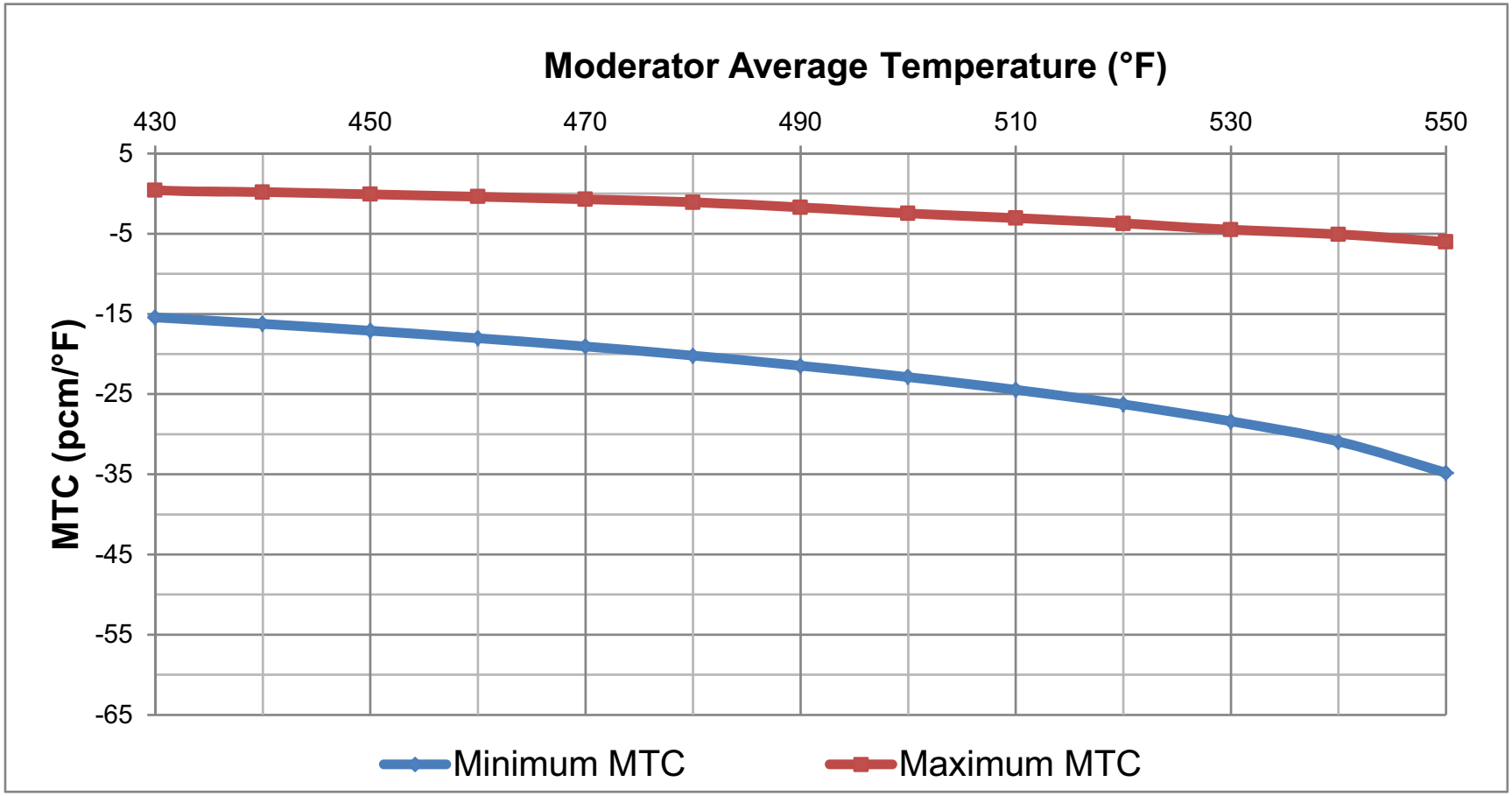

Figure 4.3-14: Moderator Temperature Coefficient of Reactivity at Zero Power

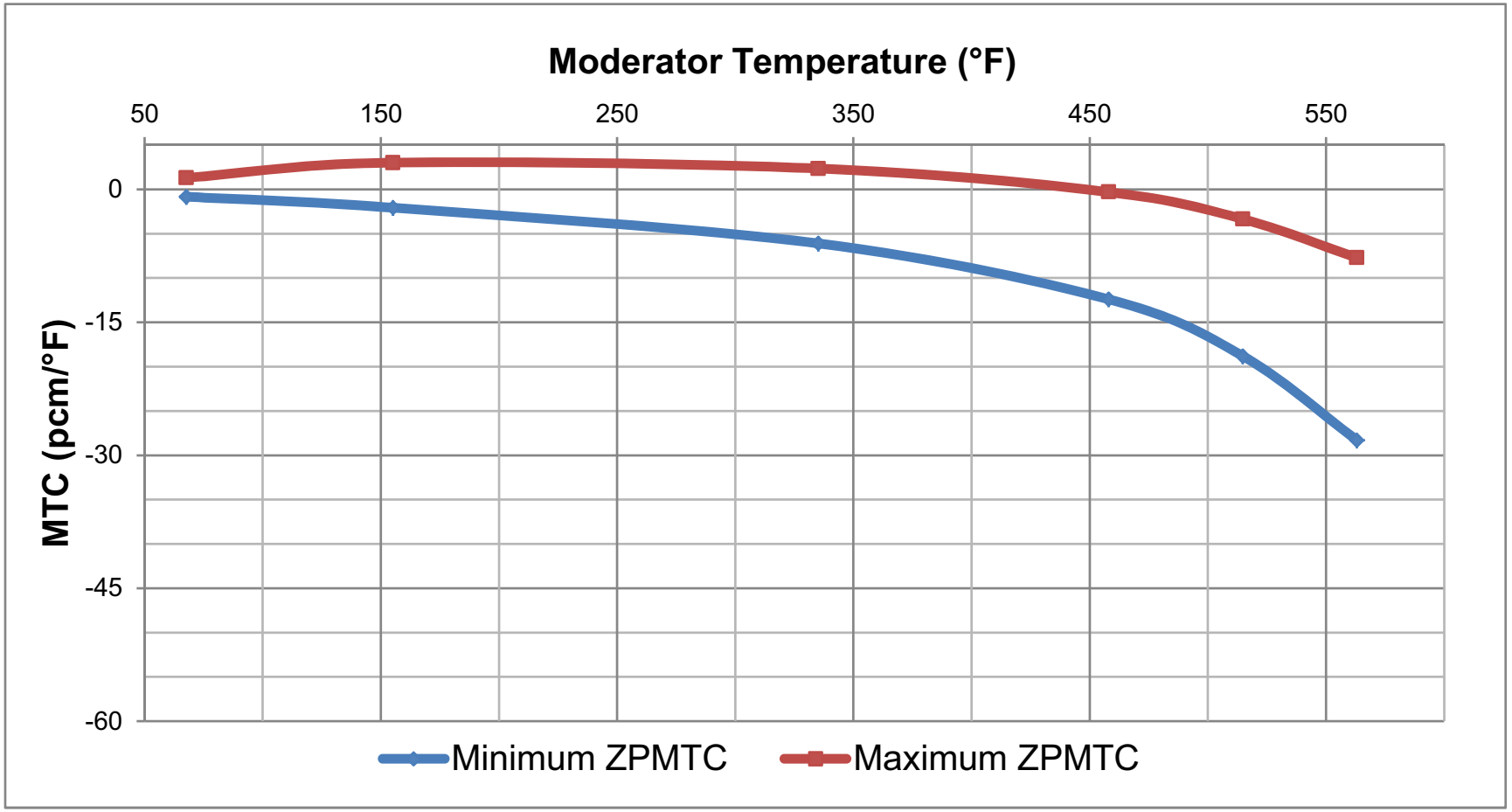

Figure 4.3-15: Maximum and Minimum Power Defect

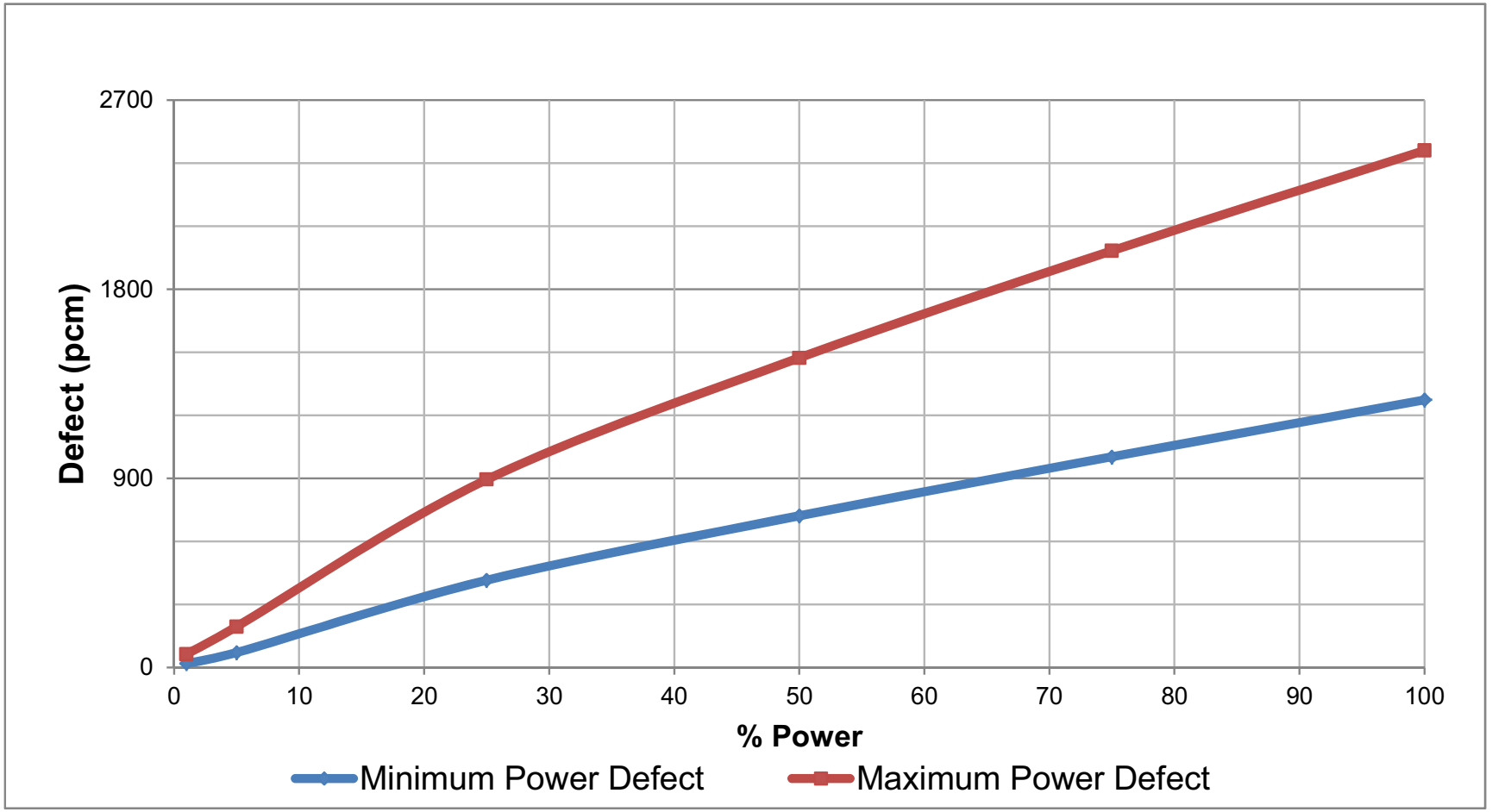

Figure 4.3-16: Maximum and Minimum Power Coefficient

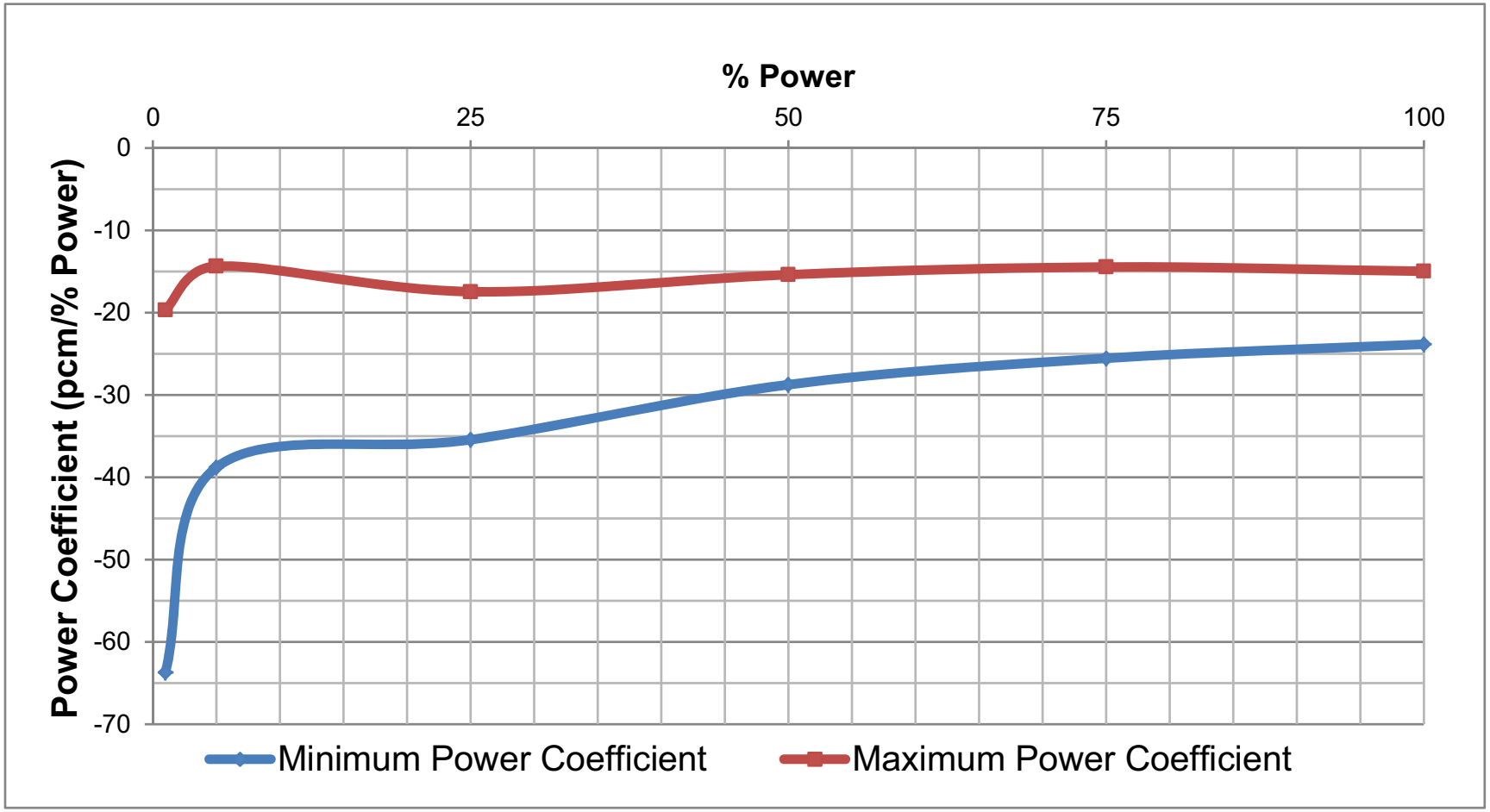

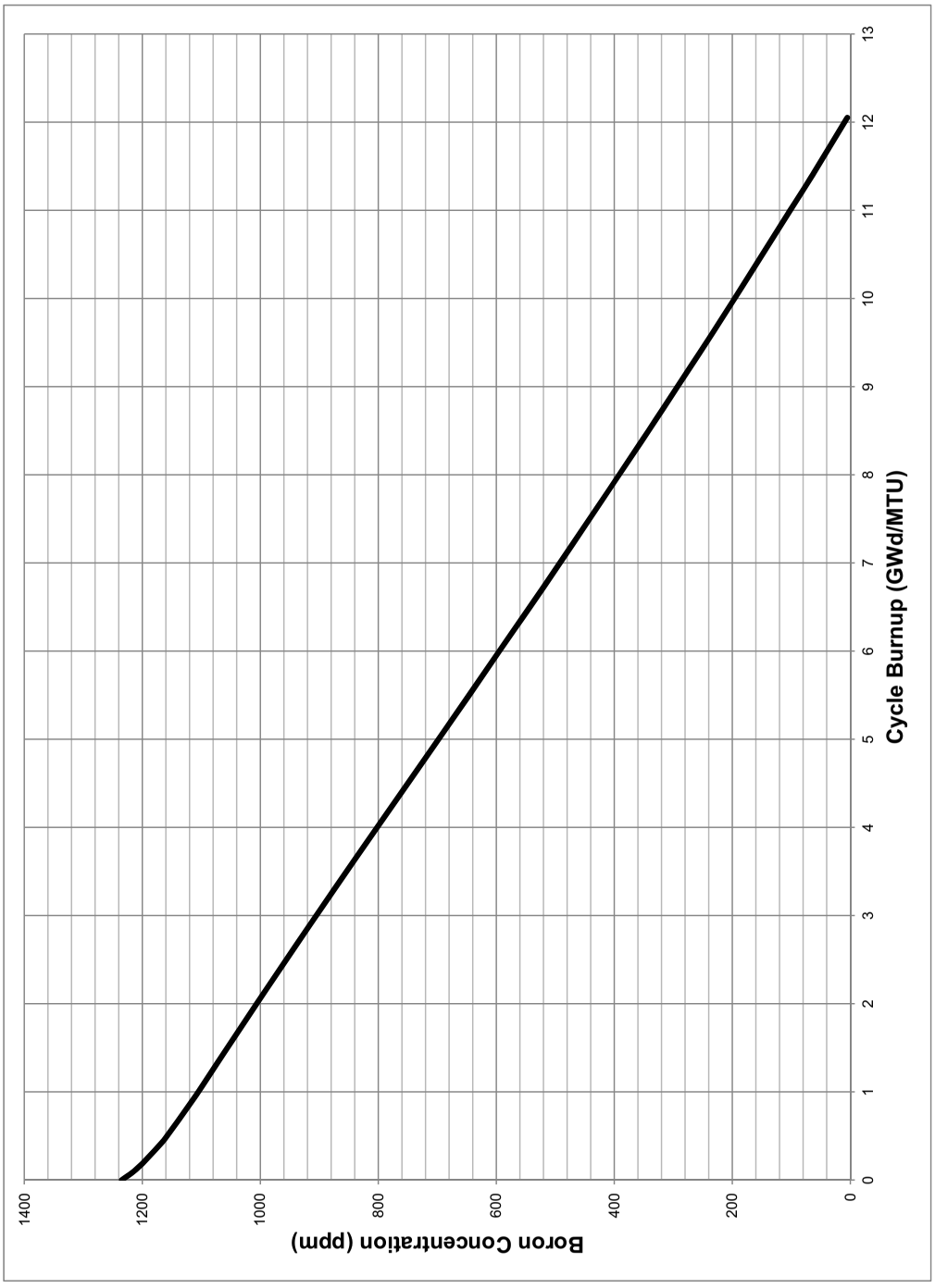

Figure 4.3-17: Boron Letdown Curve for Equilibrium Cycle

Figure 4.3-18: Control Rod and Incore Instrument Locations

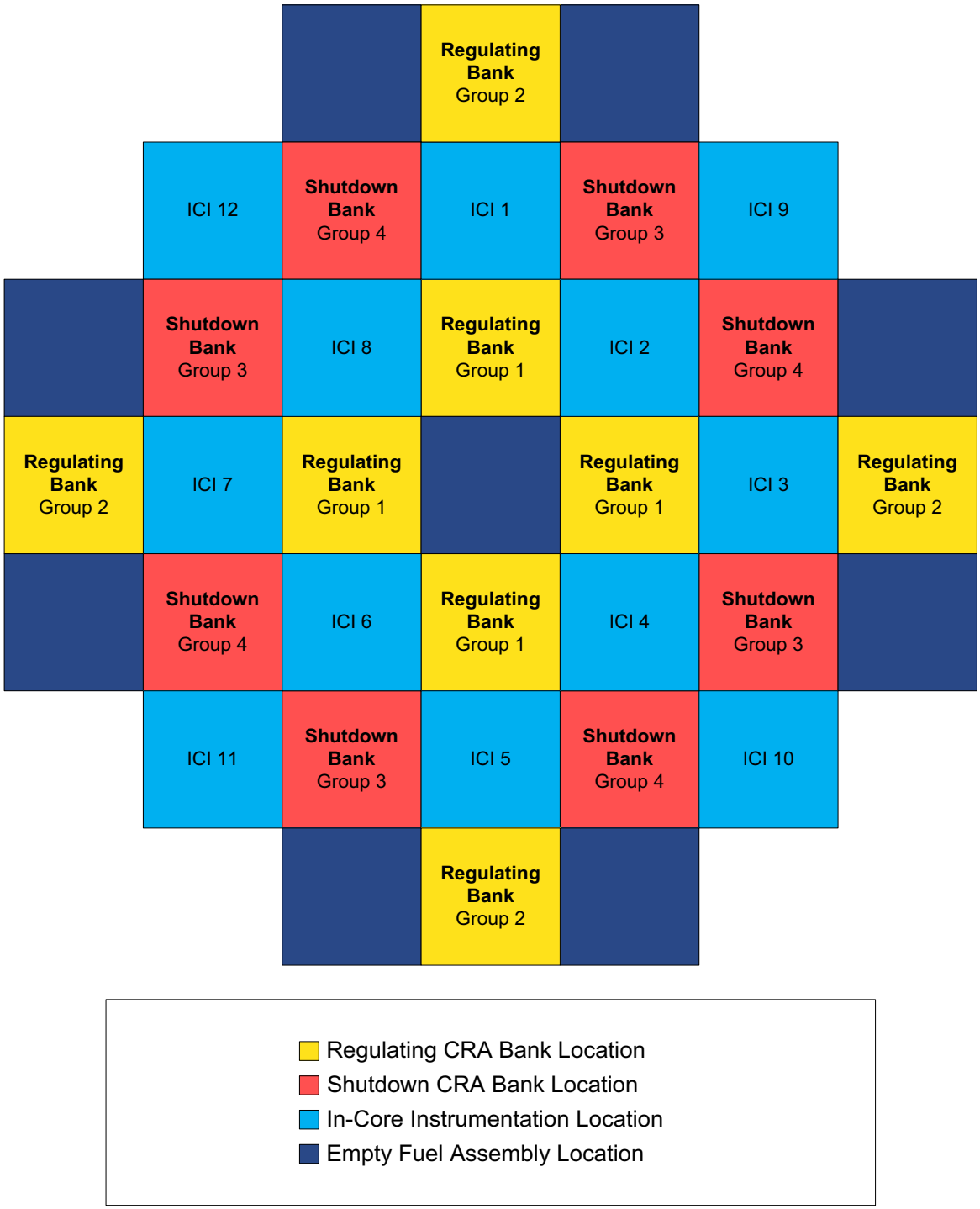

Figure 4.3-19: Differential Rod Worth at Beginning, Middle and End of Cycle from 0% to 100% Power

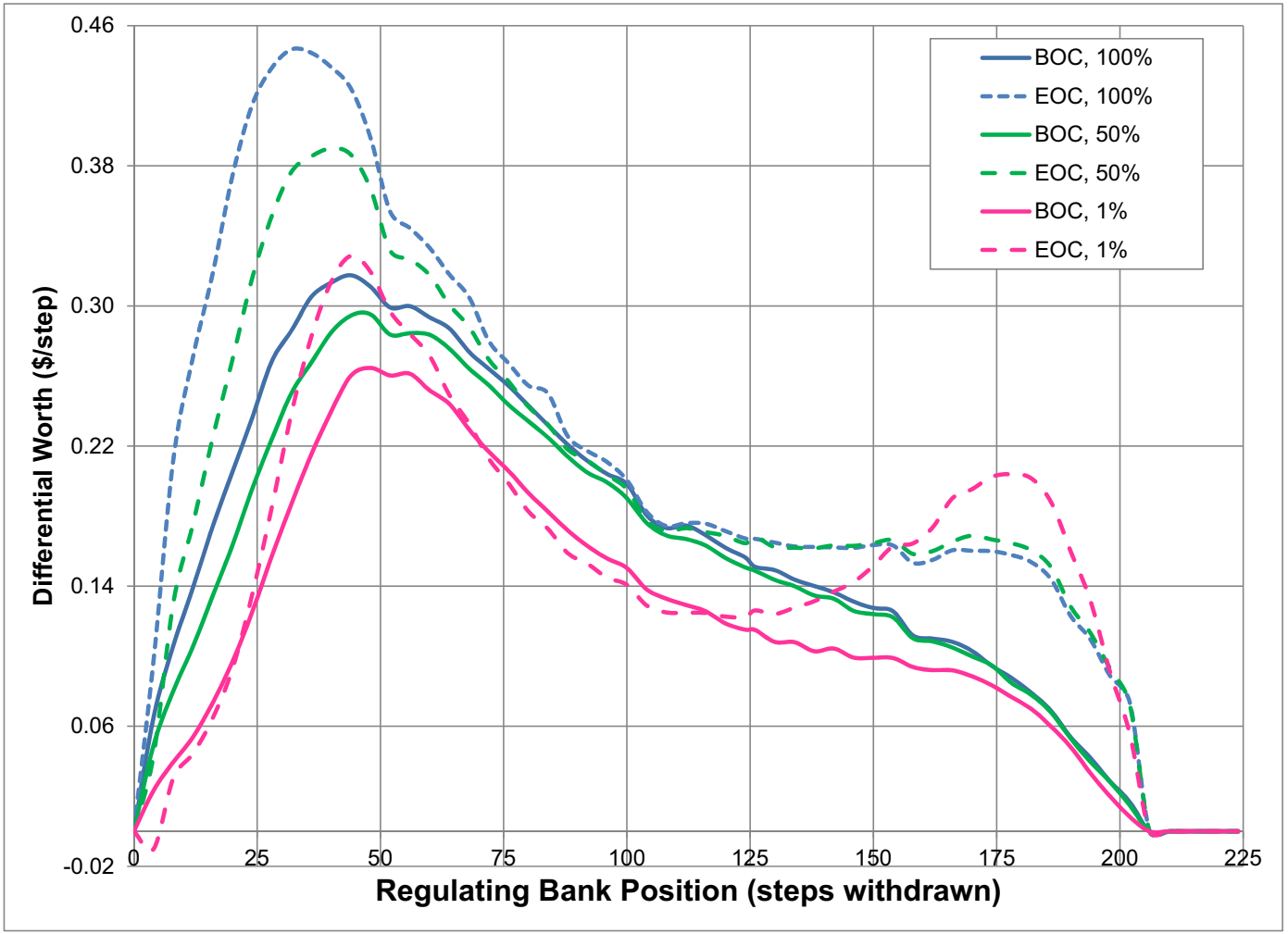

Figure 4.3-20: Integral Regulating Bank Worth for Withdrawal from the Power Dependent Insertion Limits

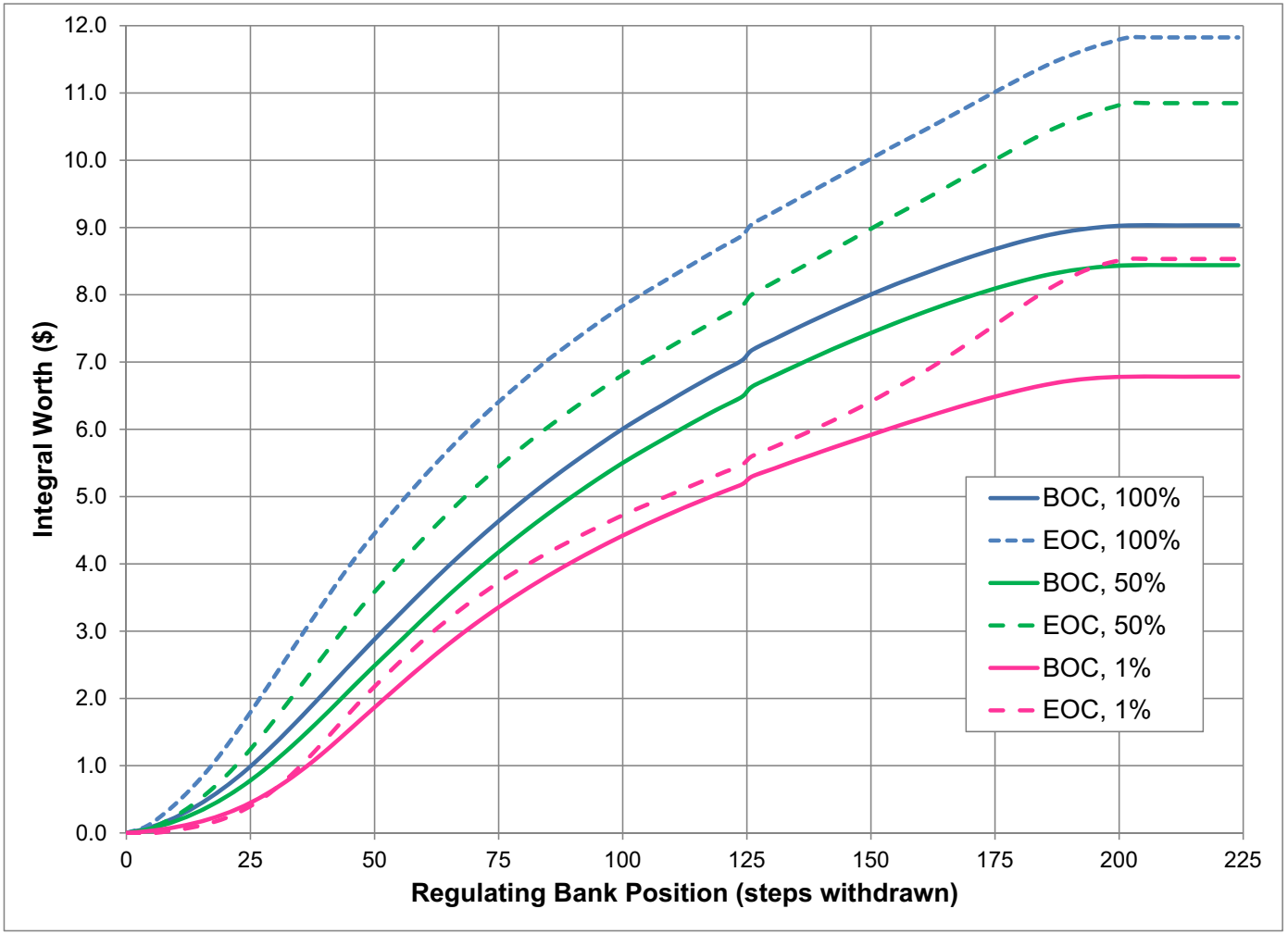

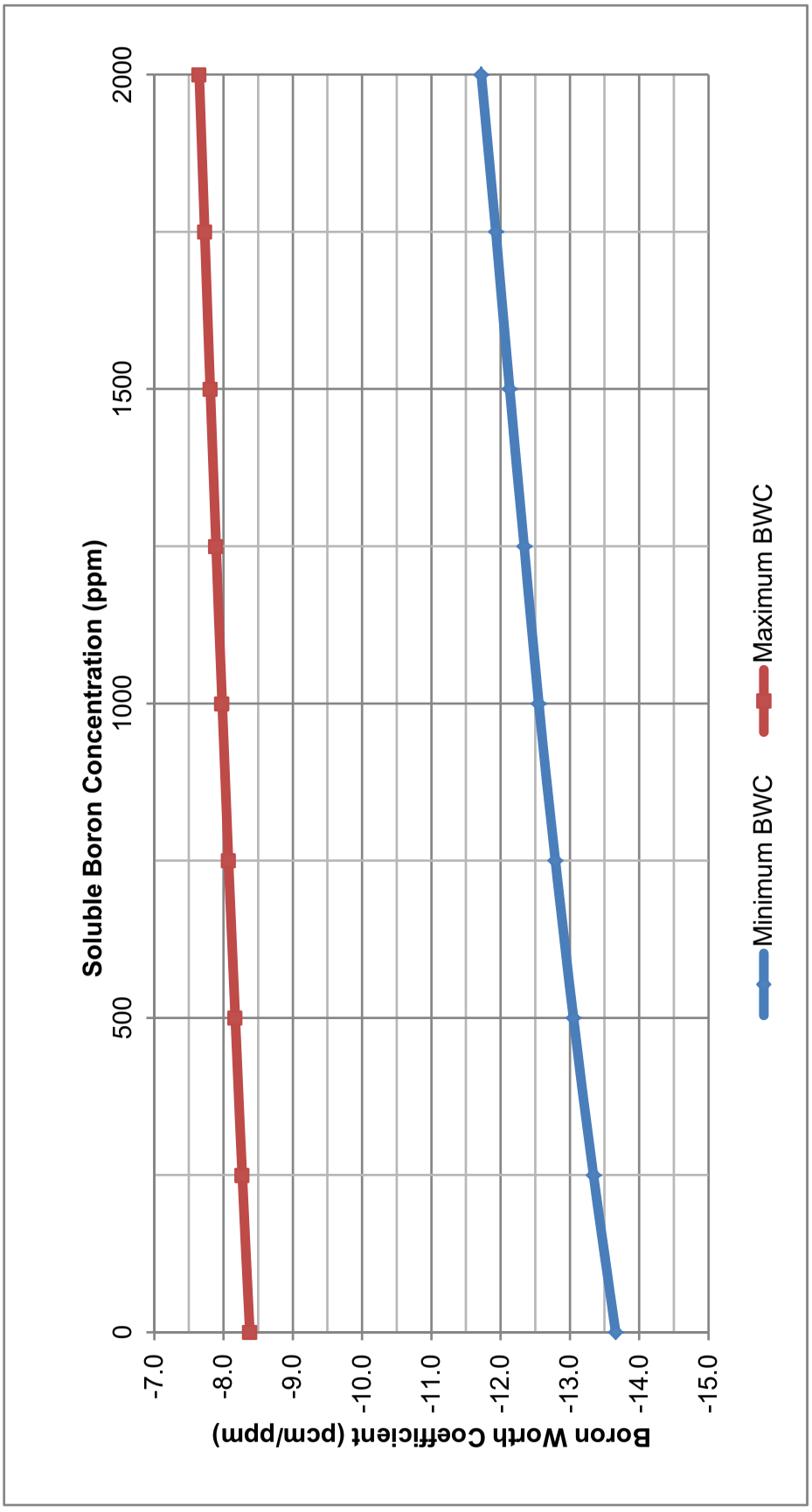

Figure 4.3-21: Boron Worth Coefficient

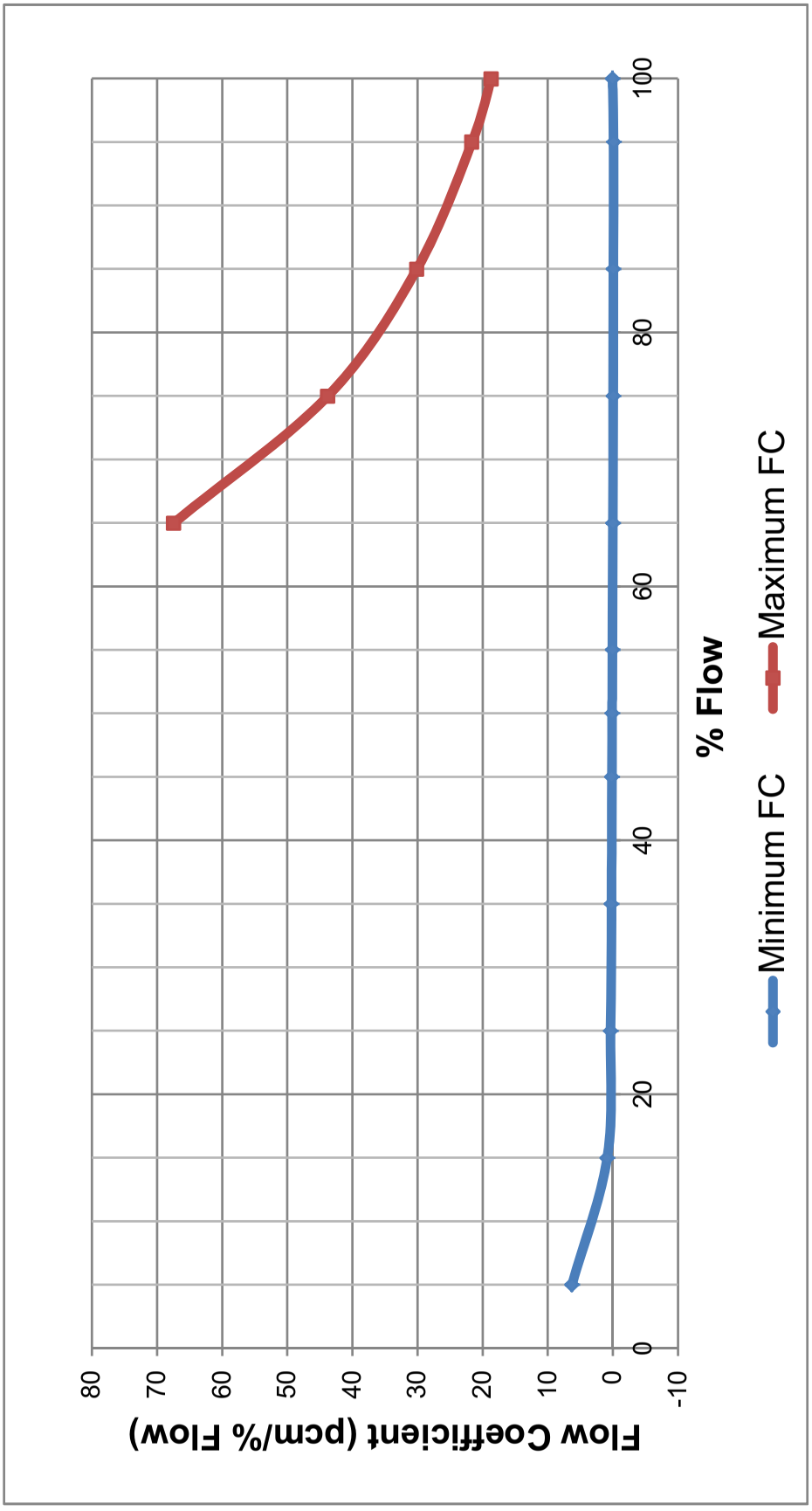

Figure 4.3-22: Flow Coefficient of Reactivity (Maximum and Minimum)

Figure 4.3-23: Control Rod Position versus Time after Trip

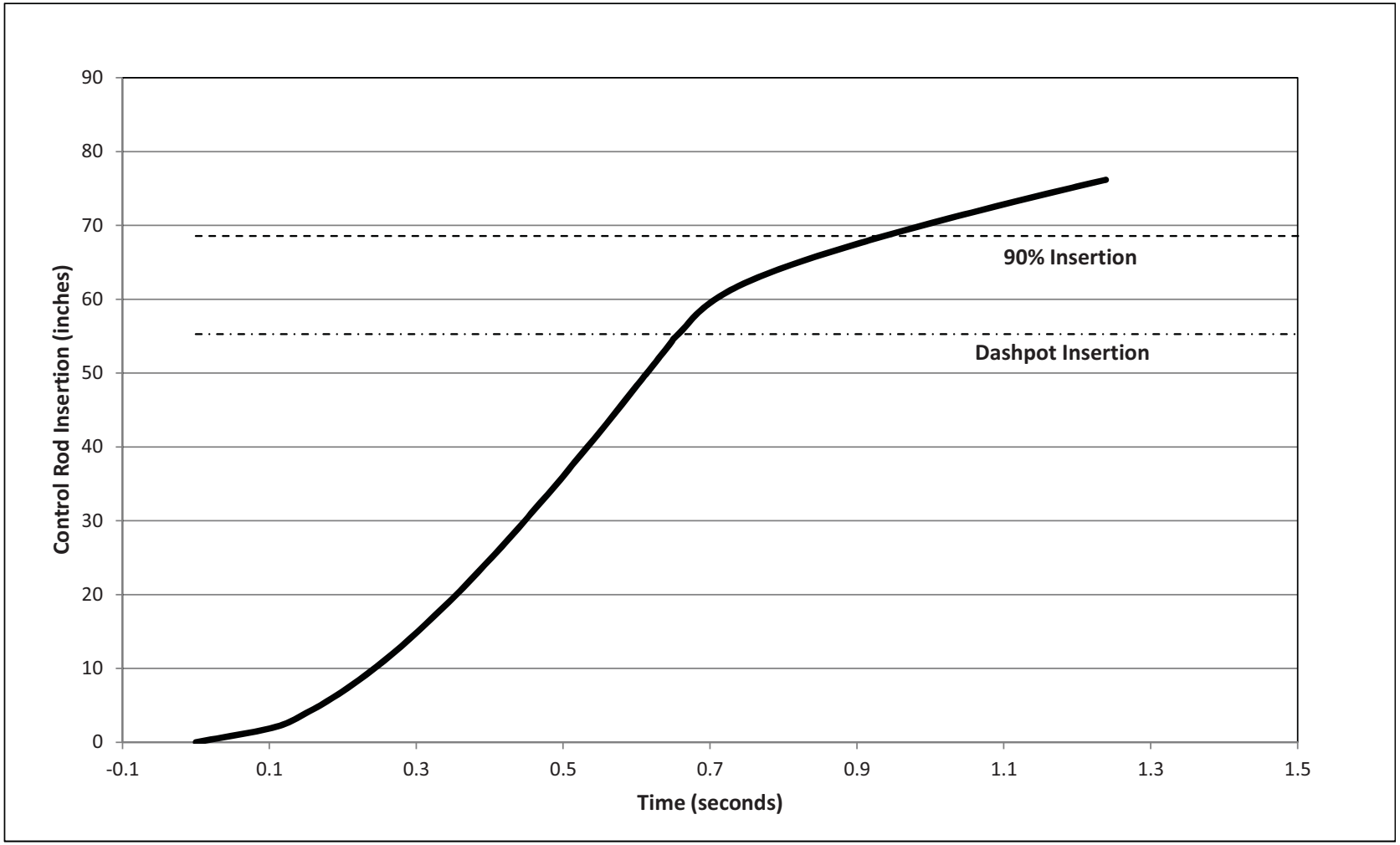

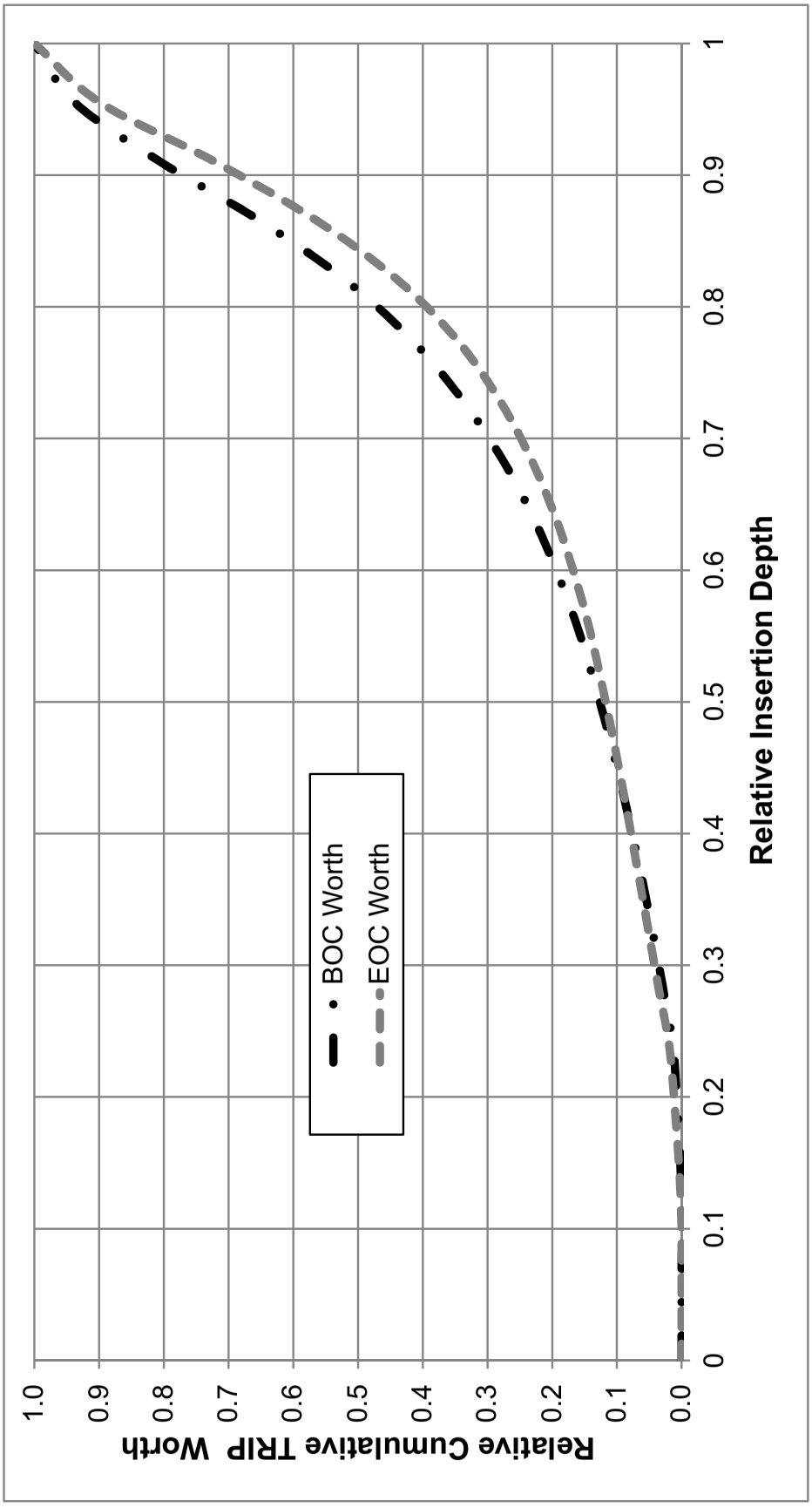

Figure 4.3-24: Reactivity Worth versus Control Rod Position

Figure 4.3-25: Cross-section view of MCNP6 Model for Vessel Irradiation Flux Calculation

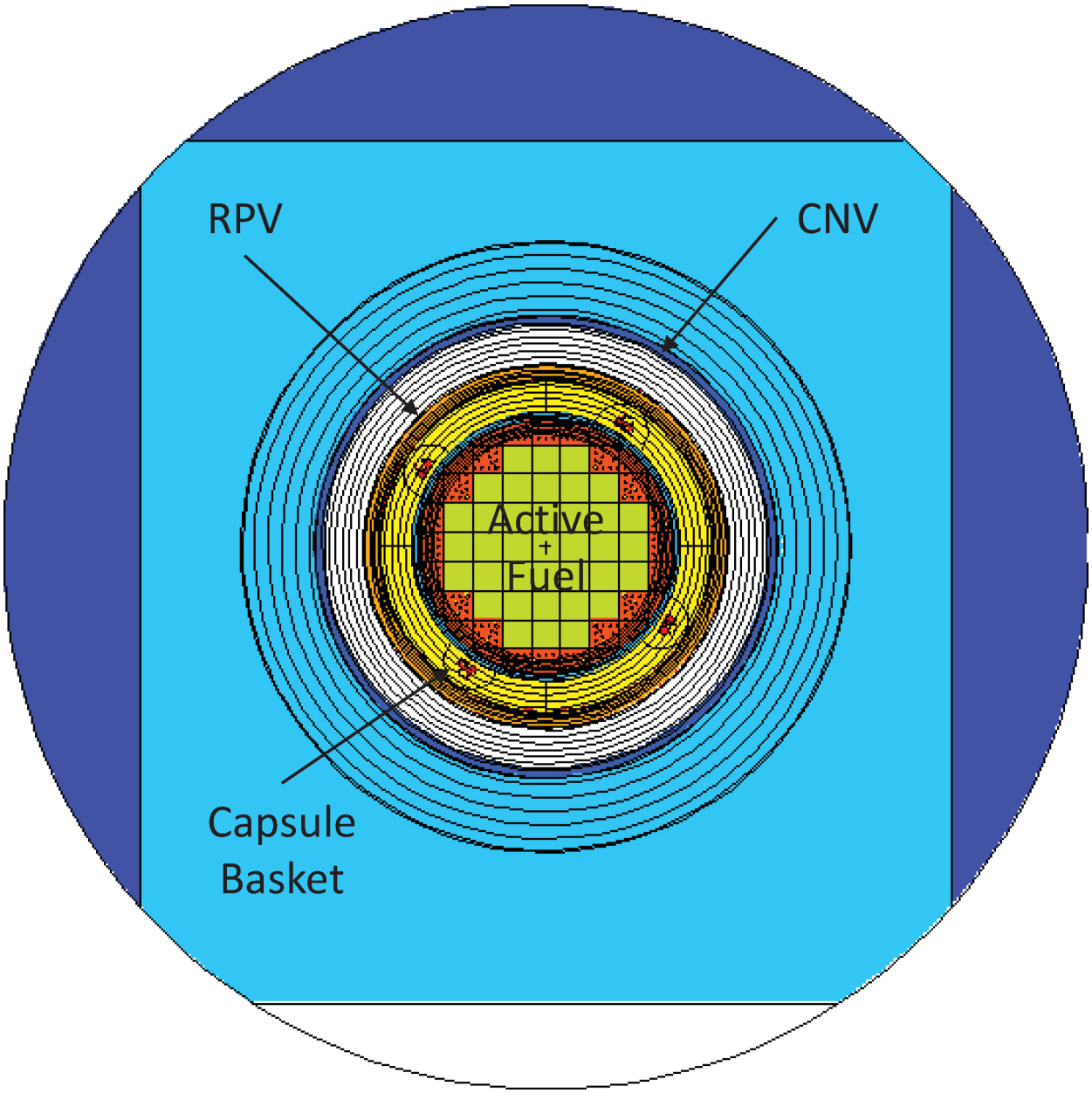

Figure 4.3-26: Typical Axial Xenon Oscillation for 100% Power at Beginning of Cycle

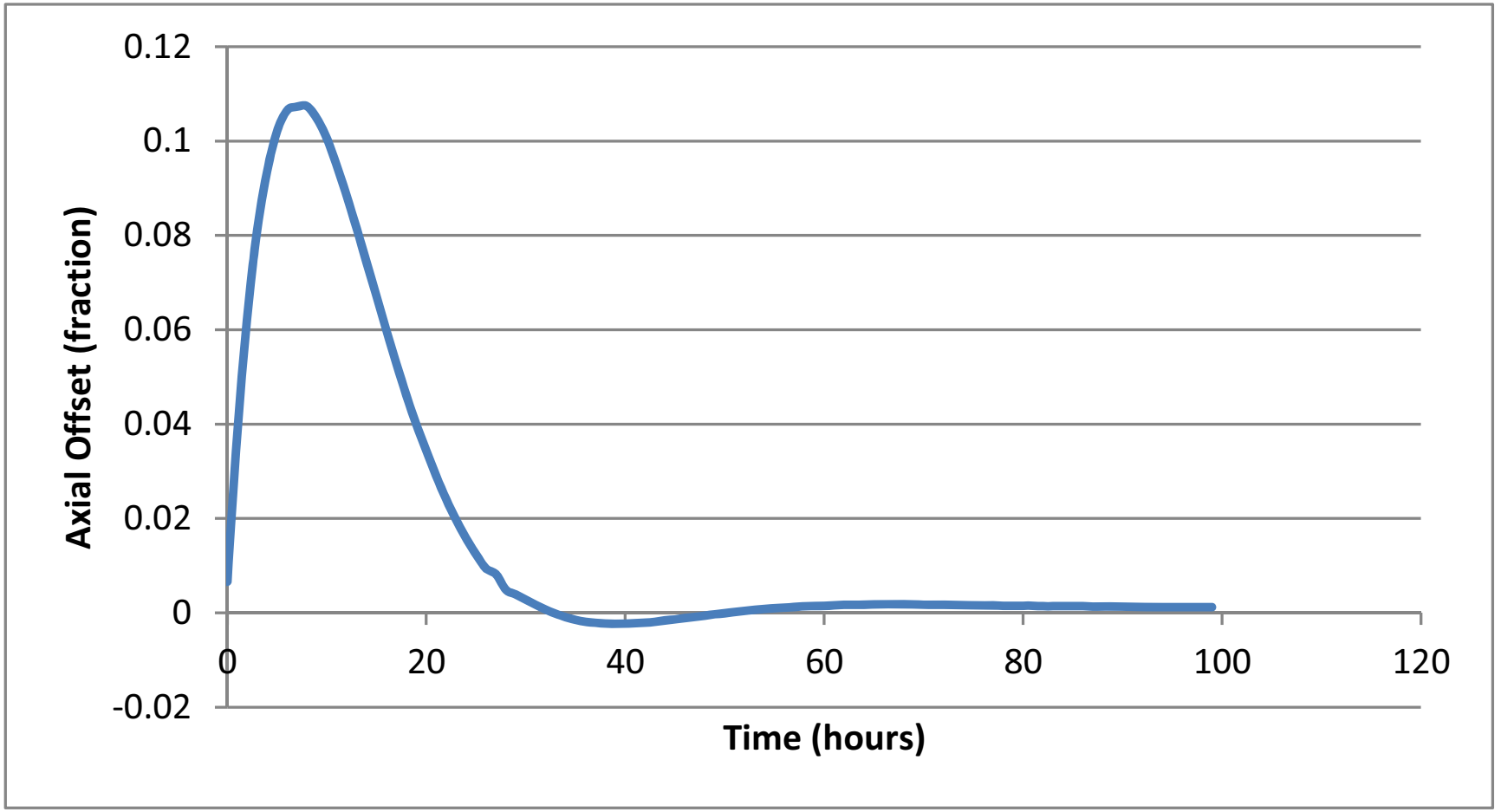

4.4 Thermal and Hydraulic Design

The thermal-hydraulic design of the NuScale Power Module (NPM) provides cooling for fuel and core components and protects the fuel and cladding during off normal conditions. Adherence to a set of specified acceptable fuel design limits (SAFDLs) preserves the integrity of the fuel and cladding and prevents release of fission products from the fuel.

The NPM is a natural circulation pressurized water reactor (PWR) with integral, once-through, helical coil steam generators (SGs). The driving force for natural circulation flow is the pressure head caused by the lower density water in the core and the higher density water in the downcomer. This pressure head varies with power and as a result there is a unique steady-state flow at each power level.

The methodology and analysis tools (i.e., licensing methodology) used in the thermal-hydraulic design are summarized in this section and described in detail in the referenced NuScale topical reports. The VIPRE-01 code is used for steady-state and transient subchannel fuel and temperature calculations. The PIM code is used for thermal-hydraulic stability calculations. The subchannel steady state results provided in this section and the transient results in Chapter 15 are performed in accordance with the methodology, including all restrictions, defined in Reference 4.4-3. The methodology is used to establish the power peaking limits and protect SAFDLs without using thermal margin-specific trips. Fuel rod thermal evaluations are performed at rated power and during transients up to the design limit burnup to verify the fuel temperature and integrity design bases described in Section 4.2.1 are satisfied. These analyses also provide input for the initial fuel rod thermal conditions used in Chapter 15 transient analyses.

Hydraulic flow instabilities are precluded by a regional exclusion solution. Detection and suppression of hydraulic instabilities is not required.

4.4.1 Design Basis

The design bases for the thermal-hydraulic design of the reactor are discussed below. The design bases for the mechanical design of the fuel are discussed in Section 4.2.1. The instrumentation and controls system design features that address the monitoring requirements in General Design Criterion (GDC) 13 and the protection system requirements in GDC 20 are described in Section 7.1.

Consistent with GDC 10, the thermal-hydraulic design of the reactor core includes sufficient margin to critical heat flux (CHF) to ensure adequate heat transfer with a 95-percent probability at the 95-percent (95/95) confidence level so that SAFDLS are not exceeded during any condition of normal operation, including the effects of anticipated operational occurrences (AOOs) and conditions that result in unstable power oscillations with the reactor trip system available.

Consistent with GDC 12, the thermal-hydraulic design of the core includes design and operational limits that preclude power instability such that fuel design limits are not exceeded.

The following are the design bases for the NuScale thermal-hydraulic design:

4.4.1.1 Critical Heat Flux

Adequate heat transfer from the fuel cladding to the reactor coolant is provided by assuring that critical heat flux limits are met during normal operation, AOOs, and infrequent events (IE). NuScale-specific CHF correlations are used to ensure that CHF does not occur with a 95 percent probability at a 95 percent confidence level during normal operation and abnormal operating occurrences. For some accidents, some rods may be predicted to exceed CHF criteria as long as the requirements of 10 CFR 100 are met.

4.4.1.2 Fuel Temperature

For normal operation and AOOs, the fuel melting temperature is not exceeded in any part of the core. These analyses are performed at rated power and during transients up to the design limit burnup as described in Section 4.2.

4.4.1.3 Core Flow

The core flow design basis is that 91.5 percent of the minimum design flow passes through the core and provides fuel cooling. This is based on a bypass flow of 8.5 percent which accounts for flow through the fuel assembly guide tubes, the reflector block, and the gap between the reflector block and the core barrel.

4.4.1.4 Hydrodynamic Stability

The hydrodynamic stability design basis is that normal operation and AOO events do not lead to hydrodynamic instability as discussed in Section 4.4.7.

4.4.2 Description of Thermal and Hydraulic Design of the Reactor Core

The NPM uses natural circulation to drive the flow in the reactor coolant system (RCS) to provide core heat removal during normal plant operation, AOOs, infrequent events (IEs), and accidents. A description of the thermal-hydraulic characteristics of the core is provided in the following sections.

4.4.2.1 Summary Comparison

Figure 5.1-3 shows the significant hydraulic features of the natural circulation flow path. Table 4.4-1 provides geometrical information on the key components of the RPV flow path.

Table 4.4-2 and the Subchannel Analysis Methodology topical report (Reference 4.4-3) provide the relevant parameters for the thermal-hydraulic evaluation of core performance of the NPM. Table 4.4-2 also provides similar information for other recent PWR designs for comparison purposes.

Table 4.4-3 summarizes the applicable ranges for some of the existing CHF and departure from nucleate boiling (DNB) correlations in the public domain. The Babcock

and Wilcox B&W-2 and Westinghouse W-3 CHF correlations were developed for their specific fuel assembly applications. The Electric Power Research Institute EPRI-1 critical heat flux correlation and the Atomic Energy of Canada Limited (AECL) critical heat flux look-up table were developed for general applications. The NuScale natural circulation flow conditions include conditions that are outside of the CHF test data provided by the B&W, EPRI, and Westinghouse correlations. Therefore, several test programs were conducted to obtain CHF test data for the NuScale reactor fuel design. These programs culminated in the development of the NuScale NSP2, NSP4, and Extended Hench-Levy CHF correlations which are described in Section 4.4.2.7.

4.4.2.2 Critical Heat Flux

The overall margin for protecting the fuel cladding SAFDLs is established by an analysis limit that accounts for testing uncertainties, manufacturing tolerances, and consideration of non-testing variations, such as rod bow, measurement uncertainties and instrumentation delays. Figure 4.4-1 provides a depiction of the NSP2 and NSP4 critical heat flux ratio (CHFR) limits and thermal margins.

For subchannel analysis, the key fuel failure mechanism is clad overheating in off-nominal conditions, such as AOOs, infrequent events, and accidents. Fuel rod failure occurs when the heat transfer coefficient between the fuel rod clad and coolant degrades significantly to due to the formation of a continuous vapor layer on the fuel rod. The degradation of the heat transfer coefficient in a two-phase flow condition is dependent on local conditions such as pressure, flow rate, coolant quality, and boiling regime. Various terms have been used to describe this phenomenon, including CHF, departure from nucleate boiling, critical power ratio, boiling crisis, boiling transition, burnout, and dryout.

The low flow steady-state nominal conditions and hypothetical transient and accident conditions in the NPM suggest that both the "DNB" and "Dryout" CHF mechanisms are relevant. "CHF" is a more general term, including both "DNB" and "Dryout," which are specific CHF mechanisms. For internal consistency in modeling the range of NuScale-specific phenomena, NuScale thermal margin analyses use the generic term CHF.

The parameter of interest for preventing the occurrence of CHF is the ratio of the critical heat flux to local heat flux, or CHFR:

$$CHFR = q''_{CHF} / q''_{local} \qquad \text{Eq. 4.4-1}$$

where

q''_{CHF} = critical heat flux, 10^6 btu/hr-ft^2, and

q''_{local} = local heat flux, 10^6 btu/hr-ft^2.

The NuScale CHFR limit for the NSP2 correlation that corresponds to a 95 percent probability of CHF at a 95 percent confidence level is 1.17. The NuScale CHFR limit for

the NSP4 correlation that corresponds to a 95 percent probability of CHF at a 95 percent confidence level is 1.21. The NSP2 and NSP4 critical heat flux correlations are used to evaluate thermal margin for normal operation, AOOs, infrequent events, and accidents, with the exception of those characterized by rapid depressurization. Events exhibiting a rapid depressurization are evaluated to a CHFR limit using the Extended Hench-Levy critical heat flux correlation. The Extended Hench-Levy critical heat flux correlation limit and range of applicability are provided in Appendix B of Reference 4.4-8.

The range of applicability of the NSP2 CHF correlation is:

Pressure, psia	300 to 2300
Local Mass Flux, $10^6 lb_m/hr\text{-}ft^2$	0.110 to 0.700
Local equilibrium quality, %	≤ 90.0
Inlet equilibrium quality, %	≤ 0

The range of applicability for the NSP4 correlation is:

Pressure, psia	500 to 2300
Mass flux, 10^6 lbm/hr-ft^2	0.116 to 0.635
Local equilibrium quality, %	≤ 95
Inlet equilibrium quality, %	≤ 0

The transient response of the reactor system is dependent on the initial power distribution. Limits provided by the core system and the protection system ensure that the design meets CHF design bases for AOOs. The core operating limits report (COLR) specifies the cycle-specific, power-peaking limits that maintain the core power distribution within prescribed limits during power operation. These power-peaking limits are expressed as limits on total heat flux (F_Q), enthalpy rise ($F_{\Delta H}$), and axial peak (F_Z). These power peaking factors are functions of burnup and power level. Section 4.3 provides additional discussion about the development and use of these limits.

- Enthalpy rise hot channel factor ($F_{\Delta H}$) is the ratio of the power in the hot rod divided by the power in the average rod. This all rods out (ARO) limit ensures that the design basis value for the CHFR is met for normal operation, operational transients, and IEs.
- The heat flux hot channel factor (or total peaking factor), F_Q, is the ratio of maximum local heat flux on the surface of a fuel rod to the average fuel rod heat flux. The maximum F_Q value is used to calculate the peak linear heat generation rate. The maximum F_Q value is utilized to ensure the specified acceptable fuel design limit for fuel centerline melting is not exceeded.
- Axial Peaking Factor (F_Z), is defined as the maximum relative power at any axial point in a fuel rod divided by the average power of the fuel rod. F_Z can be defined for a rod, an assembly, or the entire core.

The Module Protection System (MPS) automatically initiates and controls the protective actions necessary to mitigate the effects of the design basis events (DBEs)

identified in Table 7.1-1. The MPS reactor trip functions are listed in Table 7.1-3, including the associated parameter and analytical limits.

The core design and thermal limits are developed such that the thermal margin criteria are not exceeded for normal operation and AOOs. Specifically, there is a 95-percent probability at the 95-percent confidence level (95/95) that the hot rod in the core does not experience a CHF condition. For the purpose of this analysis, the CHF is assumed to occur if the subchannel analysis-calculated CHFR is less than the allowable limit. For IEs and accidents, the total number of fuel rods that exceed the criteria are assumed to fail and are used in determining the radiological dose source term.

4.4.2.3 Linear Heat Generation Rate

Limits on axial peaking factor are not required because the limits on F_Q and $F_{\Delta H}$ maintain a sufficiently flat power distribution, and axial peaking is treated in a multi-layered approach involving both operational restrictions and analysis.

A limit on peak linear heat generation rate (PLHGR) is specified to help ensure that fuel performance limits are not exceeded. The design limit on PLHGR maintains the fuel temperature below the centerline melt criterion and limits the peak cladding temperature so cladding-coolant chemical interactions remain within the acceptable range.

The total heat flux peaking factor (F_Q) is used to calculate the PLHGR. Section 4.3 provides a discussion on the calculation of the PLHGR based on the linear heat generation (LHGR) and the design F_Q.

4.4.2.4 Subchannel Analytical Results

Figure 4.4-2 through Figure 4.4-8 provide maps of the typical distribution of thermal hydraulic parameters throughout the NuScale core. These steady state analyses are performed using VIPRE-01 and are based on an equilibrium cycle power distribution at 100 percent power. The equilibrium cycle is the reference cycle described in Section 4.3. Each rod and subchannel in the one-eighth core is modeled in this analysis. Figure 4.4-2 provides the enthalpy rise hot channel factor for each individual rod ($F_{\Delta H}$) in the one-eighth core. For the best estimate analysis, the MCHFR for the entire core (using the NSP4 correlation) is 9.6 (compared to the 95/95 design safety limit of 1.21). Figure 4.4-4 shows the maximum clad outer wall temperature for each rod in the core. Figure 4.4-5 shows the maximum rod heat flux, Figure 4.4-6 the average channel mass flux, and Figure 4.4-7 the exit equilibrium quality for each subchannel. Figure 4.4-8 provides the coolant temperature at the exit of each subchannel. These values are best estimate values in that they do not include the uncertainties that are discussed later in this section and that are applied in a subchannel analysis. A figure for void fraction is not provided because the channel exit void fractions are zero except for the hot channel which is 0.01. Table 4.4-7 shows the exit void fractions for the core average and hot channel for the equilibrium power distribution in Figure 4.4-2. In addition, Table 4.4-7 shows the same void fraction values using the conservative 24-channel subchannel model with all uncertainties applied. The 24-channel model is described in Section 4.4.4.5.2 and in Reference 4.4-3.

It is important to maintain subcooled margin in the riser (area above the control rod guide tubes) during normal operation to ensure that margin-to-thermal-hydraulic stability is maintained as discussed later in Section 4.4.7. A reactor trip actuates 5 degrees F before the core outlet average temperature reaches saturation (Section 7.1).

4.4.2.5 Core Coolant Flow Distribution

The NuScale design uses natural circulation, and there is no active control of the core flow. The core inlet flow distribution is dependent upon the geometry of the RCS loop, including the lower core plate and bypass flow paths. The core bypass flow paths are discussed in Section 4.4.3.1. There are flow inlets for each of the fuel assemblies in the core, similar to currently licensed PWR fuel designs. However, the design of the NPM is unique because the flow distribution is dependent upon the buoyancy-driven flow rate and vessel design. The core inlet flow distribution changes based on power level, axial and radial power distribution, and core average temperature. The inlet flow distribution is determined by computational fluid dynamics. The analysis indicates that at full power the peripheral assemblies receive from 3.5 to 4.5 percent less than average flow, the central assembly receives up to 3.5 percent less than average, and the assemblies located between the central assembly and the peripheral assemblies receive up to 3.6 percent more flow than the average assembly.

Several inlet flow distributions are evaluated in Reference 4.4-3 to understand the effect on CHF. For up to a 15 percent inlet flow reduction to the hot fuel assembly, the flows equalize after the flow reaches approximately one-third of the active fuel length, resulting in an insignificant decrease in MCFHR. Additionally, for a given radial power distribution, there was no sensitivity observed to the inlet flow distribution. A 5 percent reduction in the flow to the hot assembly is used in the subchannel analysis.

4.4.2.5.1 Core Coolant Temperature Distribution

As discussed in Reference 4.4-3, the core inlet temperature distribution is a boundary condition input for steady-state and transient subchannel analysis that is dependent on nuclear steam supply system design geometry. In the helical coil SG design, the primary RCS flow is on the shell side and the secondary feedwater flow is through the tubes. The concentric geometry of the SGs relative to the core removes any asymmetric helical coil SG influences on the coolant through the downcomer into the core inlet. A computational fluid dynamics calculation for the RCS loop determines the core inlet temperature distribution for several power levels and power distributions in the NPM design. The largest deviation in core inlet temperature to a fuel assembly is less than 0.25 degrees F from the average inlet temperature. A uniform core inlet temperature that is 5 degrees F higher than design is assumed in the subchannel analysis for AOOs, infrequent events, and accidents.

4.4.2.5.2 Turbulent Mixing

The turbulent mixing model within VIPRE-01 accounts for the exchange of enthalpy and momentum between adjacent subchannels caused by turbulent flow. The coefficient for turbulent mixing and the turbulent momentum factor are

the two inputs needed for this model. This mixing model is incorporated into the VIPRE-01 energy and momentum equations, which is dependent on the amount of turbulent crossflow per unit length.

The NuScale turbulent mixing coefficient is determined from thermal mixing tests and the value is fuel-design specific. This value is further justified based on parametric sensitivity analysis described in Reference 4.4-3.

The value for the turbulent momentum parameter is not measured and is justified based on parametric sensitivity analysis provided in Reference 4.4-3. The sensitivity study results demonstrate that the NPM base model is not sensitive to the turbulent momentum parameter.

4.4.2.6 Core Pressure Drops and Hydraulic Loads

4.4.2.6.1 Hydraulic Loads

The NuScale fuel assemblies do not experience liftoff from the lower core plate under normal operating conditions and AOOs as described in Section 4.2. A liftoff analysis is performed using the hydraulic flow loads from zero percent to 102 percent power. The analysis considers the weight of a fuel assembly, the displaced fuel assembly volume, the fuel assembly springs, the maximum design flow rate, and the core average temperature. The calculated maximum hydraulic lift force is a small fraction of the assembly weight.

4.4.2.6.2 Core Pressure Drop

Flow testing on a full-scale prototype fuel assembly was performed to establish flow component loss coefficients and other related flow characterization parameters for the NuScale fuel assembly. The form loss coefficients are used in the fuel assembly liftoff analysis and the subchannel analysis. Fuel assembly pressure drop tests were performed for a range of steady-state conditions as part of the CHF testing program. The pressure drop across the core at full power conditions is provided in Reference 4.4-3.

4.4.2.7 Correlations and Physical Data

As discussed in the Critical Heat Flux topical report (Reference 4.4-1), CHF tests were performed at Stern Laboratories and at the AREVA KATHY test facility. These tests obtained steady-state CHF data used in the creation and validation of the NSP2 and NSP4 critical heat flux correlations. The Stern tests were performed on an assembly comparable to the NuScale fuel design, but with simple non-mixing spacer grids rather than the HMP™ and HTP™ spacer grids. As described in Section 4.2, the NuScale fuel assembly contains four intermediate spacer grids (HTP™) which induce a swirling flow pattern in the coolant and a single HMP™ non-mixing grid at the bottom of the assembly. The three Stern tests provide data over a range that encompasses the NPM operating parameter values and are used to develop a base CHF correlation. A set of CHF tests from the AREVA KATHY facility tested an assembly design that included the HMP™ spacer grids. The test was conducted with two different axial power profiles as described in Reference 4.4-1. The tests included both unit cell (four fuel rods) and cells

containing guide tubes (three fuel rods and a guide tube). The Stern data provides the basis for the NSP2 correlation and the AREVA data validates the NSP2 correlation and provides the basis for the NSP4 correlation that conservatively predicts NuFuel HTP2™ critical heat flux performance.

The Extended Hench-Levy correlation (Reference 4.4-8) is based on Stern data with the KATHY data providing validation to conservatively predict NuFuel HTP2™ critical heat flux performance for an inadvertent opening of a reactor pressure vessel valve event.

Comparisons between Stern Laboratories and KATHY data can be found in Reference 4.4-1.

The limiting non-loss-of-coolant accident (LOCA) analyses in Chapter 15 are performed using NRELAP5 code. Once the limiting cases for each transient are identified, the determination of the thermal margin is performed using the VIPRE-01 subchannel core model with the NSP4 critical heat flux correlation. This subchannel model is described in detail in Reference 4.4-3. It is used with a conservative radial and axial power distribution and with all uncertainties applied deterministically as described in the reference.

The limiting rapid depressurization analyses in Chapter 15 are performed using the NRELAP5 code. Determination of thermal margin is also performed using the NRELAP5 code with the Extended Hench-Levy critical heat flux correlation as detailed in Appendix B of Reference 4.4-8.

4.4.2.8 Thermal Effects of Operational Transients

The subchannel analysis approach described below demonstrates that thermal-margin specific trips are not necessary to mitigate AOOs. The CHF analyses demonstrate that safety limits are met with the minimal operational constraints described in Section 4.4.3.2.

This section also demonstrates that hydraulic flow instabilities are precluded by reactor trip signals that occur prior to the development of any flow instabilities so that detection and suppression of hydraulic instabilities is not required.

4.4.2.9 Uncertainties in Estimates

Uncertainties or biases are incorporated into the subchannel methodology to provide conservatism. These uncertainties establish the design limit for the CHF correlation as shown in Figure 4.4-1. The derivation of the penalties or conservative bias are discussed in Reference 4.4-3. Uncertainties in the CHF correlation, analytical methods, operating conditions, physical inputs, core inlet flow distribution, and core exit pressure are considered in the subchannel analysis.

4.4.2.9.1 Correlation Uncertainties

There are uncertainties that are accounted for in subchannel safety analysis calculations, including those from the analysis method, physical manufacturing

design inputs to the model, and operating conditions. The application of uncertainties in the NuScale subchannel methodology is deterministic, which means that the uncertainty associated with a parameter is applied in the conservative direction without considering the statistical combination of the uncertainties.

4.4.2.9.1.1 Analysis Method Uncertainties

The analysis method uncertainties include the computer code uncertainty and CHF correlation uncertainty. The computer code uncertainty comes from axial and radial modeling and the approximations in the governing constitutive equations in the VIPRE-01 code. The adequacy of the axial and radial models were confirmed with sensitivity studies.

Code comparisons to data in applicable ranges are used to reduce code uncertainty. Most of this test validation is by benchmarking to COBRA-FLX (Reference 4.4-5), an approved subchannel analysis code with an approved Safety Evaluation Report (Reference 4.4-6). The benchmark results for VIPRE-01 compare well for conditions anticipated for NuScale Power Plant applications and establish that no penalty is needed for computer code calculation bias.

The CHF correlation uncertainty is included in the 95/95 minimum critical heat flux ratio (MCHFR) safety limit of the NuScale-specific NSP2 and NSP4 CHF correlations. The CHF correlations are developed from the local conditions derived from a simulated subchannel model of the CHF test, using the subchannel software, in this case VIPRE-01. Therefore, the uncertainty in the computer code is included in the CHF correlation itself.

The CHF correlation development inherently accounts for VIPRE-01 code uncertainty and the 95/95 CHF design limit accounts for this uncertainty. For this reason, no additional penalties for uncertainty in analysis method are added to the subchannel calculations.

4.4.2.9.1.2 Uncertainty in Operating Conditions

The operating boundary conditions are input into the subchannel analysis to account for measurement uncertainty. The values for these uncertainties are based on the instrumentation used for monitoring and are plant specific. The measurement uncertainties consist of those related to core power, system flow, core inlet temperature, and core exit pressure. The operating uncertainties are comparable to those used in the industry and are discussed in Reference 4.4-3.

The core bypass flow is important because bypass flow is not available for heat transfer from the cladding. The core inlet flow boundary condition accounts for the appropriate bypass flow. The bypass values used for safety analysis are determined as analytical maximum values rather than best-estimate values.

4.4.2.9.2 Uncertainties in Physical Data Inputs

The following uncertainties in physical data used in the VIPRE-01 subchannel analysis are accounted for in the VIPRE-01 subchannel analysis model:

- enthalpy rise engineering uncertainty ($F^E_{\Delta H}$)
- heat flux engineering uncertainty (F^E_Q)
- LHGR engineering uncertainty (F^E_{LHGR})
- radial power distribution uncertainty
- fuel rod bow and assembly bow uncertainty
- core inlet flow distribution uncertainty
- core exit pressure distribution uncertainty

The enthalpy rise engineering uncertainty ($F^E_{\Delta H}$) is applied to the hot channel to account for small fabrication uncertainties related to allowable manufacturing tolerances. This factor accounts for variations in pellet diameter, pellet density, enrichment, fuel rod diameter, and fuel rod pitch.

The $F_{\Delta H}$ hot channel factor uncertainty penalty factor is directly applied to the hot rod $F_{\Delta H}$. For transients that use the fully detailed model and pin-by-pin $F_{\Delta H}$ distribution, the hot channel factor for enthalpy rise is applied to the hot rod, independent of the location.

The heat flux engineering uncertainty factor (F^E_Q) accounts for the small manufacturing uncertainties (pellet density, enrichment, fuel rod surface area) that affect the local heat flux. For application of the heat flux engineering uncertainty, the heat flux from the conduction model is applied as a direct penalty to the VIPRE-01-calculated MCHFR by increasing the CHF 95/95 limit.

The LHGR hot channel factor is very similar to the heat flux hot channel factor, except that the fuel rod surface area uncertainty is excluded because the fuel rod outer diameter does not significantly impact the LHGR of the pellet. The LHGR engineering uncertainty (F^E_{LHGR}) is used directly in the subchannel analysis.

The (F^E_{LHGR}) hot channel factor is applicable for PLHGR fuel centerline melt calculations. This uncertainty factor is used as a penalty on the PLHGR. The radial power distribution uncertainty is related to the neutronics code that is used for the radial power distribution inputs. The power of rods a few rows away from the hot rod/channel have a negligible impact on the MCHFR. With the hot rod in the subchannel model placed at the design limit $F_{\Delta H}$, and any neutronic code uncertainty accounted for in the core design, no radial power distribution penalty needs to be applied.

For the asymmetric events that use augmentation factors to account for a larger $F_{\Delta H}$ due to the asymmetry, the relative change in $F_{\Delta H}$ is applied to the hot rod and negates the need for bias or uncertainty impacts on results. For calculations that use a pin-by-pin or fully detailed power distribution for $F_{\Delta H}$, it is conservative without additional factors in that the peak rod conditions are conservative. A radial distribution uncertainty is not applied because conditions far away from the hot rod have a negligible effect on MCHFR.

Fuel rod bowing can have a negative impact on CHF because of reduced flow area in the hot channel. Determination of the necessity of a rod bow penalty is performed for MCHFR and LHGR applications. For MCHFR, a penalty is derived based on the magnitude of the gap closure and the reduction in CHF to reach failure in bowed rods.

The penalty for rod bow is applied externally to VIPRE-01 by increasing the CHF analysis limit that is used for margin comparison. The penalty is applied and determined for the highest exposure of any assembly in the core, regardless of where the hot channel MCHFR occurs. The CHF analysis limit used for thermal margin evaluations biases the 95/95 MCHFR design limit by the penalty for potential rod or assembly bowing. The penalty for rod bow is 3 percent as described in Reference 4.4-3. This penalty is a conservative value based on the AREVA methodology for rod bow in Reference 4.4-2, which was demonstrated to be applicable for the NuScale fuel design in Reference 4.4-7.

The F^E_Q and rod bow penalties are both applied to the MCHFR design limit in accordance with the methodology in Reference 4.4-3. As shown in Figure 4.4-1, the 95/95 MCHFR design limit for the NSP4 CHF correlation is 1.21. The CHF analysis limit becomes 1.284 with the F^E_Q and rod bow penalties applied.

As discussed in Reference 4.4-3, the RCS pressure bias is not consistent across all conditions. As a result, case dependent bias directions on pressure are utilized to ensure a conservative calculation of MCHFR.

Core Inlet Flow Distribution Uncertainty

The core inlet flow distribution is discussed in Section 4.4.2.5. For the subchannel analysis methodology, inlet flow distribution uncertainty is applied to the hot or limiting assembly as shown in the distributions presented in Reference 4.4-3. The open lattice of the NuScale core allows flow redistribution to occur for inlet flow imbalances and the 5 percent reduction to the hot assembly assumed has a minimal effect on MCHFR.

Core Exit Pressure Distribution Uncertainty

The open upper plenum design allows for pressure equilibrium and no core exit pressure distribution uncertainty is necessary for the subchannel analyses.

4.4.2.10 Flux Tilt Considerations

Radial tilt is a condition where the power is not symmetric between azimuthally symmetric fuel assemblies. Azimuthal power tilt is an allowable limit on operation. Once the flux tilt is beyond an allowable threshold, actions are required to remedy the condition.

The design $F_{\Delta H}$ safety limit inherently accounts for the radial tilt, expressed as:

$$F_{\Delta H}^{TS} = F_{\Delta H}(1 + T_q)$$

where,

$F_{\Delta H}^{TS}$ = COLR enthalpy rise design peaking factor,

$F_{\Delta H}$ = Design limit for core design calculations, and

T_q = azimuthal tilt.

The design limit is met by accounting for radial tilt due to asymmetric power peaking. Radial tilt is evaluated in core design calculations by inducing xenon oscillations or transients. Xenon transients are triggered by inserting control rod banks or single control rods as discussed in Section 4.3.2.7. The maximum calculated radial peaking factor after the resulting tilt is then compared to the COLR $F_{\Delta H}$ design peaking factor to ensure that it is below the limit.

The subchannel analysis methodology requires no additional factor to account for radial tilt as described in Reference 4.4-3. Table 4.4-4 lists the uncertainties used in the subchannel analyses of AOOs. The development of the uncertainties and the values used in the subchannel analysis are provided in Reference 4.4-3.

4.4.3 Description of the Thermal and Hydraulic Design of the Reactor Coolant System

The NPM is a self-contained nuclear steam supply system comprised of a reactor core, a pressurizer, and two SGs integrated within the RPV. The RPV is an approximately cylindrical steel vessel. The upper and lower heads are torispherical. The pressurizer baffle plate is integrated with the steam plenums, and has orifices to allow surges of water into and out of the pressurizer, and acts as a thermal and hydraulic barrier.

Figure 5.1-1 is a diagram of an NPM and shows the RPV within the containment vessel. Figure 5.1-2 provides a simplified diagram of the RCS. Figure 5.1-3 denotes and describes the major RPV loop flow paths during normal, steady-state, and full-power operating conditions.

4.4.3.1 Plant Configuration Data

Table 5.1-2 lists the nominal operating parameters of the RCS at various power levels. Table 4.4-1 provides geometrical information on the key components of the RPV flow path.

4.4.3.1.1 Core Bypass Flow

The subchannel analysis considers the flow through the heated core and does not consider the flow that effectively bypasses the fuel rods and is not available to remove heat.

The following flow paths allow flow to bypass the core and reduce flow through the fuel assemblies:

- reflector block cooling channels
- fuel assembly guide tubes and instrument tubes

Best-estimate flow, maximum flow, and minimum flow are calculated for the applicable design considerations. These calculations account for the uncertainties in the component flow resistances and the thermal head.

4.4.3.1.1.1 Reflector Cooling Channel Bypass

The reflector blocks surrounding the core have several cooling channels that allow flow to pass through the reflector blocks. A conservative value for the reflector cooling channel bypass fraction for steady-state and transients is provided in Reference 4.4-3.

4.4.3.1.1.2 Guide Tube and Instrument Tube Bypass

The maximum amount of bypass flow for the guide tubes and instrument tubes for the fuel assemblies is provided in Reference 4.4-3.

The total bypass flow used in the subchannel analysis is 8.5 percent.

4.4.3.2 Analytical Design Operating Restrictions

Figure 4.4-9 provides the operating map showing analytical and normal operating conditions. The green dotted line with T_{cold}, T_{avg}, and T_{hot} identified represent nominal full power operating conditions. T_{avg} remains fixed above 15 percent rated thermal power (RTP); T_{cold} and T_{hot} vary along the green dotted line as power is increased or decreased. The solid blue and black dotted lines illustrate the normal T_{avg} and RCS pressure operating ranges, excluding the T_{avg} during startup with the reactor at less than 15 percent RTP.

The analytical limits on the operating range that are illustrated as the outer box (red on three sides, blue at minimum critical temperature) constrained by the following considerations:

- Upper RCS pressure bound: analytical limit protects against exceeding RPV pressure limits for reactivity and heatup events
- Lower RCS pressure bound: analytical limit ensures riser subcooling is maintained.
- Left-hand temperature boundary: analytical limit on minimum temperature for criticality
- Right-hand average temperature limit: analytical riser temperature limit protects against exceeding MCHFR limits for reactivity and heatup events.

If hot leg temperature is below 600 degrees F, the low pressure analytical limit is constant at 1600 psia. If hot leg temperature is above 600 degrees F, then the low pressure analytical limit increases to 1720 psia. The saturation curve and a parallel, 5 degrees F margin are illustrated on the right side of the figure showing the margin to saturation in the riser based on the analytical limits shown.

4.4.3.3 Thermal Margin Limit Map

A series of CHF calculations are performed for a range of power levels between hot zero power (HZP) and HFP to establish trends and operating conditions of the limiting MCHFR, and to determine the limiting axial flux shapes for subchannel calculations. The limiting axial flux shape is determined based on a nuclear analysis (Section 4.3) of all of the possible axial flux shapes that could occur during the equilibrium cycle from operation within the operating limits. The operating limits in this context are the axial offset window, the power dependent insertion limits, and the cycle burnup. The analysis of axial flux shapes is described in Section 4.3. From these axial shapes, limiting top-peaked, middle-peaked, and bottom-peaked shapes are identified at 5 percent, 25 percent, 50 percent, 75 percent, and 102 percent. At each power level, a subchannel analysis is performed using VIPRE-01 to determine the MCHFR for a top-peaked, a middle-peaked, and a bottom-peaked shape. The MCHFR calculations are performed including the deterministically combined uncertainties discussed in Section 4.4.2.9 and summarized in Table 4.4-4. The results of this analysis identify a unique limiting shape for each power level. These limiting axial flux shapes are used to develop the thermal margin limit map.

The thermal margin limit map provides the inlet temperature and power level where operation is allowed to ensure that there are no fuel failures due to CHF and that the core exit conditions are not at saturation. The CHF limit prevents fuel failures and the core exit saturation limit ensures margin for thermal-hydraulic stability.

Using the limiting axial shapes determined from the power-flow analyses described previously, a set of thermal margin limit cases are performed with the VIPRE-01 subchannel model. These cases vary inlet temperature, pressure, and power level that result in a MCHFR at the 95/95 limit. These cases provide the MCHFR component of the thermal margin limit map.

A set of thermal margin limit cases are also performed with VIPRE-01 to determine the core inlet temperature that results in core exit saturation temperature as a function of power.

Figure 4.4-11 provides a plot of the resulting thermal margin limit map that includes both the MCHFR and core exit saturation components. The saturation limits (dashed lines) correspond to the combination of core inlet temperature and power that result in core average outlet temperature being at the saturation temperature. There are two dashed lines based on the natural circulation flow rates that correspond to the allowed minimum and maximum core average temperature at each power level. The solid curve is the combination of inlet temperature and power level that results in a MCHFR being at the design limit. The MCHFR calculations are performed assuming the limiting radial and axial power distributions previously discussed. These calculations are also performed including the deterministically combined uncertainties discussed in Section 4.4.2.9. As can be seen from the figure, the CHF analysis limit portion of the thermal margin limit map is well above 100 percent power.

4.4.3.3.1 Flow Stability Exclusion Regions

The NuScale flow stability protection solution uses a regional exclusion solution as described in the "Evaluation Methodology for Stability Analysis of the NuScale Power Module" topical report (Reference 4.4-4). The region is defined by a single point specifying riser subcooling margin. The stability exclusion region is protected by automatic MPS protective action.

Section 15.9.2 describes stability analysis application methodology using the PIM computer code. The methodology specifies the type and scope of the generic analysis used to define the exclusion region as well as the margins and the analytical limit for the reactor protection trips required to prevent unstable flow oscillations.

4.4.3.4 Power-Maneuvering Characteristics

While power maneuvering operations within the capability of the rod control system are anticipated to support power demands, continuous power maneuvering is not assumed in the analysis of the reference equilibrium cycle, as indicated in Section 4.3. However, planned continuous power maneuvering will be considered as part of a cycle-specific core design using the methodologies described in Technical Specification 5.6.3. The limiting axial flux shape that is described in Section 4.4.4.3 will include the impact of planned power maneuvering. Power control is accomplished using boron control and control rod positioning.

Section 4.3.2 describes the analysis used to generate the wide range of normal operation axial power shapes used to establish operating limits for normal steady state and power control operations. These limiting power distributions are controlled during operation by technical specifications that require operation within the axial offset (AO) window and within the power dependent insertion limits (PDILs).

The fixed in-core flux measurements and resulting power distribution continuously displayed in the control room and provide further assurance that the power distributions both axially and radially are not exceeded. Operation outside these limits is not allowed by the plant technical specifications.

4.4.3.5 Thermal and Hydraulic Characteristics Summary Table

Table 4.4-2 summarizes the thermal-hydraulic characteristics of the NPM.

4.4.4 Evaluation

Conformance to GDC 10 requirements is demonstrated by establishing SAFDLs and ensuring that the plant stays within the SAFDLs. These limits ensure that the fuel clad is not breached (and thus this fission product barrier remains intact), that fuel system dimensions remain within operational tolerances, and that functional capabilities are not reduced below those assumed in the safety analysis. The subchannel core thermal-hydraulic analysis determines that the MCHFR is maintained above the 95/95 limit during normal operation and AOOs, ensuring the SAFDLs are satisfied and fuel cladding integrity is demonstrated. The thermal margin criteria are not exceeded for normal operation and AOOs. For IEs and accidents, the total number of fuel rods that exceed the criteria and are assumed to fail is used as input for radiological dose calculation purposes.

4.4.4.1 Critical Heat Flux Correlation

The functional form of the NSP2 and NSP4 critical heat flux correlations are expressed as a curve fit to a number of physical parameters including:

- pressure
- cold wall factor
- boiling length
- local mass flux
- local equilibrium quality

The coefficients of the critical heat flux correlations are determined with a cross-validation process and linear least-squares regression based on local condition parameters calculated with the VIPRE-01 subchannel thermal-hydraulics code. The form of the equation and correlation coefficients and the details of the development of the correlations are provided in Reference 4.4-1. Details of the development for the Extended Hench-Levy critical heat flux correlation are provided in Appendix B of Reference 4.4-8.

4.4.4.2 Core Hydraulics

As discussed in Section 4.4.2.5.1, a uniform inlet temperature distribution is assumed that is 5 degrees F above the expected inlet temperature.

Table 4.4-5 lists the principal flow elements in the RPV flow path and describes the flow path.

4.4.4.3 Influence of Power Distribution

The subchannel analysis basemodel is developed to conservatively represent a cycle-specific core as described in Reference 4.4-3. The model preserves limiting core

conditions along with the operational envelope specified in the cycle-specific COLR. The envelope accounts for power distribution throughout the core using design peaking factors in combination with the limiting RCS parameters such as flow and pressure. An eighth-core symmetric subchannel analysis model is used to capture the limiting conditions of the cycle-specific core.

The radial power distribution for the core is characterized by the enthalpy rise hot channel factor $F_{\Delta H}$, which is the ratio of the maximum integrated rod power within the core to the average rod power. $F_{\Delta H}$ is variable depending on the cycle design, the exposure, fuel composition, burnable poison loading, operational history, and thermal-hydraulic conditions. As a result, the location of the peak $F_{\Delta H}$ fuel rod changes throughout an operating cycle.

A conservative core power distribution that bounds the cycle-specific or time-in-life dependent radial power distribution is used to make the radial power distribution independent of specific cycle core designs. The analysis for each cycle loading pattern confirms that this limiting radial power distribution is bounding for the fuel cycle.

The Core Operating Limit Report (COLR) imposes a limitation on the peak value of $F_{\Delta H}$, and therefore limits the highest value for any fuel rod at hot full power. The $F_{\Delta H}$ peaking design limit, also known as the core operating limit peaking factor, is increased for lower power levels, allowing a linear increase to HZP.

The total peaking factor (F_Q) is the ratio of the maximum local heat flux on the surface of a fuel rod to the average fuel rod heat flux. The maximum F_Q value is used to calculate the peak LHGR.

A limiting axial flux shape is used in the subchannel analysis. Similar to the radial power distribution, the limiting axial flux shapes are developed to be bounding for most cycles, however, the conservatism of the axial flux shapes used in the subchannel analysis is confirmed for each cycle.

In summary, the subchannel methodology is developed to use bounding radial and axial power distributions. It should be noted that the radial power distribution used in the subchannel analysis is higher (i.e. more conservative) than the value in the COLR. This is because of the application of the biases to account for uncertainties due to engineering hot channel factors are applied as multipliers on the $F_{\Delta H}$ value from the COLR as described in Reference 4.4-3.

The development of bounding axial and radial flux shapes is explained in detail in Reference 4.4-3.

4.4.4.3.1 Influence of Power Distribution During Transients

For most Chapter 15 transients that do not involve CRA motion, the bounding axial and radial power distributions developed in the previous sections are conservative and are used. If the events occur from reduced power, the radial power distribution

is augmented in accordance with the higher $F_{\Delta H}$ allowed at lower powers. Similarly, the limiting axial flux shape for the analyzed power is used.

For Chapter 15 events that involve CRA motion, such as Section 15.4 events, the radial power distribution at the time of peak core power is determined from the event-specific nuclear analysis. The bounding power distribution determined for the steady state analysis is then augmented to reflect the higher peak $F_{\Delta H}$. This is conservative because the bounding radial power distribution used in the basemodel and most transients is characterized by a very flat power distribution around the peak rod, which minimizes energy transfer out of the channel containing the peak rod. This is described in more detail in Reference 4.4-3.

An adjustment to the bounding radial power distribution also includes penalties for $F_{\Delta H}$ measurement and engineering uncertainty on the hot rod. These penalties include the measurement uncertainty on the radial peaking as well as the engineering uncertainty for enthalpy rise. The radial power distribution prior to applying uncertainty penalties retains the conservative peak-to-average for the hot assembly, while the rod in which MCHFR is determined accounts for the applicable uncertainties.

The CHF limiting axial power shape based on core-average axial power is sufficient to be used for most transient analyses. Generally, the core-average axial power shape does not deviate significantly from the spectrum of shapes already considered within the power shapes analysis, and the subchannel limiting axial power shape is held constant during these events. The combination of the core-average axial power shape of initiating power level with the conservative radial power distribution and core hydraulic boundary conditions from NRELAP5 provides a conservative MCHFR calculation. For events where the axial flux shape changes, a specific analysis is performed to determine the axial flux shape that is conservative for the event.

4.4.4.4 Core Thermal Response

The core thermal response during AOOs, IEs, and accidents is presented in Chapter 15.

Low power and shutdown operation is described in Section 19.1.6 and the probabilistic risk assessment for the operation is addressed. The NPM natural circulation design does not require mid-loop operation during shutdown conditions. The core is always submerged in a pool of water so the core is not subjected to mid-loop thermal-hydraulic conditions during refueling operations.

4.4.4.5 Analytical Methods

4.4.4.5.1 Reactor Coolant System Flow Determination

The reactor coolant system (RCS) flow loop is comprised of the fuel assembly region, core bypass region, upper core plate, CRA guide tubes, CRA guide tube support plate, riser transition, control rod drive shaft support, upper riser turn to annulus, steam generator, downcomer transition, downcomer to lower plenum

turn, and the lower core plate. The volumes, flow areas, and volume lengths used to perform the flow calculation are provided in Table 4.4-1. The driving force for flow is the buoyancy arising from the density differences around the RCS flow loop. The primary contributors to pressure loss in the system are the fuel assembly and steam generator regions. These pressure losses are confirmed by testing. The remaining pressure drops are determined analytically. The steady state flow is calculated using the thermal-hydraulic software NRELAP5 as discussed in Section 5.1.4.

Three RCS flow rates are defined as a function of reactor power level, maximum design, best estimate, and minimum design. The best estimate flow is the most likely value for the primary coolant flow rate. This flow is based on the best estimate values of the friction and form losses in the RCS loop, and the amount of core bypass flow. Maximum design flow is the highest expected value for the primary coolant flow rate. The maximum design flow accounts for uncertainties in the RCS loop form losses, the uncertainty in the core bypass flow, and the uncertainty in the heat transfer capability of the SG. The minimum design flow is the lowest expected value for the primary coolant flow rate. The minimum design flow accounts for uncertainties in the RCS loop friction and form losses (including the influence of crud and corrosion), the uncertainty in the core bypass flow, and the uncertainty in the heat transfer capability of the SG. At full power, the maximum design flow is 12.5 percent greater than the best estimate flow and the minimum design flow is 8.3 percent less than the best estimate flow. The minimum design flow is used in subchannel calculations and is provided in Table 4.4-2. Bypass flow is discussed in Section 4.4.3.1.1.

RCS flow is measured continuously using four sets of ultrasonic transducers located in the four quadrants of the RPV wall in the downcomer region. These instruments are discussed further in Section 7.1.1. The ultrasonically determined flow is calibrated against a heat balance calculated flow. The ultrasonic flow is displayed in the control room. Increased pressure drop due to long term effects such as crud deposition would be identified by trending of the continuous flow measurement.

The thermal design analysis methodology encompasses the basis for the subchannel model and its application. The thermal hydraulics of the reactor core are modeled using VIPRE-01 with a one-pass approach in which all the characteristics of the hot channel are captured, including inter-channel feedback. The core is analyzed using eighth-core symmetry. Analyzed core designs may not necessarily be eighth-core symmetric; however, the conservatisms used in the model account for the insignificant non-symmetries in the core design as further described in Reference 4.4-3.

4.4.4.5.2 Subchannel Model

The subchannel analysis basemodel is developed in a conservative manner such that it bounds specific cycle core designs. The subchannel model is a 24-channel, one-eighth core model. The model is detailed in the region surrounding the peak power rod with decreasing detail farther away from the hot rod. The decreasing detail is accomplished by combining channels (called lumped channels). Sensitivity studies show that the rod power a few rods removed from the hot rod has minimal

effect on the MCHFR. Other aspects of the basis for the model are discussed in Section 4.4.3 and Section 4.4.4. The design inputs to construct the subchannel model are:

- RCS conditions
  - core thermal power
  - flow rate and core bypass fraction
  - core inlet temperature, turbulent mixing and temperature distribution
  - system pressure
- power distribution
  - radial peaking
  - axial peaking
- mechanical fuel design information
  - fuel array geometry and loss coefficients
  - pellet and clad dimensions
  - material properties for the fuel, clad, and the pellet-to-clad gap
- fuel performance data
  - gap width, fill gas volume, composition, and pressure
  - fuel centerline and volumetric average fuel temperatures
  - fuel and clad surface temperatures

The effect of crud on the flow and enthalpy distribution in the core is directly modeled in the VIPRE-01 subchannel analyses with respect to fuel rod heat transfer. In addition, conservative analysis of the effects of crud deposition on the fuel rod surface over a range of pellet-to-clad gap conductances, crud thicknesses, and crud conductivities are explicitly included in the fuel heat transfer inputs used in the subchannel analysis methodology to bound the effect on CHFR calculations. The effect of a reduced flow area as a result of crud deposition on the outer surface of the fuel rod is not directly modeled in the VIPRE-01 subchannel evaluations as it is an insignificant reduction in flow area, and thus an insignificant impact on calculated CHFR.

Reference 4.4-3 provides details about the methodology used to analyze the thermal and hydraulic response of the fuel and core coolant, including the correlations used for heat transfer, void fraction, and pressure drop.

4.4.4.6 Fuel Rod Conduction

Conduction of heat through the fuel rod directly impacts thermal margin to CHF for transient analyses. The VIPRE-01 one-dimensional conduction model is used for the fuel rod starting from the centerline of the fuel pellet outward to the cladding surface. VIPRE-01 does not model the phenomenon associated with fuel rod behavior changes caused by fuel exposure. The VIPRE-01 fuel and cladding temperatures are calibrated to

match or conservatively bound the fuel performance code (COPERNIC) results as described in Reference 4.4-3. Fuel conduction temperature calculations include the effects of crud deposition on the fuel rods.

Table 4.4-8 provides the peak fuel temperature at the core average linear heat rate of 2.5 kw/ft. In addition, the peak fuel temperature is also shown at the peak linear heat rate of 6.5 kw/ft, both values demonstrating significant margin to fuel melting.

4.4.4.7 Fuel Design-Specific Inputs

Fuel design-specific information is used in the subchannel basemodel. Spacer grid loss coefficients and friction factor are derived from pressure drop tests. These are applied in the subchannel analysis as described in Reference 4.4-3.

Operating conditions covering normal operation, AOOs, IEs, and accidents were translated into the ranges listed in Table 4.4-6 as the nominal (full-power), non-LOCA and LOCA operating states.

4.4.5 Testing and Verification

Testing is performed in accordance with the plant test program described in Section 14.2.

4.4.5.1 Testing Prior to Startup

An RCS flow test is conducted following fuel loading but prior to criticality. This flow test is conducted using heat from the CVCS system to provide the motive force for natural circulation. The purpose of this test is to provide confirmation of the thermal-hydraulic aspects of the design prior to going critical.

4.4.5.2 Initial Power and During Operation

During power ascension, core power distribution measurements and inlet and outlet thermocouple measurements are taken to confirm that the peaking factors used in the thermal-hydraulic design are conservative. In addition, RCS flow measurement is performed during power ascension following refueling outages. This flow measurement, with analytical biases applied to account for flow uncertainties related to allowable secondary side perturbations and core axial flux offset ranges, provides confirmation that the RCS loop resistance used in the thermal-hydraulic design and Chapter 15 transient and accident analyses remains bounding.

4.4.5.3 Component Inspections

Fuel assembly component surveillance is performed during refueling outages as described in Section 4.2.4.6.

4.4.6 Instrumentations Requirements

4.4.6.1 Incore Instrumentation System

The in-core instrumentation system (ICIS) uses neutron flux measurements in twelve (12) fuel assemblies to determine a three-dimensional power distribution in the core (see Section 4.3). During startup testing (Section 14.2), this power distribution is compared to the power distribution assumed in the thermal-hydraulic analysis to ensure that the peaking factor used in the analysis is conservative.

In addition, temperature is continuously monitored at the inlet and outlet of the 12 fuel assemblies and this information is used to verify that proper flow rates are being used in the thermal-hydraulic analysis. The location of the 12 assemblies that contain the incore flux and inlet and outlet temperature detectors is shown in Figure 4.3-18.

The conservatism of the VIPRE-01 subchannel code is established by comparison against experimental data and other computer code analyses as described in Reference 4.4-3.

4.4.6.2 Module Protection System

The following MPS reactor trips provide automatic protection of the reactor core safety limits:

- RCS high pressure
- RCS low pressure (above 600 degrees F) and low-low pressure
- nuclear high power trip

These protective trips ensure that MCHFR limits are not exceeded and that fuel centerline temperature stays below the melting point. These trips also ensure that average enthalpy in the riser is less than the enthalpy of saturated liquid and that core exit quality is within the limits defined by the CHF correlation.

There is no CHF related trip in the NuScale design because the CHF limits are at high power levels and the reactor is tripped before CHF limits are approached (see Figure 4.4-11).

A detect and suppress system is not used for stability in the NPM design because MPS protective actuations are achieved prior to reaching the flow stability exclusion region as discussed in Section 4.4.7.3.

The technical specifications include operating limits and system operability requirements, which ensure the thermal-hydraulic performance of the core. The reactor trip setpoints in the MPS include margin-to-safety limits for the monitored parameters. The MPS and reactor protective trips are described in Section 7.1.

The NPM design does not include a loose parts monitoring system because:

- The low fluid velocities resulting from natural circulation flow combined with a design that has only small lines entering the RPV minimizes the potential for loose parts entering or being generated in the RPV.
- The NPM design uses corrosion-resistant materials and has a flow-induced vibration program (Section 3.9) that further minimizes the potential for loose parts being generated in the RPV.
- During startup operation, a foreign materials exclusion program minimizes the potential for loose parts entering the RPV.
- Underwater vessel inspections during refueling outage verify that there are no loose parts in the RPV.

In addition the NuScale fuel assembly has a mesh filter at the bottom of each fuel assembly (Section 4.2) that filters out loose parts that could enter the fuel assembly.

4.4.7 Flow Stability

This section describes the evaluation of flow stability for the NPM.

4.4.7.1 Approach

The evaluation of unstable flow oscillations in the NPM includes a detailed phenomenological review of possible modes of instability and operating conditions that may result in instability. Details of the methodology are provided in Reference 4.4-4, including generic boundary conditions of anticipated transients where unstable oscillations may occur. Section 15.9 demonstrates that the NPM-specific design is protected from unstable flow oscillations when operation is limited to a defined pressure-temperature exclusion zone.

The phenomenological review identifies the limiting instability mode as natural circulation instability.

The approach for stability protection in the NPM is regional-exclusion rather than the detection-and-suppression. The operational domain identified with potential instability is characterized by loss of subcooling in the riser that leads to vapor generation above the core. This condition is excluded by the MPS protective actions.

In the demonstration of the methodology, no instabilities are identified to occur over the range of power evaluated because riser subcooling margin is not lost. The MPS actuation precludes onset of instability on loss of subcooling with sufficient margin to accommodate instrumentation time delays.

4.4.7.1.1 Phenomenological Description of NuScale Power Module Stability

There are several key design and arrangement considerations of the NuScale design that define the stability phenomena of importance.

The NPM design is a small modular integrated PWR. The helical coil SGs are integrated within the RPV and the primary coolant flow is driven by natural

circulation. The density difference between the relatively high-temperature flow exiting the core and the lower-temperature flow returning through the downcomer annulus creates the natural circulation driving head.

Various feedback mechanisms are possible and special consideration is given to coupling the SG dynamics and the flow stability in the primary loop. Feedback coupling between the thermal-hydraulic phenomena and the neutron kinetics is important. This is particularly the case where coolant and fuel rod temperatures provide reactivity feedback, and the core power response affects the coolant temperature and the density head that drives the flow and influences its stability.

4.4.7.1.2 Instability Mode Classification

The instability modes are broadly classified as static or dynamic. A list of the instability modes under each category and the mechanism for each mode is described in Table 4.4-9. The relevance of each instability mode to the NuScale design is designated as not applicable, excluded as limited by other phenomena, or applicable.

4.4.7.2 Analysis Methodologies

4.4.7.2.1 PIM Code

The PIM code simulates the flow dynamics in the NuScale RCS loop with optimal resolution of its stability. The extensive experience in the field of boiling water reactor stability analysis, both numerical and first principle understanding, is used in addressing single-phase natural circulation stability, which is unique to the NPM.

The PIM code applies the general theory and numerical methods of the RAMONA code, but is not a direct derivative of the coding. The PIM code has been developed independently to suit the geometry and specific needs of the NuScale reactor. The main advantage of the RAMONA-type algorithm used in PIM is the absence or insignificance of numerical damping that affects other time-domain codes, and requires extensive study and adjustment before they can be successfully benchmarked and reliably used.

Frequency-domain methods are not affected by numerical damping as much as some time-domain methods, but they are not used for NuScale as they require linearization of the governing equations. While linearization is accurate for small perturbations, and properly identifies the decay ratio and the conditions at the onset of instability, it is not suitable to analyze the stability of a highly-nonlinear system such as a natural circulation loop. A linearized model would not be able to discover the importance of nonlinearities that may be manifested at relatively small perturbation amplitudes. However, the RAMONA-type algorithm used by PIM is fully capable of representing the nonlinear interactions inherent in the natural circulation flow.

The PIM code approximates the reactor vessel geometry and flow. The approximations are founded on basic assumptions regarding the geometry, the representation of the flow fields, and various interactions and feedback

mechanisms. The major assumptions are listed below. More details about modeling assumptions, their impact, and justifications are given in Reference 4.4-4:

- The flow around the primary loop is one-dimensional, while the flow area varies along the flow path.
- The flow in the core is represented by a single channel. This assumption is reasonable given that the individual fuel assemblies are not closed channels and cross flow between assemblies is allowed.
- Power generation in the core is represented by a point-kinetics model. Accordingly, the axial power shape is invariant.
- The flow in the RCS loop is modeled as non-equilibrium, two-phase flow in which a drift flux formulation accounts for mechanical (velocity) differences between the liquid phase and the vapor phase (if any vapor exists).
- The pressurizer is not modeled. Pressure is specified by code input and the dependence of thermodynamic properties on pressure is uniform.
- A simplified model for ambient heat losses along the downcomer to the containment vessel provides representative estimates for this small effect on natural circulation driving head, which has some effect on stability at low-power conditions.
- The solid structures within the RPV, with the exception of the fuel rods in the core and the SG tubes, are assumed to have no heat exchange with the circulating fluid.
- The total core thermal power, flow rate, pressure, and inlet temperature are specified initial conditions for the RCS and SG secondary side. The specified conditions are based on plant performance operational predictions associated with plant design activities, or as chosen for sensitivity studies.

The geometry representation of the NPM pressure vessel for the numerical simulation is given in Figure 4.4-12. The core is represented by a heated section at the bottom of the riser. The cold leg annulus is represented as a one-dimensional pipe with a generally-varying cross section area. The helical coils of the SGs fill part of the cold leg volume and heat is exchanged between the downward flow in the RCS loop and the secondary side (inside the helical coil SG tubes). The dashed line represents a pressure boundary condition that is imposed by the pressurizer.

4.4.7.3 Stability Protection Solution

Section 4.4.3.3.1 describes how the NPM meets GDC 12 requirements by using an operating domain that is protected by MPS reactor trips in the exclusion region where the reactor is not allowed to operate. The exclusion region, defined by the area in the operating map where stability criteria are not met, is enforced automatically by the MPS trip setpoints.

The reactor operating maps for the NuScale reactor are described in Section 4.4.3.3.

In summary, a detection and suppression solution is not used for the NuScale design. Flow stability is ensured by maintaining a suitable operating region using an exclusion region solution.

4.4.8 References

4.4-1 NuScale Power, LLC, “NuScale Power Critical Heat Flux Correlations,” TR-0116-21012, Rev. 1, November 2017.

4.4-2 AREVA Inc., "Computational Procedure for Evaluating Fuel Rod Bowing," XN-75-32(P)(A), Supplement 1-4, February 1983.

4.4-3 NuScale Power, LLC, "Subchannel Analysis Methodology," TR-0915-17564-P, Rev. 1, February 2017.

4.4-4 NuScale Power, LLC, "Evaluation Methodology for Stability Analysis of the NuScale Power Module," TR-0516-49417-P, Rev. 0, July 2016.

4.4-5 AREVA NP Inc., “COBRA-FLX: A Core Thermal-Hydraulic Analysis Code Topical Report,” ANP-10311P, Rev. 0, March 2010.

4.4-6 Bahadur, Sher, U.S. Nuclear Regulatory Commission, letter to Pedro Salas, AREVA NP, Inc., January 29, 2013, Agencywide Document Access and Management System (ADAMS) Accession No. ML13135A053.

4.4-7 NuScale Power, LLC, “Applicability of AREVA Fuel Methodology for the NuScale Design,” TR-0116-20825-P-A, Rev. 1, June 2016.

4.4-8 NuScale Power, LLC, “Loss-of-Coolant Accident Evaluation Model,” TR-0516-49422-P, Rev. 0, December 2016.

Table 4.4-1: Geometries of Reactor Coolant System Components

RCS Region	Total RCS Region Volume (ft^3)	RCS Sub-region Description	Average Flow Area (ft^2)	Length (ft)
Riser	635	Lower riser and transition	24.9	9.4
		Upper riser and riser turn	15.4	26.0
Downcomer	1199	Downcomer (including steam generators)	25.7	46.0
Core	89	Fuel assemblies	10.3	7.9
		Reflector cooling channel	0.9	7.9
Pressurizer	578	Pressurizer heaters / main steam plenums	36.1	1.7
		Cylindrical pressurizer	61.4	6.9
		Reactor pressure vessel top head	41.2	2.2

Note: Nominal values

Table 4.4-2: Plant Reactor Design Comparison

Parameter	NuScale	US-EPR	US-APWR
Key Reactor Parameter			
Core thermal output (MWt)	160	4590	4451
System pressure (psia)	1850	2250	2250
Number of loops	NA	4	4
Inlet temperature (°F) [best estimate (BE) flow]	497	563.4	550.6
Core average temperature (°F) (BE flow)	543	596.8	588.8
Average temperature rise in core (°F) (BE flow)	100	62.7	72.1
Minimum design flow (lb/hr)	4.27E+6	173E+6	168E+6
Maximum design flow (lb/hr)	5.24E+6	195E+6	188E+6
Best estimate flow (lb/hr)	4.66E+6	180E+6	175E+6
Core bypass flow (%)	8.5	5.5	9.0
Average linear power density (kW/ft)	2.5	5.22	4.65
Peak linear power for normal operating conditions (kW/ft)	5.0	13.6	12.1
Normal operation peak heat flux (10^6 Btu/hr-ft^2)	0.171	.460	0.421
Total heat flux hot channel factor (F_Q)	2.0	2.60	2.60
Heat transfer area on fuel surface (ft^2)	6,275	86,166	91,360
Normal operation core average heat flux (Btu/hr-ft^2)	85,044	177,036	162,000
Core flow area (ft^2)	9.79	63.6	68.0
Core average coolant mass velocity (10^6 lbm/hr-ft^2) (BE)	0.49	2.8	2.25
Core average coolant velocity (ft/sec)	2.7	16	14.1
Core			
Equivalent diameter of active core (in)	59.28	148.3	119.7
Number of fuel assemblies	37	241	257
Fuel Assembly			
Effective fuel length (in.)	95.89	165.4	165.4
Nominal fuel weight per assembly (lb)	550	1182	1350
Rods per fuel assembly	264	264	264
Fuel Assembly pitch (in.)	8.466	8.466	8.466
Fuel rod pitch (in.)	0.496	0.496	0.496
Number of grids per assembly	5	10	11
Fuel Rod			
Cladding outside diameter (in.)	0.374	0.374	0.374
Pellet-cladding gap (in.)	0.00325	0.0033	0.0033
Cladding material	M5®	M5®	ZIRLO
Fuel column length (in.)	78.74	160	165.4
Fuel pellet diameter (in.)	0.3195	0.3195	0.322
Fuel pellet density (% theoretical density)	96.0	96.0	97

Note: These values are provided for comparison purposes only. More detailed information is provided for NuScale in Table 4.1-1, Table 4.1-2, and Reference 4.4-3. Table 5.1-1 provides additional information on NuScale RCS flow.

Table 4.4-3: Applicable Ranges of Existing Critical Heat Flux Models

	B&W-2	W-3	EPRI-1	AECL CHF Look Up Table
Pressure (psia)	2002 to 2393	1001 to 2306	203 to 2451	15 to 2901
Mass flux (lb/hr-ft^2)	749,880 to 4,000,080	999,840 to 4,999,920	199,840 to 4,100,360	0 to 5,898,740
Thermodynamic quality	-0.03 to 0.20	-0.15 to 0.15	-0.25 to 0.75	-0.50 to 1.00

Note: Ranges are approximate

Table 4.4-4: Subchannel Methodology Parameter Biases

Parameter	Conservative Bias Direction	Location Applied
Reactor power measurement uncertainty	Increase	VIPRE-01 or NRELAP5 input
Core inlet flow rate uncertainty	Decrease	VIPRE-01 or NRELAP5 input
Core bypass flow	Decrease	VIPRE-01 or NRELAP5 input
Core exit pressure	Case Dependent	VIPRE-01 or NRELAP5 input
Core inlet temperature	Increase	VIPRE-01 or NRELAP5 input
Core inlet flow distribution uncertainty	Decrease	VIPRE-01 model hot assembly
$F^{U}_{\Delta H}$ Uncertainty	Increase	Hot rod peaking (root-sum-square)
$F_{\Delta H}$ Rodded peaking	Increase	Limiting assembly peaking
$F^{E}_{\Delta H}$ Engineering uncertainty	Increase	Hot rod peaking (root-sum-square)
$F_{\Delta H}$ Augmentation for asymmetric events	Increase	Limiting assembly peaking
F^{E}_{Q} Engineering uncertainty	Increase	CHF analysis limit
Fuel rod bowing	Increase	CHF analysis limit

Notes:

1) The uncertainty bias for measurement of core power, system flow, system pressure, and core inlet temperature are accounted for in NRELAP5 transient analysis boundary conditions provided using non-LOCA transient methodology. These uncertainties are applied when performing steady-state analyses or analyses that do not involve NRELAP5 Non-LOCA methodology. Uncertainty values are provided in Reference 4.4-3.
2) Core inlet flow bias is zero because the minimum design system flow rate accounts for uncertainties throughout the RCS loop. The NRELAP5 transient simulations include the implementation of the flow loss uncertainties.
3) The rodded peaking value is used for all MCHFR analyses except those that start from HZP. The HZP cases use a PDIL-ARO factor at HZP conditions.
4) Augmentation for asymmetric events varies based on the event-specific neutronic calculation.

Table 4.4-5: Summary of Reactor Coolant System Loop Flow Elements

Flow Element	Hydraulic Phenomena
Core support blocks in downcomer	Flow over obstructions and drag due to four blocks in annulus
Downcomer-to-lower plenum turn	Flow turning through 180 degrees along thickened corners. Forward and reverse losses are considered due to possible flow reversal during plant startup.
Lower core plate	Flow through thick-edged orifice. Forward and reverse losses are considered due to possible flow reversal during plant startup.
Core	Flow through nozzles and spacer grids
Upper core plate	Flow through thick-edged orifice. Forward and reverse losses are considered due to possible flow reversal during plant startup.
Control rod assembly Guide Tubes	Parallel flow in interstitial area of tube bundle
Control rod assembly guide tube support plate	Flow through plate which resembles a screen
Riser transition	Flow through converging nozzle
Control rod drive shaft support	Flow through plate which is treated as six round edges
Pressurizer baffle	Flow through sudden contraction and sudden expansion. Forward and reverse losses are the same.
Upper riser turn to annulus	Flow turning through 180 degrees and drag from eight hanger braces
Downcomer through steam generator	Flow over tubes
Downcomer transition	Flow through converging nozzle
Upper core support blocks	Flow over obstructions and drag due to four blocks in annulus

Table 4.4-6: Reactor Operating Conditions

Operating State	Pressure (psia)	Mass Flux ($lb/hr\text{-}ft^2$)	Inlet Subcooling (°F)
Nominal (full-power) operation	1,850	442,400	135
Non-LOCA	1450 to 2180	36,870 to 589,870	36 to 135
LOCA	73 to 1,850	0 to 37,340	0 to 135

Table 4.4-7: Void Fraction at Exit of Core

Parameter (at core exit)	Equilibrium Cycle (without uncertainties)	24-Channel Subchannel Analysis (with all uncertainties applied)
Core Average Void Fraction	0.0	0.0
Hot Channel Void Fraction	0.01	0.36

Table 4.4-8: Peak Fuel Pellet Temperatures

Parameter	Value
Core Average Centerline Pellet Temperature (2.5 kw/ft)	1375
Hot Rod Centerline Pellet Temperature (6.5 kw/ft)	2075

Table 4.4-9: Applicability of Instability Mechanisms

Instability	Mechanism	Applicable to NuScale	Rationale for Determination
Static Instabilities	Governed by steady-state characteristics of the system		
Flow excursion or Ledinegg instability	Determined by the relationship between the pressure drop characteristic of a boiling channel and the pressure drop characteristic imposed by an external system (e.g., a pump).	Yes	There is no possibility for negative slope of the $\Delta P(\dot{m})$ in the case of single-phase natural circulation and it can be demonstrated that in a substantially unconstricted flow path like the primary circuit in the NPM that this condition is also absent even under two-phase conditions. Reference 4.4-4 demonstrates there is no negative slope at any power at the steady-state balanced loop operating points where $\Delta P = 0$. Moreover, no negative slope was found anywhere on the curve. Therefore, the flow excursion mode is not possible in the NPM.
Boiling crisis	Higher heat flux than the flux that can be transferred by nucleate boiling.	No	Reactor operation is restricted such that a margin to boiling transition is achieved by maintaining the minimum CHF ratio above correlation limits.
Flow pattern (relaxation) instability transition	Flow regime transitions influence the pressure drop and create inflections of the pressure drop versus flow rate that may result in instability. Flow regime transitions include laminar-to-turbulent transitions and bubbly-to-annular flow transitions.	No	Flow regime transitions cannot cause instabilities in the NPM. Bubbly-to-annular flow regime transitions occur at high steam qualities and are well outside the operational range of the NPM, which is single-phase flow with minimal, if any, local subcooled boiling. Other instability modes become excited at lower steam quality in the NPM riser and, therefore, the boiling regime transitions are bounded by these other phenomena.
Flashing instability	Relevant for heaters located under a tall riser Hot (at or near saturation) liquid rises to lower pressure elevation. Evaporation at reduced pressure (flashing) drives flow disturbance.	Yes	Observed only in low-pressure systems with pressures much lower than NPM operating pressure
Bumping Geysering	Periodic or chaotic oscillations caused by cyclical vapor generation in a tall riser. Similar to flashing instability, except vapor is generated in the heater and expands in the riser. Possible liquid thermodynamic metastable state (superheated) caused by low flow and lack of nucleation sites.	No	Possible only in low-pressure systems, and therefore not a primary instability mode in NPM.

Table 4.4-9: Applicability of Instability Mechanisms (Continued)

Instability	Mechanism	Applicable to NuScale	Rationale for Determination
Dynamic instabilities	Governed by inertia, feedback, and overall system response.		
Pressure-drop oscillations	Oscillations are the dynamic extension of Ledinegg static instability. Pressure drop versus flow rate is a multi-valued function. Transition from one flow state to the other is accompanied by a storage mechanism, such as compressing a volume of vapor, which causes a delayed rebound and cyclical transitions ensue.	Yes	The necessary condition of a multi-valued pressure drop versus flow rate has been excluded in the NPM as shown in the Ledinegg analysis.
Acoustic oscillations	Resonance of pressure waves. Thermal energy feeds and sustains the instability. In the compression phase, direct contact between the liquid phase and the heated surface is forced by collapsing a vapor film and heat transfer is enhanced while in the rarefaction phase the vapor film is reestablished, and the cycle is repeated. High velocity flow may also provide the mechanical energy to excite the standing waves.	No	There is no mechanism for feeding and sustaining this type of instability in the NPM as discussed in Reference 4.4-4.

Table 4.4-9: Applicability of Instability Mechanisms (Continued)

Instability	Mechanism	Applicable to NuScale	Rationale for Determination
Density-wave oscillations	Occurs in vertical heated channels with or without boiling. Any flow perturbation at the inlet generates effects that propagate (wave) up the channel. Decreasing inlet mass flow rate results in increasing the flow enthalpy and lowers the density either by liquid expansion in the case of single-phase flow or through increased vapor generation. At steady state or quasi-steady state, or for very low frequency perturbation, the inlet flow perturbation generates a negative feedback so that the system returns to its initial state and is stable. Specifically, a perturbation decreasing the inlet mass flow rate results in lowering the density in the channel, thus increasing the buoyancy pressure head, which tends to restore the original flow rate. However, dependent on the frequency of the perturbation, sufficiently strong delayed feedback can be destabilizing. Delay mechanism is the time to propagate the density wave to transverse the heated channel length. For resonant frequency, the delayed effects of perturbation reach the channel exit at the time the inlet perturbation reverses phase and the original perturbation is reinforced. At this frequency, the system is destabilized given sufficiently strong feedback, which can occur when the power is increased. For a single-phase heated channel, instability is conceivable only for long heated channels as the density change of liquid due to change in enthalpy is relatively small. Conversely, boiling increases the mixture density response to enthalpy change, making a boiling channel less stable compared to the single-phase case. In addition, in the two-phase case, the feedback from an initial inlet flow perturbation is not limited to density head, but includes the response of friction pressure drop, which is significant due to the two-phase multiplier.	Yes	Density wave instability is seldom observed without compounding factors in nuclear systems. While density waves are present normally in a heated channel, they can occur in a heated channel connected to a tall adiabatic riser as in the simplified boiling water reactor natural circulation. Density wave instability is a concern for the flow in the secondary side of the SG of the NPM and must be addressed. Density waves in the primary circuit are part of a compound interconnected phenomena of a potential natural circulation riser instability and must be addressed as an integral process with various components.
Xenon instability	Pure neutronic phenomenon.	No	Xenon stability calculations for the NPM core demonstrate that these oscillations are highly stable as a pure instability mode. Refer to Section 4.3.

Table 4.4-9: Applicability of Instability Mechanisms (Continued)

Instability	Mechanism	Applicable to NuScale	Rationale for Determination
Natural circulation instability	Natural circulation system includes two legs: a riser and a downcomer. The dynamics of the flow in the two legs depends on the heater source and heat sink, and their respective location. The natural circulation instability mechanism of interest for the NPM has the heater located under a tall riser and the heat sink located near the top of the cold leg. A perturbation increasing the flow rate results in a reduction in the heater exit temperature and an increase in its density. The density perturbation travels up the riser and there is a time delay before the new density is distributed throughout the length of the riser. This delayed feedback is negative because the difference in temperature between the riser and the cold leg is diminished reducing the density difference that drives the flow. If this delayed negative feedback is sufficiently strong, the flow is destabilized and undergoes growing oscillations. The riser boils in the case of high friction in the loop that reduces flow, or if power input is sufficiently increased. The density response to an enthalpy perturbation is much higher in the case of phase change than in the case of single-phase thermal expansion. The boiling natural circulation loop can be destabilized more readily than a single-phase loop.	Yes	Natural circulation instability is a possible mode for the NPM and is evaluated in depth. The evaluation includes other compounding phenomena not discussed in the description of the fundamental instability given above. These compounding phenomena include the feedback from nuclear reactivity and the dynamics of the heat exchanger.
Coupled compound instability modes	Compound instability modes include secondary phenomena that influence or modify the primary mechanism significantly.		
Parallel channel instability	Common headers alter the boundary conditions under which a single channel would have operated. The common pressure drop boundary condition allows for multiple oscillation modes depending on the phase difference among the oscillations in each channel. The fixed pressure drop boundary condition is destabilizing and, therefore, a set of two channels connected in parallel are less stable than a single one. For two channels oscillating out of phase, the common pressure drop fluctuation is eliminated (in the linear limit) as the effects of the flow oscillations in the two channels cancel out.	No	Parallel channel instability in the NPM core has been dispositioned in Reference 4.4-4 and is not a concern.
Primary circuit flow coupling to secondary side of SG	See discussion in Reference 4.4-4.	Yes	SG secondary-side flow coupling to the RPV-side flow is restricted to the effects of the total secondary flow. Out-of-phase flow oscillations in the tubes are self-cancelling and result in no net oscillatory effects.

Table 4.4-9: Applicability of Instability Mechanisms (Continued)

Instability	Mechanism	Applicable to NuScale	Rationale for Determination
Neutronic coupling with natural circulation instability	Takes effects of the neutron reactivity feedback into account. A flow increase perturbation at the core inlet reduces the core exit temperature at constant power. Reduced moderator temperature adds positive reactivity and the power is increased if the moderator temperature coefficient is negative. Power increase offsets core exit temperature reduction and the reactivity response becomes milder (reduced gain). However, the time delay involved in these processes could reinforce the perturbation if the resulting phase shift is large.	Yes	The reactivity-to-power and power-to-heat flux phenomena are important and are included in stability evaluations of the primary coolant flow in the NPM. Reference 4.4-4 provides the rational for this conclusion.
NPM circulation instability	Stability of the flow in a natural circulation loop with constant heater power and constant density cold leg is compounded to include reactivity-to-power feedback. Ideal SG assumption is relaxed with more realistic modeling of the heat transfer dynamics. System operating conditions may include parts in which the flow is two-phase because of subcooled boiling in the core and flashing in the riser.	Yes	The main NPM instability mode is natural circulation instability, also called riser instability mode. Evaluations rely on detailed numerical techniques in which a dynamic system is constructed using nonlinear equations the conservation of mass, momentum, and energy. Equations and governing equations for fission power dynamics and heat transfer.

Figure 4.4-1: Critical Heat Flux Ratio Limits and Thermal Margins

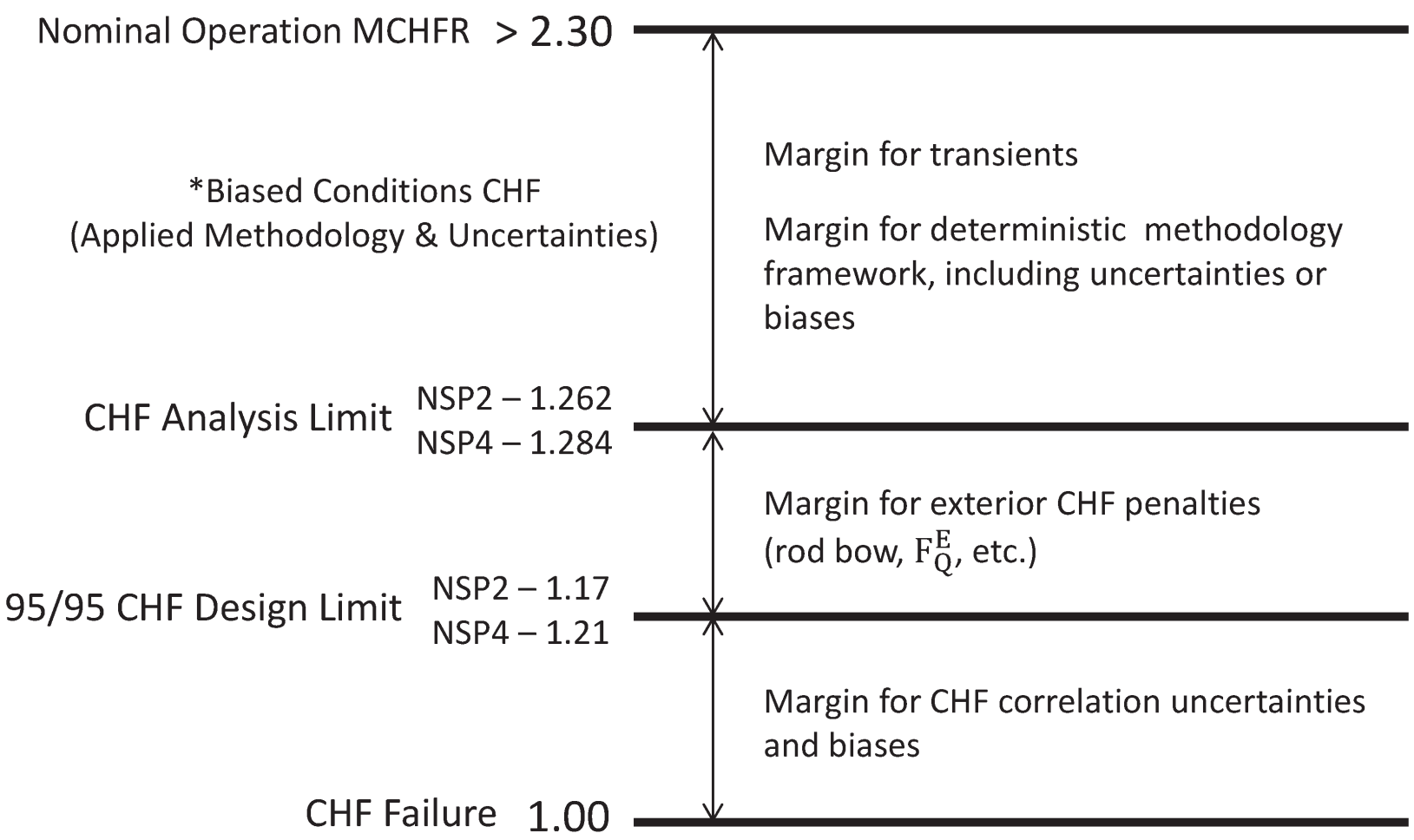

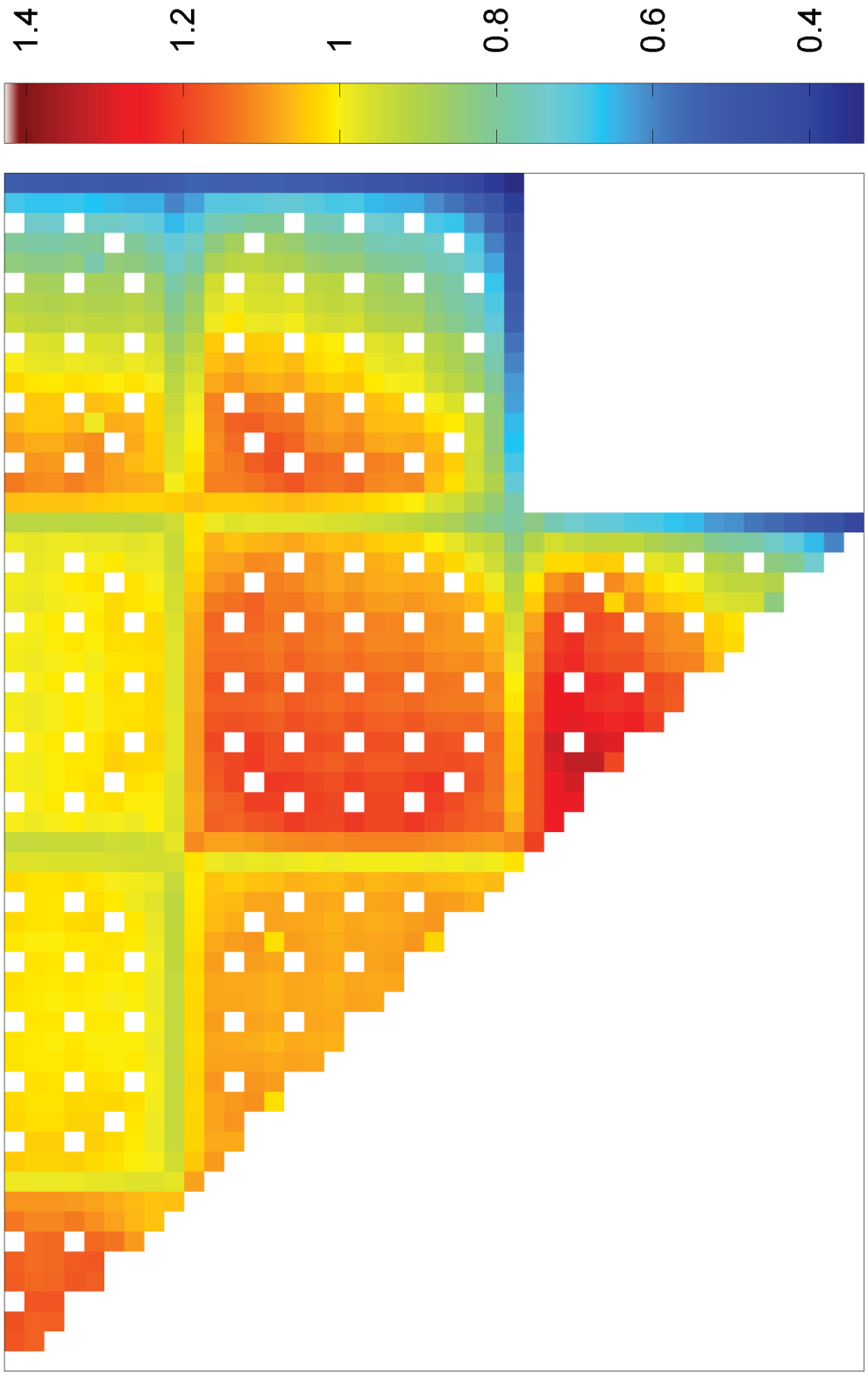

Figure 4.4-2: Radial Power Distribution
(Ratio of Peak Rod Power to Average Rod Power)

Figure 4.4-3: Not Used

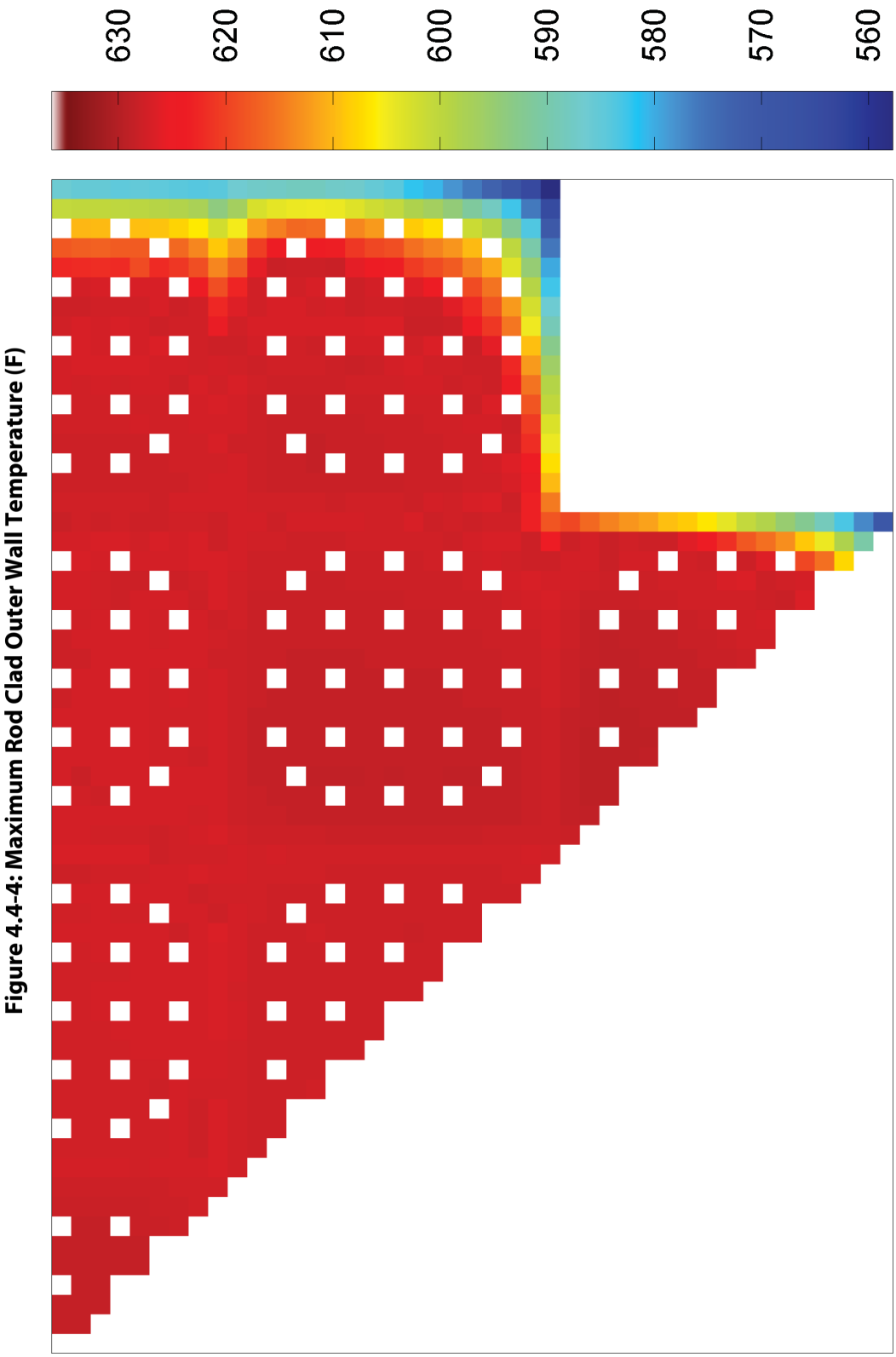

Figure 4.4-4: Maximum Rod Clad Outer Wall Temperature (F)

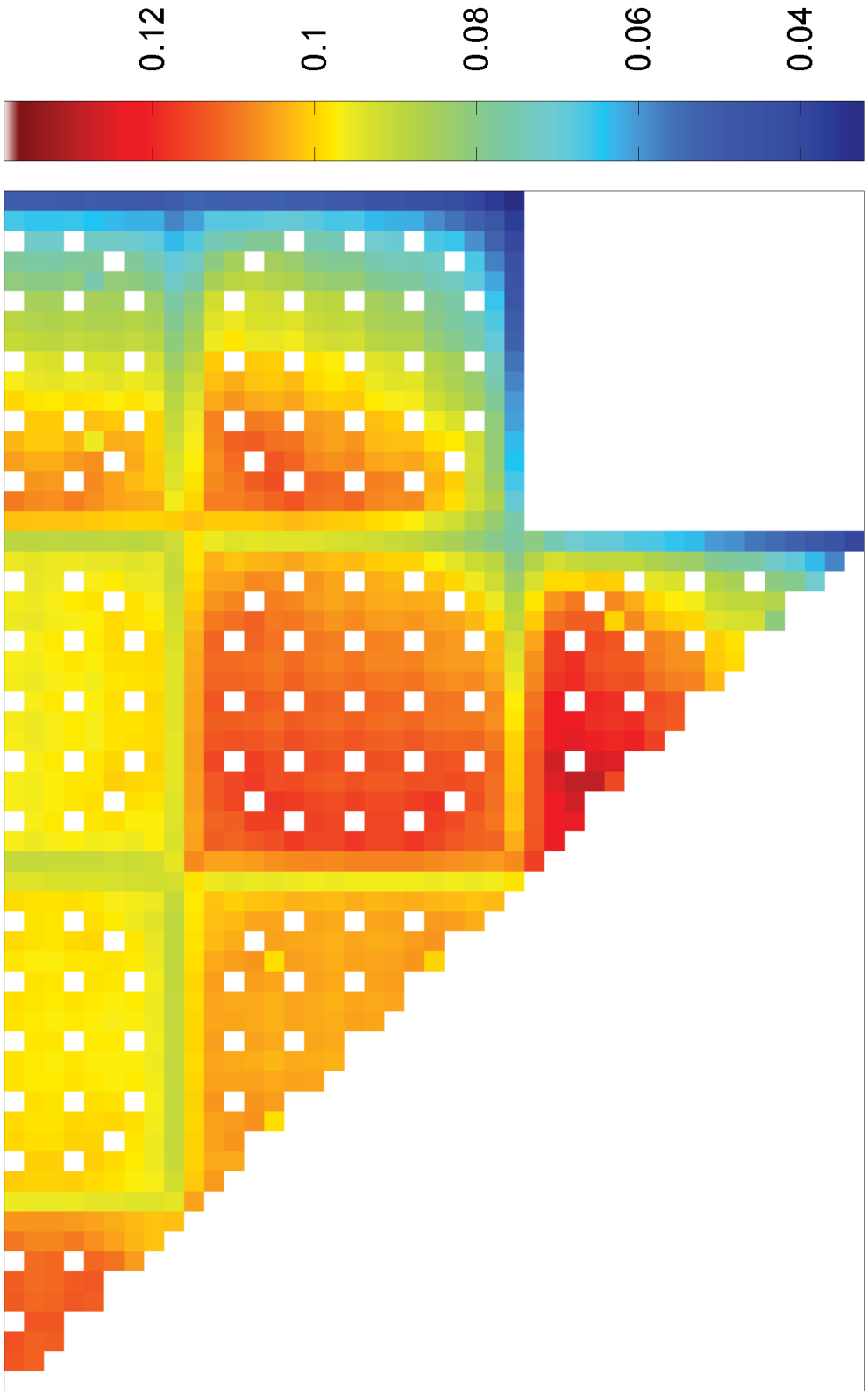
0.12
0.1
0.08
0.06
0.04
Figure 4.4-5: Maximum Rod Heat Flux (MBtu/hr-ft2)

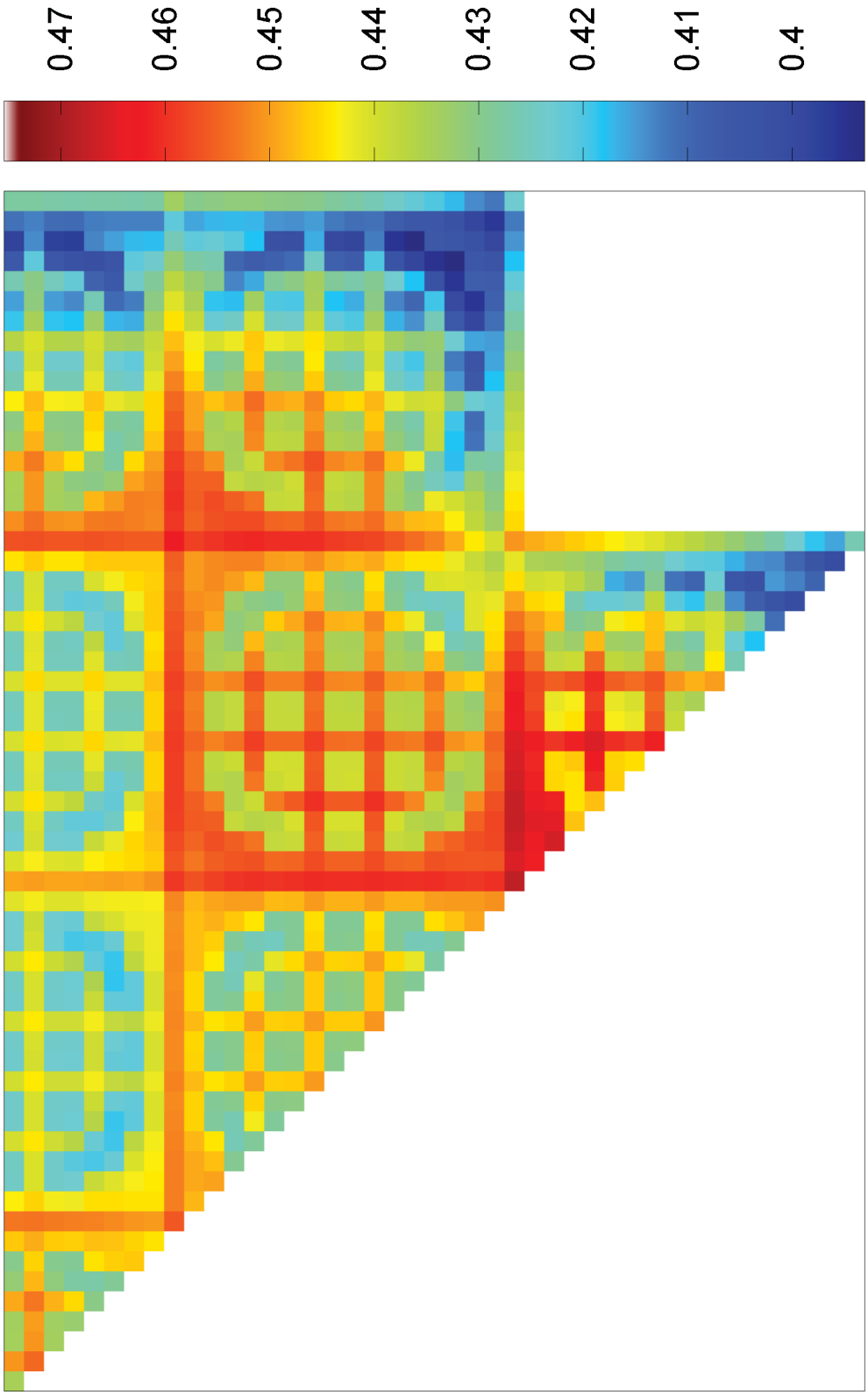

Figure 4.4-6: Average Channel Mass Flux (Mlbm/hr-ft^2)

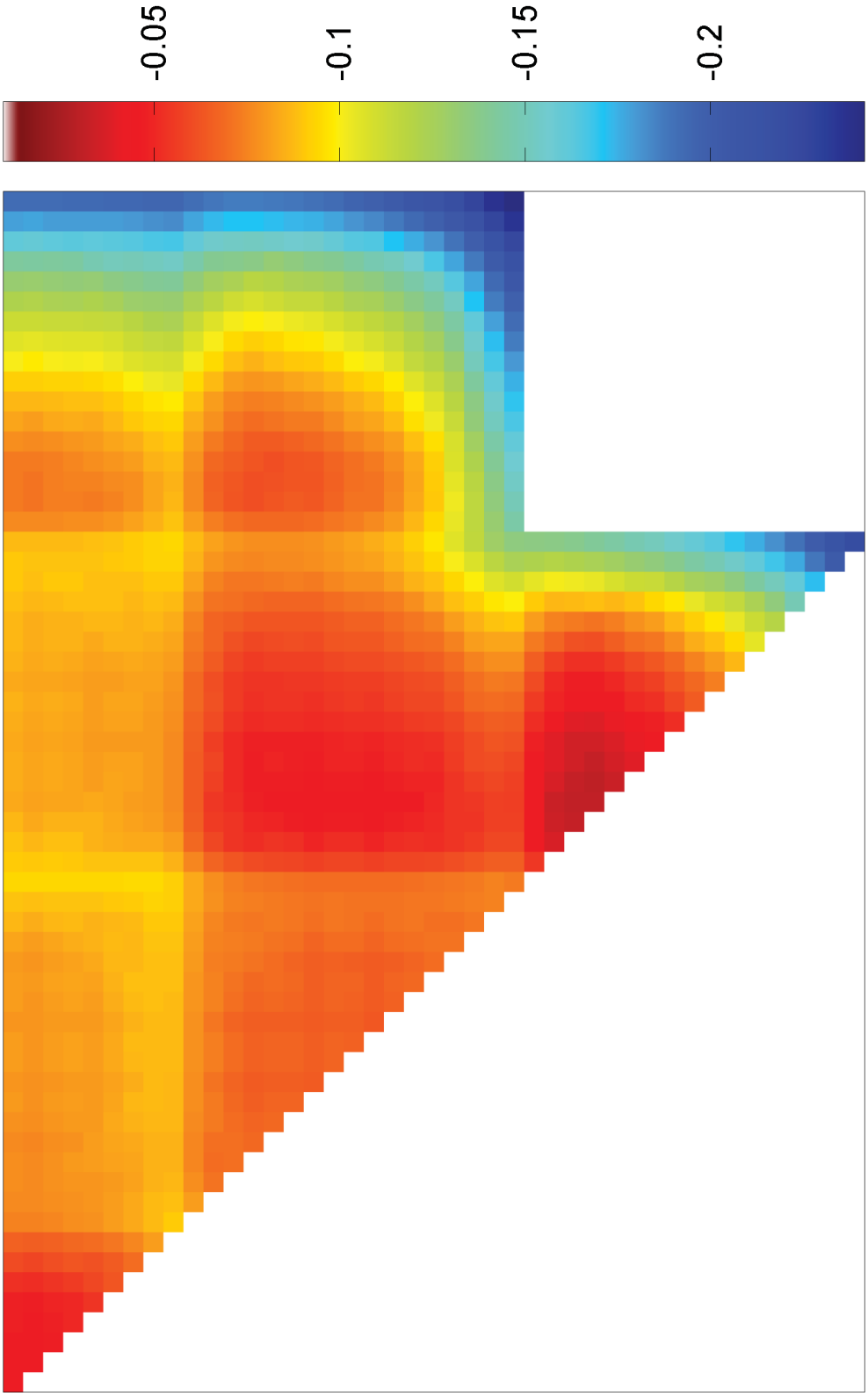

Figure 4.4-7: Maximum Channel Equilibrium Quality (fraction)

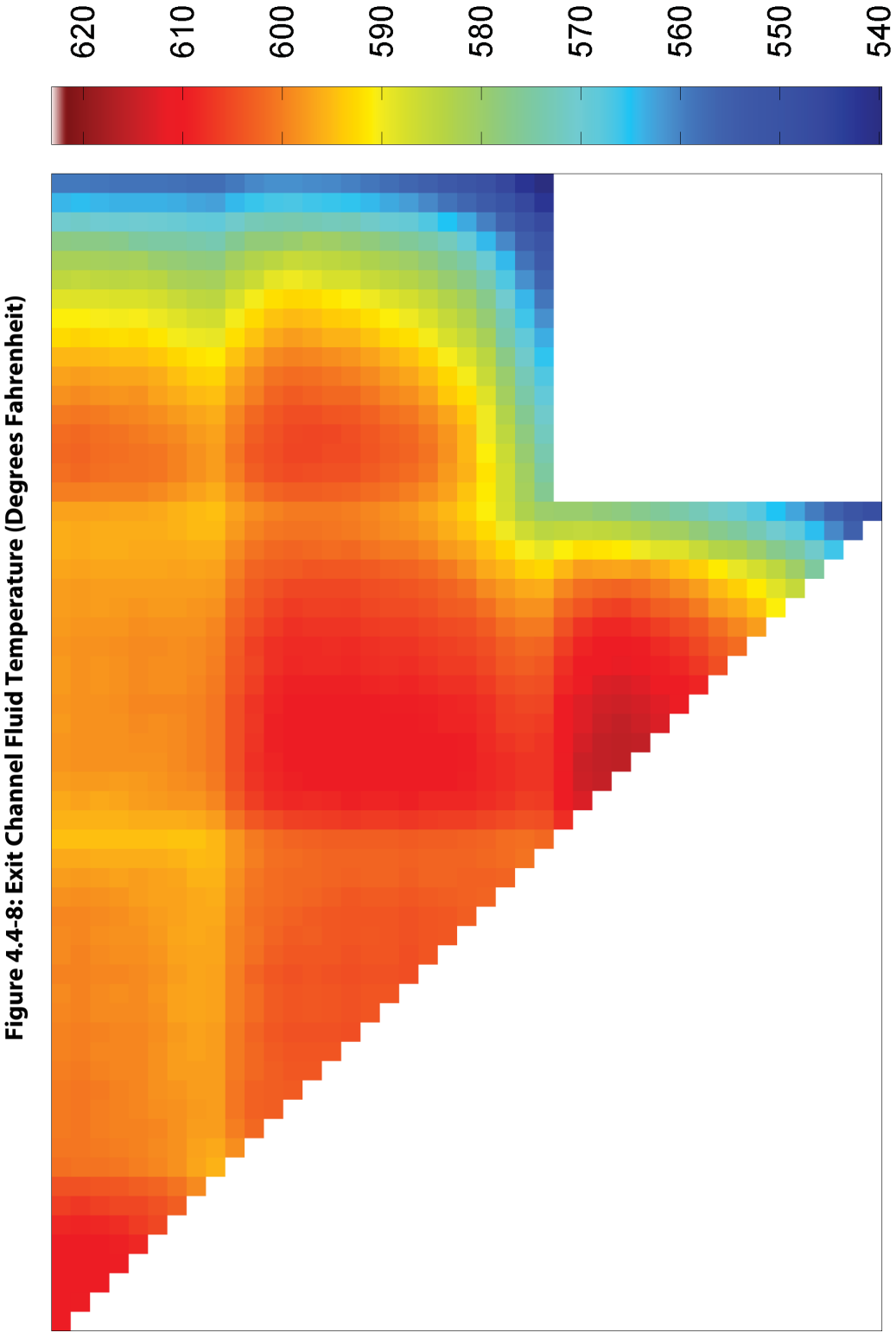

Figure 4.4-8: Exit Channel Fluid Temperature (Degrees Fahrenheit)

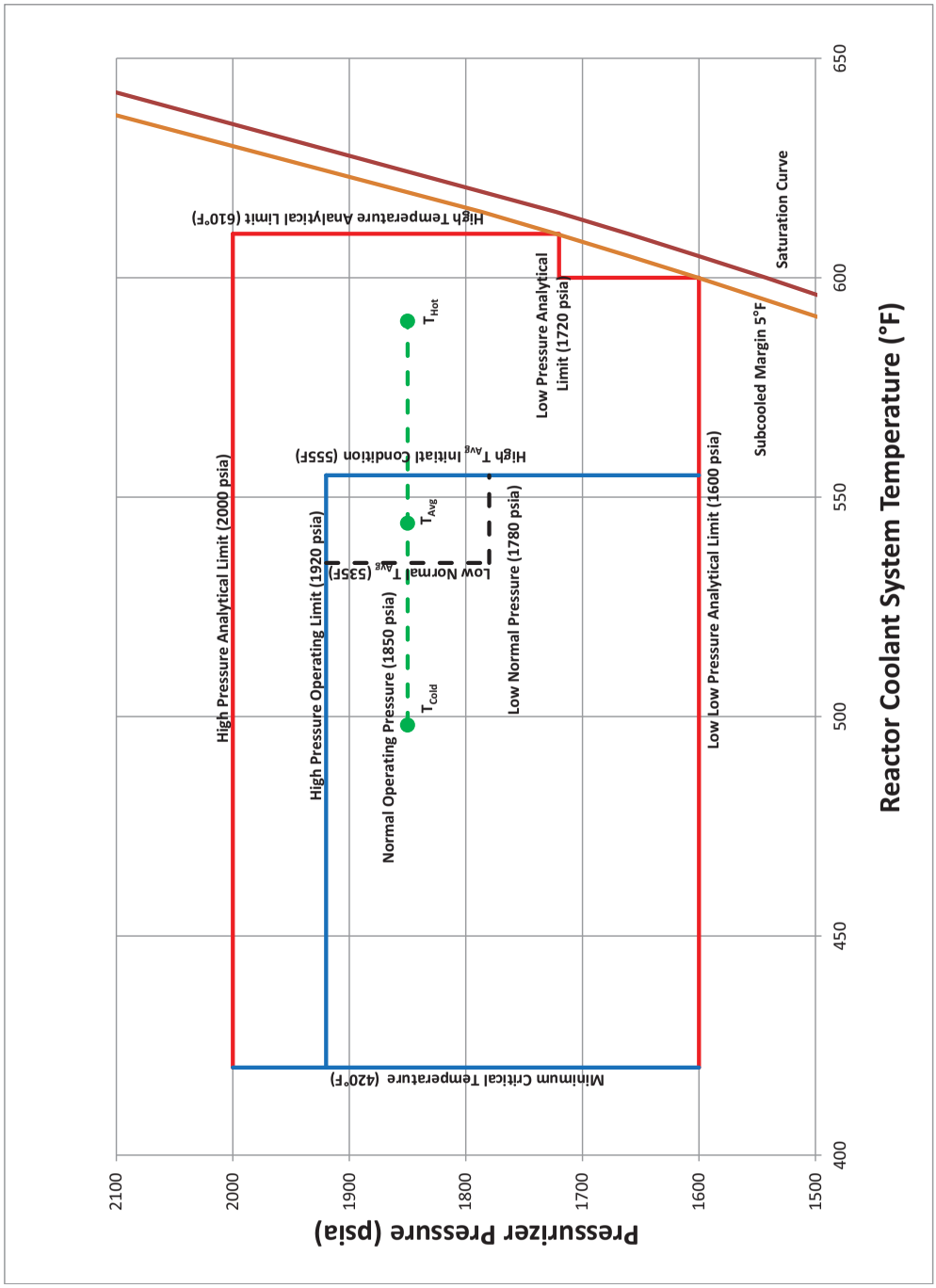

Figure 4.4-9: Analytical Design Operating Limits

Figure 4.4-10: Not Used

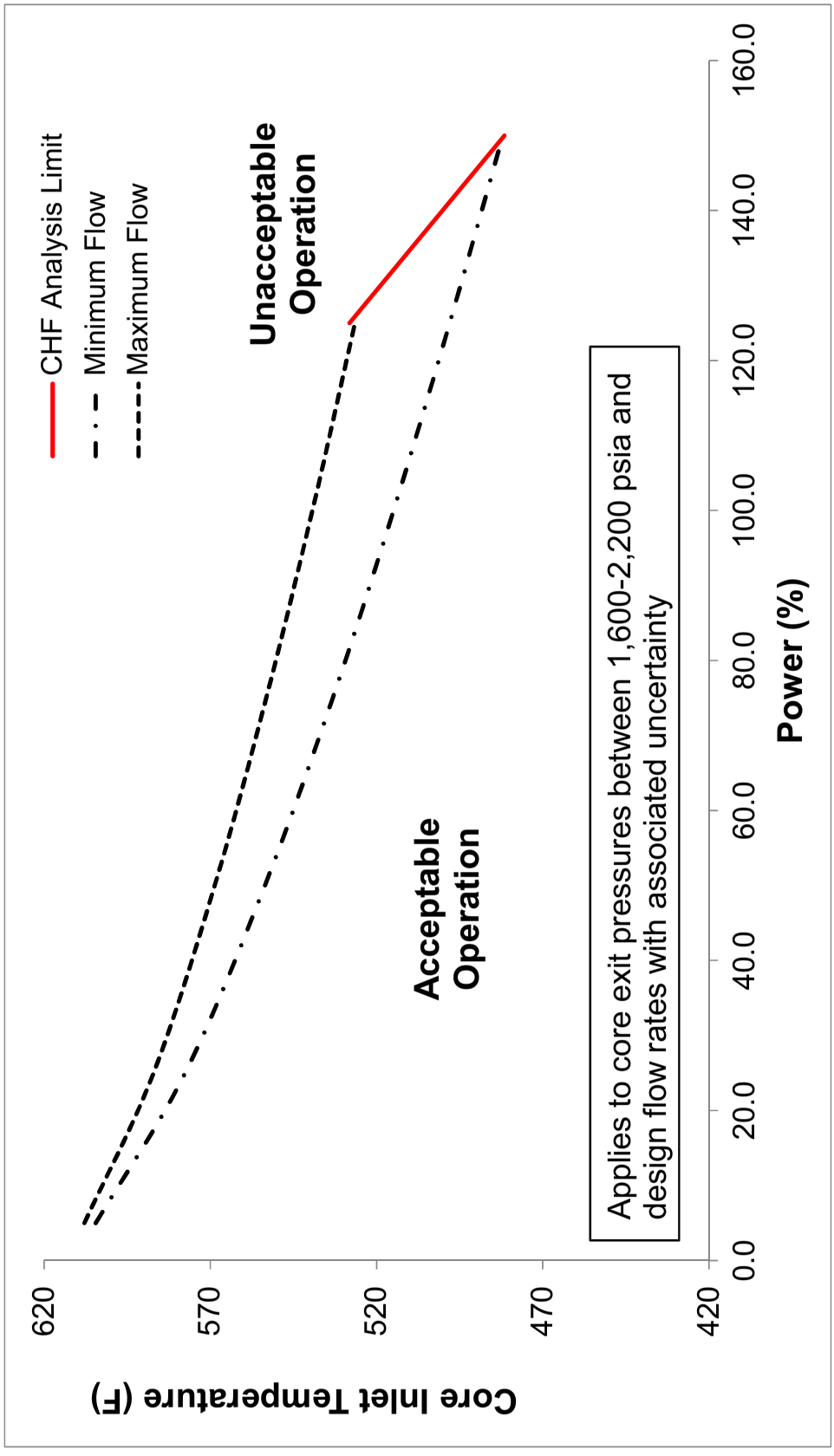

Figure 4.4-11: Thermal Margin Limit Map

Figure 4.4-12: Illustration of the Geometry Representation for the Stability Analysis

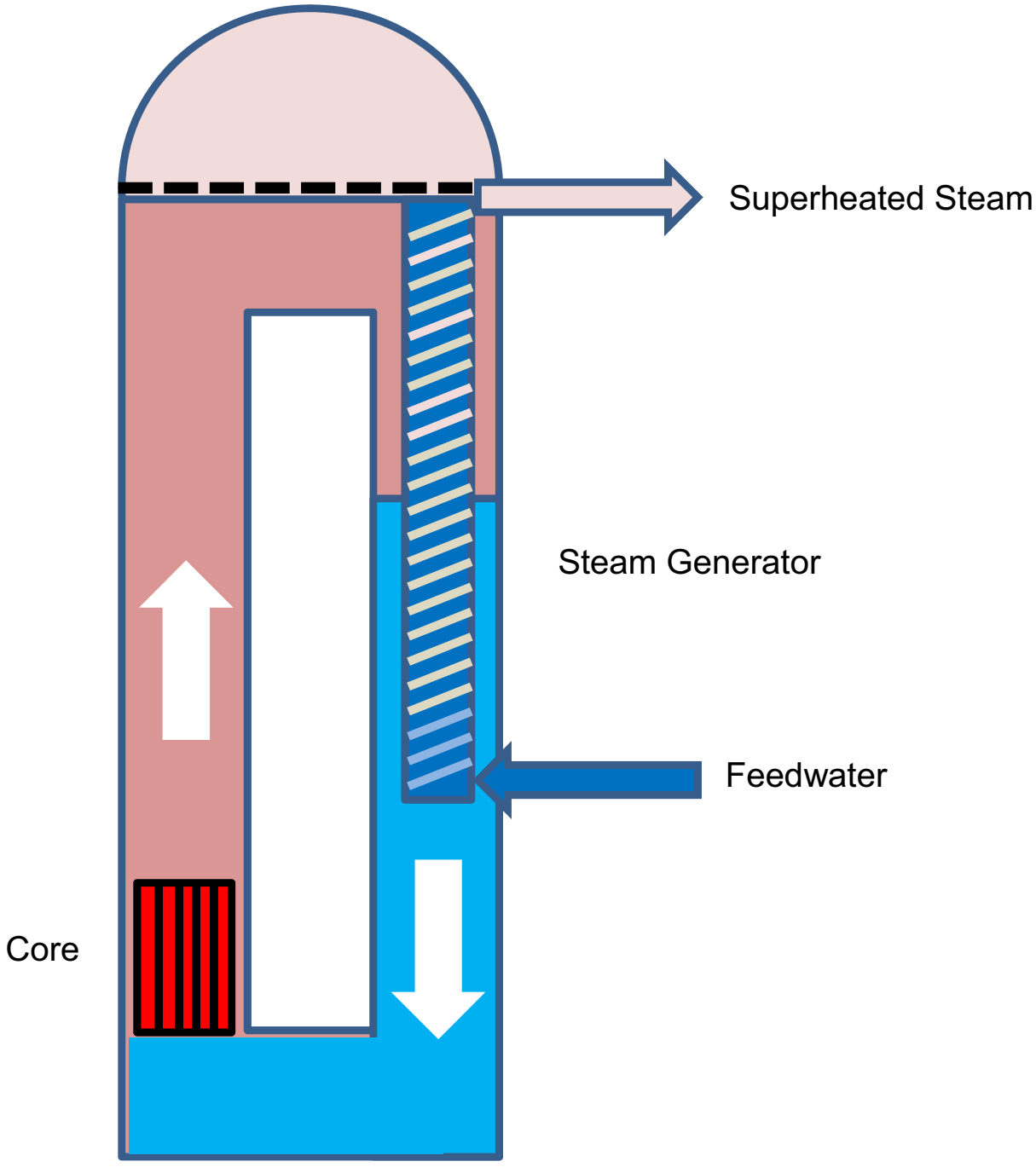

4.5 Reactor Materials

4.5.1 Control Rod Drive System Structural Materials

The control rod drive system (CRDS) consists of the control rod drive mechanisms (CRDMs) and the related mechanical components that provide the means for control rod assembly insertion into the core as described in Section 4.6. Portions of the CRDS are a part of the reactor coolant pressure boundary (RCPB) as described in Section 5.2.

The CRDS materials discussed in this section include the CRDMs and extend to the coupling interface with the control rod assemblies (CRAs) in the reactor vessel. Figures 4.6-1, 4.6-5 and 4.6-6 are illustrations of the CRDM-to-CRA interface. Materials for the pressure-retaining components of the CRDMs are listed in Table 5.2-4 and include the latch housing, the rod travel housing, and the rod travel housing plug.

Section 3.9.4 provides the details of the mechanical testing, seismic analysis of the CRDS, components life cycle testing, and mechanism functional tests. Operating experience of the CRDS design is discussed in Section 3.9.4 and Section 4.6.

4.5.1.1 Materials Specifications

The CRDMs are mounted above the pressurizer of the reactor pressure vessel and inside the containment vessel. The CRDM internal components can be exposed to primary coolant or saturated steam and non-condensable gases. Prior to module movement for refueling, the containment vessel is partially flooded with borated water, but the CRDMs are not normally submerged. However, the material design of the external surfaces of the CRDM include consideration of inadvertent submergence into borated water during module movement or refueling. The inside surface of the CRDM cooling tubes and cooling water connector is exposed to component cooling water. CRDM materials are selected to be compatible with the applicable fluid environments.

Portions of the CRDM that establish the RCPB are classified as Quality Group A and are designed, fabricated, constructed, tested, and inspected as Class 1 in accordance with Section III of the American Society of Mechanical Engineers (ASME) Boiler and Pressure Vessel Code (BPVC) and the applicable conditions promulgated in 10 CFR 50.55a.(b). The CRDM materials, including weld materials, conform to fabrication, construction, and testing requirements of BPVC, Section III, Subsection NB. The materials selected for fabrication conform to the applicable material specifications provided in BPVC, Section II and meet the requirements of BPVC, Section III, Article NB-2000.

As a conservative measure to minimize the potential for leakage of the fluid system inside containment, the CRDM coil heat exchangers, cooling tubes, and cooling water connectors are classified as Quality Group B (Section 3.2) and are designed, fabricated, constructed, tested, and inspected as Class 2 in accordance with Section III of the ASME BPV Code and the applicable conditions promulgated in 10 CFR 50.55a.(d). The CRDM coil heat exchanger, cooling tubes, and cooling water connector materials, including weld materials, conform to fabrication, construction, and testing requirements of ASME BPV Code, Section III, Subsection NC. The materials selected for fabrication conform to

the applicable material specifications provided in ASME BPV Code, Section II and meet the requirements of ASME BPV Code, Section III, Article NC-2000.

Table 4.5-1 lists the CRDM materials, including the material grade, class, or type, as applicable. Materials exposed to borated pool water, primary reactor coolant, saturated steam and non-condensable gases, or component cooling water are corrosion-resistant stainless steels, nickel-based alloys, and, to a limited extent, cobalt-based alloys. These materials are selected from materials proven in light-water reactor operation and for their compatibility with the reactor coolant as specified in ASME BPV Code, Section III, Paragraphs NB-2160 or NC-2160 and Subsubarticles NB-3120 or NC-3120, as applicable.

CRDS pressure-retaining components are not fabricated or manufactured from cast austenitic stainless steel. Use of cold-worked austenitic stainless steel is avoided to the extent practicable during fabrication of CRDS structural components. Austenitic and martensitic stainless steel with yield strength greater than 90,000 psi, as determined by the 0.2 percent offset method, are not used in the fabrication of the CRDS structural components.

4.5.1.2 Austenitic Stainless Steel Components

Processing and welding of unstablized American Iron and Steel Institute (AISI) Type 3XX series austenitic stainless steels for pressure-retaining parts comply with Regulatory Guide (RG) 1.44, Revision 1, to prevent sensitization and stress corrosion cracking. Austenitic stainless steel is procured in the solution-annealed condition. When rapidly cooled by means other than water quenching, non-sensitization of base materials is verified by test in accordance with Practice A or Practice E of American Society for Testing and Materials (ASTM) A262 (Reference 4.5-1) as required by RG 1.44.

For AISI Type 3XX series austenitic stainless steel subjected to sensitizing temperatures subsequent to solution heat treatment, the carbon content is limited to no more than 0.03 weight percent (wt%).

CRDM weld filler metals listed in Table 4.5-1 are in accordance, as applicable, with SFA-5.4 and SFA-5.9, of ASME BPV Code, Section II, Part C. They are analyzed for delta ferrite content and limited to a ferrite number (FN) of 5FN to 20FN in accordance with RG 1.31, Revision 4, and ASME BPV Code, Section III, Paragraphs NB-2433 or NC-2433, as applicable. Carbon content of austenitic stainless steel weld filler metals is limited to no more than 0.03 wt%.

Section 5.2.3 describes the controls used to minimize the introduction of potentially harmful contaminants including chlorides, fluorides, and low melting point alloys on the surface of austenitic stainless steel components. Such controls are also applicable to stainless steels used in the CRDM. In accordance with RG 1.44, cleaning solutions, processing equipment, degreasing agents, and other foreign materials are removed during processing prior to elevated temperature treatments. Acid pickling is avoided on stainless steel and not used on sensitized austenitic stainless steel.

4.5.1.3 Other Materials

The use of martensitic stainless steel is limited to Type 410 with a minimum tempering temperature of 1050 degrees F to prevent temper embrittlement and stress-corrosion cracking.

Nickel-chromium based alloy X-750 is used for the CRDM springs and cobalt-based alloys Haynes 25 and Stellite 6 are used for wear-resistant parts as identified in Table 4.5-1. These materials have been used in existing pressurized water reactor (PWR) CRDMs for the same function with satisfactory performance. The material of the rod drive expansion plug and pins associated with gripper components is Haynes 25. Stellite 6 material is limited to hardfacing of the CRDM gripper latch arm tips. To minimize the possibility of stress-corrosion cracking failures, the CRDM springs and wear-resistant parts are procured in the same heat treatment condition as previously used in the industry. Alloy X-750 spring material and heat treatment conform to the requirements of AMS 5698 or AMS 5699. There have been no operating experience reports of stress-corrosion cracking of Alloy X-750 CRDM springs fabricated from AMS 5698 and AMS 5699. For Alloy X-750, the cobalt impurity is maintained as low as possible and does not exceed 1 percent. To minimize cobalt intrusion into the reactor coolant, low-cobalt or cobalt-free alloys may be used for wear-resistant CRDM parts if their wear and corrosion resistance are qualified by testing.

4.5.1.4 Material Cleaning and Cleanliness Control

Cleaning of CRDMs complies with the ASME NQA-1 requirements (Reference 4.5-2). The final surface cleanness meets the requirements for "Class B" of Subpart 2.1.

Handling, storage, and shipping of CRDMs comply with ASME NQA-1-2008, Part 1, Requirement 13. Packaging, shipment, handling, and storage of CRDMs meet the requirements of "Level B" of ASME NQA-1a-2009, Part II, Subpart 2.2 (Reference 4.5-2).

4.5.2 Reactor Internals and Core Support Structure Materials

Figures 3.9-1 through 3.9-4 show the reactor vessel internals (RVI) subassemblies with components that comprise the RVI. The RVI consist of core support assembly, lower riser assembly, upper riser assembly, flow diverter, and pressurizer spray nozzles. The RVI do not contain any cast austenitic stainless steel components.

4.5.2.1 Materials Specifications

Table 4.5-2 lists the RVI materials and associated specifications, including the material grade, class, or type as applicable. The portions of the RVI performing a core support function are designed and fabricated as Class CS in accordance with ASME BPV Code, Section III, Subsection NG. The materials for core support structures and threaded structural fasteners conform to the requirements of ASME BPV Code, Section III, Subsubarticle NG-2120, and the applicable requirements of ASME BPV Code, Section II, Part D, Tables 2A, 2B, and 4. The remaining portions of the RVI are designated as internal structures and are designed to conform to ASME BPV Code, Section III, Article NG-3000 considering the requirements of Paragraph NG-1122(c).

The design of RVI has considered peak neutron fluence in the materials surrounding the core. Neutron irradiation-induced degradations such as irradiation-assisted stress corrosion cracking, void-swelling, stress-relaxation, and irradiation embrittlement have been evaluated using material aging degradation mechanism screening criteria of the Electric Power Research Institute (EPRI) materials reliability program (Reference 4.5-3). The components meeting the screening criteria are the incore instrumentation guide tube (ICIGT) flags and welds, fuel pins and caps, shared fuel pins and nuts, the intermediate reflector blocks and alignment pins, the lower core plate, and the core barrel. In addition, components identified as susceptible to irradiation-induced stress relaxation are also included for potential wear due to loosening. Components screening in for neutron degradation are included for augmented visual inspection.

4.5.2.2 Control on Welding

The welding of RVI materials conform to the applicable requirements of ASME BPV Code, Section III, Articles NG-2000, NG-4000, and NG-5000. Welding is conducted utilizing procedures qualified according to the rules of ASME BPV Code, Sections III, Subarticle NG-4300 and Section IX. Welders and welding operators are qualified in accordance with ASME BPV Code Section IX and RG 1.71, Revision 1.

Electroslag welding is not permitted on RVI and core structural supports. Additional information regarding welding of austenitic stainless steel RCPB materials provided in Section 5.2.3 is also applicable to the welding of RVI and core support components.

4.5.2.3 Nondestructive Examination

Nondestructive examinations of core support structure materials, including tubular products, conform to the requirements of ASME BPV Code, Section III, Subarticle NG-2500 utilizing the methods of ASME BPV Code, Section V and acceptance standards of Subarticle NG-5300.

4.5.2.4 Fabrication and Processing of Austenitic Stainless Steel Components

Most RVI base metal is fabricated from Type 304/304L austenitic stainless steel. Austenitic stainless steel parts are fabricated from materials procured in the solution-annealed condition. Use of cold worked austenitic stainless steel is avoided to the extent practicable during fabrication of the RVI and core support structure. Austenitic stainless steel used in the RVI and core support components does not exceed a yield strength of 90,000 psi as determined by the 0.2 percent offset method.

Processing and welding of unstablized AISI Type 3XX series austenitic stainless steels comply with RG 1.44 to prevent sensitization and stress-corrosion cracking. When rapidly cooled by means other than water quenching, non-sensitization of base materials is verified by test in accordance with Practice A or Practice E of ASTM A262 (Reference 4.5-1) as required by RG 1.44.

For AISI Type 3XX series austenitic stainless steel subjected to sensitizing temperatures subsequent to solution heat treatment, the carbon content is limited to no more than 0.03 wt%.

RVI weld filler metals and associated specifications listed in Table 4.5-2 are in accordance with ASME BPV Code, Section II, Part C. They are analyzed for delta ferrite content and limited to a ferrite number of 5FN to 20FN in accordance with RG 1.31 and ASME BPV Code, Section III, Paragraph NG-2433. Carbon content of austenitic stainless steel weld filler metals is limited to no more than 0.03 wt%.

Tools for abrasive work such as grinding, polishing, or wire brushing are not permitted to be contaminated by previous usage on ferritic carbon steel or other materials that could contribute to intergranular cracking or stress-corrosion cracking.

Section 5.2.3 describes the controls used to minimize the introduction of potentially harmful contaminants including chlorides, fluorides, and low melting point alloys on the surface of austenitic stainless steel components. In accordance with RG 1.44, cleaning solutions, processing equipment, degreasing agents, and other foreign materials are removed during processing prior to elevated temperature treatments. Acid pickling is avoided on stainless steel and not used on sensitized austenitic stainless steel.

4.5.2.5 Other Materials

Materials exposed to primary reactor coolant are corrosion-resistant stainless steels, nickel-based alloys, and, to a limited extent, cobalt-based alloys. These materials are selected from materials proven in light-water reactor operation and for their compatibility with the reactor coolant as specified in ASME BPV Code, Section III, Paragraph NG-2160 and Subsubarticle NG-3120.

Alloy 600 base metal and Alloy 82/182 weld metal are not used in the RVI and core support structure design.

Washers used in the RVI upper riser assembly are nickel-based Alloy 718. These washers utilize the same final solution annealing and precipitation-hardening treatment process as used for Alloy 718 threaded fasteners. Refer to Section 3.13.1 for further discussion regarding the annealing and precipitation-hardening treatment for Alloy 718 materials. The RVI upper riser assembly washers are not in tension and, as a result, they are not susceptible to stress corrosion cracking.

4.5.3 References

4.5-1 American Society for Testing and Materials, “Standard Practices for Detecting Susceptibility to Intergranular Attack in Austenitic Stainless Steels,” ASTM A262-15, West Conshohocken, PA.

4.5-2 American Society of Mechanical Engineers, Quality Assurance Requirements for Nuclear Facility Applications, ASME NQA-1-2008/1a-2009 Addenda, New York, NY.

4.5-3 Electric Power Research Institute, "Materials Reliability Program: PWR Internals Material Aging Degradation Mechanism Screening and Threshold Values (MRP-175)," EPRI #1012081, Palo Alto, CA, December 2005.

4.5-4 Electric Power Research Institute, "Materials Reliability Program: Resistance to Primary Water Stress Corrosion Cracking of Alloys 690, 52, and 152 in Pressurized Water Reactors (MRP-111)," EPRI #1009801, Palo Alto, CA, March 2004.

4.5-5 Electric Power Research Institute, "Materials Reliability Program: Resistance to Primary Water Stress Corrosion Cracking of Alloy 690 in Pressurized Water Reactors (MRP-258)," EPRI #1019086, Palo Alto, CA, August 2009.

Table 4.5-1: Control Rod Drive Mechanism Materials

Component	Material Designation (Grade, Class, or Type)
Latch Mechanism Assembly	
Magnetic parts: plungers, poles, keys	Type 410
Springs	Alloy X-750 (UNS N07750), AMS 5698 or AMS 5699
Wear parts: latch pins, pivot pins, plunger pin, key pins	Haynes Alloy 25
Latch links Latch arms Lock plungers Guide tubes, support tubes Shims and lock cups	Type 304
Hardfacing for latch arm tips	Stellite 6 or Low cobalt or cobalt-free material
Lock screws	Type 316
Water-Cooled Coil Stacks	
Magnetic parts: housings and flux rings Cooling tube Housing through bolts	Type 410
Non-magnetic parts	Type 304
Wire	Class N insulated copper
Drive Rod & Remote Disconnect Assembly	
Drive rod Drive rod coupling, coupling sleeve Remote disconnect rod Remote disconnect button and button insert	Type 410
Drive rod lower spring retainer Remote disconnect coupling expansion nut Drive rod collar dowel Remote disconnect rod union Remote disconnect upper spring retaining collar Remote disconnect shoulder nut	Type 304
Remote disconnect lower and upper springs	Alloy X-750 (UNS N07750), AMS 5698 or AMS 5699
Remote disconnect expansion plug	Haynes Alloy 25
Latch Housing Assembly	
Flux rings, shield rings	Type 410
Housing thermal shield	Type 304
CRDM Weld Filler Metals (Note 2)	
Welding electrode materials	E308, E308L, E316, E316L
Welding rod materials	ER308, ER308L, ER316, ER316L
CRDM RCPB Components	**Refer to Section 5.2**

Note 1: All listed materials, except the water-cooled coil stacks, are exposed to RCS coolant.
Note 2: 0.03% maximum carbon

Table 4.5-2: Reactor Vessel Internal Materials

Component	Specification	Material Designation (Grade, Class, or Type)
Core Support Assembly		
Core barrel	SA-965	Type 304/304L; Grade F304/F304L
Reflector blocks	SA-965 or SA-182	Type 304/304L; Grade F304/F304L
Lower core plate	SA-965 or SA-240	Type 304/304L
Alignment pins for reflectors Shared fuel pin and fuel pin nuts	SA-479	Type 304/304L
Alignment pins for lower core plate	SA-193	Type 304; Grade B8
Upper support blocks	SA-479 or SA-240	Type 304/304L
Socket Head Cap Screw	SA-193	Grade B8, Class 1
Alignment Dowel	SA-193	Grade B8, Class 1
Reactor Vessel Surveillance Capsule Assembly		
Capsule basket, protection guide, support Specimen enclosure Screw locking caps	SA-240	Type 304/304L
Plugs and dowel pins Screws	SA-479	Type 304/304L
Upper Riser Assembly		
Upper riser transition and section Riser backing strips Upper CRD supports Upper riser hanger ring and hanger braces Chemical volume and control system (CVCS) injection piping support Incore instrumentation centering plate Flow diverter	SA-240	Type 304/304L
Upper riser hanger threaded structural fasteners Upper riser hanger alignment pins	SA-479	Type 304
Upper riser bellows CVCS injection flexible pipe	N/A	Type 304L
CVCS injection piping	SA-312	Seamless; Grade TP304/TP304L
CVCS injection piping end cap CVCS injection piping elbow	SA-182	Grade F304/F304L
Incore instrumentation guide tubes (ICIGTs) - 1-12	SA-213	Grade TP304/TP304L
Pressurizer spray nozzles	SA-479	Grade TP304/TP304L
Washers	SB-637	Alloy 718 (UNS N07718)
Lower Riser Assembly		
Lower riser section, transition, and spacer Upper core plate ICIGT support ICIGT flags CRA guide tube support plates CRD alignment cones, CRA cards, CRA lower flange	SA-240	Type 304/304L
Lower riser trunnions Fuel pins and fuel pin caps	SA-479	Type 304/304L
ICIGTs - 1 ICIGTs - 2 inner and outer assemblies	SA-213	Grade TP304/TP304L
CRA guide tubes	SA-312	Seamless; Grade TP304/TP304L

Table 4.5-2: Reactor Vessel Internal Materials (Continued)

Component	Specification	Material Designation (Grade, Class, or Type)
RVIs Weld Filler Metals		
Welding electrode materials	SFA-5.4	E308, E308L, E316, E316L
Welding rod materials	SFA-5.9	ER308, ER308L, ER316, ER316L
Flux and metal cored welding electrode/rod materials	SFA-5.22	E308TX, E308LTX, E316TX, E316LTX

4.6 Functional Design of Control Rod Drive System

The design of the control rod drive system (CRDS) and its supporting structures, systems, and components provides the functional capability to achieve safe shutdown and maintain the fuel cladding acceptance criteria during anticipated operational occurrences (AOOs), infrequent events and accidents.

The CRDS performs the following safety-related functions:

- releases the control rod assemblies during a reactor trip
- maintains the pressure boundary of the reactor pressure vessel

The CRDS performs the following non safety-related functions:

- latching, holding, and maneuvering the CRAs during reactor startup, power operation, and shutdown
- provides rod position indication
- protects fuel integrity during reactor disassembly and reassembly prior to and after refueling

4.6.1 Description of the Control Rod Drive System

The CRDS includes the control rod drive mechanisms (CRDMs) and all electrical and instrumentation and controls components, including rod position indicators, to operate the CRDMs. The CRDM includes the control rod drive shaft, which extends to the coupling interface with the control rod assemblies (CRAs) in the reactor pressure vessel. The CRDS supports the CRA by latching, holding, and maneuvering the CRA during reactor startup, power operation, and shutdown in response to signals from the control rod drive power converter and controller assembly, and in releasing the CRA during a reactor trip. The CRDS also includes the rod position indicator cabinets and cables, CRDM power cables, and cooling water supply and return piping inside containment. The mechanical design of the CRDM is described in Section 3.9.4 and the design of the CRA is described in Section 4.2.2. The instrumentation and controls for the CRDS are described in Section 7.0.4.

Figure 4.6-1 through Figure 4.6-5 illustrate the principal features of the CRDS. Figure 4.6-1 is a simplified drawing showing an overview of the location of the various components of the CRDS relative to the reactor pressure vessel (RPV) and the containment vessel (CNV). It includes the CRDMs and supports, control rod drive shafts, internal CRDS supports, and CRA guide tubes. The CRDMs are located on top of the RPV and laterally constrained at two elevations above in order to limit relative lateral seismic motion, yet allow for unrestricted axial expansion. The long control rod drive shafts are located inside the RPV, and aligned laterally by CRDS support structures that are part of the reactor vessel internals (RVI). Further details are provided in Section 3.9.4.1. The electromagnetic load transfer across the primary pressure boundary is facilitated by electromagnetic coils on the outside (Figure 4.6-3) that engage a set of magnetic poles connected to latches on the inside (Figure 4.6-5), in order to move the control rod drive shaft in a predetermined stepping sequence (refer to Section 3.9.4.1.2). Figure 4.6-2 provides an illustration of the CRDM electromagnetic coils and housings, including the pressure housings. The major components of the CRDM are annotated, and detailed in the subsequent figures. The power and cooling water connectors are located on top of the mast assembly and sensor

coil for ease of access through the removable cover on top of the CNV (Figure 4.6-1). Figure 4.6-3 illustrates the CRDM drive coil and embedded cooling coils shown on the right view without the coil stack housings and mast assembly. The electrical connector on top of the left view is located above the cooling water fittings for separation purposes. Figure 4.6-4 shows the layout of the rod position indicator sensor coil assemblies which are located directly above the rod travel housing. Rod position indication is facilitated by means of electromagnetic induction in the sensor coils, as the top of the control rod drive shaft travels upwards or downwards within the pressure boundary. Figure 4.6-5 provides an overview of the latch mechanism assembly (LMA), with the remote disconnect latch shown separately for better illustration. The three magnetic poles, latches and grippers on the left represent an industry-standard LMA design that performs the rod withdrawal/insertion/reactor trip functions, whereas the remote disconnect grippers (RDG) are relied upon during the remote disconnection/re-connection for NPM refueling only. Figure 4.6-6 illustrates the remote disconnection of the control rod drive shaft from the CRA that is not available in the operating NPM location, in order to preclude inadvertent CRA disengagement.

The CRDM assembly is a hermetically sealed electro-mechanical device, which moves the CRA in and out of the reactor core, and holds the CRA at any elevation within the range of CRA travel. If electrical power is interrupted to the CRDM, the control rod drive shaft is released, and the attached CRA drops into the reactor core.

The CRDMs are mounted on the RPV head, and the CRDM pressure housings are safety-related American Society of Mechanical Engineers (ASME) Class 1 pressure boundaries. The CRDS components internal to the reactor coolant pressure boundary are designed to function in borated primary coolant with up to 2000 ppm boron at primary coolant pressures and temperatures ranging from ambient conditions to 650 degrees F design temperature and 2,100 psia RPV design pressure. During normal operating conditions the upper portion of the RPV and the CRDM pressure housing are in contact with saturated steam on the inside at 625 degrees F and 1850 psia. The lower portion of the drive rod is submerged in the primary coolant at hot leg temperature flowing upward through the upper riser and CRA guide tubes. The electric coil operating conditions require active cooling by water through a CRDS cooling water distribution header to cooling tubes in the drive coils of each CRDM as shown in Figure 4.6-3. The cooling requirements for the CRDMs are provided by the reactor component cooling water system (RCCWS) in Section 9.2.2. The RCCWS is designed to maintain the CRDM winding temperature below the design maximum temperature of 356 degrees Fahrenheit.

The CRDS cooling line is branched into supply lines inside the containment vessel to each individual CRDM. After passing through the CRDM cooling tubes, the flexible return lines rejoin into a single return header leaving containment. A thermal relief valve is provided on the return header to provide overpressure protection for the CRDS cooling piping during a containment isolation event.

The structural materials of construction for the CRDS are discussed in detail in Section 4.5.1.

4.6.2 Evaluations of the Control Rod Drive System

This section describes how the design of the CRDS conforms to General Design Criteria (GDC) 4, 23, 25, 26, 28, 29 of 10 CFR 50, Appendix A. The design also conforms to Principal Design Criteria (PDC) 27.

GDC 4 is applicable to the CRDS design as it requires the structures, systems, and components important to safety to be designed to accommodate the effects of and to be compatible with the environmental conditions during normal plant operation as well as during postulated accidents as a result of equipment failures and external events. The CRDS provides the capability to safely shut down the reactor during normal operations and AOOs and either prevents or mitigates the consequences associated with postulated accident scenarios. The CRDS design features comply with GDC 4 requirement for designing the CRDS to be compatible with the environmental conditions. The CRDS components located inside the containment are protected against dynamic effects as described in Section 3.6. The CRDS structures, systems, and components are located inside the Reactor Building, which is a Seismic Category I structure designed to protect from events and conditions outside the NuScale Power Plant. The CRDS ability to perform the required safety-related functions will not be compromised by adverse environmental conditions. The control rod drive shafts are immersed in 590 degrees F water during normal full power operation. The upper portion of the control rod drive shafts penetrate the pressurizer and are exposed to a steam environment at about 625 degrees F. The control rod drive shafts and latch mechanisms are designed to 650 degrees F and are able to operate without the typical liquid drag forces experienced by CRDMs in the current PWR fleet.

GDC 23 requires that the protection system be designed to fail into a safe state in the event of adverse conditions or environments. The CRDM provides positive core reactivity control through the use of movable CRAs. The movable CRAs provide reactivity control for modes of operation when the NPM is installed in its operating location. During transition to the refueling area, and during refueling activities, the CRA are inserted and the associated CRDM is disconnected from the CRDS. The CRDM, in conjunction with the module protection system, actuate the control rods to perform safety-related functions when necessary to provide core protection during normal operation, AOOs, and accidents. The CRDM is designed to fail in a safe condition, even under adverse conditions, that prevents damage to the fuel cladding and excessive reactivity changes during failure. Loss of electrical power to the reactor trip breaker will initiate a reactor trip, causing rods to drop into the core to shut down the reactor.

GDC 25 requires that the protection system be designed to ensure that specified acceptable fuel design limits are not exceeded for any single malfunction of the reactivity control systems. Chapter 15 safety analyses demonstrate that the CRDS with any assumed credible failure of any single active component is capable of performing a reactor trip when plant parameters exceed the reactor trip setpoint, in accordance with GDC 25.

GDC 26 is applicable to the CRDS design, as the CRDS is one of the independent reactivity control systems. It is designed with appropriate margin to assure its reactivity control function under conditions of normal operation including AOOs. The CRDS facilitates reliable operator control by performing a safe shutdown (i.e., reactor trip) via gravity-dropping of the CRAs on a reactor trip signal or loss of power. The CRDS is designed

such that core reactivity can be safely controlled and that sufficient negative reactivity exists to maintain the core subcritical under cold conditions.

PDC 27 requires that the two independent reactivity control systems (control rods and soluble boron system) are capable of reliably controlling reactivity changes to assure that under postulated accident conditions and with appropriate margin for stuck rods the capability to cool the core is maintained. The analyses in Chapter 15 demonstrate that, with a stuck rod, the capability to cool the core is maintained. The insertion of all CRAs is required to hold the reactor core subcritical under cold conditions.

GDC 28 requires that the effects of postulated reactivity insertion accidents neither result in damage to the reactor coolant pressure boundary, nor cause sufficient damage to impair the capability to cool the core. A postulated failure of the CRDS causing a rod ejection has the potential to result in a relatively high rate of positive reactivity insertion, which could challenge specified acceptable fuel design limits. The rod ejection accident is not analyzed as a loss-of-coolant accident event. To prevent a mechanical failure of the CRDM housings, the CRDM nozzles are designed to be an integral part of the RPV. The CRDM pressure housings are full penetration welded to the safe ends of the CRDM nozzles. The safe-end-to-CRDM nozzle welds and safe-end-to-CRDM pressure housing welds are inspected to ASME Class 1 requirements. However, a failure of the CRDM pressure housing is postulated to provide a limiting reactivity insertion event in Section 15.4. The REA analysis presented in Section 15.4 demonstrates that GDC 28 is met by ensuring that the effects of a postulated rod ejection event meet the acceptance criteria in the SRP.

GDC 29 is applicable to the CRDS design, as the CRDS, in conjunction with reactor protection systems, is designed to assure an extremely high probability of accomplishing its safety-related functions in the event of AOOs. The CRDS fulfills its safety-related functions to control the reactor within fuel and plant limits during AOOs despite a single failure of the system. The CRDS accomplishes safe shutdown (i.e., reactor trip) via gravity-dropping of the CRAs on a reactor trip signal or loss of electrical power. The CRDM pressure housing is an ASME Class 1 pressure boundary for the reactor coolant for all ASME service levels.

The safety-related reactor trip function of the CRDS is initiated by the module protection system through the reactor trip system, which isolates the CRDS power converter and controller assembly from the normal direct current power system. Failures of the CRDM have been evaluated in a failure modes and effects analysis. Effectiveness of the CRDS, despite possible single failures, is demonstrated in Chapter 15, which shows the CRDS performs a reactor trip when plant parameters exceed the reactor trip setpoint. Therefore, the reactor is placed in a subcritical condition with any assumed credible failure of any single active component.

Section 3.6 demonstrates that all CRDS essential equipment is protected from common-mode failure caused by leakage or rupture of moderate- and high-energy lines, the dynamic and environmental effects of postulated breaks, and potential jet impingement to ensure compliance with GDC 4.

The CRDS instruments are not covered by ASME Boiler and Pressure Vessel Code, but instrument lines are subject to these requirements. The CRDM components inside the CNV are located near high- and moderate-fluid system piping, such as reactor coolant system

piping, feedwater piping, and steam piping. Loads from moderate- and high-energy line breaks are included in the stress analysis for CRDS components that are designed per the rules of the ASME Boiler and Pressure Vessel Code.

The jet impingement loads generated from high energy line breaks inside the CNV are analyzed as described in Section 3.6. The main steam and feedwater system lines meet the criteria for leak-before-break (LBB) (see Section 3.6.3). Therefore, circumferential and longitudinal breaks that could impinge on the CRDMs are not postulated. For the other high energy lines inside containment that do not qualify for LBB, these lines are small (NPS 2). The line size limits the energy of jet impingement loads. Based on the low jet pressure load and heavy walled construction of the CRDMs, jet impingement does not adversely affect CRDM scram functionality.

There are also jet impingement loads expected from opening the reactor safety valves and the emergency core cooling system reactor vent valves, which vent to the containment. A fluid jet diffuser is provided at the outlet of these valves to dissipate the energy of the fluid jet in order to protect the essential SSC in the region of containment near the RPV head.

The essential control elements of the CRDS (those required to provide reactor trip) are provided by the module protection system and are isolated from nonessential portions of the rod control system provided by the module control system, as described in Section 7.0.

4.6.3 Testing and Verification of the Control Rod Drive System

The CRDS prototype testing is described in Section 3.9.4 and Section 4.2.4. The testing of the prototype includes conceptual (mock-up) testing, prototype performance testing, stability testing, endurance testing and production testing.

The pre-operational and initial startup tests that are performed to verify the proper function of the CRDS are described in Section 14.2. They include insertion, withdrawal and drop time testing, and hydrostatic tests. Inservice tests are conducted to verify the operability of the CRDS on a periodic basis and are described in the Technical Specifications.

4.6.4 Information for Combined Performance of Reactivity Systems

Single or common cause failures of the CRDS do not prevent proper operation of the reactor trip function. There are no reactor trip function failures that prevent proper functioning of the engineered safety features actuation system. Section 7.2 provides the details that support this conclusion.

As indicated in Section 4.3, there are two independent reactivity control systems in accordance with GDC 26; the CRDS and the addition of soluble boron by the CVCS. The CVCS is not a safety-related system, so boration is not credited for reactivity control in the safety analyses presented in Chapter 15. The design bases and capabilities of the CVCS are discussed in Section 9.3. The CRDS is the reactivity control system that is credited in the design basis safety analyses.

4.6.5 Evaluations of Combined Performance

Chapter 15 demonstrates that for all design basis events, the CRDS is capable of maintaining the reactor within acceptable limits, assuming that the most reactive control rod is stuck out.

Figure 4.6-1: Overview of Control Rod Drive Mechanism Locations in Relation to the Reactor Pressure Vessel and Containment Vessel

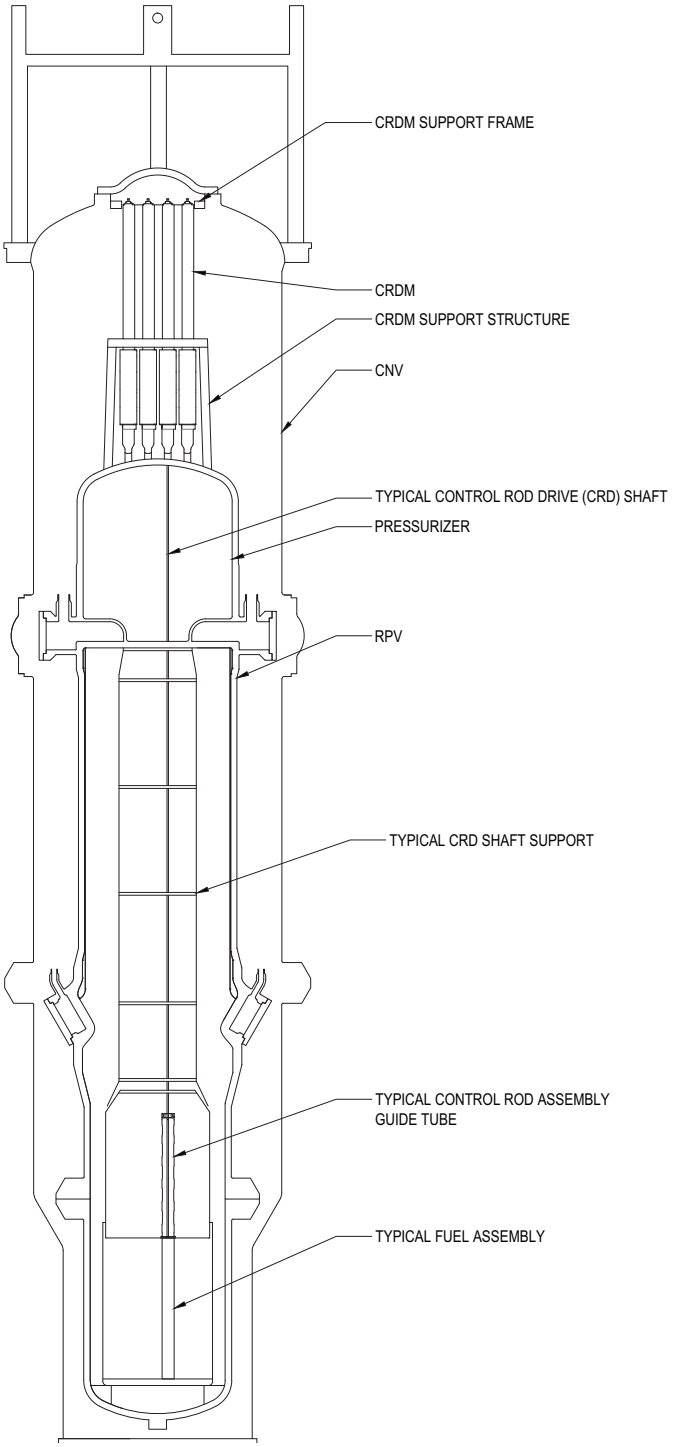

Figure 4.6-2: Control Rod Drive Mechanism Coils and Housings

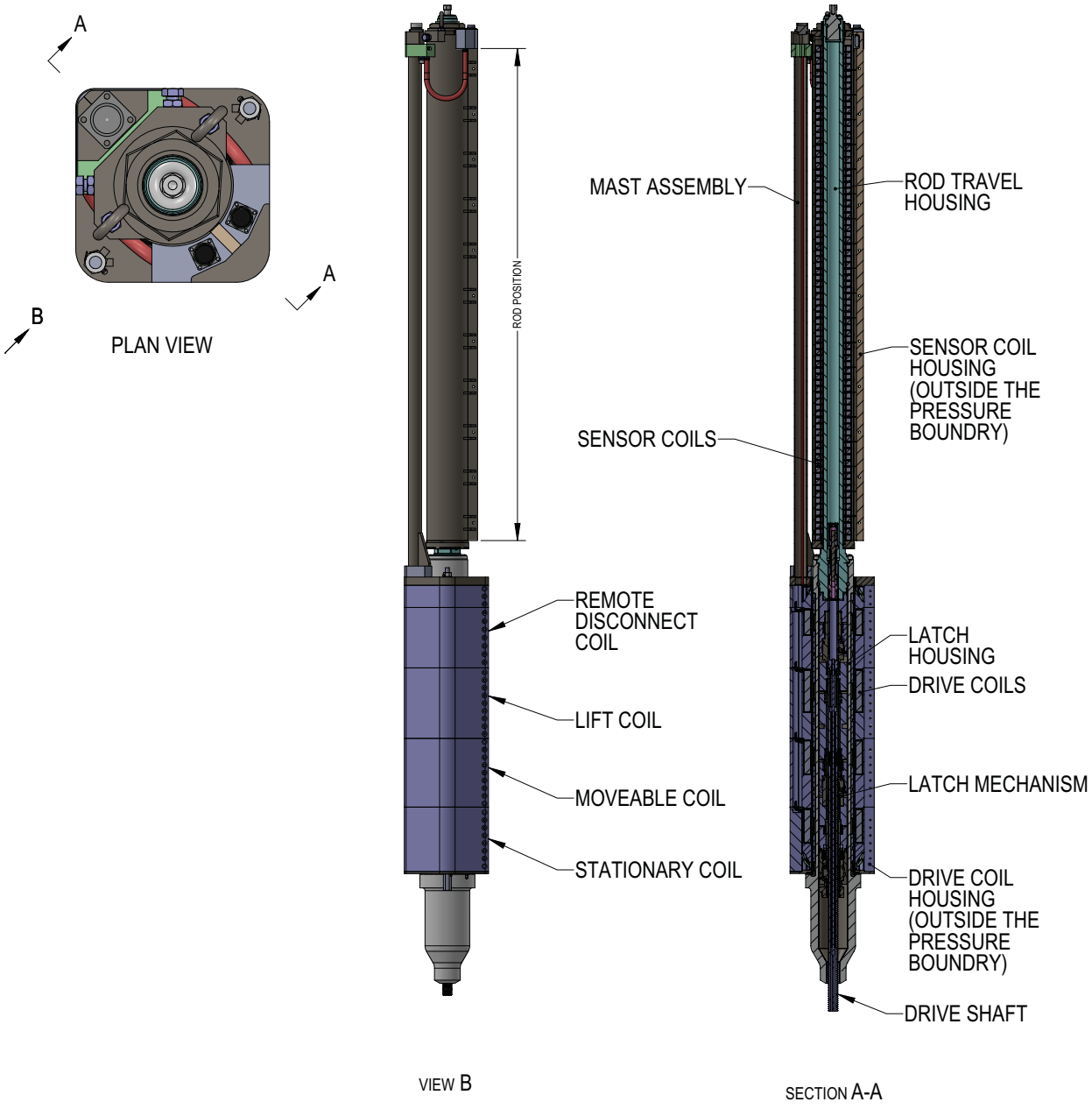

Figure 4.6-3: Control Rod Drive Mechanism Drive Coil and Cooling Detail

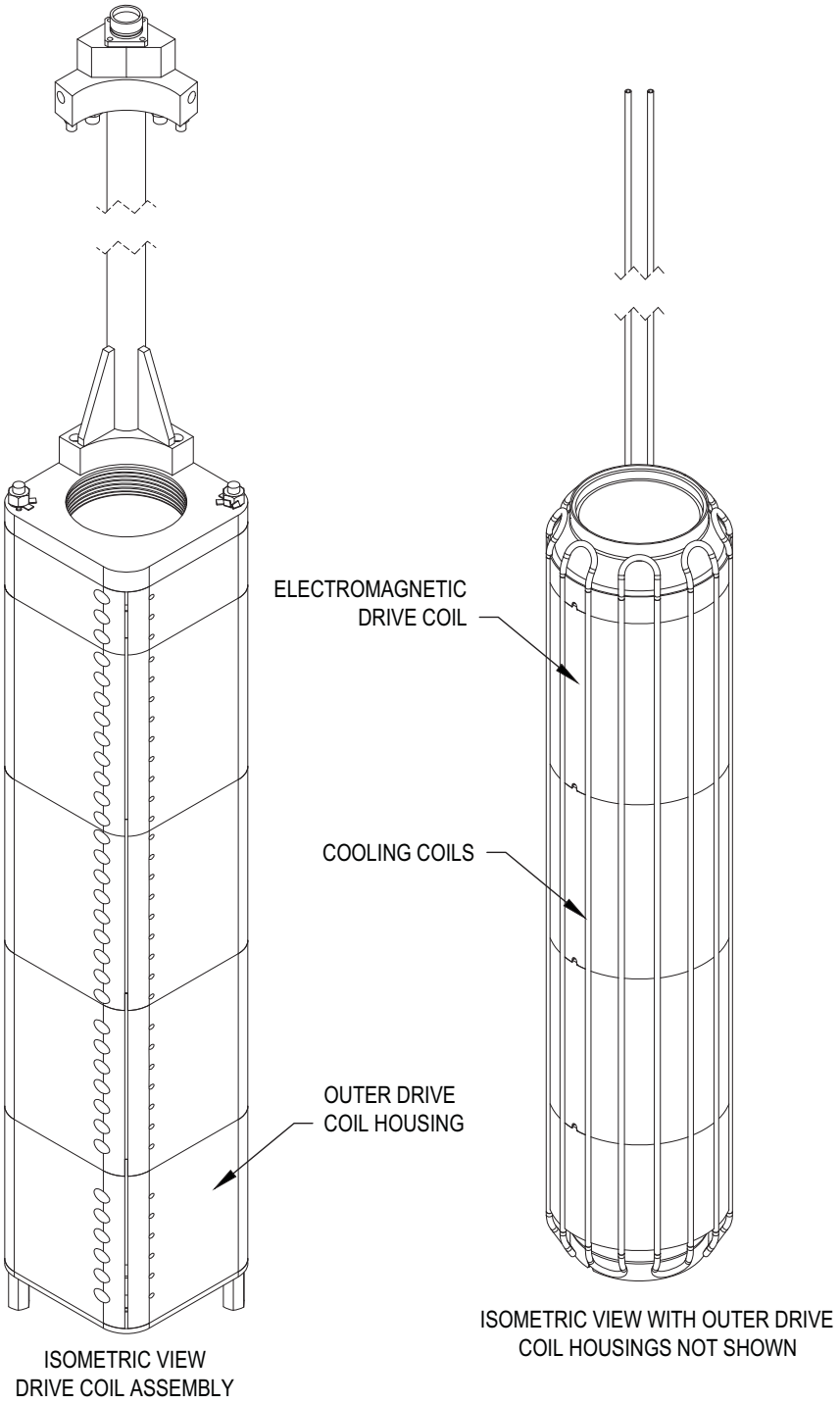

Figure 4.6-4: Layout of Sensor Coil Assembly

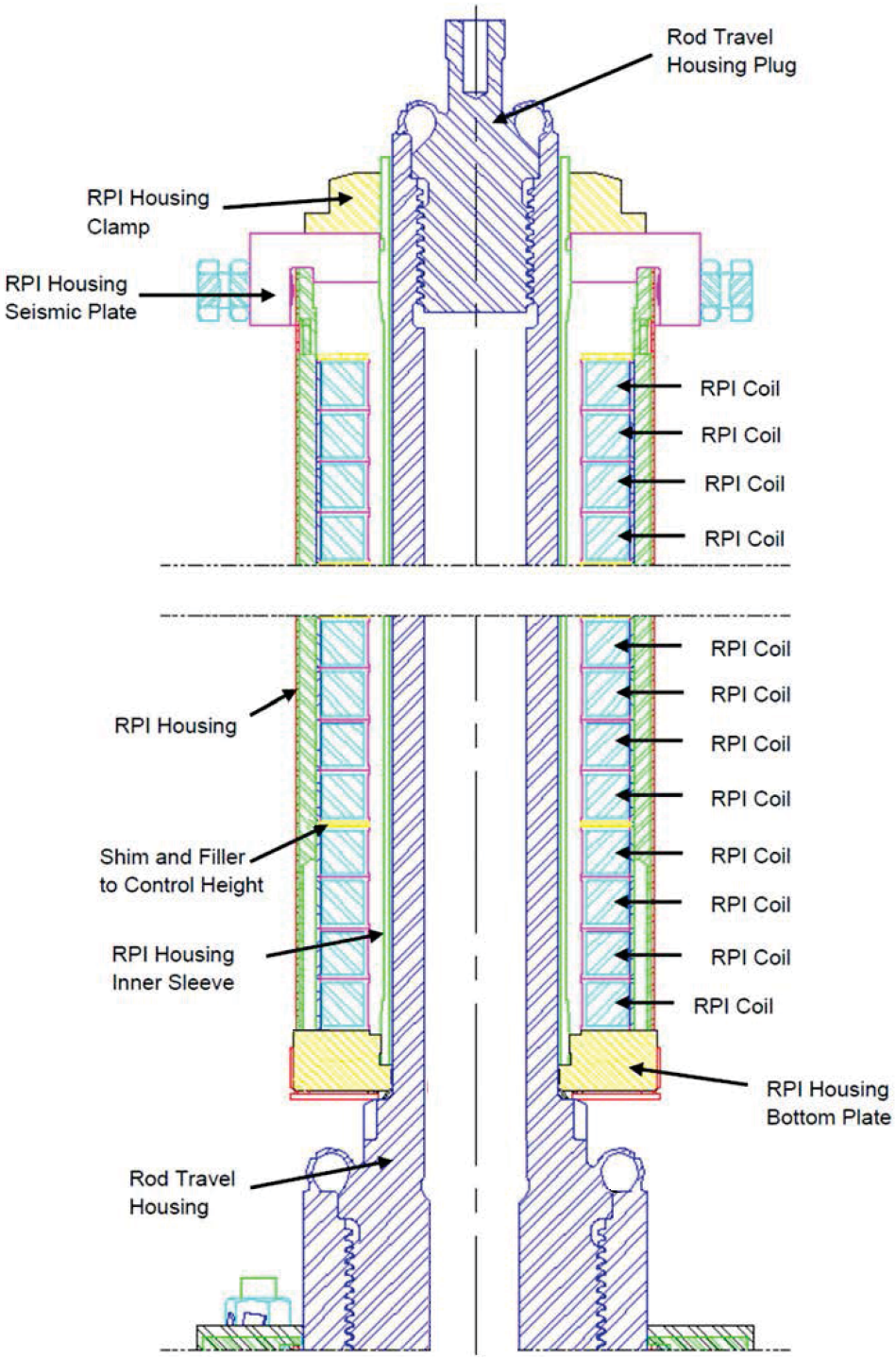

Figure 4.6-5: Overview of Latch Mechanism Assembly

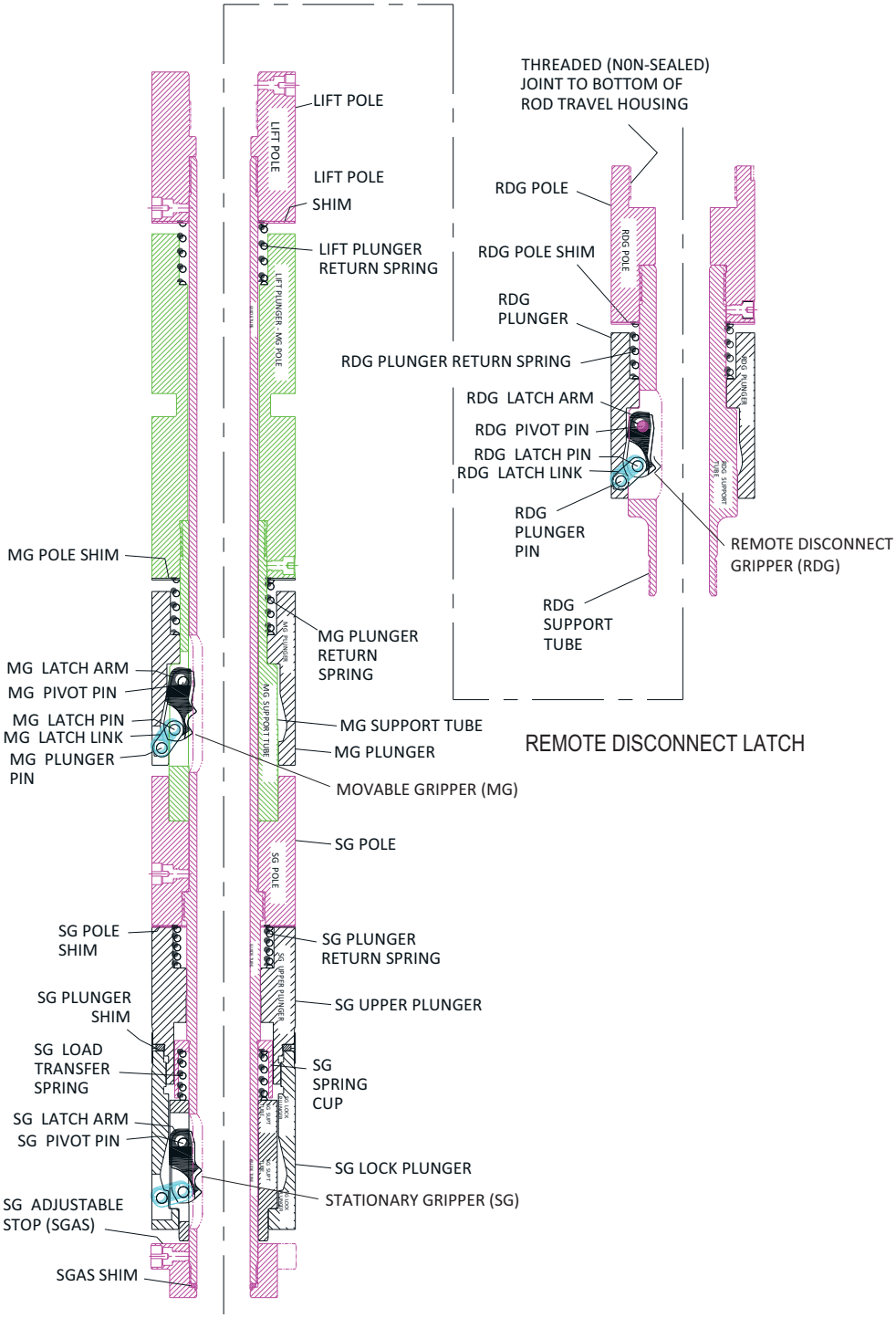

Figure 4.6-6: Control Rod Drive Mechanism Drive Shaft Interface with Control Rod Assembly